Role of the Synovial Membrane in Osteoarthritis Pathogenesis and Cartilage Repair

Robert M. Stefani

Submitted in partial fulfillment of the
requirements for the degree of
Doctor of Philosophy
in the Graduate School of Arts and Sciences

COLUMBIA UNIVERSITY

2020

ABSTRACT

Role of the Synovial Membrane in Osteoarthritis Pathogenesis and Cartilage Repair

Robert M. Stefani

Osteoarthritis (OA) affects an estimated 250 million people worldwide, representing an enormous economic and social burden across demographic groups. While classically attributed to 'wear and tear' of the articular cartilage, there is a growing appreciation that OA is a whole-joint disease with a complex etiology involving the synovium and surrounding tissues. The synovium is a specialized connective tissue membrane that envelops the diarthrodial joint and maintains the synovial fluid environment through molecular secretion as well as bi-directional filtration of these constituents, nutrients, and cellular waste products. Moreover, synovium-derived cells have been directly implicated in both the native repair response as well as degradation of articular cartilage.

Much of the existing research of synovium has been conducted in the context of rheumatoid arthritis (RA). And while synovitis is a key feature of both RA and OA, clinical reports have described OA synovium as distinct in its cellular and structural composition, molecular secretion, and chronic onset. However, literature studies have not adequately addressed the mechanisms by which alterations in synovium structure-function affect joint and cartilage health, particularly the contribution of different cell types within the synovium to solute transport and lubrication. The

work described in this dissertation addresses these knowledge gaps in the context of existing and emerging OA therapies, namely glucocorticoids and electrical stimulation.

We anticipate that a more comprehensive characterization of changes to the synovium composition, secretion of key metabolic mediators, lubrication properties, as well as its ability to regulate solute transport in and out of the joint space will not only contribute to our basic science understanding of the synovium but also the development and modification of therapeutic strategies aimed at restoring and maintaining joint health. This characterization will be facilitated by our laboratory's expertise in tissue engineering and explant culture, IL-1 and DEX stimulation, and electrical stimulation of joint tissues. The approach of using an engineered synovium model is attractive in that quantitative high throughput *in vitro* mechanistic studies can be performed on tissues that are fabricated from cells derived from normal and OA synovium of patients and corresponding immune cells at defined density and cell type ratios. It also facilitates isolating effects of certain cell types or starting composition that are found in explant specimens.

Intra-articular glucocorticoid injections are commonly administered to patients in an effort to control inflammation and pain. And while these high dose injections are known to have significant detrimental local and systemic effects, comparatively low doses of dexamethasone (DEX), a synthetic glucocorticoid, are known to have pro-anabolic and anti-catabolic effects on cartilage cultures. Our laboratory has published extensively on the benefits of DEX stimulation in growth and maintenance of engineered and explanted cartilage as well as chondroprotection from pro-inflammatory cytokines (e.g interleukin-1; IL-1), both in juvenile bovine basic science and adult canine preclinical systems. However, the concomitant effects of DEX on synovium structure-function have not been elucidated.

In Part I, we describe a functional tissue engineered synovium model that was validated against explant behavior. We were able to recapitulate many of the unique structural and functional characteristics of synovium, including protein expression, intimal lining formation, solute transport, and friction coefficient. Additionally, changes in engineered synovium structure-function mirrored that of explants when treated with IL-1 or DEX. The engineered synovium model was then expanded to include resident macrophage-like synoviocytes (MLS), demonstrating the key role that these cells play in structural reorganization of synovium. The model was also translated to human cells, showing the potential of the system for personalized medicine. Finally, motivated by insights into solute transport in the synovium as well as its strong anti-inflammatory response to DEX, we developed a sustained low-dose DEX delivery platform for mitigating synovial inflammation while simultaneously stimulating cartilage growth. Utilizing a preclinical adult canine model, we showed that extended intra-articular delivery of DEX improved functional outcomes and cartilage tissue quality.

In Part II, we evaluated synovium behavior and cartilage repair in response to modes of electrical stimulation. Electrical stimulation of cells and tissues has been a topic of interest for decades, owed in part to the knowledge that endogenous electric field (EF) gradients guide cell behavior during embryogenesis and wound healing. Pulsed electromagnetic fields (PEMFs) have been used in a clinical setting to stimulate bone repair and alleviate pain, however their use for OA and cartilage repair is controversial. Culture studied of PEMFs have shown anti-catabolic and pro-anabolic effects on isolated FLS and cartilage, respectively. And previous work in our laboratory demonstrated directed 2D migration of synoviocytes and chondrocytes in response to direct current (DC) EF stimulation. These modes of electrical stimulation have not been explored in synovium

explants, so it is unclear to what extent the observed phenomena translate to the 3D tissue environment.

For the first time, we characterized the biological response of both healthy bovine and OA human synovium explants, showing distinct anti-inflammatory behavior in bovine tissues and a highly variable response in arthritic human tissues, likely due to different inflammatory cell content. Motivated by the potent anti-inflammatory effect seen in normal tissue and previous work showing a pro-anabolic effect on cartilage, the PEMF system was then adapted for use with a preclinical adult canine model of engineered cartilage repair. In this model, PEMFs significantly enhanced functional outcomes and cartilage tissue quality. Finally, we investigated the potential for direct synovial cell-mediated cartilage repair via induced migration with DC EFs. By developing and validating a novel tissue-scale bioreactor capable of applying DC EFs in sterile culture conditions to three-dimensional constructs, we showed increased recruitment of synovial repair cells to the site of a cartilage wound.

Taken together, the sum of the work builds on existing therapeutic strategies by developing models to understand the contribution of the synovium to joint maintenance and repair. By modeling dexamethasone- and electrical- induced changes to composition and function of synovium and cartilage, via complementary explant and engineered approaches, valuable mechanistic insights into osteoarthritis pathogenesis and cartilage repair were gathered. These findings lay the groundwork for more complex and personalized *in vitro* models of OA and motivate future work to capitalize on knowledge of the functional plasticity of the synovium to develop synovium-targeted strategies for OA treatment and prevention.

Table of Contents

List of Figures

List of Tables

List of Abbreviations

αMEM	alpha Minimum Essential Medium
ACI	autologous chondrocyte implantation
ANOVA	analysis of variance
BM	serum-free basal medium
CM	serum-free chondrogenic medium
COL	collagen
CTL	control
DAPI	4’,6-Diamidino-2-Phenylindole, Dihydrochloride
DC	direct current
DEX	dexamethasone
DiI	1,1’-Dioctadecyl-3,3,3’,3’-Tetramethylindocarbocyanine Perchlorate
DMEM	Dulbecco’s Modified Eagle’s Medium
DNA	Deoxyribonucleic Acid
DW	dry weight
ECM	extracellular matrix
EF	electric field
FBS	fetal bovine serum
FGF	fibroblast growth factor
FLS	fibroblast-like synoviocyte
GAG	glycosaminoglycan
HA	hyaluronan
HSD	honest significant difference
IL	interleukin
ITS	Insulin-Transferrin-Selenium
MACI	matrix-assisted chondrocyte implantation
MCSF	macrophage colony stimulating factor
MLS	macrophage-like synoviocyte
MMP	matrix metalloproteinase

MTT	3-(4,5-Dimethyl-2-thiazolyl)-2,5-diphenyl-2H-tetrazolium bromide
MW	molecular weight
NGF	nerve growth factor
NO	nitric oxide
OA	osteoarthritis
OCA	osteochondral allograft
OAT	osteochondral autograft transfer
PBS	phosphate buffered saline
PEMF	pulsed electromagnetic field
PFA	paraformaldehyde
RA	rheumatoid arthritis
SDSC	synovium-derived stem cell
TGF	transforming growth factor
TNF	tumor necrosis factor
WW	wet weight

Acknowledgments

I would like to first acknowledge the funding sources for my graduate research: Columbia University, National Institutes of Health, United States Department of Defense, Musculoskeletal Transplant Foundation, New York State Stem Cell Science, Orthopaedic Scientific Research Foundation, and IGEA Clinical Biophysics. Without the financial support of these organizations, the work in this dissertation would not have been possible.

Secondly, thank you to my committee members: Clark Hung, Gerard Ateshian, Jimi Cook, Chloe Bulinski, and Helen Lu. I am extremely lucky to have had each of you guide and support me throughout my graduate career. I am especially grateful to Clark, who has been an incredible advisor, mentor, and friend. Clark's knowledge and creativity have inspired me to be a better scientist and researcher. Thank you to Gerard for his thoughtful critiques, fascinating history lessons, and always being willing to lend a hand with computational modeling. Thank you to Jimi for taking such an active and supportive role in my research. Thank you to Chloe for being my resource for anything biology related and for the many fun conversations along the way. Many thanks to Helen for her research support and always being a friendly face around the office. Thank you to Roshan Shah for his mentorship and enthusiasm for the synovium project. Thank you to Amy Reilein at the Biological Sciences Imaging Facility, Aaron Stoker and Chantelle Bozynski at University of Missouri, Ruggero Cadossi and Stefania Setti at IGEA, Eric Semler and Marc Jacobs at MTF, Kacey Marra and Adam Cottrill at University of Pittsburgh. Thank you to the current and former BME staff, who are the unsung heroes of the department: Arthur Autz, Michelle Cintron, Karen Evans, Zachary Corter, James Ihn, Paulette Louissaint, Jarmaine Lomax, and Keith Yeager.

Thank you to all the members of the Cellular Engineering Lab, past and present: Terri-Ann Kelly, Andrea Tan, Sonal Sampat, Adam Nover, Brendan Roach, Amy Silverstein, Eben Estell, Andy Lee, Lianna Gangi, Hagar Kenawy, Matt Pellicore, Lance Murphy, Will Yu, Saiti Halder, Colden Lyons, Charlie Cai, Sofia Barbosa, and Neeraj Sakhrani. A special thanks to Adam for showing me the ropes when I was a lowly first year and getting me my first CEL publication. Thanks to Amy for partnering up to get the synovium project up and running. Thanks to Roachie for making sure I wasn't slacking off and generally being a pain in the you-know-what. Thanks to Eben for his camaraderie, whether talking about the latest Google device or thrashing me on the squash courts. Thanks to Andy, Lianna, Hagar, Matt, and Lance for taking it easy on me as I've gotten used to my role as lab elder (and for picking up the slack as my presence in lab has waned). Special thanks to Saiti for sticking it out with me for her entire undergraduate career. My first paper would not have gotten done without her tireless efforts and enthusiasm. And last, but not least, thank you to Andrea for her wisdom, mentorship, and friendship.

Thank you to the members of the Musculoskeletal Biomechanics Lab: Mike Albro, Sevan Oungoulian, Brian Jones, Alex Cigan, Bob Nims, Krista Durney, Chieh Hou, Brandon Zimmerman, Jay Shim, Courtney Schaeffer, Claire Sise, and Katie Spack. I hope we can keep the fantasy football league going for years to come. Special thanks to Sevan for the career advice and Bob for all of his help with FEBio.

Thank you to my parents and brother for being my support system. I didn't get to visit you guys as often as I would have liked these past years in grad school, but I promise I will make up for it now. Thanks to my grandparents, who have supported me so much along the way. And above all, thank you Maka for being such an amazing partner over the last four years. She has made me a better person and I could not have accomplished any of this without her love and support.

Chapter 1

Introduction

The synovium is a specialized connective tissue membrane that envelops the diarthrodial joint and maintains the composition of the synovial fluid. While the synovium has long been implicated in the etiology of rheumatoid arthritis (RA), and thus the subject of extensive research efforts in this context, there is comparatively little known about the role of synovium in post-traumatic and idiopathic osteoarthritis (OA). Our laboratory has vast experience in applying chemical, electrical, and mechanical stimuli to native and engineered cartilage tissues in order to better understand cartilage growth, healing, and OA progression. However, the concomitant and likely interactive effects of these stimuli on the synovium, as well as downstream consequences on cartilage and overall joint function, have largely been gleaned from culture studies of isolated cells or clinical reports. In order to provide a more complete understanding of synovium behavior that can be leveraged to improve on existing cartilage repair strategies and to inspire new treatments targeting synovial function, the motivation of the work in this dissertation is two-fold: 1) characterize synovium structure-function in response to pro-inflammatory cytokine insult and glucocorticoid treatment; 2) investigate electrotherapeutic strategies for modulating synovium behavior and cartilage repair.

To guide this effort **(Figure 1.1)**, two overarching hypotheses are presented, accompanied by specific aims and rationale. The broader clinical and societal significance of the work is then described, followed by an overview of the relevant literature, including diarthrodial joint structure-function, current repair modalities, and models.

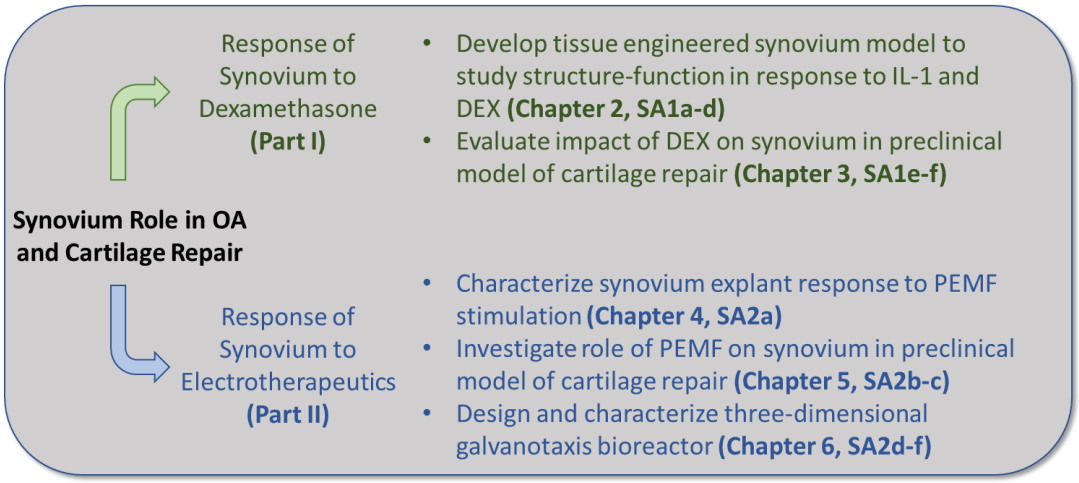

Figure 1.1 Organizational structure of dissertation.

1.1 Hypotheses and Specific Aims

Global Hypothesis (Part I): Synovium structure-function, and by extension OA and cartilage repair, is modulated by interleukin-1 (IL-1) and dexamethasone (DEX).

Specific Aim 1a: To develop a fibroblast-like synoviocyte (FLS)-based engineered synovium to facilitate evaluation of structure-function, and validate against baseline properties of native tissue explants.

Specific Aim 1b: To evaluate the response of the engineered synovium described in SA1a and native tissue explants to IL-1 insult and DEX treatment.

Specific Aim 1c: To incorporate tissue-resident macrophage-like synoviocytes (MLS) into the engineered synovium model and use cell tracking techniques to observe behavior.

Specific Aim 1d: To translate the engineered synovium model to a human system, and evaluate the role of blood-derived T lymphocytes in synovium response to IL-1 and DEX.

Despite the critical role of the synovium in joint and cartilage health, there is a striking lack of quantitative structure-function data. This is partly the result of a lack of adequate *in vitro* synovium models. Useful insights can be gleaned from *in vivo* monitoring of tracer molecules, however these lack the resolution to provide mechanistic insights and limit other quantitative assessments (Levick

and McDonald, 1989; Myers et al., 1995). For example, there is an apparent increase in synovium permeability that has been inferred from decreased HA content in the synovial fluid and increased HA in the serum (Scanzello and Goldring, 2012a). In contrast, a recent *in vivo* study reported that 500 kDa dextran was retained in the arthritic joint longer than in the healthy joint, while 10 kDa was similar for both. This observation may be associated with changing composition and thickness of the synovium (Myers et al., 1995), however these conflicting findings highlight the need for more sophisticated synovium models.

Explant studies are undoubtedly an important tool, but they have limited utility due to low supply of healthy human tissue. Specimens from clinical patients are highly damaged, contaminated with fat and capsular tissue, making them hard to manipulate and limiting the functional analysis that can be performed *in vitro* (McNamara et al., 2010). Studying the response of synovial explants to pro-inflammatory stimuli is further complicated by stark differences in cell and matrix content due to disease state, donor, and harvest site (Smith, 2011). Meanwhile, simpler 2D monolayer studies of FLS from our laboratory (Estell et al., 2017; Silverstein et al., 2017) and others (Blewis et al., 2010b; Sun et al., 2003; Utomo et al., 2016), as well as those of 3D micropellet synovium culture (Kiener et al., 2010), are valuable tools for studying the biological changes to synovium cell secretion profiles. However, the former lacks normal tissue structure and organization, and the latter is a spherical microtissue rather than sheet-like membrane necessary for bulk characterization of composition, solute transport, and lubrication.

Our laboratory has extensive experience evaluating the response of engineered and explanted cartilage to pro-inflammatory cytokine (i.e. IL-1) and anti-inflammatory drug (i.e. DEX) stimulation (Bian et al., 2010; Lima et al., 2008b). Intra-articular DEX injections have been used for decades to treat joint inflammation and pain (Cederlöf and Jonson, 1966; Grodzinsky et al.,

2017; Heard et al., 2015; Lu et al., 2011; Sherman et al., 2015), however evidence for their use remains inconclusive (American Academy of Orthopaedic Surgeons Board of Directors, 2013). In addition to the role that the synovium likely plays in drug clearance, these glucocorticoids are known to have a significant anti-inflammatory effect and modulate cell biosynthesis in the joint (Lu et al., 2011; Roach et al., 2016a), likely playing a role on FLS and local immune cells as well (Reyes et al., 2008). In better understanding synovium structure-function, especially in the context of current pharmaceutical treatments, researchers may be able to better predict and influence outcomes, perhaps by developing targeted synovium therapies (Jérémie Sellam and Berenbaum, 2010; Sutton et al., 2009).

To this end, these studies aim to build on this knowledge to develop complementary engineered and explanted synovium models to investigate how IL-1 and DEX alter synovium structure-function **(Chapter 2)**. The approach of using a surrogate synovium model is attractive in that quantitative transport and lubrication measurements and other high throughput *in vitro* mechanistic studies can be performed on tissues that are fabricated from cells derived from small clinical biopsies and blood (Bondeson et al., 2010). Development of *in vitro* human models will be especially valuable due to limitations with translatability in animal systems (Bendele, 2001). It also facilitates isolating effects of certain cell types (i.e. FLS vs. MLS or T Lymphocytes) or starting composition (i.e. intima vs. sub-intima or fibrous vs. fatty) that are found in explant specimens. Building on a previous microtissue approach that demonstrates the unique ability of FLS to reconstitute many of the structural aspects of synovium (Kiener et al., 2006), *we hypothesized that an engineered synovial membrane can recreate structure-function of native tissue. Further, cytokine- or glucocorticoid-induced changes to solute transport and lubrication properties can be related to changes in architecture and composition.*

Specific Aim 1e: To develop a sustained, low-dose, intra-articular DEX delivery platform, consisting of PLGA microspheres embedded within an acellular agarose implant, for improving joint repair.

Specific Aim 1f: To evaluate the acellular DEX implant from SA1d in an adult canine preclinical model of osteochondral autograft transfer (OAT). Determine impact on cartilage repair tissue and synovium.

Data from animal studies and early clinical trials suggest that early inhibition of the intra-articular inflammatory response post-traumatic injury of the knee may improve clinical outcomes (Olson et al., 2014). However, intra-articular glucocorticoid injection doses are necessarily high due to the high clearance rate of the steroid from the joint space (Armstrong et al., 1981; Habib, 2009). Repeated high-dose injections (Backes et al., 2013; Ikeuchi et al., 2014) have been associated with adverse effects on growth of articular and growth plate chondrocytes (Chrysis et al., 2003; Dragoo et al., 2012), synoviocytes (Sherman et al., 2015), and osteoblasts (Allen, 1996). Meanwhile, comparatively low doses of DEX serve as a critical pro-anabolic and anti-catabolic factor in chondrogenic cultures (Florine et al., 2013; Lima et al., 2007; Lu et al., 2011). An optimal delivery system for sustained low (therapeutic) dose of DEX to the synovial joint is not currently available for clinical use in cartilage restoration (Bajpayee et al., 2017). To this end, an intra-articular extended-release delivery system was developed and evaluated in a preclinical model of cartilage repair **(Chapter 3)**. Motivated by the synovium response to DEX elucidated by SA1a-d, *we hypothesized that sustained low-dose DEX delivery would support repair outcomes via dual pro-anabolic and anti-catabolic effect on cartilage and synovium.*

<u>Global Hypothesis (Part II)</u>: Electrical stimulation supports joint health and repair via anti-catabolic, pro-anabolic, and galvanotactic effects on synovium and cartilage.

<u>Specific Aim 2a:</u> To characterize the response of healthy and OA synovial explants to pulsed electromagnetic fields (PEMFs) in baseline, IL-1, and DEX-treated conditions.

Aside from clinical evidence indicating a modulatory effect on pain (Betti et al., 1999; Zorzi et al., 2007), little is known about how PEMF may alter the behavior of synovial tissue. Recently, much work has been done to characterize a potential anti-inflammatory effect of PEMF on isolated bovine and human OA FLS via the adenosine receptor complex (De Mattei et al., 2009; Ongaro et al., 2012; Varani et al., 2008). However the distribution and quantity of FLS, MLS, and non-resident immune cells in the synovium changes dramatically based on stage of OA and donor (O'Brien et al., 2017; Utomo et al., 2016), potentially creating a more complex response to PEMF. Studies have evaluated the response of macrophage cell lines to PEMF, showing variable effects on inflammatory mediators (Akan et al., 2010; Kawczyk-Krupka et al., 2002; Ross and Harrison, 2013). Moreover, cellular response is likely to be affected by cell-cell and cell-matrix interactions only present in native tissues. Motivated by results from studies in SA1a-d that showed IL, DEX, and OA-induced fluidity in cell phenotype, these studies aim to evaluate how chemical environment and disease state affect response to PEMF **(Chapter 4)**. Specifically, *we hypothesized that PEMFs would decrease markers of inflammation in healthy bovine tissues and have an inconsistent effect on human OA tissues. Further, we hypothesized that the effect of PEMF would be altered by concurrent chemical treatment.*

Specific Aim 2b: To develop an optimal PEMF dosing strategy for improving joint repair.
Specific Aim 2c: To evaluate the PEMF strategy in an adult canine preclinical model of engineered osteochondral repair. Determine impact on cartilage repair tissue and synovium.

Clinical studies of PEMFs have shown improvements in function following microfracture, matrix-assisted chondrocyte implantation (MACI®), bone marrow-derived stem cell transplantation, and osteochondral allograft (OCA) (Cadossi et al., 2014; Collarile et al., 2018; Iwasa and Reddi, 2018). However, while these initial studies were promising, PEMFs have remained controversial for cartilage repair due to inconclusive clinical evidence of robust efficacy and few mechanistic studies on the matter (Bjordal et al., 2007; Gobbi et al., 2014). We suspect that the conflicting data may stem from differences in methods and strengths/duty cycle of applied electric fields, anatomic geometry, repair type, and contributions from surrounding tissues. Informed by response of synovial tissue elucidated in SA2a and optimization of cartilage behavior in SA2b, these studies aim to provide a comprehensive analysis of clinical outcomes in conjunction with tissue level analyses of cartilage and synovium **(Chapter 5)**. As engineered cartilage is especially susceptible to impacts from sub-optimal implantation properties and pro-inflammatory cytokines (Djouad et al., 2009; Hunter and Levenston, 2004; Obradovic et al., 2001b; Spalazzi et al., 2008), *we hypothesized that a standardized and optimized PEMF strategy would serve a dual role of stimulating cartilage anabolism and suppressing synovial inflammation following joint repair.*

Specific Aim 2d: To investigate direct current electrical field (DC EF)-induced migration of adherent synovial immune cell populations.
Specific Aim 2e: To evaluate DC EF-induced migration of FLS within a collagen hydrogel matrix.

Specific Aim 2f: To design, build, and validate a bioreactor capable of applying DC EFs to three-dimensional tissue specimens. Evaluate migration of synovial repair cells within a model cartilage defect.

FLS, which are sometimes referred to as synovium-derived stem cells (SDSCs), can be differentiated to make cartilage *in vitro*, making them an attractive target cell source for cartilage repair strategies (Bilgen et al., 2007; Rui et al., 2010; Sampat et al., 2011a). FLS are recruited to the site of partial thickness defects *in vivo*, however the efficiency of their migration into the wound site is generally insufficient for effective healing (Hunziker and Rosenberg, 1996). Meanwhile, proliferation of resident MLS and infiltration of peripheral blood mononuclear cells (PBMCs) contribute to the pro-inflammatory environment and further joint degeneration (O'Brien et al., 2017; Utomo et al., 2016).

DC EFs may allow the selective homing of repair cells and exclusion of immune cells. Our laboratory has shown that in 2D culture, both chondrocytes and FLS exhibit preferential cathodal or anodal migration, dependent on passage number (Chao et al., 2000; Finkelstein et al., 2007; Tan et al., 2011). Meanwhile, evidence suggests that macrophages preferentially migrate towards the anode (Orida and Feldman, 1982). Divergent galvanotactic behavior of fibroblasts and macrophages has been alluded to more recently as well (Douglas et al., 2019). However, galvanotaxis of FLS and MLS (or adherent PBMCs) has not been explored in a 3D repair model, either as a method to increase homing of FLS repair cells or to exclude inflammatory cells. Such an *in vitro* model will be crucial in translating culture findings to a preclinical system that will ostensibly require implanted electrodes. To this end, these studies aim to investigate galvanotaxis of adherent PBMCs and develop new methods to evaluate galvanotactic behavior in three-dimensional biomimetic tissue specimens **(Chapter 6)**. *We hypothesized that adherent PBMCs*

and FLS exposed to DC EFs, in 2D and 3D, respectively, would exhibit directed migration. Furthermore, development of new bioreactor approaches would facilitate application of DC EFs to three-dimensional synovium and cartilage specimens in biomimetic configurations.

1.2 Significance

OA is a degenerative condition that affects an estimated 250 million people worldwide, representing an enormous economic and psychosocial burden for patients and their families (Hunter and Bierma-Zeinstra, 2019). While classically attributed to 'wear and tear' of the articular cartilage, there is a growing appreciation that OA is a whole-joint disease with complex etiology involving the synovium and surrounding tissues (Bhattaram and Chandrasekharan, 2016; Loeser et al., 2012; Scanzello and Goldring, 2012a). Pathologic changes to the synovium architecture and composition often precede the presence of cartilage damage (Hügle and Geurts, 2017), suggesting a potentially critical role in early disease pathogenesis. And while synovitis is a key feature of both rheumatoid arthritis (RA) and OA, clinical reports have described OA synovium as distinct in its cellular and structural composition, molecular secretion, and chronic onset (Bondeson, 2015; Furuzawa-Carballeda et al., 2008; Hitchon and El-Gabalawy, 2011; Penatti et al., 2017; Jeremie Sellam and Berenbaum, 2010; Sutton et al., 2009; Wenham and Conaghan, 2010).

A better understanding of synovium transport and response to DEX may facilitate development of improved treatment strategies aimed at modulating synovium behavior and improving drug residence time. Furthermore, development of more effective pain treatments may help to mitigate the spread of opioid abuse (Goesling et al., 2016). In addition to drug clearance, the filtration and secretion function of the synovium defines the synovial fluid composition of lubricants, such as hyaluronan (HA). HA in healthy joints has an extremely large average

molecular weight (MW) (1-6 MDa), which has shown anti-inflammatory (Cooper et al., 2008; Lee and Cowman, 1994), chondroprotective (Bauer et al., 2016), and lubricating (Blewis et al., 2010a) properties. HA is degraded in OA and these smaller fragments (e.g. <200kDa) promote a pro-inflammatory phenotype (McKee et al., 1996) and reduce synovial fluid viscosity thereby increasing joint friction and tissue wear (Fam et al., 2009).

While many OA cases are considered idiopathic, a large number arise secondary to a traumatic event. It has been reported that approximately 60% of knee arthroscopies find chondral lesions, 67% of which can be categorized as focal defects (Widuchowski et al., 2007). Improving cartilage repair and restoration surgeries via modulation of synovium structure-function may reduce rehabilitation times, costs, and the demand for total joint arthroplasty (TJA), as well as facilitate the adoption of engineered cartilage technologies. Electrotherapeutics hold potential as low-cost, low-risk, non-invasive adjunctive therapies for improving cartilage repair. Low intensity PEMFs have been shown to reduce joint inflammation and pain (Betti et al., 1999; Zorzi et al., 2007) and are clinically-approved for treatment of arthritis (De Mattei et al., 2009; Ongaro et al., 2012; Varani et al., 2008). Alternatively, DC EFs may enable selective homing of target cells to defect sites, thus augmenting natural repair processes (Katagiri et al., 2017).

In understanding the complex interactions as well as individual cellular, biochemical, and functional changes that arise in OA synovium and cartilage, researchers may be able to better predict and influence outcomes (Attur et al., 2010; Scanzello and Goldring, 2012b). We believe that it is this lack of knowledge that contributes to the conflicting and inconclusive results of many current OA therapies, including glucocorticoid injections and electrotherapeutics (American Academy of Orthopaedic Surgeons Board of Directors, 2013). To this end, studies presented in **Part I** of this dissertation established an engineered synovial membrane that shares key

compositional, structural, and functional properties of native tissue in both IL-1 and DEX-treated culture conditions **(Chapter 2)**. We then elucidated the impact of sustained low-dose DEX on synovium and cartilage in a preclinical OAT repair model **(Chapter 3)**.

In **Part II**, investigation of the synovium was expanded to investigate the response to non-invasive electrical stimulation modalities. We first determined the biological response of healthy or OA synovium explants to PEMF stimulation in both pro-inflammatory and anti-inflammatory culture conditions **(Chapter 4)** and then further evaluated the impact of PEMF on synovium and cartilage in a preclinical engineered cartilage repair model **(Chapter 5)**. Finally, DC EFs were explored as a potential method of stimulating homing of synovial repair cells to a cartilage defect in a 3D culture system **(Chapter 6)**.

1.3 Background

1.3.1 Diarthrodial Joint Structure and Function

1.3.1.1 Normal Synovium

The synovium envelops the diarthrodial joint and plays a key regulatory role in defining the composition of the synovial fluid through bi-directional filtration (Blewis et al., 2010a) as well as biosynthesis of critical boundary lubricants such as lubricin and hyaluronic acid (HA) (Blewis et al., 2010b; Schmidt and Sah, 2007). Characterized by a unique intima/sub-intima architecture, synovium is distinct from other barrier membranes found in the body (Kiener et al., 2010). The synovial intima is composed of a dense collagenous matrix (primarily type I and IV) (Smith, 2011) with cells interspersed, lacking a distinct basement membrane (Barland et al., 1962). The normal intimal lining **(Figure 1.2A)**, which is in direct contact with the synovial fluid, is about 1-4 cells thick and composed of approximately 90% FLS and 10% MLS (Valencia et al., 2004). The sub-

intimal layer of the synovium is ~5 mm thick and relatively acellular and heterogeneous. In addition to a sparse population of FLS and MLS, the tissue is highly vascularized with nerves in close proximity to the vessels (Haywood and Walsh, 2001; Levick and McDonald, 1995; Price et al., 1996; Smith, 2011). Depending on the depth and joint location, extracellular matrix (ECM) consists of a mixture of fibrous and collagenous (type I, III, IV, V and VI) dense connective tissue regions and adipose.

FLS are key contributors to the articular cartilage niche, contributing molecules important for lubrication, ECM turnover, and inflammation (Kiener et al., 2010). In addition to expressing common MSC markers (Alegre-Aguarón et al., 2014), these cells can also be identified the surface expression of decay accelerating factor (CD55), vascular cell adhesion molecule-1 (VCAM-1), and calcium-dependent adhesion molecule-1 (cadherin-11) (Ospelt, 2017). FLS interact with the ECM and the sub-intima through integrins, such as the $\alpha_1\beta_{1,}$ $\alpha_2\beta_1$, $\alpha_4\beta_1$ integrins and intercellular adhesion molecule (ICAM-1) (Agarwal and Brenner, 2006; Bartok and Firestein, 2010; Kiener et al., 2010; Valencia et al., 2004). They have been shown to secrete lubricin and HA, both key components of joint lubrication (Jay, 1992; Jay et al., 2007, 2000a), and respond to and contribute to the secretion of inflammatory cytokines into the synovial fluid (Kiener et al., 2010). MLS also secrete catabolic factors and function to remove waste and pathogens from the joint (Jeremie Sellam and Berenbaum, 2010). MLS are identifiable by positive expression of CD11b, CD14, CD45, CD68 and CD163 (Bartok and Firestein, 2010; Edwards, 1982).

The synovium is convoluted and known to come into contact with large portion of the articular surfaces (Palmer, 1967), ostensibly undergoing both fluid and tissue shear loading during normal daily activities. Synovial cells are highly responsive to shear loading, which is in part mediated by viscous HA in synovial fluid (Estell et al., 2017). In healthy joints, the MW of HA is

very large (1-6 MDa) and has anti-inflammatory (Cooper et al., 2008; Lee and Cowman, 1994), chondroprotective (Bauer et al., 2016), and lubricating (Blewis et al., 2010a) properties. The clearance of large molecules (i.e. HA and lubricin) from the joint is approximately one half every 38 hours (Levick, J. R., et al., 1999). Water and smaller proteins (i.e. cytokines) in the synovial fluid are replaced about every two hours (Levick, J. R., et al., 1999). This leads to small molecules (MW<10kDa) quickly reaching equilibrium in plasma and synovial fluid (Gerwin et al., 2006).

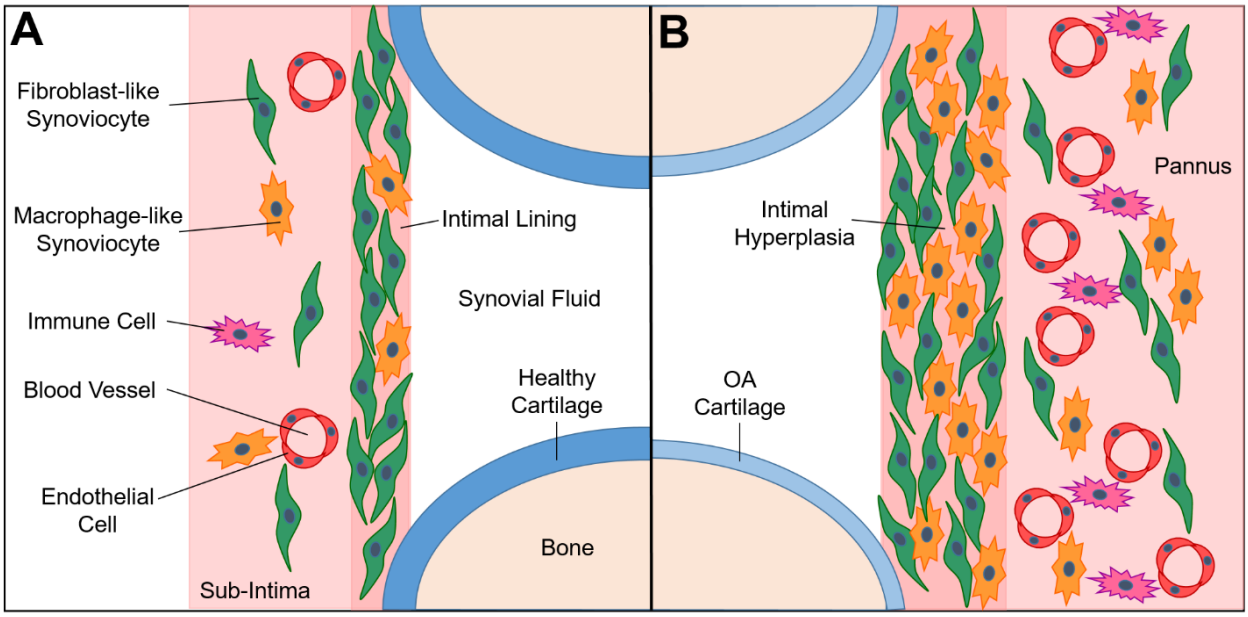

Figure 1.2 Relevant synovium anatomy. **(A)** Normal synovium is comprised of ~90% FLS and ~10% MLS. **(B)** OA synovium composition and structure changes dramatically, coinciding with altered secretion of lubricants and inflammatory mediators.

1.3.1.2 OA Synovium

The OA synovium thickens into a pannus-like structure with an increase in intimal cellularity (hyperplasia), fibrosis, vascularity, and innervation **(Figure 1.2B)** (Mathiessen and Conaghan, 2017; Shibakawa et al., 2003; Wenham and Conaghan, 2010; Yuan et al., 2004). The hyperplastic response includes a drastically changing distribution and quantity of tissue-resident FLS and MLS,

depending on the stage of OA (O'Brien et al., 2017; Utomo et al., 2016). There is a concurrent infiltration of macrophages, lymphocytes, and other immune cells from the vasculature and secretion of pro-inflammatory cytokines, all of which are thought to contribute to the progression of joint degeneration (Blewis et al., 2010b; Kiener et al., 2006; Scanzello and Goldring, 2012a; Sutton et al., 2009). Infiltrating mononuclear cells are predominately $CD14^+$ monocytes/macrophages and $CD4^+$ T lymphocytes (Moradi et al., 2015), estimated in one study to represent ~65% and 22% of the immune cells in the OA synovium, respectively (Pessler et al., 2008). Meanwhile, other studies have found negligible quantities of T lymphocytes in OA synovium (Bondeson et al., 2010).

Synovial inflammation is a key feature of OA, although distinct from that of rheumatoid arthritis RA (Ene et al., 2015; Hitchon and El-Gabalawy, 2011; Pelletier et al., 2001). Synovitis can be detected through imaging modalities such as MRI and ultrasound as the patients also have greater amount of synovial fluid volume with a total increase in lubricant content (although lower total concentration) (Blewis et al., 2010a; Mathiessen and Conaghan, 2017; Jeremie Sellam and Berenbaum, 2010). Normally large HA chains are degraded and these fragments promote a pro-inflammatory phenotype (McKee et al., 1996) and reduced synovial fluid viscosity that increases joint friction and tissue wear (Fam et al., 2009). Additionally, decreased HA chain length exacerbates lubricant loss from the joint (Sabaratnam S. et al., 2005). Similar loss of lubricants has been observed following ACL injury, implicating this mechanism in secondary OA as well as primary (Elsaid et al., 2008).

1.3.1.3 Articular Cartilage and Repair Strategies

Articular cartilage is a dense white connective tissue that covers our mobile joints and provides load-bearing support and lubrication (Lai et al., 1991). It has a highly specialized and organized structure, consisting of the superficial zone, middle zone, deep zone, and calcified zone (Carballo et al., 2017). The composition of each zone varies, however the primary ECM components are collagen (75% of tissue dry weight) and proteoglycan (20-30% of tissue dry weight) (Brocklehurst et al., 1984). The biomechanical behavior of articular cartilage is typically modeled as a biphasic mixture containing a liquid (80% of tissue wet weight) and a solid phase composed of porous matrix (Ateshian et al., 1997). It is the interaction of these phases that give cartilage its high compressive strength, mainly through fluid pressurization via charged proteoglycan molecules.

The avascular nature of articular cartilage and dense extracellular matrix confer a poor healing capacity whereby localized regions of tissue damage can lead to joint degeneration and OA (Hehenberger et al., 1998; Kloth, 2005). Cartilage repair and restoration surgeries, such as microfracture, OAT, OCA, and cell-culture techniques (e.g. autologous chondrocyte implantation; ACI) are each limited by a number of factors, including availability of graft tissue, donor site morbidity, and difficulty in matching size and surface contours (Andrade et al., 2016; Bugbee et al., 2016; Nover et al., 2015; Shimozono et al., 2019). In attempts to overcome some of these issues, a number of engineered cartilage technologies (e.g. MACI) are progressing through the clinical pipeline (Iwasa et al., 2009; Pietschmann et al., 2009).

The effectiveness and longevity of cartilage restoration treatments can also be limited by the impact of proinflammatory cytokines on graft incorporation and integrity (Djouad et al., 2009; Hunter and Levenston, 2004; Obradovic et al., 2001b; Spalazzi et al., 2008). Synovial fluid from injured knees is known to negatively affect chondrogenesis (Yang et al., 2006), with interleukins

specifically linked to adverse integrative repair (Wilusz et al., 2008). Iatrogenic cartilage injury can further hamper outcomes; chondrocyte death can occur due to osmolarity differences in saline, contact with blood, or drying during open procedures (Amin et al., 2017; Hooiveld et al., 2003; Sgaglione and Kerker, 2008). Furthermore, cartilage grafts often suffer from reduced viability and metabolic activity caused by extended preservation (Nover et al., 2015) or method of graft harvest and delivery (Sgaglione and Kerker, 2008).

1.3.2 Osteoarthritis and Joint Repair Models

1.3.2.1 Synovium-Based Models

A number of models exist with which to study aspects of synovium structure-function, each with inherent strengths and limitations **(Table 1.1)**. *In vivo* studies utilizing tracer molecules have offered important insights on solute transport across the synovium, but provide a challenge in resolving mechanisms below the whole-joint level (Levick, J. R., et al., 1999; Levick and McDonald, 1995, 1989) due to the inherent confounding variables of the *in vivo* environment including ill-defined boundary conditions arising from vasculature throughout the sub-intima (Bhattaram and Chandrasekharan, 2016). Studying the response of synovial explants to pro-inflammatory stimuli is a complex task due to stark differences in cell and matrix content due to disease state, donor, and harvest site (Smith, 2011). The few studies that have cultured synovium explants have focused mainly on biochemical response to cytokine treatment (Fichadiya et al., 2016; Labens et al., 2013). Human synovial explants treated with IL-1β or tumor necrosis factor-α (TNFα) were shown to secrete increased concentration of inflammatory mediators such as prostaglandin-E2 (PGE2) (Hardy et al., 2002), IL-6, and IL-8 (Beekhuizen et al., 2011).

In an effort to work with a simpler and more reproducible system, some have opted to model synovium as a confluent FLS monolayer. This focus is facilitated by high proliferation in 2D monolayers, whereby FLS exclude both the MLS and contaminating blood cells at early passage (Kiener et al., 2006). In response to IL-1β and TNFα, human OA FLS rapidly proliferate and secrete increased concentrations of lubricant molecules (e.g. HA and lubricin), cytokines, nitric oxide (NO), PGE2, and matrix metalloproteinases (MMPs) (Blewis et al., 2010a, 2010b; Furuzawa-Carballeda et al., 2008; Gitter et al., 1989; Hamilton et al., 1994; Pulkki, 1986). Similar synovium-like monolayers have been cultured on various substrates, including filter membranes (Blasioli et al., 2014; Blewis et al., 2010a), temperature responsive dishes (Mitani et al., 2014), and suspension (Warnock et al., 2014, 2013). Systems consisting of filter membranes enable functional transport measurements (Blewis et al., 2010a) and the dual compartments of Transwells® are especially useful for co-culture with cells or tissues such as macrophages (Blasioli et al., 2014; Peck et al., 2018) or cartilage (Peck et al., 2018; Pretzel et al., 2009). However, simple cell layers lack the dense ECM and three-dimensional architecture of the intima and sub-intima that play an integral role in the function of native tissue.

Some have described engineered models of synovium, each demonstrating varying levels of complexity to closer resemble native tissue while avoiding the pitfalls of explant tissue. One research group created an engineered model of RA synovium consisting of 25 µl microtissues seeded with 5.0×10^6 FLS per ml. These tissues demonstrated an ability to reorganize into the intimal lining architecture, secrete lubricin, support macrophage survival, and create a hyperplastic tissue in response to TNFα exposure (Kiener et al., 2010, 2006; Kiener and Brenner, 2005; Valencia et al., 2004). Yet despite reproducing synovial cell behavior in this engineered synovium model, the constructs lacked proper explant controls, were too small for direct protein

measurements, and not in a biomimetic membrane configuration necessary for bulk functional measures.

Table 1.1 Comparison of *in vitro* synovium models.

	Cell Monolayer (Blewis et al., 2010a)	**TE RA Micropellet** (Kiener et al., 2010)	**Native Explants** (Swärd et al., 2017; van Buul et al., 2012)	**TE Synovial Membrane** (Stefani et al., 2018)
Gross Morphology	X	X	✓	✓
Structural organization	X	✓	✓	✓
ECM content	X	✓	✓	✓
Cell content	X	✓	✓	✓
Molecular secretion	✓	✓	✓	✓
Solute transport measurements	✓	X	✓/X	✓
Friction and lubricant measurements	✓	X	✓/X	✓
Defined geometry and initial content	✓	✓	X	✓
Clinical specimen availability	✓	✓	X	✓
High throughput mechanistic studies	✓	✓	X	✓

1.3.2.2 Cartilage-Based Models

IL-1 and DEX stimulation of engineered and explanted cartilage tissues have been widely used to model the OA and post-injury joint environment (Lima et al., 2008c; Andrea R Tan et al., 2015). Behavior of engineered adult cartilage has been validated against explanted tissues (Lima et al., 2008c; Ng et al., 2010). Engineered tissues are useful for *in vitro* modeling due to their consistent geometry, composition, and growth, which allow for reliable mechanical and biochemical

assessments with higher sample size.

There is currently a limited understanding of the inter-relationship between the synovium (including FLS and MLS) and cartilage explants in OA, particularly in the presence of inflammatory mediators. Co-culture of bovine, canine, or human cartilage and synovium explants from healthy and OA donors exposed to injurious compression or cytokine insult (IL-1 or TNFα) resulted in increased tissue degradation (decreased collagen and proteoglycan content) and increased levels of inflammatory mediators such as MMPs, NO and PGE2 (Beekhuizen et al., 2011; Cook et al., 2007; Hardy et al., 2002; Lee et al., 2009; Swärd et al., 2017; van Buul et al., 2012). Similarly, co-culture of OA synoviocytes with alginate encapsulated OA chondrocytes resulted in decreased proteoglycan synthesis and increased PGE2 expression, an effect that was only further magnified by treatment with IL-1β (Huch et al., 2001). However, co-culturing injured cartilage with healthy FLS had a protective effect on cartilage (Lee et al., 2013). Overall, many co-culture studies only looked at the effects of co-culture on cartilage tissue, generally ignoring reciprocal changes to the synovium (Cook et al., 2007; Patwari et al., 2009).

1.3.3 Dexamethasone

1.3.3.1 Clinical Use

Intra-articular glucocorticoid injections have been used for decades to treat joint inflammation and pain (Cederlöf and Jonson, 1966; Grodzinsky et al., 2017; Heard et al., 2015; Lu et al., 2011; Sherman et al., 2015). However, injection doses are necessarily high (4 mg per knee) due to the high clearance rate of the steroid from the joint space, where serum levels can peak within hours to a couple of days after administration (Armstrong et al., 1981; Habib, 2009). Repeated high-dose injections (Backes et al., 2013; Ikeuchi et al., 2014) have been associated with adverse effects on

growth of articular and growth plate chondrocytes (Chrysis et al., 2003; Dragoo et al., 2012), synoviocytes (Sherman et al., 2015), and osteoblasts (Allen, 1996). Impairment of healing or infections can be other undesired side effects of glucocorticoids (Sherman et al., 2015). These side effects, as well as risks of systemic absorption, typically limit patients to 2-4 injections per year (Armstrong et al., 1981; Berthelot et al., 2013; Habib, 2009; McAlindon et al., 2017; Neustadt, 2006; Younes et al., 2007). As a result, current guidance does not recommend for or against the use of intraarticular glucocorticoids (American Academy of Orthopaedic Surgeons Board of Directors, 2013).

To provide extended low-dose glucocorticoid delivery, an intra-articular microsphere injection of triamcinolone acetonide (TA) has recently been approved by the FDA. In advanced OA patients, these TA-MS injections provided better pain relief and longer joint residence time than bolus TA injection (Bodick et al., 2015; Kraus et al., 2018; Spitzer et al., 2019). However, TA-loaded MS did not affect cartilage pathology in this clinical trial (Spitzer et al., 2019) or an *in vivo* rat model of OA (Rudnik-Jansen et al., 2017). The product was not evaluated for cartilage repair.

1.3.3.2 *In Vitro* Use

DEX, a synthetic glucocorticoid, is a common media supplement for chondrogenic and osteogenic cultures. Used at relatively low doses (100 nM), it stimulates anabolism in immature tissues and contributes to maintenance of mature tissues *in vitro* (Bian et al., 2010; Lima et al., 2008c, 2007). Lu and co-workers have reported that DEX concentrations as low as 1 nM were sufficient to protect cartilage explants against TNF-α, and concentrations of 100 nM to 10 μM enhanced cartilage explant sulfate incorporation and suppressed GAG loss to the media (Lu et al., 2011). It has also

been reported to inhibit collagen degradation of cartilage explants in response to IL-1 and plasminogen (Saito et al., 1999). Although typically administered via bolus dose, it has been demonstrated that *in vitro* sustained DEX release from poly(lactic-co-glycolic acid) (PLGA) microspheres (MS) promotes development of functional engineered cartilage and confers protection from pro-inflammatory cytokine-induced tissue degradation (Roach et al., 2016b).

1.3.4 Electrotherapeutics

1.3.4.1 Pulsed Electromagnetic Fields

Historically, PEMFs have been used in a clinical setting to treat delayed unions of bone fractures (Becker et al., 1977). Low intensity PEMFs have also been used to reduce joint inflammation and pain (Betti et al., 1999; Zorzi et al., 2007) and is clinically-approved for treatment of arthritis (De Mattei et al., 2009; Gobbi et al., 2014; Ongaro et al., 2012; Ryang We et al., 2013; Trock et al., 1993; Varani et al., 2008). More recently, PEMFs were shown to improve function following microfracture, MACI, bone marrow-derived cell transplantation, and OCA (Cadossi et al., 2014; Collarile et al., 2018; Iwasa and Reddi, 2018). However, while these initial clinical studies were promising, PEMFs have remained controversial for arthritis and cartilage repair due to limited clinical evidence of robust efficacy and few mechanistic studies on the matter (American Academy of Orthopaedic Surgeons Board of Directors, 2013; Bjordal et al., 2007; Gobbi et al., 2014).

Controlled laboratory experiments have suggested several potential mechanisms of action. *In vitro* studies have established PEMFs as a modulator of inflammatory signaling in isolated chondrocytes and FLS (De Mattei et al., 2009; Vincenzi et al., 2013). Specifically, it has been shown that PEMF may attenuate inflammation through the adenosine pathway (De Mattei et al., 2009; Ongaro et al., 2012; Varani et al., 2008). PEMFs have also been shown to increase

chondrocyte proliferation and matrix production (Mattei et al., 2001; Ongaro et al., 2011) as well as chondro-differentiation of MSCs (Esposito et al., 2013). Enhanced proteoglycan synthesis was also observed in bovine and human OA cartilage explants (De Mattei et al., 2007; Ongaro et al., 2011). Nevertheless, *in vivo* studies have struggled to reproduce positive culture results in synovium and cartilage. In autologous cartilage repair in sheep, enhancement of subchondral bone integration was observed, however cartilage and synovium were not significantly affected (Benazzo et al., 2008).

1.3.4.2 Direct Current Electrical Fields

Endogenously generated EF gradients are known to guide cell migration in developing embryos (Robinson, 1985). Analogous to their role in development, both pulsed and continuous DC EF gradients of 1-10 V/cm guide cell migration in regeneration following connective tissue injuries in adult animals (Baker et al., 1974; Lippiello et al., 1990; Nessler and Mass, 1987; Soong et al., 1990). Pulsed DC EFs have been used therapeutically in humans (Kloth, 2005), especially for promoting healing of non-joining bone fractures and dermatological wounds, including diabetic or pressure-induced ulcers (Braddock et al., 1999). The use of DC EFs of strengths ranging from 0.1-10 V/cm is known to induce directed movement (galvanotaxis) and shape change (galvanotropism) in a number of musculoskeletal cells *in vitro*, such as chondrocytes, ligament fibroblasts, meniscal fibrochondrocytes, and FLS **(Table 1.2)** (Chao et al., 2007, 2000; Finkelstein et al., 2007; Gunja et al., 2011; Tan et al., 2011). Exposed to a DC EF of 6 V/cm, FLS exhibited anodal migration at P1 and cathodal migration at P4 and directed velocity of up to 5 μm/hr (A. R. Tan et al., 2015a).

The translation of these findings to biomimetic and/or 3D configuration is unclear, however, as these and other studies have been performed primarily in 2D or modified 2D culture

systems. Most 2D galvanotaxis systems have the advantage of simple and repeatable measurements that also allow real-time microscopic analysis (Chao et al., 2007, 2000; O'Connell et al., 2015; Tan et al., 2011). Cell phenotype and behavior is known to change drastically based on substrate and 3D environment (Sun et al., 2006). In order to better model how cells might migrate *in vivo*, others have created pseudo-3D culture systems capable of applying pulsed and continuous DC EFs to cells (Sun et al., 2004; Wu et al., 2014; Yuan et al., 2014; Zhao et al., 1996). These set-ups are typically unable to accommodate irregularly sized explants and/or TE constructs, instead examining single cells on an acellular substrate.

Table 1.2 Summary of *in vitro* galvanotaxis studies.

System/Substrate	Cell Type	E-Field, media	Directed Velocity	Direction	References
2D Glass Slide	Chondrocytes	6 V/cm DC, 5% FBS	6.21 µm/hr	Cathode (P2) or anode (P4)	(O'Connell et al., 2015)
2D Glass Slide	Chondrocytes	10 V/cm DC, 5% FBS	17.59 µm/hr	Cathode (P1)	(Chao et al., 2000)
2D Glass Slide	Synovial Fibroblasts	6 V/cm DC, 5% FBS	~5 µm/hr	Anode (P1) or Cathode (P4)	(A. R. Tan et al., 2015b)
3D Confluent Cell Sheets	Epithelial cells	1.5 V/cm DC, 10% FBS	~15 µm/hr	Cathode	(Zhao et al., 1996)
3D Collagen Gel on glass slide	Fibrosarcoma HT1080	0.1 V/cm DC, 10% FBS	13.74 µm/hr	Perpendicular to EF	(Sun et al., 2004)
3D Fibrin Matrix on TC dish	MSCs and HUVECs	3 V/cm pulsed (2ms and 1 Hz), 10% FBS	~8 µm/hr	Perpendicular to EF	(Yuan et al., 2014)

Part I

Dexamethasone as a Catabolic and Anabolic Mediator in Synovium and Cartilage

Chapter 2

Explanted and Engineered Synovium: Complementary Approaches to Evaluate Structure-Function in Response to Chemical Stimuli

2.1 Introduction

In both OA and acute joint injury, architectural and compositional changes to the synovial membrane affect secretion, lubrication, and transport behavior in the synovium, contributing to an altered joint homeostatic environment (Elsaid et al., 2008; Mwangi et al., 2018; Smith, 2011). Yet, despite the appreciation for the role that the synovium plays in cartilage and joint health, quantitative structure-function data for this tissue remain incomplete. We anticipate that through development of a functional tissue engineered synovium model, limitations of explant culture systems can be overcome while also avoiding the pitfalls of simpler monolayer culture systems **(Table 1.1)**. Our laboratory has extensive experience evaluating the response of engineered and explanted cartilage to pro-inflammatory cytokine (i.e. IL-1) and anti-inflammatory drug (i.e. DEX) stimulation (Bian et al., 2010; Lima et al., 2008b). DEX, a glucocorticoid, is widely used in joint applications, both clinically and in culture **(1.3.3)**, however it is unclear how it affects synovium behavior.

To this end, we aimed to build on this knowledge by developing complementary engineered and explanted synovium models to investigate how these chemical stimuli alter

synovium structure-function. Here, we modified an existing Matrigel-based micropellet approach, where FLS-only constructs were able to reorganize in an intimal lining architecture that became hyperplastic in the presence of TNFα, secrete lubricin, and support blood monocyte survival (Kiener et al., 2010, 2006; Kiener and Brenner, 2005; Valencia et al., 2004). Matrigel shares many ECM constituents of native synovium and supports synovial cell assays for studying pro-inflammatory cytokine effects on proliferation and cell infiltration (Kiener et al., 2010; Kiener and Brenner, 2005; Lee et al., 2007; Valencia et al., 2004). Building on this approach, *we hypothesized that an engineered synovial membrane can recreate structure-function of native tissue. Further, cytokine- or glucocorticoid-induced changes to solute transport and lubrication properties can be related to changes in architecture and composition.*

To this end, we first describe the development of a juvenile bovine FLS-based engineered synovium, cultured as a flat, disk-shaped membrane in a Transwell insert (SA1a). Second, the fully formed engineered synovium was subjected to IL-1 and DEX treatment, and changes to structure-function were compared to explant tissue (SA1b). The bovine model was then expanded to include labeled MLS in order to track cell response (SA1c). Finally, engineered synovium was prepared using passaged human FLS and co-cultured with human T lymphocytes in IL-1 and DEX treated conditions (SA1d).

2.2 Bovine FLS-based Engineered Synovium Responds Similarly to Interleukin-1 and Dexamethasone as Explants in Culture

2.2.1 Introduction

In this section, studies are described to characterize and validate the FLS-based engineered synovium in baseline as well as IL-1 and DEX-treated conditions (SA1a-b). A basic science bovine system was selected for development and validation due to the robust and consistent growth

exhibited by engineered constructs and ease of procurement of synovial explants, which facilitated model validation by comparing engineered and native tissues. Engineered constructs were prepared by encapsulating FLS in Matrigel (Kiener and Brenner, 2005; Lee et al., 2007) and allowing gelation directly in a Transwell to create a flat, disk-shaped construct. Constructs were then pre-cultured to allow cellular reorganization into an intimal lining layer with underlying sub-intimal layer. First, key baseline features of native synovium structure-function were assessed. Tissue behavior was then compared in response to IL and DEX stimulation. This included ECM and cell content, and for the first time, quantitative measurements of solute transport and lubrication function.

2.2.2 Materials and Methods

2.2.2.1 Synovium Explant Harvest

Fresh synovial tissue was harvested from discarded (IACUC-exempt) bovine calf knee joints (2-4 weeks old). Explants were collected from the region adjacent to the medial and lateral femoral condyles **(Figure 2.1)**. For subsequent *in vitro* experiments, tissue was pooled from 4 donor animals and diced into consistent ~5 mm × 5 mm pieces. Prior to studies, explants were maintained for up to two weeks in serum-free basal media (BM) consisting of DMEM supplemented with 50 μg/mL L-proline (Cat. No. P5607; Sigma), 100 μg/mL sodium pyruvate (Cat. No. S8636; Sigma), 1% ITS™+ Premix (contains insulin, transferrin, selenous acid, BSA, and linoleic acid; Cat. No. 354352; Corning), 1% antibiotic–antimycotic, and 50 μg/mL ascorbic acid-2-phosphate.

Figure 2.1 Bovine synovium explant harvest. Synovium (arrow) was harvested from the medial and lateral femoral condyles of juvenile bovine knees.

2.2.2.2 Formation of Tissue Engineered Synovium Constructs

Synovium was digested in collagenase type II (Cat. No. LS004177; Worthington Biochemical Corporation) for 2 hours with stirring at 37°C. Digested synovial cells were filtered through a 70 µm porous nylon mesh. Viable cells were counted and plated at a density of 1.76×10^3 cells/cm^2 for expansion. The mixed population of primary synovial cells was expanded for two passages in α-Minimum Essential Medium (αMEM; Cat. No. 12000022; ThermoFisher) containing 10% fetal bovine serum (FBS; Cat. No. S11550; Atlanta Biologicals), 1% antibiotic-antimycotic (Cat. No. 15240062; ThermoFisher), and 5 ng/ml fibroblast growth factor-2 (FGF-2; Cat. No. PHG0264; ThermoFisher) (Alegre-Aguarón et al., 2014; Sampat et al., 2011b; A. R. Tan et al., 2015a). The resulting population of FLS was suspended at 5×10^6 cells/ml in 7 mg/ml Matrigel (Cat. No. 354234; Corning) **(Figure 2.2A)**. For biochemical and histological analyses, constructs were cast in 6.5 mm Transwells with 3 µm polyester filter membranes (Cat. No. 3472; Corning), resulting in disk-shaped specimens attached to the underlying filter (volume = 100 µl, diameter = 6.48 mm, thickness = 3.03 mm). Specimen dimensions were calculated based on gel volume and Transwell

geometry. Transport analyses were conducted using a parallel set of TE specimens cast in a scaled-down (volume = 25 µl, diameter = 4.27 mm, height = 1.70 mm) 4.26 mm Transwell system (Cat. No. 3385; Corning). To induce ECM deposition and the stratified intimal/subintimal organization, constructs were initially cultured in Dulbecco's Modified Eagle's Medium (DMEM; Cat. No. 12100046; ThermoFisher) supplemented with 10% FBS, 1% antibiotic-antimycotic, and 50 µg/ml ascorbic acid-2-phosphate (Cat. No. A8960; Sigma) for 21 days in the upper compartment of the Transwell only **(Figure 2.2B)**. During this period, the basolateral compartment was left empty and media in the luminal compartment was changed three times per week. Luminal media volumes were 100 µl and 300 µl for 4.26 mm and 6.5 mm Transwells, respectively.

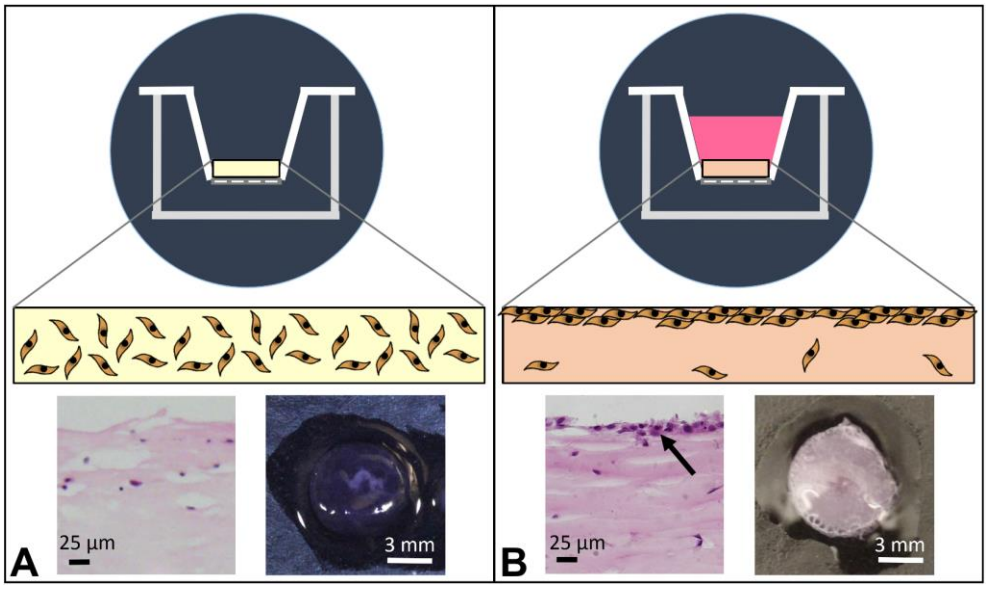

Figure 2.2 Schematic of engineered synovium formation. (A) The construct is initially cast in the luminal compartment of a Transwell insert. Cells are suspended within the Matrigel matrix in a random orientation. Representative day 0 histology (left) and gross morphology (right). (B) During the 21-day pre-culture period, media is only supplemented in the luminal compartment. This induces cellular reorganization into a stratified architecture (intima and sub-intima). Matrix deposition also occurs during this period, resulting in a membranous construct. Representative day 21 histology (left) and gross morphology (right).

2.2.2.3 *In Vitro* Chemical Stimulation

TE constructs and explants (EXP) were individually cultured for two weeks in one of four conditions: serum-free BM (CTL), 100 nM DEX, 10 ng/ml IL-1, or both DEX and IL-1 (ILDEX) (Lima et al., 2008b; Roach et al., 2016a). For TE constructs, media was introduced to both luminal and basolateral compartments, and media was changed three times per week. Basolateral media volumes were 200 µl and 700 µl for 4.26 mm and 6.5 mm Transwells, respectively. Individual EXP specimens were cultured in 1 ml media each, again with media changes three times per week. TE synovium was harvested at day 21 (initial maturity, start of treatment) and day 35 (end of two-week treatment) for biochemical, histological, and transport analyses. Synovium explants were harvested at day 0 (initial harvest, start of treatment) and day 14 (end of two-week treatment).

2.2.2.4 Functional Assessment of Tissue Permeability

Three different solutions were prepared, each containing a different FITC-labeled dextran diluted in PBS (10 kDa, 0.5 mg/ml, Cat. No. D1820; 70 kDa, 0.5 mg/ml, Cat. No. D1822; 500 kDa, 0.2 mg/ml, Cat. No. D7136; ThermoFisher). Small dextrans were selected to resemble the MW of the pro-inflammatory cytokines IL1α (17 kDa) and TNFα (17 kDa), as well as TGFβ3 (27 kDa), MMP-2 (72 kDa), and small MW HA. Lubricin (200-400 kDa) concentrations are 0.3-0.4 mg/ml (Levick, J. R., et al., 1999) and 0.11-0.18 mg/ml (Levick, J. R., et al., 1999) in healthy and OA knees, respectively, whereas HA (27-10,000 kDa) concentrations are on the order of 1-4 mg/ml, depending on disease state (Levick, J. R., et al., 1999).

At time zero, 50 µl of FITC-labeled dextran in PBS solution was added to the upper (luminal) compartment of the Transwell (n=7-8 per media-solute size pairing) **(Figure 2.3C)**. PBS (150 µl) was added below the Transwell (basolateral) and was collected and replenished with fresh

PBS at 0, 1, 2, 4, 8, 24, 48, and 72-hour time points. The basolateral solute concentration was quantified for each time point using a fluorescent plate reader (SpectraFluor Plus, Tecan) at an excitation and emission wavelength of 495 nm and 519 nm, respectively. Clearance, defined as the amount of dextran collected from the basolateral compartment as a function of the starting amount of dextran in the luminal compartment, was plotted as a function of time. Apparent permeability (P_d) was computed as a function of solute flux (J_s), area of the filter (S), and solute concentration difference in the luminal and basolateral compartment (ΔC): $P_d = J_s/(S\Delta C)$ (Garcia et al., 2011; Yuan and Rigor, 2010). For this computation, it was assumed that solute flux was determined entirely by diffusion. In a similar manner, permeability of 70 kDa dextran was assessed in CTL and IL-treated bovine explants (n=3-4) by affixing a piece of tissue to a larger 6.5 mm Transwell using a silicone gasket **(Figure 2.3B, D)**. The DEX group was omitted from explant transport analysis due to sample size limitations related to the large amount of explant tissue required to make these measurements. However, solute transport in native explants was visualized qualitatively using confocal imaging.

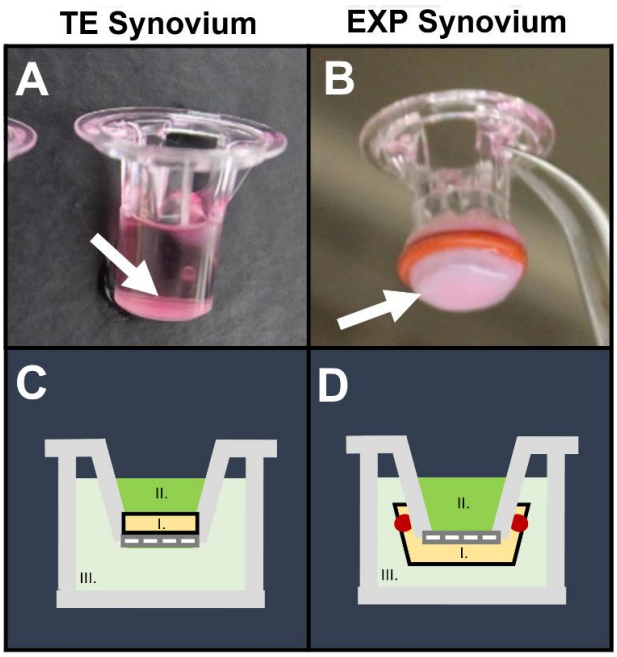

Figure 2.3 Schematic of solute transport studies in TE synovium and explants. **(A)** TE synovium (arrow) was cultured and tested *in situ* on a 4.26 mm Transwell insert. **(B)** Synovium explant (arrow) was secured to the underside of a 6.5 mm Transwell insert using a rubber gasket (red); Change in permeability of FITC-labeled dextran in **(C)** TE and **(D)** explant synovium (I) was assessed using a Transwell system. The dextran suspension (II) was placed in the luminal compartment (i.e. the synovial cavity). PBS (III) was added to the basolateral compartment (i.e. the fibrous capsule and associated vasculature) and sampled at time points to quantify joint clearance.

2.2.2.5 Functional Assessment of Tissue Friction

Baseline minimum friction coefficient of bovine TE and explant synovium (n=3) was determined using a custom loading device, as described in (Estell, 2018). Briefly, a multiaxial load cell made continuous measurements of normal and friction forces during reciprocal sliding of synovium against a glass platen at 1 mm/s with 25 kPa contact pressure applied. Friction coefficients were calculated for each cycle from the ratio of the two forces and averaged over a 1 hr test. During testing, tissues were completely submerged in PBS.

Separately, spatially-varying modulus of the synovium was measured using atomic force microscopy (AFM, Asylum MFP 3D Bio Infinity). At each of 5 different “local test regions” (100 μm × 100 μm) synovium specimens were subjected to 5 elastic modulus indentation tests (Krishnan et al., 2004).

2.2.2.6 Biochemistry

Bovine TE constructs (n=8-10) and explants (n=9-10) were frozen at -20 °C. Lyophilized samples were weighed to obtain specimen dry weight (DW) prior to digestion. Samples were solubilized by incubating for 16 hours at 56 °C in 0.5 mg/mL proteinase K (Cat. No. 193504; MP Biomedicals) in 50 mM Tris buffered saline containing 1 mM EDTA, 1 mM iodoacetamide (Cat. No. 12227-1000; Acros), and 10 mg/mL pepstatin A (Cat. No. BP2671100; Fisher) (Riesle et al., 1998). DNA and collagen content were analyzed using the Picogreen (Cat. No. P11496; ThermoFisher) and orthohydroxyproline (OHP) assays, respectively. The OHP assay was performed as previously described (Hollander et al., 1994).

2.2.2.7 Media Analyses

Media samples were assayed using a HA Quantikine ELISA Kit (Cat. No. DHYAL0; R&D Systems). To account for variations in size of the specimens, HA values were normalized to the final dry weight of the associated specimens. Additionally, NO was assayed using a Griess Reagent Kit (Cat. No. G7921; ThermoFisher). Agarose gel (0.5% w/v in TAE buffer) electrophoresis (~2.3 V/cm for 6 hours) and subsequent staining with 0.005% Stains-All (Cat. No. E9379; Sigma) in 50% ethanol was used to determine relative MW distributions for pooled TE and EXP samples (Lee and Cowman, 1994). A HiMark™ pre-stained protein ladder (Cat. No. LC5699;

ThermoFisher) and ~1.5-1.8 MDa HA (Cat. No. 53747; Sigma) were used as approximate MW standards. A solution of 50% (v/v) juvenile bovine synovial fluid in PBS was added as an additional comparison. ImageJ was used to generate size distribution histograms from imaged gels and quantify peak location and area under curve.

2.2.2.8 Histological and Immunohistochemical Characterization

4% paraformaldehyde-fixed samples (TE and EXP) were embedded in paraffin wax and sectioned in 8 μm slices. Deparaffinized sections were stained with hematoxylin and eosin (H&E) to determine cell distribution and picrosirius red to determine collagen distribution. Samples were immunohistochemically stained for collagen type I (Smith, 2011) (1:200; rabbit polyclonal; Cat. No. ab34710; Abcam), collagen type IV (Smith, 2011) (1:500; rabbit polyclonal; Cat. No. ab6586; Abcam), lubricin (Jay et al., 2000b) (1:250; rabbit polyclonal; Cat. No. ab28484; Abcam), CD-14 (Zimmermann et al., 2001) (1:200; rabbit polyclonal; Cat. No. ab203294; Abcam), and cadherin-11 (Lee et al., 2007) (1:40; goat polyclonal; Cat. No. AF1790; R&D Systems) using a 3,3'Diaminobenzidine (DAB) Substrate Kit (Cat. No. ab64238; Abcam). Briefly, heat mediated epitope retrieval was performed for 10 minutes at 98 °C in citrate buffer (pH 6) prior to commencing the DAB protocol. The sections were counterstained with hematoxylin. Isotype controls were prepared to rule out non-specific staining.

2.2.2.9 Statistics

Data sets were tested for normality and homogeneity using the Kolmogorov-Smirnov Test and Bartlett's test, respectively. If possible, non-normal data was log-transformed to achieve normal distribution for subsequent parametric tests. Otherwise, non-normal and non-homogeneous bovine

data were analyzed using the Kruskal Wallis test and Dunn's post-hoc test. Normal and homogeneous data sets were analyzed using one- or two-way analysis of variance (ANOVA) with Tukey honest significant difference (HSD) post-hoc test. A Pearson (r) or Spearman (rs) correlation coefficient was computed for relevant comparisons with $\alpha=0.05$. All statistical tests were performed in Graphpad Prism 7 (La Jolla, CA). Values are presented as mean ± standard deviation.

2.2.3 Results

2.2.3.1 Baseline Comparison of TE and Explant Synovium

Mature day 21 TE synovium exhibited structural characteristics of native synovium. TE synovium exhibited an opaque, flat morphology, reminiscent of the membranous appearance of native tissue explants **(Figure 2.4A-B)**. The formation of the intimal lining, a key characteristic of synovium, was confirmed with H&E **(Figure 2.4C-D)**. Three-dimensional z-stack reconstructions of confocal images showed similar patterns of cellular organization in each tissue **(Figure 2.4E-F)**. Additionally, TE synovium expressed critical proteins of interest in the native synovium. Lubricin **(Figure 2.4G-H)**, cadherin-11 **(Figure 2.4I-J)**, collagen type I **(Figure 2.4M-N)**, and collagen type IV **(Figure 2.4O-P)** were highly expressed in the intimal lining layer, but also throughout the sub-intima. CD14 expression **(Figure 2.4K-L)**, indicative of MLS or monocyte phenotype, was low in each tissue. TE and explant synovium had statistically similar baseline permeability and minimum friction coefficient **(Figure 2.5A-B)**. Furthermore, a similar distribution of elastic modulus was observed in the two tissue types, however a higher proportion of EXP regions had lower modulus than in TE **(Figure 2.5C)**.

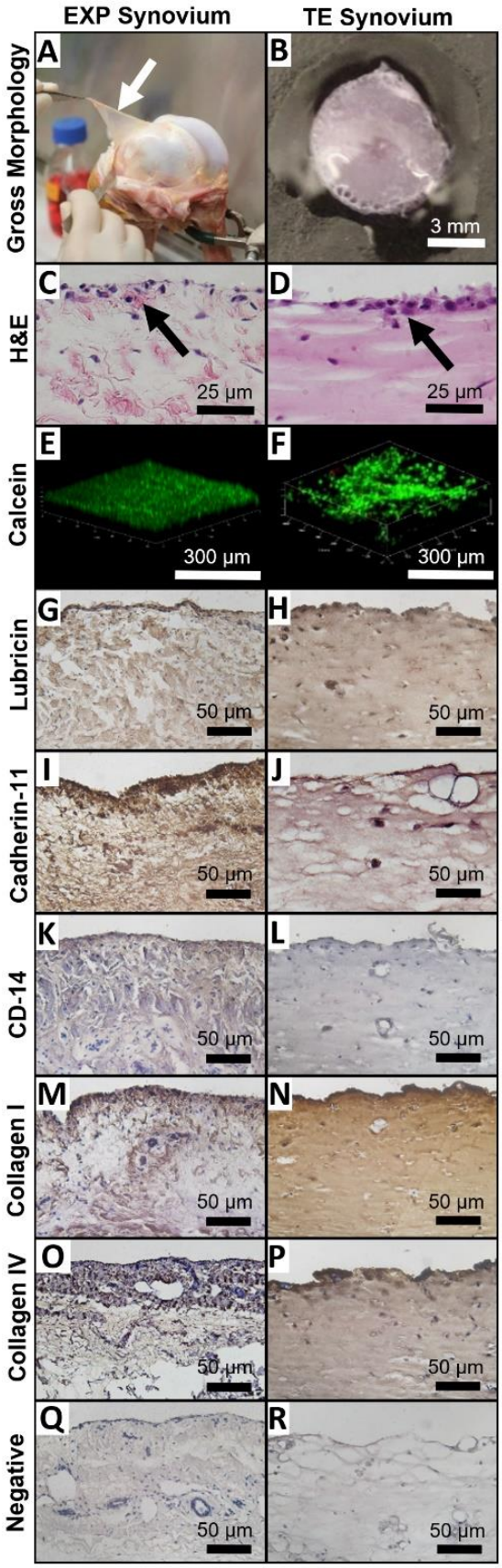

Figure 2.4 Structure and composition of bovine explant and TE synovium. **(A)** Explant and **(B)** TE synovium displayed an opaque, flat, membranous morphology. **(C, D)** A 1-4 cell thick intimal lining layer was observed using H&E. **(E, F)** 3D z-stack reconstruction with cells labeled with calcein-AM (green) showed similar cellular localization to the surface of the tissue with fewer subintimal cells. Positive immunohistochemical staining was visualized with DAB Peroxidase and cells were counterstained with hematoxylin. Both tissues showed **(G and H)** lubricin and **(I and J)** cadherin-11 expression. **(K)** CD14 expression was extremely low in EXP synovium, as expected for "healthy" synovium containing primarily FLS, whereas **(L)** TE synovium had negative staining. **(M and N)** Type I and **(O and P)** type IV collagen were also present in both tissues. **(Q and R)** Corresponding isotype controls showed the absence of non-specific staining.

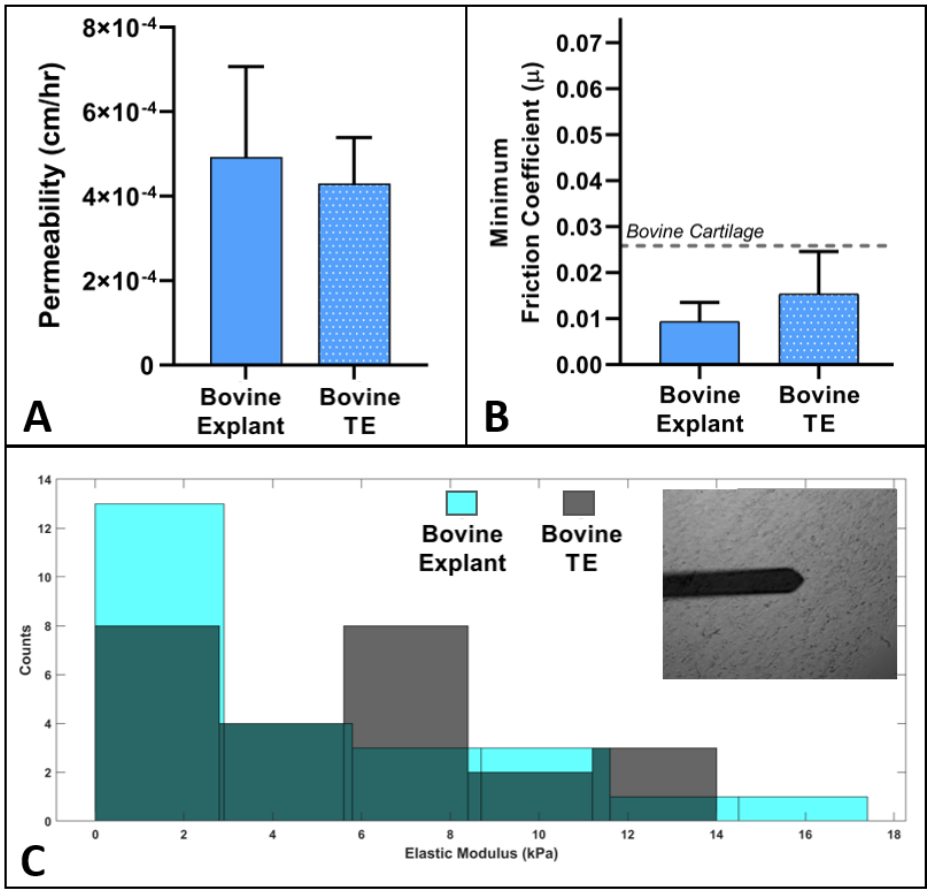

Figure 2.5 Baseline permeability and mechanical properties of explant and TE synovium. **(A)** Mean permeability of 70 kDa FITC-dextran was similar in EXP (n=3) and TE (n=7) synovium. **(B)** Minimum equilibrium friction coefficient was similar in EXP (n=3) and TE (n=3) synovium (Estell, 2018). **(C)** Histogram of AFM elastic modulus measurements for EXP and TE synovium, inset: tip of AFM probe on explant.

2.2.3.2 Lubricant Secretion

Robust lubricin staining was observed in EXP and TE synovium for both CTL and IL groups, with comparatively weaker staining in DEX groups **(Figure 2.6A)**. HA secretion in IL groups was significantly higher than CTL in TE synovium and bovine explants ($p<0.05$) with a near twofold increase, and to a lesser extent in TE synovium treated with DEX ($p<0.05$) **(Figure 2.6B)**. Gel electrophoresis of pooled specimens **(Figure 2.6C, D)** showed that both CTL and DEX-treated EXP and TE specimens had greater proportions of high MW HA compared to their IL-treated

counterparts. The 1.5 MDa HA standard and bovine synovial fluid contained predominantly high (>460 kDa) MW HA, although a large size range with multiple peaks was observed in each **(Figure 2.6D)**. Further, of the high MW HA (>460 kDa) in explant specimens, CTL and DEX-treated explants had predominantly higher MW HA than IL-treated explants.

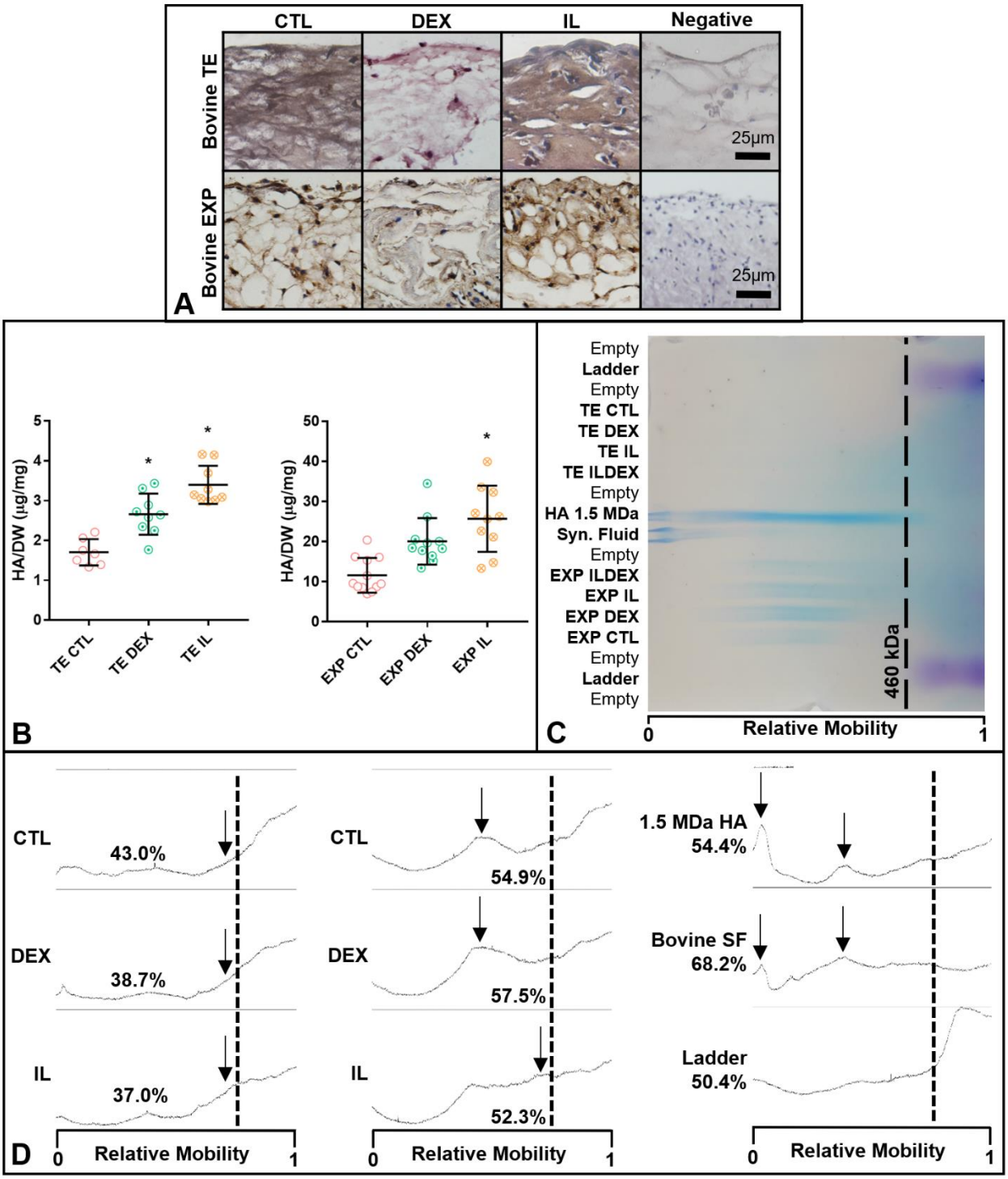

Figure 2.6 Lubricin and HA secretion in bovine TE and EXP synovium. **(A)** Robust lubricin expression (reddish brown) was observed in CTL and IL groups for both EXP and TE synovium, with comparatively weaker staining in DEX groups. **(B)** Overall, bovine TE and EXP synovium had elevated HA secretion in response to DEX and IL treatment, *p<0.05 vs. CTL, †p<0.05 vs.

DEX. **(C)** Agarose gel electrophoresis (HA, blue; ladder, purple) showed approximate HA size distribution of **(D)** pooled experimental groups and standard molecules of interest. In both EXP and TE synovium, wide HA MW distributions were observed, with the highest proportion of high MW HA (lower relative mobility) being estimated in CTL and DEX-treated groups. Peaks (arrows) represented mobility of the predominant high MW HA for a given group. The upper size limit of the ladder was 460 kDa (dotted line), which was used as a cut-off point to approximate the relative amounts of small and large MW HA in the given sample. Lower MWs could not be accurately resolved in the given gel conditions (low agarose concentration and high voltage) that were otherwise necessary for HA mobility.

2.2.3.3 Structure-Function Response

Total collagen content, normalized to average initial collagen content in the given tissue type, was significantly lower in DEX-treated TE synovium compared to CTL ($p<0.05$) **(Figure 2.7A)**. A similar trend was observed in IL-treated TE synovium ($p=0.270$). No significant differences were observed in collagen of bovine explants **(Figure 2.7B)**. DNA content, normalized to initial DNA content, was elevated in IL-treated TE ($p=0.163$) and bovine explant ($p=0.136$) synovium relative to their CTL counterparts **(Figure 2.7C, D)**. When comparing the relative change in ratio of collagen to DNA, COL/DNA was significantly lower in TE DEX and TE IL relative to TE CTL ($p<0.05$) **(Figure 2.7E)**. A similar trend of decreased COL/DNA in bovine EXP IL was seen compared to CTL ($p=0.104$) **(Figure 2.7F)**.

Similarities were observed in structural changes undergone by TE and EXP synovium, as visualized with H&E and picrosirius red histology **(Figure 2.8)**. CTL specimens were especially fibrous, with strong picrosirius red staining and associated large gaps present in the ECM. DEX specimens had increased intimal cellularity and slightly denser matrix. IL specimens had further increased intimal cellularity and very dense collagen matrix present throughout the tissue.

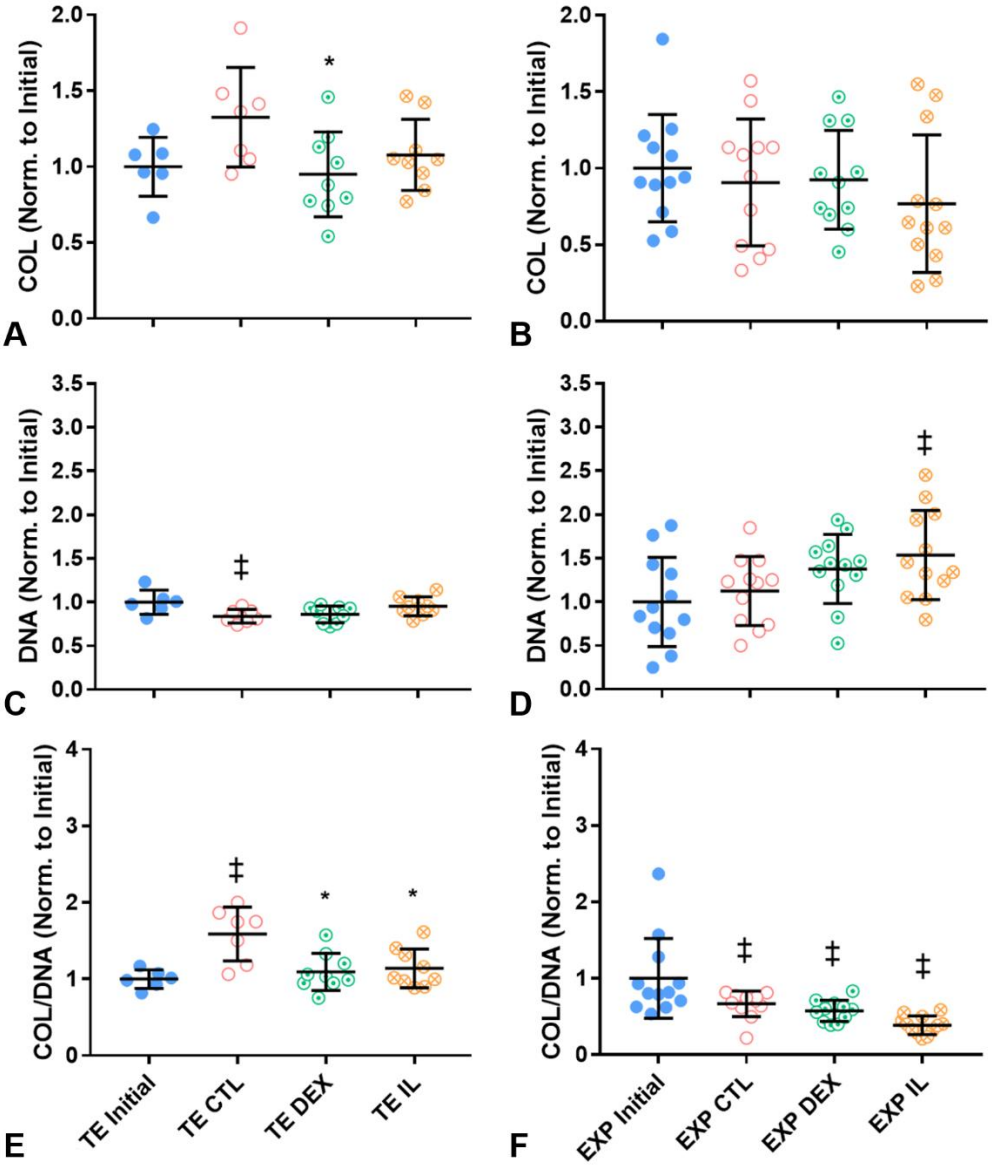

Figure 2.7 Total collagen and DNA content in bovine TE and explant synovium. **(A)** Change in total collagen was significantly lower in DEX-treated TE synovium relative to CTL ($p<0.05$), and a similar trend was observed in IL-treated TE synovium ($p=0.2698$). **(B)** Total collagen was statistically unchanged in all bovine explant groups. Change in DNA was elevated with IL treatment relative to CTL for **(C)** bovine TE synovium ($p=0.163$) and **(D)** EXP synovium ($p=0.136$). DNA significantly decreased compared to initial values in TE CTL and increased compared to initial values in EXP IL ($p<0.05$). Change in COL/DNA was significantly lower in DEX- and IL-treated groups compared to CTL for **(E)** bovine TE synovium ($p<0.05$), and similar trends were seen for **(F)** EXP IL ($p=0.104$); *$p<0.05$ vs. CTL, †$p<0.05$ vs. DEX, ‡$p<0.05$ vs. Initial.

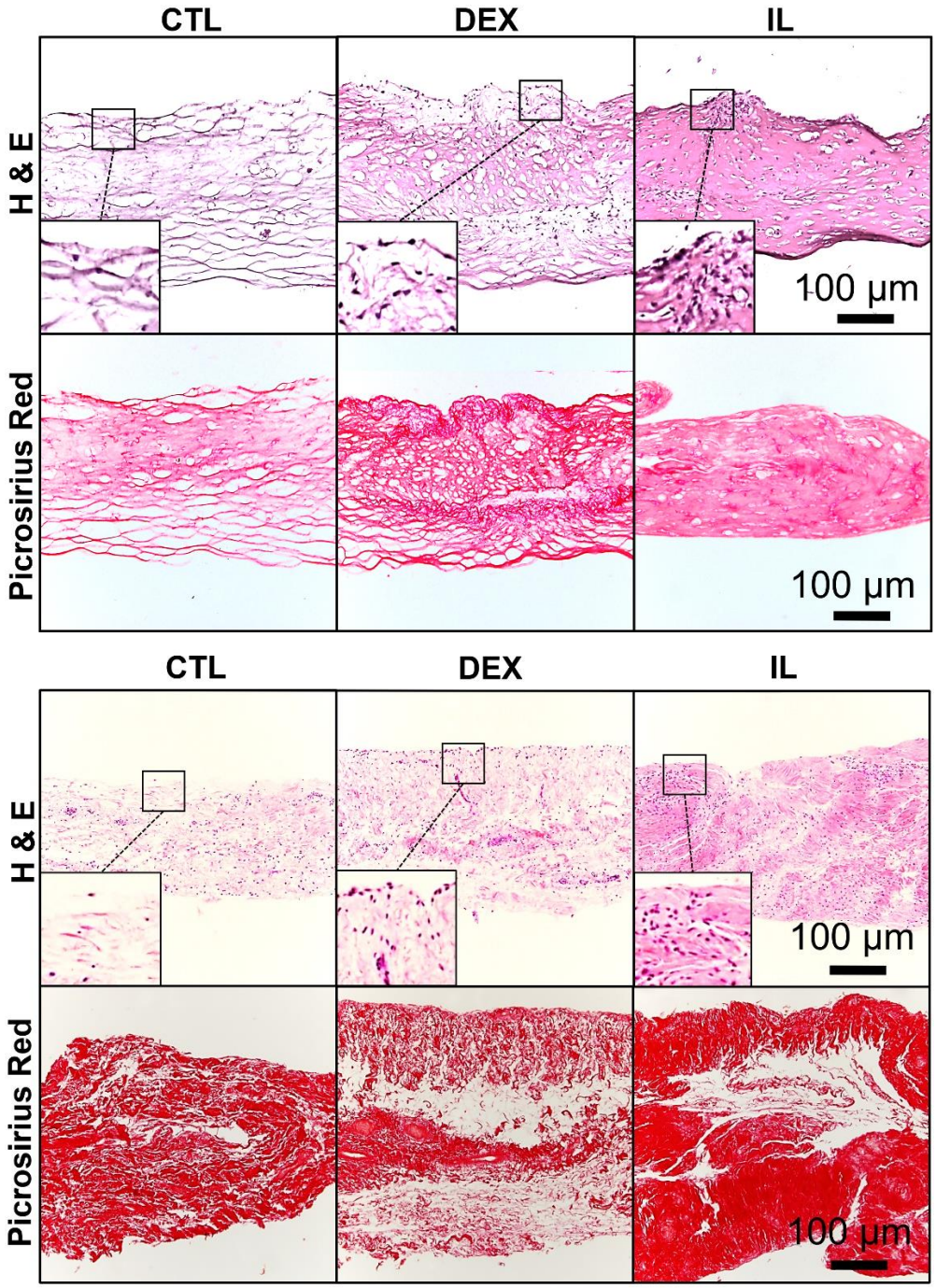

Figure 2.8 H&E and picrosirius red histology of bovine TE and EXP synovium. Similarities were observed in structural changes undergone by TE (upper) and EXP (lower) synovium, as visualized with H&E and picrosirius red staining. CTL specimens were especially fibrous, with strong picrosirius red staining and associated large gaps present in the ECM. DEX specimens had increased intimal cellularity and slightly denser matrix staining. IL specimens had further increased intimal cellularity and very dense collagen matrix present throughout the tissue.

For solute transport analysis, the two separate fluid reservoirs modeled different compartments within the joint. The luminal compartment modeled synovial fluid while the basolateral compartment modeled the extra-capsular space. Total clearance over 72 hours **(Figure 2.9A, C, E)** mimicked differences in permeability **(Figure 2.9B, D, F)** in each group, with higher clearance correlating to higher permeability values, as expected. Cell-free Matrigel controls (not plotted) consistently had significantly higher clearance than TE constructs over the 72-hour measurement period ($p<0.05$). Cell-free controls vs. TE constructs had 72-hour dextran clearances of (~56% vs. ~25%) for 10 kDa, (~24% vs. ~13%) for 70 kDa, and (~17% vs. ~5%) for 500 kDa. Overall, permeability in TE synovium **(Figure 2.9A-F)** was significantly decreased with increasing solute MW ($p<0.05$). Both DEX and IL resulted in decreased permeability of the 70 kDa solute ($p<0.05$), with approximate decreases of 28% and 26%, respectively **(Figure 2.9D)**. In TE synovium, decreased collagen to DNA ratio (COL/DNA) was strongly correlated with observed decreases in permeability of 70 kDa dextran ($r(2) = 0.9736$, $p = 0.0264$). Specifically, DEX and IL specimens had lower COL/DNA compared to CTL **(Figure 2.7E)** and similarly had lower permeability **(Figure 2.9D)**. No significant differences or correlations were observed with the 10 kDa and 500 kDa solutes.

Total 72-hour clearance of 70 kDa dextran was significantly higher in EXP compared to TE specimens ($p<0.05$), however variance was quite high compared to TE constructs. Permeability of 70 kDa dextran was statistically similar in TE synovium and bovine explants, with coefficients of $4.3 \times 10^{-4} \pm 1.1 \times 10^{-4}$ cm/hr and $4.9 \times 10^{-4} \pm 2.1 \times 10^{-4}$ cm/hr, respectively. Permeability of 70 kDa dextran in CTL bovine explants increased twofold ($p=0.0941$), while IL-treated explants remained unchanged ($p=0.88$) **(Figure 2.9H)**. No significant correlation between permeability coefficient and COL/DNA was observed in bovine explants ($rs(1) = -0.3210$, $p = 0.7920$). A

representative confocal image showed diffusion primarily occurring in the intercellular spaces **(Figure 2.9I)**.

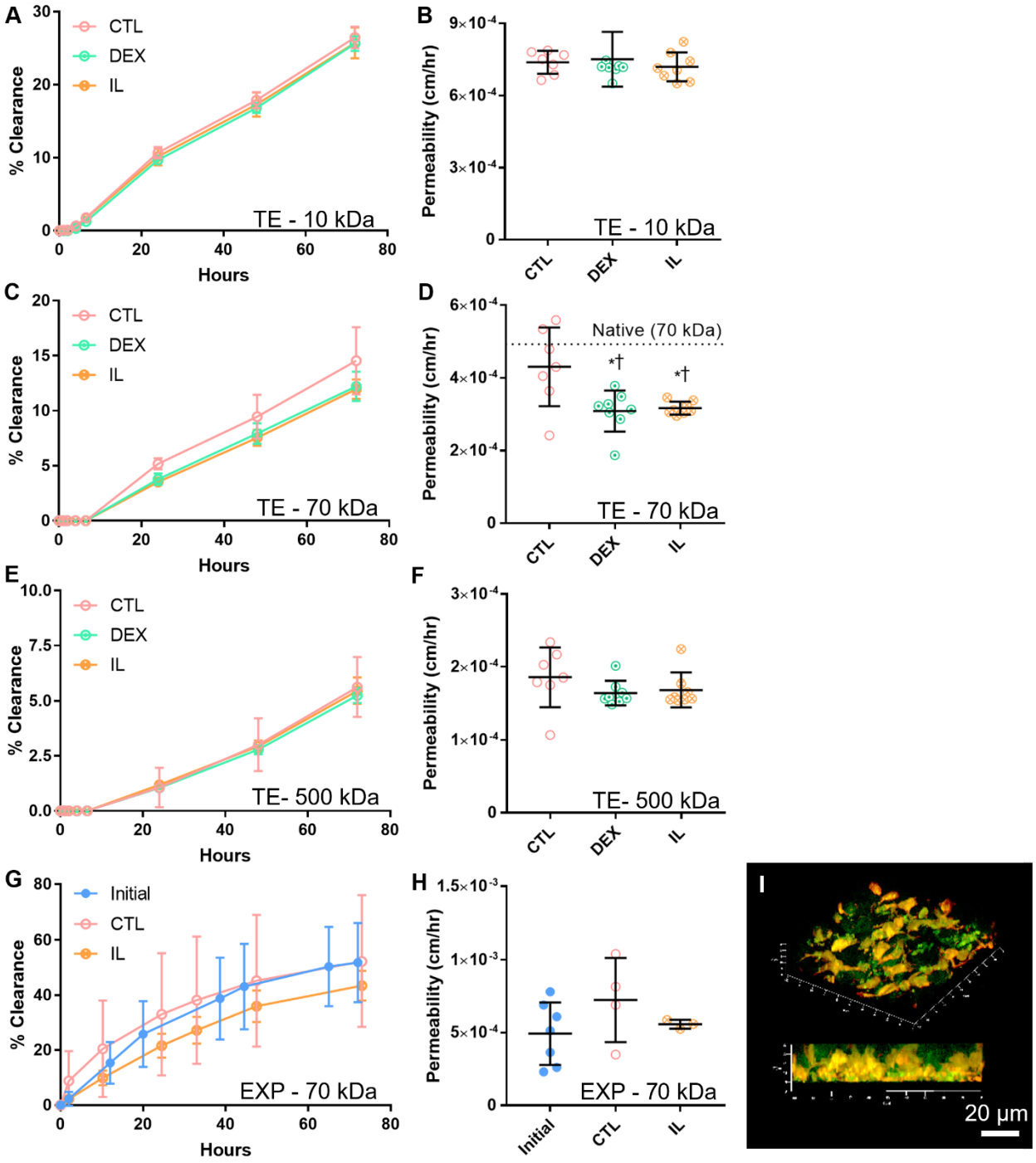

Figure 2.9 Cumulative clearance of dextran and corresponding permeability values were presented for 10 kDa, 70 kDa, and 500 kDa sizes in TE specimens **(A-F)** and for the 70 kDa size

in bovine EXP specimens **(G-H)**. **(D)** Both DEX- and IL-treated TE groups exhibited decreased permeability relative to CTL with 70 kDa dextran only. Permeability of 70 kDa dextran in CTL did not differ significantly from native tissue (dotted line, value from **7H**), whereas DEX and IL specimens were significantly lower (*p<0.05 vs. CTL, †p<0.05 vs. native). **(G-H)** In EXP synovium (N=3-4), permeability in CTL increased over time and was higher than IL-treated tissue, but neither observation was statistically significant (p=0.0941 and p=0.3448, respectively). **(I)** Representative 3D confocal image of 70 kDa FITC-Dextran (green) and resident cells (red-orange) within a living synovium explant showed diffusion occurring in intercellular spaces.

2.2.3.4 Inflammatory Response

NO secretion per DNA was elevated in IL-treated TE synovium and bovine explants compared to corresponding DEX groups (p<0.05) **(Figure 2.10A, C)**. Day 0 bovine TE synovium and explants consisted primarily of $CD14^-$ cells **(Figure 2.10B, D)**. In both tissue types, relatively intense CD14 staining (reddish-brown) was observed in CTL and IL specimens. DEX-treated tissues had relatively less intense staining compared to CTL and IL, however elevated compared to initial.

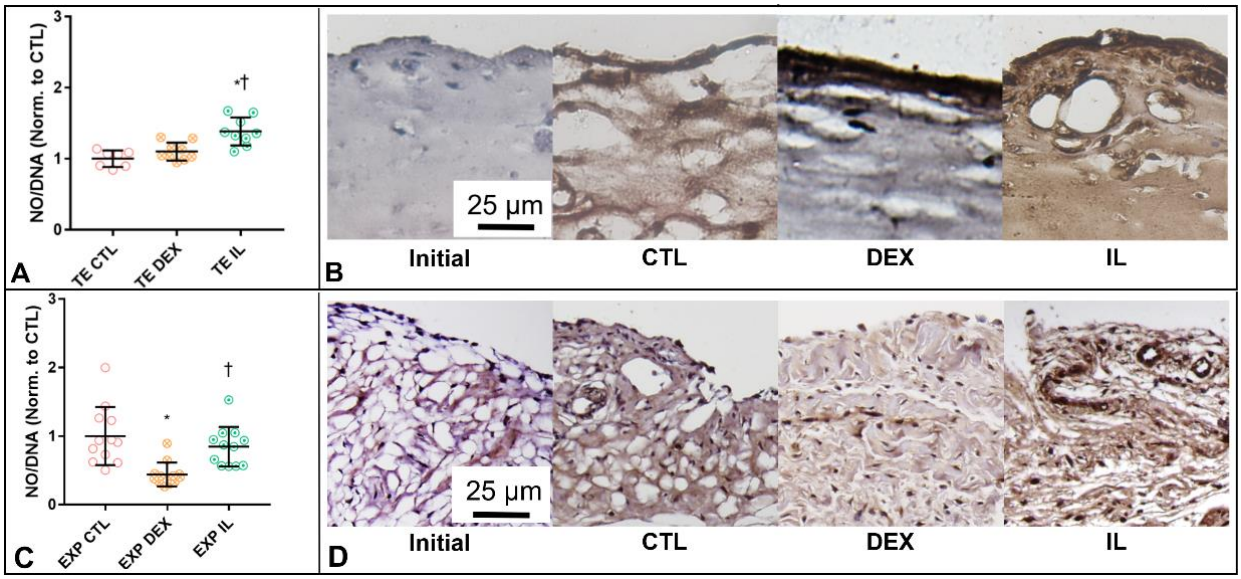

Figure 2.10 Nitric oxide secretion and CD14 expression in TE synovium and explants. NO production in bovine **(A)** TE and **(C)** explant synovium was elevated in response to IL treatment,

*p<0.05 vs. CTL, †p<0.05 vs. DEX. Elevated CD14 expression (reddish brown) was observed in **(B)** TE and **(D)** explant tissue treated with IL. An increase was also seen in CTL groups, but CD14 staining was less intense for DEX specimens.

2.2.4 Discussion

The findings of these studies support the specific hypothesis linked to SA1a-b and, by extension, the global hypothesis of Part I. Similarities in baseline structural, biochemical, solute transport, and friction properties were observed in bovine TE synovium and native synovium explants. Furthermore, similar IL-1 and DEX-induced changes in structure-function were observed. Specifically, engineered synovium allowed quantitative correlations between structure and solute transport function that are not possible with other culture techniques.

The FLS-only TE synovium exhibited a defined intimal lining layer and expressed lubricin and cadherin-11, among other markers of native synovium **(Figure 2.4)**. TE and explant synovium also had similar baseline permeability to 70 kDa dextran and minimum friction coefficient **(Figure 2.5)**. Increased HA secretion in response to IL and DEX was characteristic of TE and native tissue **(Figure 2.6)**. Relative size determination by gel electrophoresis showed a shift to lower MW HA in IL-treated specimens compared to CTL and DEX **(Figure 2.6)**. A similar trend has been observed in OA patients, where the proportion of pro-inflammatory, low MW HA in the joint (Jiang et al., 2011) tends to increase due to the breakdown of larger MW HA (Stern, 2004). Synovium explants from healthy and OA donors exposed to cytokine insult have increased concentration of pro-inflammatory mediators such as MMPs, NO and PGE2 (Beekhuizen et al., 2011; Cook et al., 2007; Hardy et al., 2002; Lee et al., 2009; Swärd et al., 2017; van Buul et al., 2012). On the other hand, glucocorticoids are known to have a significant anti-inflammatory effect

and to modulate cell biosynthesis in the joint (Roach et al., 2016a), likely influencing FLS as well (Reyes et al., 2008). Similar trends in NO secretion were observed in our specimens **(Figure 2.10)**.

The concentration of lubricin, another lubricant molecule, was decreased in the ECM of DEX-treated and control bovine explants, whereas it was maintained or increased in IL-treated groups **(Figure 2.6)**. It is possible that greater levels of secreted lubricants in the media for DEX groups are correlated to lower levels within the tissue itself; however, additional studies will be required to confirm this. OA synovial fluid contains decreased concentrations of lubricin (Blewis et al., 2010a; Elsaid et al., 2008; Mathiessen and Conaghan, 2017; Jeremie Sellam and Berenbaum, 2010), despite reports that human OA FLS rapidly proliferate and secrete increased concentrations of lubricant molecules (e.g. HA and lubricin) when treated with IL-1β and TNF-α *in vitro* (Blewis et al., 2010a, 2010b; Furuzawa-Carballeda et al., 2008; Gitter et al., 1989; Hamilton et al., 1994; Pulkki, 1986). Overall, it is presumed that the relative balance between aberrant cytokine and lubricant production in the joint and altered transport properties determines synovial fluid content of lubricant molecules.

Permeability of 500 kDa dextran was ~1.6-1.9 $\times$ 10^{-4} cm/hr in TE synovium, which is similar to that of lubricin and HA (~0.36-1.8 $\times$ 10^{-4} cm/hr) in membranes of physiologic pore size (50 nm) (Blewis et al., 2007). Permeability of 70 kDa dextran was statistically similar in TE synovium and bovine explants, with coefficients of 4.3 $\times$ 10^{-4} $\pm$ 1.1 $\times$ 10^{-4} cm/hr and 4.9 $\times$ 10^{-4} $\pm$ 2.1 $\times$ 10^{-4} cm/hr, respectively. Furthermore, the observed relationship between increasing solute size and decreased permeability parallels *in vivo* findings of the rabbit knee, which showed increased clearance of low MW HA ($\leq$500 kDa) compared to high MW HA (~2,200 kDa) (Coleman P. J. et al., 2004a; Sabaratnam S. et al., 2005). As 10 kDa dextran permeability was similar across studies, this size solute can likely diffuse freely through even small intercellular

spaces. On the other hand, molecules of 500 kDa and above diffuse very slowly. Future studies can investigate whether more accurate modeling, including computational analyses of the transport can resolve differences in behavior of higher MW solutes.

Under the conditions of the current studies, treating TE synovium with DEX or IL resulted in a ~20% reduction in 70 kDa dextran permeability **(Figure 2.9)**. A similar decrease in permeability was observed in IL vs CTL bovine explant tissues, however there was a high degree of statistical variance arising from the inherent challenges in harvesting uniform synovium samples from the joint **(Figure 2.9)**. This functional change was related to lower collagen in DEX-treated TE synovium and greater DNA in TE synovium treated with IL. In fact, the relative ratio of COL/DNA (i.e. ECM vs. cells) in DEX- and IL-treated groups for both TE synovium and bovine explants was lower than CTL **(Figure 2.7)**. In TE synovium, this lower COL/DNA was strongly correlated with observed lower permeability of 70 kDa dextran ($r^2 = 0.97$, $p = 0.0264$). Though for bovine explant synovium, no significant correlation was detected, so it is unclear to what extent the ECM contributes to native tissue transport behavior.

Others have described similar transport mechanisms in the synovium, which are facilitated by ECM volume fractions (primarily collagen fibrils and GAGs) and limited by the space occupied by cells (Blewis et al., 2007). A similar mechanism was observed here, with solute diffusion in native synovium occurring primarily around cells and through the interstitial ECM **(Figure 2.9)**. This potential mechanism is further supported by histological findings **(Figure 2.8)**, which showed intimal hyperplasia in both DEX and IL-treated TE specimens. This structural change was mirrored in explanted tissue, as well as increased collagen compaction in IL-treated groups relative to CTL. Future studies will be necessary to assess the relative importance of these structural changes to transport function compared to bulk ECM content and inflammatory characteristics.

Despite the similarity between transport characteristics of native and engineered synovium presented herein, it should be noted that the results of our *in vitro* solute transport are seemingly in contrast with reports of increased HA clearance from arthritic joints (Coleman P. J. et al., 2004b; Fraser et al., 1993), as well as elevated degradative enzymes associated with tissue breakdown and possible increased permeability (Marks and Donaldson, 2005). Notably, IL-1 is known to induce breakdown of endothelial layers and thereby increase permeability in blood-brain barrier models (Labus et al., 2014). Aside from the increased complexity of interpreting solute transport in the synovial joint, a living organ at the tissue level, it is speculated that this difference may be due to the competing contributions of higher clearance due to breakdown of HA and the thickening of the intimal layer, which may hinder transport. A recent study of dextran clearance in destabilized rat knees supports this hypothesis, showing slower transport of 500 kDa dextran and an apparent thickening of synovium in the destabilized joints (Mwangi et al., 2018). The downward shift in HA MW was recreated in our EXP and TE synovium experiments in response to interleukin **(Figure 2.6)**.

It is also likely that dextran does not fully recreate the complex tertiary structure of large MW HA or exhibit the same binding characteristics. Future work should examine various sizes of HA, however endogenous HA synthesis/breakdown in cultures and the high polydispersity of commercially available HA products may confound results. Furthermore, as additional variables are added to increase the complexity of our TE model, such as to examine the effects of vascular-mediated clearance (Bhattaram and Chandrasekharan, 2016; Levick, J. R., et al., 1999), synovial fluid shear, hydrostatic pressure, and strain-dependent permeability, there may be more convergence of our culture findings with those *in vivo*.

While correlations between structure and function may be limited by the different size Transwells used, it was necessary to fabricate engineered synovium of dimensions better suited for a particular target measurement. The larger 6.5 mm Transwell system was used to grow specimens that produced measurable levels of matrix and lubricants. A scaled down 4.26 mm system was adopted for the transport analyses to enable the high throughput necessary to test multiple dextran sizes with sufficient replicates. Importantly, comparisons between TE constructs subjected to different treatments were performed on engineered synovium derived from the same size Transwell. While it is possible that tissue properties may be somewhat dependent on the Transwell size, similar structural and chemical changes were observed in response to pro-inflammatory cytokines to those reported for other configurations, such as engineered synovial microtissues (Kiener and Brenner, 2005) and FLS monolayers (Blewis et al., 2010b). For comparisons of TE synovium, initial construct dimensions as well as cell and Matrigel concentrations were kept consistent. Nevertheless, future studies will incorporate additional ELISAs and sensitive measurement techniques to allow all measurements in the scaled-down, high-throughput version of the system.

Interestingly, an apparent phenotypic shift was seen in bovine explant cultures **(Figure 2.10)** and may help to explain the similarity in the biological response of the FLS-based TE synovium and native tissues. CTL and IL-treated bovine TE synovium and explants had an increase in $CD14^{+}$ cells and decrease in $CD14^{-}$ cells, whereas treatment with DEX maintained lower CD14 expression levels. This is striking due to the lack of MLS in the engineered synovium model. There is precedent for human fibroblasts to express and secrete soluble CD14 (Sugawara et al., 1998) and other markers of M1-activated macrophages (Manferdini et al., 2017) when exposed to an inflammatory environment, so it is possible that a phenotypic shift is partially due

to trans-differentiation of FLS (Fell, 1978; Graabaek, 1984). The following section examines this phenomenon further.

2.3 MLS Content Changes Dramatically in Bovine Synovium Explant Culture and Modulates Structural Changes in Engineered Synovium

2.3.1 Introduction

The normal intimal lining is about 1-4 cells thick and composed of approximately 90% FLS and 10% MLS (Valencia et al., 2004). FLS, the primary cells in the synovium, are largely responsible for ECM production (Kiener et al., 2010; Lee et al., 2007), lubricant secretion (Jay, 1992; Jay et al., 2007, 2000a), and contribute to the cascade of inflammatory cytokines in OA synovial fluid (Kiener et al., 2010). Hence, most biological studies of isolated synoviocytes have focused on solely on this cell type. However, the hyperplastic response includes a drastically changing distribution and quantity of FLS, MLS, and other immune cells depending on the stage of OA (O'Brien et al., 2017; Utomo et al., 2016). There is a concurrent increase in polarized macrophage infiltration from the vasculature and secretion of pro-inflammatory cytokines, all of which are thought to contribute to the progression of joint degeneration (Blewis et al., 2010b; Kiener et al., 2006; Scanzello and Goldring, 2012a; Sutton et al., 2009).

Motivated both by this knowledge and the apparent phenotypic shift observed in both the FLS-only TE synovium and explants in the preceding section **(2.2)**, we sought to incorporate MLS into the engineered synovium model and track their role in structural reorganization of the intima (SA1c). It is anticipated that this added level of complexity will be necessary in order to decouple the roles of different cell types within the synovium, especially as its composition and structure changes. Here, we began by quantifying $CD14^{+}$ cells within synovium explants in response to IL

or DEX, followed by co-culturing physiologically relevant quantities of MLS to mimic structural changes at different disease states and evaluate phenotypic stability.

2.3.2 Materials and Methods

2.3.2.1 Isolation and Expansion of MLS

Synovial explant tissue from juvenile bovine (n=2-4) or human OA (n=3) knees was digested in collagenase type II for 2 hours at 37 °C. Isolated cells were counted using a hemocytometer before and after performing a CD14 Dynabeads™ (Cat. No. 11149D; ThermoFisher) selection protocol. Briefly, the mixed cell population of synovial cells was incubated in Dynabeads and magnetically separated based on CD14 expression. Dynabeads were removed from $CD14^+$ cells prior to culture via trypsinization.

For passaging, viable MLS ($CD14^+$) were plated at a density of 1.76×10^3 cells/cm^2 and expanded for two passages in αMEM containing 10% FBS, 1% antibiotic-antimycotic, and 10 ng/ml macrophage colony stimulating factor (MCSF; Cat. No. PHC9504; ThermoFisher) (Gonçalves and Mosser, 2001). FLS were passaged as previously described **(2.2.2.1)**.

2.3.2.2 Cell Ratio Determination

For quantification of initial $CD14^+$ (i.e. MLS) and $CD14^-$ (i.e. FLS) content in explant tissues, parallel groups were counted with Dynabeads (to determine relative ratio) and quantified using the Picogreen DNA assay (to determine total cell content per dry weight). The resulting ratio and total cell number were combined to give an approximation of overall cell phenotype.

2.3.2.3 Formation and Cytokine Treatment of TE Synovium with FLS and MLS

P2 bovine MLS were pre-labeled using DiI lipophilic membrane dye (Cat. No. V22885; ThermoFisher) while P2 bovine FLS remained unlabeled. TE constructs were created as described previously **(2.2.2.2)**, with the addition of three different FLS to MLS ratios: 100% FLS, 50% FLS + 50% MLS, or 100% MLS. Each group had a total combined initial cell concentration of 5×10^6 cells/ml. Pre-culture followed by treatment in CTL or IL conditions (N=2), as described earlier, was conducted.

2.3.2.4 Histology and Immunohistochemistry

TE specimens were processed for immunofluorescence. Briefly, sections were deparaffinized and heat mediated epitope retrieval was performed for 10 minutes at 98 °C in citrate buffer (pH 6). Sections were incubated overnight in CD14 primary antibody (1:200; rabbit polyclonal; Cat. No. ab203294; Abcam) followed by a 1-hour incubation in Alexa Fluor 488 secondary antibody (1:200, goat anti-rabbit, Cat. No. ab150077; Abcam). The sections were counterstained with DAPI.

2.3.2.5 Statistics

Statistical analyses were performed as previously described **(2.2.2.9)**.

2.3.3 Results

2.3.3.1 CD14 Ratio Determination in Explants

Day 0 bovine explants consisted primarily (>90%) of $CD14^-$ cells **(Figure 2.11)**. This ratio of $CD14^+$ to $CD14^-$ was did not significantly change over 14 days with DEX treatment. In CTL and IL-treated explants, both $CD14^+$ and overall cell content (% DNA/DW) increased significantly

($p<0.05$). Concurrently, $CD14^-$ content decreased significantly in both groups, dropping to approximately 30% and 13% of total cells, respectively. Meanwhile, human OA explants contained less DNA per dry weight than bovine explant specimens; however, $CD14^+$ constituted over 50% of the total cell population.

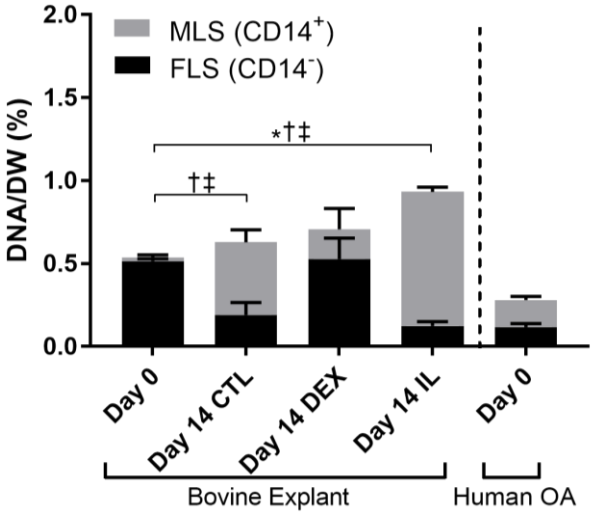

Figure 2.11 Quantification of CD14+ and CD14- cells in explant synovium. The phenotype ratio of MLS ($CD14^+$) to FLS ($CD14^-$) in EXP tissue was maintained by DEX. In CTL and IL-treated tissue, MLS content increased and FLS content decreased. Total cell content increased with IL treatment; *$p<0.05$ (total DNA), †$p<0.05$ (FLS), ‡$p<0.05$ (MLS).

2.3.3.2 TE Synovium Co-culture of FLS and MLS

The DiI membrane dye (red) robustly labeled MLS, and initial FLS to MLS ratios were qualitatively maintained over 14 days in CTL culture **(Figure 2.12A)**. Furthermore, the CD14 phenotype appeared to be stable, with red-labeled MLS also exhibiting strong positive expression of CD14 (green), while non-labeled FLS did not strongly express CD14. When treated with IL, the degree of intimal hyperplasia appeared to be dependent on the initial cell ratio, with higher

MLS to FLS ratios resulting in a thicker intima **(Figure 2.12B)**. Intimal layer formation was visible in all groups.

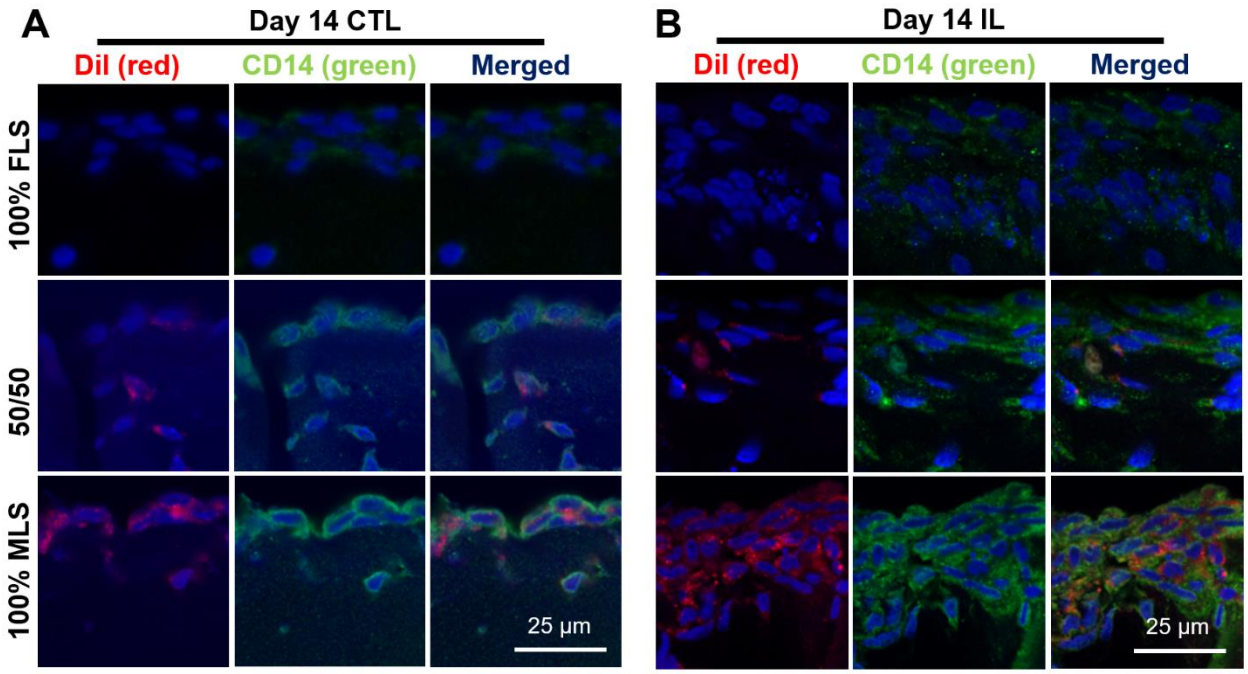

Figure 2.12 CD14 immunohistochemistry of TE synovium containing MLS and FLS. Pre-labeled MLS (DiI, red) and varying ratios of un-labeled FLS were cultured for two weeks in **(A)** CTL or **(B)** IL-supplemented media and all cells subsequently counterstained with DAPI (blue). In both CTL and IL groups, DiI (red) was co-localized with intense CD-14 expression (green). Intimal lining formation was apparent in all groups, regardless of cell type, with intimal hyperplasia apparent in groups treated with IL.

2.3.4 Discussion

The findings of these studies support the specific hypothesis linked to SA1c and, by extension, the global hypothesis of Part I. Specifically, these results highlight a strength of the engineered synovium model, where it is anticipated that the ability to define initial FLS to MLS ratios of the TE synovium may be important for modeling different stages of disease as well as understanding interactions between these cell types which is not possible *in vivo* or with native synovium

explants. The hyperplastic response to IL-1 was exacerbated by the presence of MLS **(Figure 2.12)**, which may have significant implications for transport and friction properties. Co-localization of FLS and MLS in the hyperplastic intima is characteristic of native OA tissues, as well (O'Brien et al., 2017).

A similar dual contribution to hyperplasia was observed in micropellet cultures, where FLS and monocytes "cooperated" in the TNFα-induced intimal formation (Byrne et al., 2014b, 2014a; Calvo et al., 2017). This is likely a product of both cell-cell and cell-ECM adhesive interactions in synovial remodeling (Agarwal and Brenner, 2006). FLS have been shown to play an important role in the regulation of macrophage phenotype (Donlin et al., 2014), and the reverse is likely also true. It will be informative to observe relative M1/M2 phenotype of resident and non-resident immune cells and correlating this to NO and PGE2 concentration, as well as transport and lubrication function.

CTL and IL-treated bovine synovium explants had a significant increase in $CD14^+$ cells and decrease in $CD14^-$ cells, whereas treatment with DEX maintained CD14 expression levels **(Figure 2.11)**. This confirmed the qualitative observations made in both engineered and explanted tissues in **Chapter 2.2**. Meanwhile, human OA explants were predominantly composed of $CD14^+$ cells, which was similar to the distribution observed in CTL and IL-treated explants. It is likely that a significant portion of $CD14^+$ cells in the OA human tissue were blood-derived cells, rather than resident MLS (Bhattaram and Chandrasekharan, 2016). However, there is precedent for human fibroblasts to express and secrete soluble CD14 (Sugawara et al., 1998) and other markers of M1-activated macrophages (Manferdini et al., 2017) when exposed to an inflammatory environment, so it remains possible that a phenotypic shift is partially due to transdifferentiation of FLS (Fell, 1978; Graabaek, 1984).

2.4 T Lymphocytes Modulate Engineered Human Synovium Response to Interleukin-1 and Dexamethasone

2.4.1 Introduction

The approach of using a surrogate synovium model is attractive in that quantitative transport and lubrication measurements and other high throughput *in vitro* mechanistic studies can be performed on tissues that are fabricated from cells derived from clinical biopsies and human blood specimens (Bondeson et al., 2010). In clinical OA specimens, infiltrating mononuclear cells are predominately $CD14^+$ monocytes/macrophages and $CD4^+$ T lymphocytes (Moradi et al., 2015), estimated in one study to represent ~65% and 22% of the immune cells in the OA synovium, respectively (Pessler et al., 2008). Meanwhile, other studies have found negligible quantities of T lymphocytes in OA synovium (Bondeson et al., 2010). Therefore, it is anticipated that the ability to define initial FLS to T lymphocyte ratios of the TE synovium may be important for modeling different stages and presentations of disease as well as understanding interactions between these cell types which is not possible *in vivo* or with native synovium explants. For example, differences in immune cell content may be a factor in the inconclusive evidence of intra-articular glucocorticoid effectiveness (American Academy of Orthopaedic Surgeons Board of Directors, 2013). Motivated by data validating the native-like behavior of engineered bovine synovium **(2.2, 2.3)**, in this section we explore translation of the bovine system to an *in vitro* human model (SA1d). The contribution of T lymphocytes to the response of engineered synovium to IL-1 and DEX, was also investigated.

2.4.2 Materials and Methods

2.4.2.1 Isolation and Expansion of T Lymphocytes

A fresh leukocyte-enriched blood sample (Leukopak; New York Blood Center, New York, NY) was obtained from a healthy blood donor (n=1, Type O+). The Leukopak was stored at 4°C and processed the day following collection. Briefly, a purified population of T lymphocytes was obtained using a Dynabeads FlowComp Human CD3 Kit (ThermoFisher; Cat. No. 11365D). Isolated T lymphocytes were then activated using a Dynabeads Human T-Activator CD3/CD28 Kit (ThermoFisher; Cat. No. 11131D) and expanded in Iscove's Modified Eagle Medium (IMDM) supplemented with 10% FBS and 30 units/ml interleukin-2 (IL-2; ThermoFisher, Cat No. PHC0026) for 1 week.

2.4.2.2 Optimization of T Lymphocyte 3D Culture

Activated T lymphocytes were encapsulated in 7 mg/ml Matrigel GFR (Corning; Cat No. 354230) at a concentration of 1 million cells/ml. Constructs (100 µl each) were then cultured for 1 week in one of four conditions: IMDM with 10% FBS and 30 units/ml IL-2, αMEM with 10% FBS, BM with 10 ng/ml IL-1β, or BM with 100 nM DEX. T cell-Matrigel constructs were collected at Day 0 (n=6) and 7 (n=2-4) for biochemical assessment.

2.4.2.3 Isolation of Normal Human FLS and Formation of Human TE Synovium

Normal human synovium (n=1, 33y/o white male) was obtained from the Musculoskeletal Transplant Foundation (Edison, NJ). FLS were isolated, passaged, and formed into engineered synovium constructs according to the procedure outlined in section **2.2.2.2** (96-well Transwell size), with the following modifications: P3 FLS were cast at an initial concentration of 10 million

cells/ml (instead of 5 million cells/ml) and pre-cultured for 3 months (instead of 21 days) with 20% bovine synovial fluid (Animal Technologies, Tyler, TX) supplemented media (instead of FBS). The modifications were made in response to slow tissue maturation compared to previous bovine constructs and to more closely mimic the *in vivo* environment. Following the 3-month pre-culture and maturation period, "day 0" specimens were collected and weighed prior to biochemical (n=6) and histological (n=1) analyses.

2.4.2.4 Co-Culture and Stimulation of T Lymphocytes with TE Synovium

Activated T lymphocytes were encapsulated in 7 mg/ml Matrigel GFR (Corning; Cat No. 354230) at a concentration of 1 million cells/ml. T Cell-Matrigel constructs (100 µl each) were then layered on top of TE synovium constructs in the luminal compartment of the Transwell. Co-cultures were treated in parallel with T cell-free controls for two weeks in one of three media conditions: BM (CTL), BM with 100 nM DEX, and BM with 10 ng/ml IL-1β. Specimens were collected at day 14 (n=3-6) for biochemical and histological assessments.

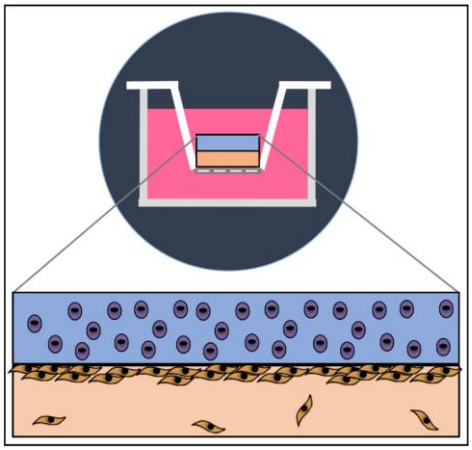

Figure 2.13 Schematic of T lymphocyte construct layered on engineered synovium. T lymphocytes (dark purple) were encapsulated within a Matrigel matrix (light purple). This construct was then placed in direct contact with mature engineered synovium (below, orange).

2.4.2.5 Biochemical Analyses

Lymphocyte-Matrigel layers were removed from co-cultures prior to weighing and assaying, so only cells that may have migrated to the engineered synovium would contribute to measured DNA content. Specimens were weighed to obtain wet weights (WW). After freezing and lyophilizing, specimens were again weighed to obtain dry weights (DW). Finally, samples were digested and assayed for DNA, as previously described **(2.2.2.6)**.

2.4.2.6 Media Analyses

Media was collected and replaced 2x per week and subsequently assayed for HA as previously described **(2.2.2.7)**.

2.4.2.7 Histology and Immunohistochemistry

Lymphocyte-Matrigel layers were removed from TE constructs prior to fixation, so that only T cells that had migrated or attached to TE constructs would be visible in resulting images. TE constructs were processed for H&E (n=1), as described in section **2.2.2.8**, and also processed for immunofluorescence. Briefly, sections were deparaffinized and heat mediated epitope retrieval was performed for 10 minutes at 98 °C in citrate buffer (pH 6). Sections were incubated for 2 hours at 4°C in CD3 (Nakamura et al., 1999) primary antibody (1:150; rabbit monoclonal [SP7]; Cat. No. ab16669; Abcam) followed by a 1-hour incubation in Alexa Fluor 488 secondary antibody (1:200, goat anti-rabbit, Cat. No. ab150077; Abcam). The sections were counterstained with DAPI.

2.4.2.8 Statistics

Statistical analyses were performed as described previously **(2.2.2.9)**.

2.4.3 Results

2.4.3.1 T Lymphocyte 3D Optimization

T lymphocytes cultured in BM+IL conditions had similar DNA content to those cultured in standard IMDM conditions (p=0.33) **(Figure 2.14)**. Meanwhile, DNA content was significantly decreased in BM+DEX and αMEM conditions compared to both BM+IL and IMDM (p<0.0001).

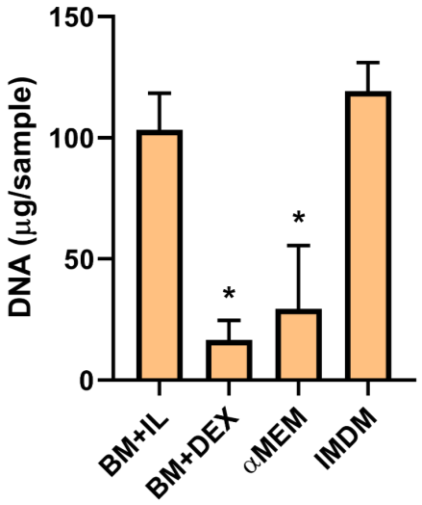

Figure 2.14 DNA content of T lymphocytes cultured in Matrigel. Basal media with 10 ng/ml IL-1 (BM+IL), basal media with DEX (BM+DEX), αMEM with 10% FBS (αMEM), and IMDM with 10% FBS and 30 units/ml IL-2 (IMDM); *p<0.0001 compared to BM+IL and IMDM.

2.4.3.2 TE Synovium with FLS±T Lymphocyte Co-Culture

Co-culture with T lymphocytes had a significant overall effect on DEX- and IL-mediated changes to DNA content in TE synovium (p=0.026) **(Figure 2.15)**. Specifically, in -T cell groups, DNA content was elevated relative to CTL in both DEX (p=0.20) and IL (p=0.024) conditions. However, in +T cell groups, DNA content was unchanged in those same media conditions (p=0.50 and p=1.0, respectively). Additionally, DNA in IL-treated specimens was elevated compared to DEX in T cell groups only (p=0.092 vs. p=0.94 for non-T cell samples).

TE synovium wet weight was not significantly affected by media or T cell condition **(Figure 2.15)**. Tissue dry weight significantly increased compared to day 0 in CTL+T cells ($p<0.001$) and IL+/-T cells ($p<0.01$ and 0.049, respectively). Meanwhile, in +T cell groups, dry weight was elevated in CTL ($p=0.0018$) and IL ($p=0.029$) compared to DEX. Overall, co-culture with T lymphocytes decreased HA secretion by approximately 28% ($p=0.093$) **(Figure 2.16)**.

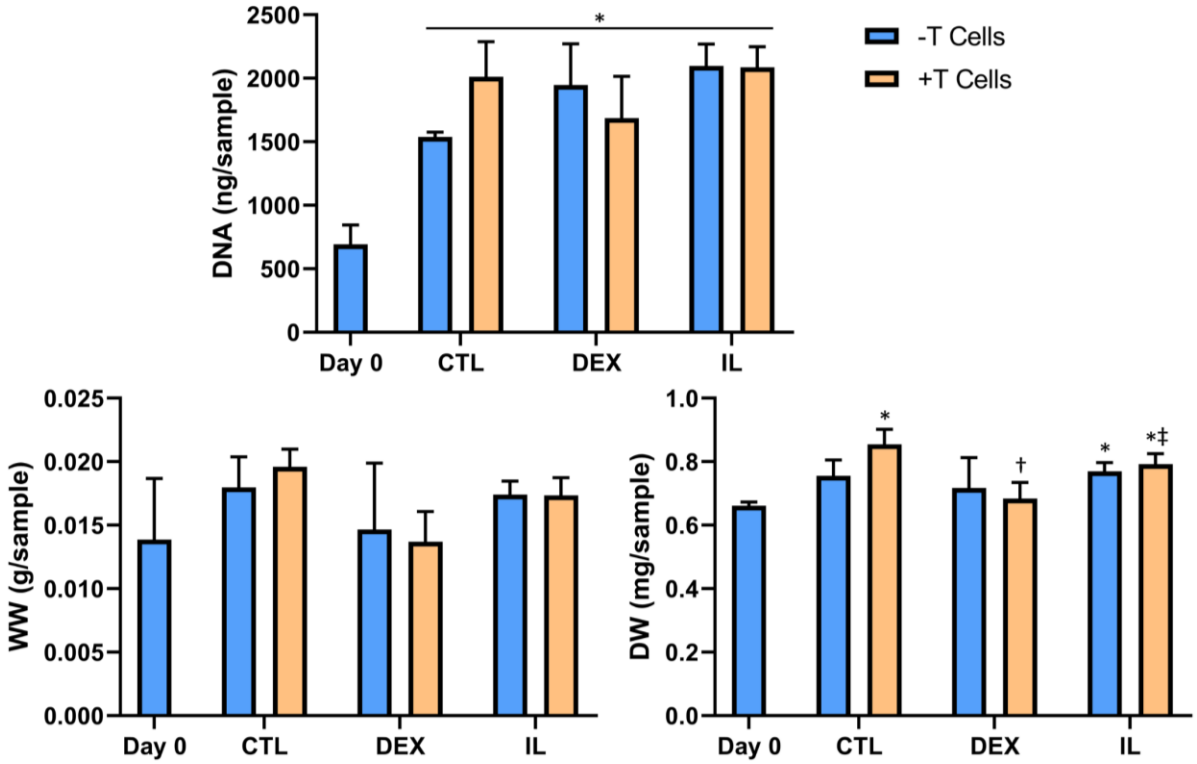

Figure 2.15 DNA content and weights of TE synovium co-cultured with T cells. *$p<0.05$ compared to Day 0, †$p<0.05$ compared to CTL, ‡$p<0.05$ compared to DEX.

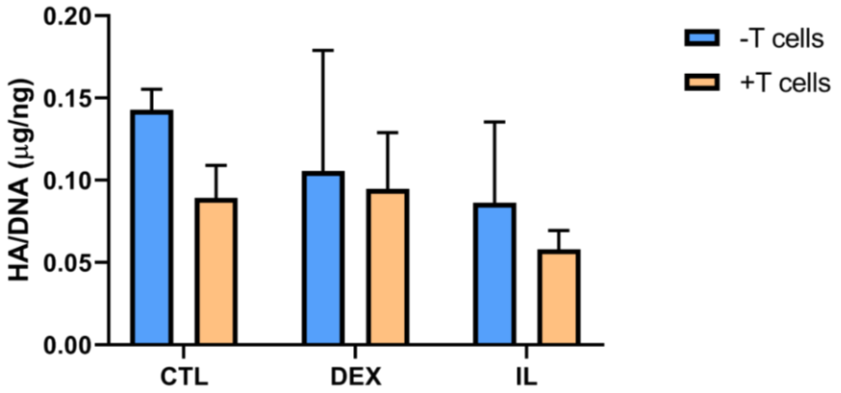

Figure 2.16 Total hyaluronan (HA) secretion of TE synovium ±T lymphocytes; (n=3-6).

Robust intimal linings (arrows) were observed in -T cell groups, with marked hyperplasia (i.e. thickened intimal cell layer) in the DEX sample **(Figure 2.17)**. Co-culture with T lymphocytes led to less of a hyperplastic response across media groups. Meanwhile immunostaining for T lymphocytes (CD3) showed that a number of these cells integrated with the intima in +T cell groups **(Figure 2.18)**.

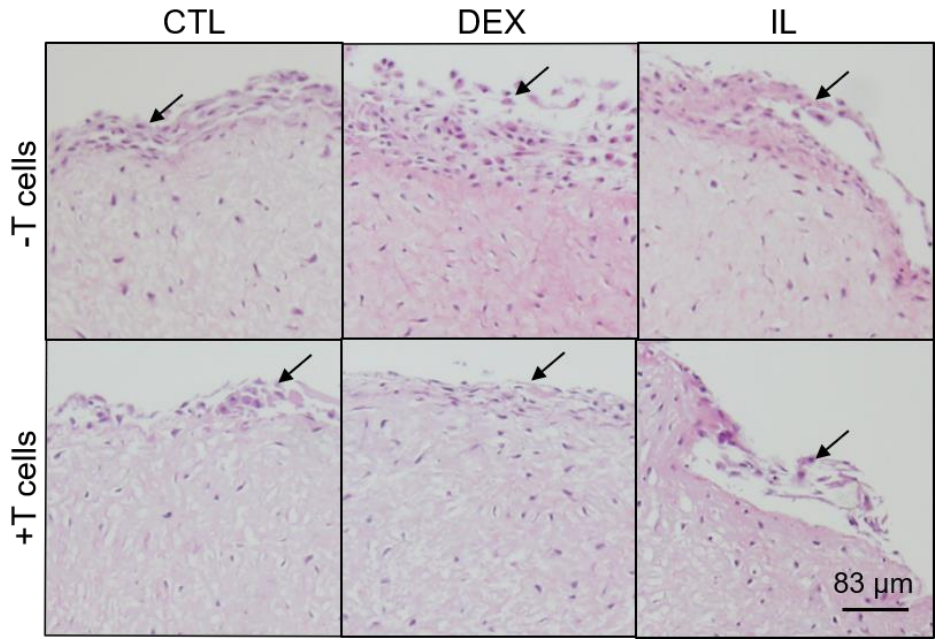

Figure 2.17 H&E of human TE synovium co-cultured with T lymphocytes. Arrows show intimal layer formation ini all groups, with a greater degree of hyperplasia in +T cell samples.

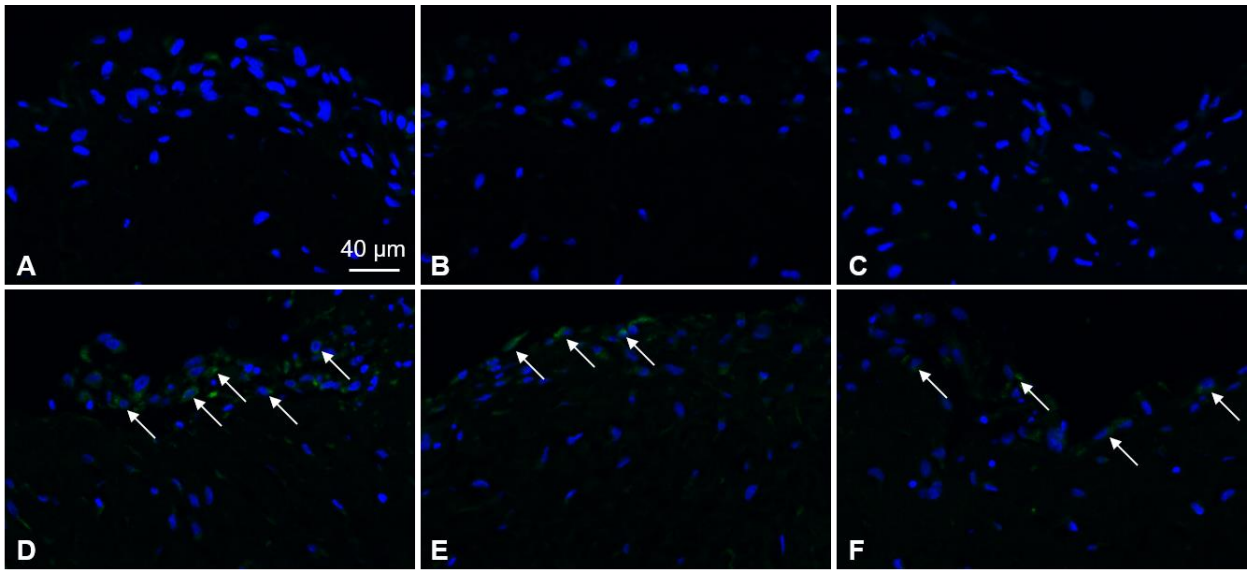

Figure 2.18 CD3 staining of human TE synovium co-cultured with T lymphocytes. **(A-C)** No T lymphocyte groups and **(D-F)** +T lymphocyte co-culture groups for **(A, D)** CTL, **(B, E)** DEX, and **(C, F)** IL treated specimens. Arrows show adherence and integration of T cells within the intimal lining of +T cell samples.

2.4.4 Discussion

The presented studies highlight a strength of the TE synovium model; with the ability to add increasing degrees of complexity, now with human-derived FLS and T lymphocytes, this model allows investigation of the role that different synovial cell populations contribute to structure-function in a more clinically relevant system (SA1d). Without T cells, human engineered synovium had similar structural characteristics to explant tissue, however HA content was not similarly modulated by IL-1 or DEX. Meanwhile, co-culture with a layer of T lymphocytes significantly altered the structural and lubricant response to IL-1 or DEX. Overall, these findings are supportive of the global hypothesis outlined for Part I, however further characterization of the human engineered synovium model and additional validation with human explant tissues need to be performed in order to clarify differences in the responses of bovine and human tissues.

In the initial analysis of T lymphocyte culture in Matrigel matrix, IL stimulation supported significantly greater cell proliferation compared to CTL or DEX conditions **(Figure 2.14)**. This is consistent with literature studies, where activation of the glucocorticoid receptor induced apoptosis in T lymphocytes (Jamieson and Yamamoto, 2000) and an activated state is required to support proliferation (Sarin et al., 1996).

In the absence of T cells, DNA content in human engineered synovium was elevated relative to CTL in both DEX and IL conditions **(Figure 2.15)**. This trend was consistent with DNA changes in bovine explant culture **(Figure 2.7D)**. Meanwhile, co-culture of engineered synovium with T lymphocytes led to the disappearance of this trend. Although T cell layers were removed from constructs prior to analysis, it was anticipated that T cells with proper cytokine stimulation (i.e. IL group) would readily proliferate, attach, and integrate with the matrix (Rocha et al., 1984; Schor, 1983), thereby contributing to overall DNA content. However, DNA content was elevated in both IL and CTL relative to DEX. T cells have been shown to bind to FLS *in vitro* (Haynes et al., 1988) and form two-way interactions with MSCs (Pober et al., 1983), and this interaction may have contributed to T cell survival in the absence of IL. This theory is supported by CD3 immunohistochemistry, which showed T cells present in the intimal lining of all three media groups **(Figure 2.18)**. However, this needs to be further evaluated, as RA models have shown that FLS do not directly affect T lymphocyte behavior and proliferation (Ohyama et al., 2002).

The human engineered synovium matured over a 3-month period, due to the lower metabolic activity of adult human cells compared to bovine. However, robust intimal linings were observed in -T cell groups, with marked hyperplasia (i.e. thickened intimal cell layer) in the DEX sample **(Figure 2.17)**. Co-culture with T lymphocytes led to a dampened hyperplastic response across media groups. Lymphocytes are thought to be drivers of synovial pannus formation, however the

cell content and distribution within the pannus structure is highly variable in native tissues (Scanzello and Goldring, 2012a). As lymphocytes are not always present in OA synovitis, it is possible that multiple mechanisms of synovial thickening exist. FLS driven hyperplasia was observed absent T cells, and T cells partially suppressed this mode of hyperplasia. At the same time, T cells integrated in the intimal lining regardless of media treatment.

Tissue dry weight significantly increased in culture for CTL+T cells and IL±T cells **(Figure 2.15)**, suggesting that although T cells were observed on DEX specimens, they likely did not contribute to a pannus-like formation. A concomitant increase in wet weight was not observed, indicating that the increased dry weight likely caused a greater degree of matrix compaction. The influence of T cell incorporation on solute transport was not evaluated here, however the engineered synovium model will facilitate these studies in the future.

Evaluating lubricant function, co-culture with T lymphocytes decreased HA secretion by approximately 28% overall, however this was unaffected by media treatment **(Figure 2.16)**. Our studies presented earlier in this chapter showed increased HA secretion in bovine tissues with both DEX and IL treatment, but MW distribution was markedly different based on media treatment **(Figure 2.6)**. It is possible that this divergence in behavior was due to the lack of HLA matching in this study, however previous work has not considered this factor (Byrne et al., 2014a; Lee et al., 2007). Both FLS and MLS express HLA-DR (Shiozawa et al., 1983), which is recognized by T cells and other leukocytes. However, HLA-DR expression may be lost in culture, as has been observed in skin fibroblasts (Branchet et al., 1992). As we observed significant proliferation in all groups, it is likely that FLS within engineered synovium also exhibited this phenotypic change and therefore did not react with mismatched T lymphocytes.

2.5 Conclusion

In this chapter, complementary engineered and explanted synovium models for evaluating changes to structure-function induced by IL-1 or DEX were described (SA1a-d). Together, we accept the hypothesis that engineered synovium can recreate structure-function of native tissue both in baseline as well as in IL-1 and DEX stimulated culture conditions. By extension, the results also support the Global Hypothesis for Part I of this dissertation **(1.1)**. First, a FLS-based engineered synovium was developed and shown to recapitulate the gross morphological, biological, and bulk functional properties of native bovine tissue **(2.2)**. This system elucidated a potential mechanism of altered solute transport in synovium; IL-1 and DEX treatment both reduced solute permeability, and this change was correlated with FLS-mediated hyperplasia and ECM synthesis. This relatively simple yet biomimetic synovium model allowed robust investigation of cellular mechanisms and macroscale tissue behavior in a controlled and repeatable system that was modified to incorporate MLS **(2.3)**. An exaggerated IL-1-induced hyperplastic response and co-localization of FLS and MLS was observed in a co-culture version of the model, highlighting the importance of MLS in synovium structure-function. Finally, the model was translated to a human system with co-cultured T lymphocytes **(2.4)**. We observed reduced intimal hyperplasia in engineered synovium co-cultured with T lymphocytes that correlated with increased specimen dry weight, suggesting an alternative T cell-mediated mechanism of hyperplasia and/or pannus formation. Overall, these studies highlight the complexity of the synovium response to IL-1 and DEX as well as the interaction of various cell types present at different stages and presentations of OA, with specific impact on synovium structure-function.

Chapter 3

Sustained Low-Dose Dexamethasone Delivery Via a PLGA Microsphere-Embedded Agarose Implant for Enhanced Osteochondral Repair

3.1 Introduction

Motivated by current limitations in osteochondral repair **(1.3.1.3)** and intra-articular DEX delivery **(1.3.3)**, as well as insights into synovium structure-function in response to IL-1 and DEX elucidated in **Chapter 2**, we sought to develop and evaluate an improved intra-articular DEX delivery strategy (SA1e-f). An optimal delivery system for sustained low (therapeutic) dose of DEX to the synovial joint is not currently available for clinical use in cartilage restoration. Toward this goal, our laboratory has demonstrated that *in vitro* local sustained DEX release from PLGA MS promotes development of functional engineered cartilage and confers protection from pro-inflammatory cytokine-induced tissue degradation (Roach et al., 2016b). Therefore, the present study was designed to provide preclinical data towards addressing a critical unmet need in orthopaedic surgery. The adult canine preclinical model was selected for its similarities to humans in patellofemoral joint pathology and presentation of pain and discomfort via changes to gait (Bendele, 2001).

To facilitate targeted drug delivery to the joint, an acellular agarose (copolymer in phase III clinical trials (Selmi et al., 2008, 2007)) hydrogel carrier with embedded DEX-loaded PLGA

microspheres (DLMS) was developed (SA1e). Drug penetration and activity was first assessed; DLMS carriers were co-cultured with engineered cartilage constructs and evaluated for $p57^{Kip2}$ expression, an indicator of glucocorticoid binding (Samuelsson et al., 1999) (Study 1a). Separately, to evaluate chondroprotection, carriers and engineered cartilage constructs were co-cultured for two weeks ± IL-1 (Study 1b). We then moved to clinically relevant osteochondral autograft transfer (OAT) for *in vivo* study (Study 2, SA1f), as it is an established procedure that may benefit from expedited host integration, support of chondrocyte growth, and reduced donor site morbidity (Sgaglione and Kerker, 2008). DLMS implants were combined with a clinically-relevant bone substrate to aid in integration (Hung et al., 2003) and press-fit into the autograft donor site and compared to intra-articular DEX injection and standard-of-care controls. The 6-month study end point was selected as the critical window for healing, integration, and cartilage restoration needed for successful functional outcomes in this preclinical model. Overall, *we hypothesized that sustained low-dose DEX delivery would have a dual anti-catabolic and pro-anabolic effect, preventing synovitis and further cartilage degeneration while simultaneously supporting the functional integrity of osteochondral autografts*.

3.2 Materials and Methods

3.2.1 Microsphere Fabrication, Characterization, and Dosing

Dexamethasone sodium phosphate (DSP; MW 516.4; Sigma D1159), a solubilized 1:1 molar equivalent of DEX (MW 392.5), was encapsulated in PLGA (75:25 lactide:glycolide, MW: 66,000-107,000; Sigma P1941) as previously described to create DLMS (Roach et al., 2016b; Rubin et al., 2009). Unloaded PLGA microspheres (ULMS) were fabricated similarly without the addition of DSP. This microsphere formulation was previously characterized (Roach, 2017).

Briefly, DLMS and ULMS had mean diameter of 46 ± 17 µm (n=543) and 25 ± 15 µm (n=411), respectively. The theoretical drug loading of DLMS was 9.1% (w/w). The actual loading capacity, determined via complete polymer hydrolysis and spectrophotometric analysis at 242 nm, was 6.3% (w/w).

To estimate proper dosing, the release profile of the microsphere formulation in agarose was characterized (Roach, 2017). Briefly, DLMS were encapsulated in 2% (w/v) agarose (Sigma; A9414) and punched into cylindrical (Ø 6 mm × 2.34 mm thickness) constructs (5.33 mg MS/ml; 350 µg MS per carrier). Constructs (n=4) were placed in individual microcentrifuge tubes with 1 ml PBS (pH 7.4), which was replaced at regular time points over 100 days. Supernatant was assayed spectrophotometrically at 242 nm and absorbance compared to a standard curve. There was an initial burst release of approximately 9.2% of the total encapsulated drug in the first 24 hours. Fitting the subsequent release data to a line over the next 99 days (R^2=0.99), an average release rate of approximately 0.9% per day was determined.

Synovial fluid volume in the canine knee (stifle) can range from <1 ml in normal animals to 3 ml or more with induced synovitis (Myers et al., 1995). Therefore, we estimated that ~1 ng DSP would be sufficient to meet the 1 nM critical threshold for chondroprotection and ~10 µg DSP to reach the upper threshold for a pro-anabolic effect (10 µM). Dosing for subsequent experiments was chosen to target this specific therapeutic window identified by Lu, et al (Lu et al., 2011).

3.2.2 Preparation and Culture of Engineered Cartilage Constructs

Articular cartilage was harvested from the knees of adult dogs (~1-year-old; n=4 joints) euthanatized for unrelated purposes. Briefly, chondrocytes were isolated via collagenase digestion,

and pooled passage 2 (P2) cells were encapsulated in agarose (2% (w/v) Type VII Agarose, Sigma A4018) to form cylindrical constructs (Ø 4 mm × 2.23 mm thickness) with an initial composition of 30 x 10^6 cells/ml (Ng et al., 2010). Constructs were initially cultured to maturity (Day 42, Young's modulus (E_Y) ~ 200kPa) in chondrogenic medium (CM) supplemented with 10 ng/ml TGFβ3 (R&D Systems #243B3200), 100 nM DEX (Sigma D4902), and 50 µg/ml ascorbic acid-2-phosphate (Sigma A8960).

At culture maturity, constructs were concentrically cored and replaced with a 2% (w/v) agarose hydrogel carrier (Ø 1.5 mm × 2.23 mm thickness) containing DLMS or ULMS (3.3 mg MS/ml) **(Figure 3.1A)**. Engineered cartilage ring-implant core (ring-core) pairs were cultured for 3 days in CM supplemented with 10 ng/ml TGFβ3 and 50 µg/ml ascorbic acid-2-phosphate (Study 1a).

For Study 1b, 2% (w/v) agarose hydrogel carriers (Ø 10 mm × 2.23 mm thickness) were encapsulated with DLMS (5.0 mg MS/ml; approximately 880 µg MS and 55 µg DSP per carrier). Mature cartilage constructs were co-cultured with the DLMS carriers for two weeks with or without application of 10 ng/ml IL-1 (recombinant human interleukin-1β; ThermoFisher PHC0816) (n=6) **(Figure 3.1B)**. To achieve the desired dosage, four hydrogel carriers were placed in a total of 25 ml media, resulting in an estimated burst delivery of 20. µg DSP (1.6 µM DEX) in the first 24 hours followed by 1.9 µg DSP (150 nM DEX) per day.

Negative DEX control carriers contained ULMS (5.0 mg MS/ml; 880 µg MS). Separately, positive controls were supplemented with 100 nM soluble DEX, which is a standard concentration for confirming chondroprotection (Lima et al., 2008c; Ng et al., 2010; Roach et al., 2016b). In each group, half of the media was replaced with fresh media 3x per week. All constructs were supplemented with TGF-β3 and ascorbic acid-2-phosphate for the entire culture period.

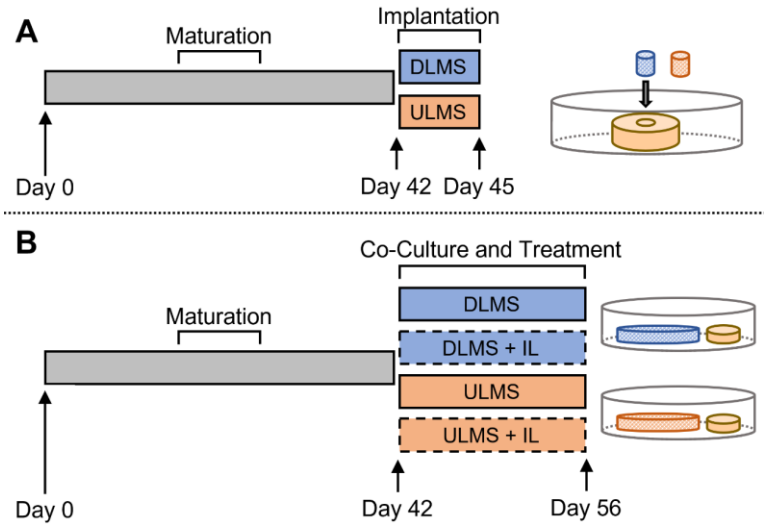

Figure 3.1 Schematic of *in vitro* dexamethasone microsphere delivery. **(A)** Following a 42-day maturation period, engineered cartilage constructs (~200 kPa) were cored and implanted with DLMS or ULMS carriers for 3 days (Study 1a). **(B)** Mature engineered cartilage constructs were divided into six experimental groups for a 14-day IL-1 stimulation period where they were co-cultured with DLMS or ULMS carriers.

3.2.3 *In Vitro* Evaluation of Delivery to Engineered Cartilage

Study 1a specimens were fixed in formalin, paraffin embedded, and sectioned (20 μm). Heat mediated epitope retrieval was performed in citrate buffer at 60°C overnight, followed by incubating in rabbit monoclonal [EP2515Y] to $p57^{Kip2}$ (Abcam; ab75974) and then goat anti-rabbit IgG secondary antibody (Alexa Fluor 488; ThermoFisher; A11034). Pixel intensity was analyzed to quantify cell DEX uptake radially away from the core (ImageJ).

For Study 1b, Young's (E_Y) and dynamic (G) moduli were measured under unconfined compression conditions (Mauck et al., 2000). Following mechanical testing, individual specimens were processed and assayed for DNA, GAG, and collagen, as previously described **(2.2.2.6)**. Values were normalized to specimen wet weight (ww). Half of each specimen was fixed in formalin and subsequently embedded in paraffin, sectioned (8 μm), and stained with safranin-o.

Resulting images were processed in ImageJ (convert to 8-bit, invert black and white) and relative pixel intensity quantified using the "plot profile" function.

3.2.4 Preclinical Canine Osteochondral Autograft Model

In preparation for the Study 2 procedure, devitalized bovine trabecular bone cores (Ø 8 mm x 5 mm thickness) were infused with 2% (w/v) agarose hydrogel mixed with DLMS (33 mg MS/ml; 3.3 mg MS and 210 µg DSP per carrier) to produce multilayered acellular osteochondral implants (1 mm gel-only region, 1 mm gel bone interface, and 4 mm bone-only) **(Figure 3.2, iii)**. From release studies, this was expected to deliver a 24-hour burst of 19 µg DSP (15-75 µM DEX; assuming 0.5-2.5 ml volume (Nade and Newbold, 1983)) per implant followed by 1.8 µg DSP (1.4-7.0 µM DEX; assuming 0.5-2.5 ml volume) per implant per day. To confirm expected release, extra implants (n=4) were placed in PBS and supernatant was collected and assayed (**3.2.1)**.

On the day of surgery, adult mongrel dogs (10 ± 1 months, 25.3 ± 3.5 kg, all female) were premedicated, anesthetized and prepared for aseptic surgery of the right knee (University of Missouri-Columbia IACUC #9167; complied with ARRIVE guidelines). Briefly, 2 doses of cefazolin (antibiotic) were given perioperatively and 2 morphine intramuscular doses plus 2 doses of oral tramadol were given for pain management. Post-operatively, a soft padded bandage was kept on the operated right hindlimb for 1 week with oral cefpodoxime (antibiotic) for 10 days.

Osteochondral autografts (Ø 8 mm diameter) **(Figure 3.2, ii)** were obtained from the trochlear ridge and sulcus terminalis and transferred to size-matched recipient defects on the neighboring trochlea or medial/lateral femoral condyle of the same knee (n=3 grafts per knee) using the Osteochondral Autograft Transfer System® (OATS®; Arthrex, Naples, FL). The empty graft donor sites **(Figure 3.2, i)** were filled with press-fit DLMS-loaded implants (OATS-DLMS;

n=6 animals, n=3 implants per animal). Dogs receiving this implant were compared to those for which there was one post-surgical DEX injection of 4 mg/knee (OATS-INJ; n=5 animals, n=3 grafts per animal; no implant) or no DEX injection (OATS-CTL; n=5 animals, n=3 grafts per animal; no implant).

Possible systemic effects of dexamethasone were assessed by daily monitoring by veterinarians, animal weights, and post mortem examination (necropsy).

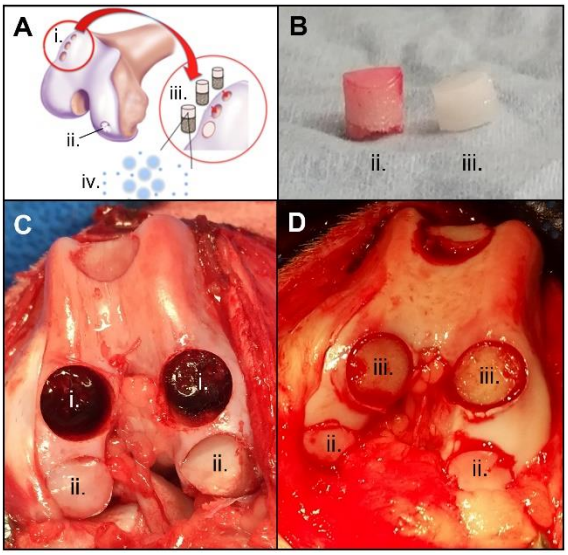

Figure 3.2 Schematic of *in vivo* OATS procedure with DEX implant. **(A)** Autograft donor site (i.), autograft repair site (ii.), DLMS implant (iii.), and dexamethasone-PLGA microsphere release (iv.); **(B)** cartilage autograft (ii.) and DLMS implant (iii.); **(C)** autograft donor (i.) and repair (ii.) sites; **(D)** Repair (ii.) and DLMS implant (iii.) sites.

3.2.5 Clinically Based Assessments

Animals were examined by a board-certified veterinary orthopaedic surgeon (JLC). Clinical lameness, functional gait, comfortable range of motion (CROM), pain, and effusion (Bozynski et al., 2015) were assessed both pre-surgery (T=0) and at the conclusion of the study period (T=6 months). Synovial fluid composition was assessed at monthly intervals (T=0, 1, 2, 3 months) with

a Luminex Multiplex Assay for IL-6 (Stannus et al., 2010), IL-8 (Lotz et al., 1992), MMP-2 (Duerr et al., n.d.), and MMP-3 (Okada et al., 1992) (ThermoFisher).

3.2.6 Histological Scoring

At the terminal time point (T=6 months), animals were sacrificed and tissue harvested for histopathology assessment. Osteochondral treatment sites including adjacent cartilage and bone were collected, fixed in formalin, and stained with H&E, picrosirius red, and toluidine blue. Synovium was harvested from four separate locations (medial/lateral trochlea and medial/lateral femoral condyle), fixed in formalin, and stained with H&E.

A modified osteochondral (OC) scoring system was used to evaluate the autograft recipient sites (Chang et al., 2014). The scoring consisted of evaluating cartilage fill, cartilage edge integration at host-graft junction, cartilage surface congruity of construct and host-construct junction, fibrosis, and inflammation.

A modified OARSI method was used to evaluate surrounding cartilage structure, chondrocyte pathology, proteoglycan staining, collagen integrity, tidemark, and subchondral bone plate (Cook et al., 2010). The OARSI method was also used to evaluate synovial pathology through microscopic examination of the lining cell, lining, and cell infiltration characteristics (Cook et al., 2010). All scoring was performed by two blinded board-certified veterinary pathologists.

DLMS implants were scanned using Micro-CT at T=0 and T=6 months to assess changes to bone fill and structure at the donor site as previously described (Liu et al., 2007).

3.2.7 Statistics

Data sets were tested for normality (Kolmogorov-Smirnov Test) and homogeneity (Bartlett's Test). When necessary, data was log-transformed to achieve normality or evaluated using equivalent nonparametric tests. For *in vitro* studies, one-way ANOVA with Tukey post hoc test (α=0.05) was used. For the *in vivo* study, functional and synovial fluid measures were compared using two-way ANOVA or corresponding mixed-effects analysis (group, time) with time as a repeated measures factor and Tukey post-hoc test (α=0.05). This data was presented as mean and standard deviation, unless otherwise noted. Analyses were performed using GraphPad Prism 8.

Ordinal scores (OARSI and OC) were analyzed using a Generalized Linear Model. Specifically, data was fit to an ordinal multinomial probability distribution and cumulative logit link function with generalized estimating equations correction for repeated measures (location, scorer). The dependent (response) variable was the score and the independent variables (predictors) were the categorical factors: group and/or repair location. Total OARSI scores were grouped into ordered categories for regression analysis to increase the number of observations per level of the dependent variable. Odds ratios (OR) and corresponding 95% CI were computed from the model's parameter estimates. Averages of non-normal datasets were presented as median (95% CI). Ordinal regression analyses were performed using IBM SPSS Statistics 25. The results of a pilot study were used to determine the sample size needed in Study 2 to achieve at least 80% power with G*Power 3 (α=0.05) (Faul et al., 2007).

3.3 Results

3.3.1 *In Situ* Evaluation of DEX Receptor Binding (Study 1a)

Cells in the surrounding cartilage ring were exposed to a radially-dependent concentration of DEX, with cartilage immediately adjacent to the DLMS-laden core expressing the most intense staining for $p57^{Kip2}$ that declined toward the edge of the construct **(Figure 3.3)**. In contrast, for ULMS constructs, mean intensity of the stain remained at baseline levels.

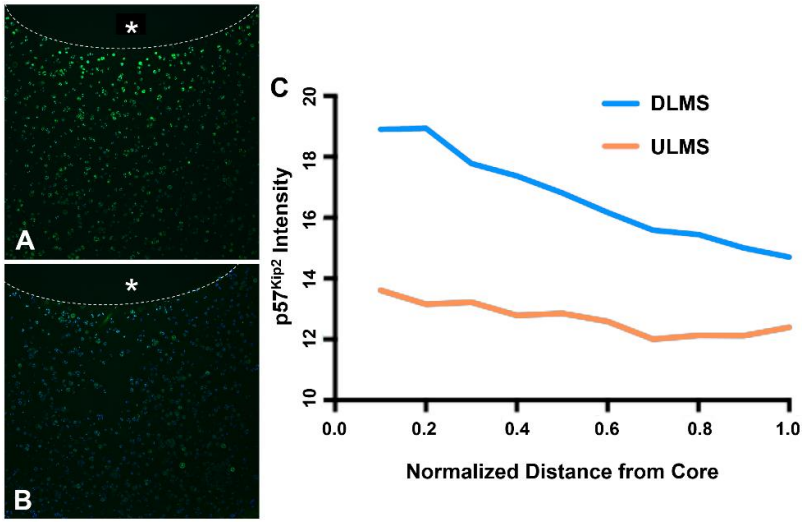

Figure 3.3 Dexamethasone penetration indicated by p57Kip2 expression. Representative immunohistochemical stain for $p57^{Kip2}$ expression (green) counterstained with DAPI. Inner core containing either **(A)** DLMS or **(B)** ULMS marked with * and boundary outlined with dotted line; **(C)** Relative pixel intensity of immunohistochemical stain expression as a function of distance away from the microsphere-embedded core (n=1).

3.3.2 *In Vitro* Chondroprotection (Study 1b)

At day 42, Young's modulus (E_Y) of the engineered cartilage constructs was 213 ± 29 kPa **(Figure 3.4A)**. Following the 14-day treatment period (day 56), E_Y of ULMS+IL specimens was significantly lower than ULMS (247 vs. 141 kPa; between-group difference, 106 kPa; p=0.048).

Meanwhile, E_Y was not significantly affected by IL insult in DLMS (256 vs. 197 kPa; between-group difference, 59.0 kPa; p=0.92). No significant between-group differences were observed in dynamic modulus (G) **(Figure 3.4B)**.

GAG/ww reached 5.5 ± 0.6% by day 42 **(Figure 3.4C)**. Following the 14-day treatment period, GAG/ww of ULMS+IL specimens was significantly lower than ULMS (5.8 vs. 4.3%; between-group difference, 1.5%; p<0.001). GAG distribution was markedly more diffuse in the periphery of ULMS and IL groups **(Figure 3.5)**. Safranin-O intensity was similar between groups at depths greater than ~150 μm. Meanwhile, GAG/ww was not significantly affected by IL insult in DLMS (6.1 vs. 5.9%; between-group difference, 0.2%; p=1.0) **(Figure 3.4C)**. GAG/ww in the DLMS+IL group was significantly greater than ULMS+IL (p<0.0001).

COL/ww was not significantly affected by IL insult, however DLMS had significantly lower content than ULMS (p=0.022) and day 42 (p<0.001) **(Figure 3.4D)**.

Positive controls for DEX protection (i.e. soluble DEX) confirmed maintenance of E_Y, G, GAG, and COL (data not shown).

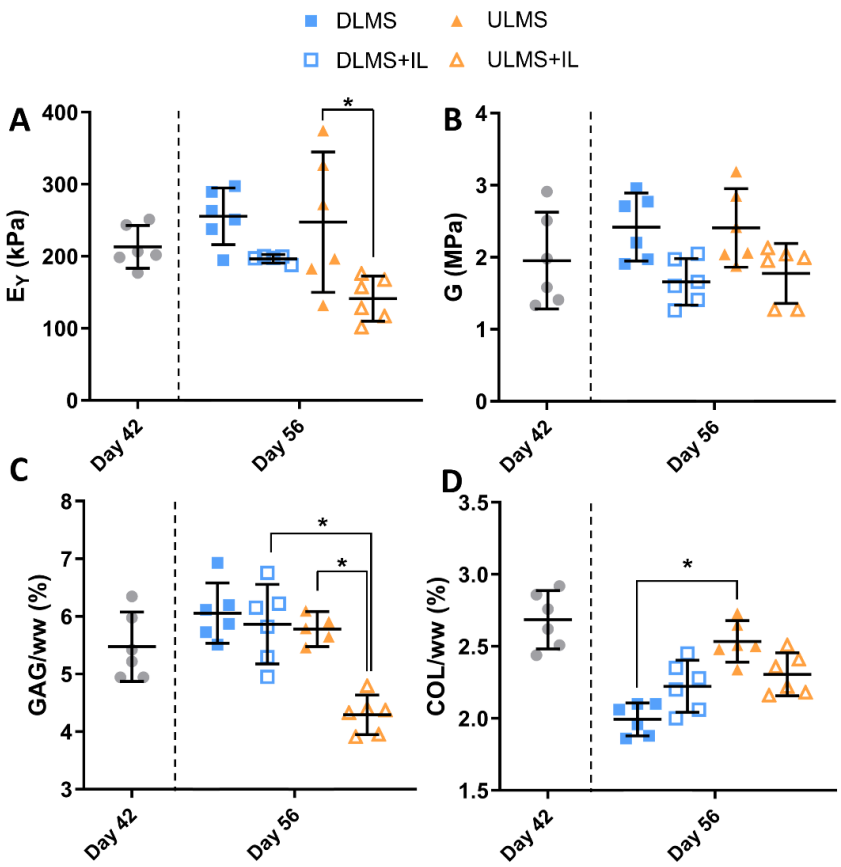

Figure 3.4 Mechanical and biochemical properties of engineered cartilage. **(A)** Young's modulus (E_Y); **(B)** Dynamic modulus (G); **(C)** GAG/ww (%); **(D)** COL/ww (%); *p<0.05. (bars show mean and 95% CI)

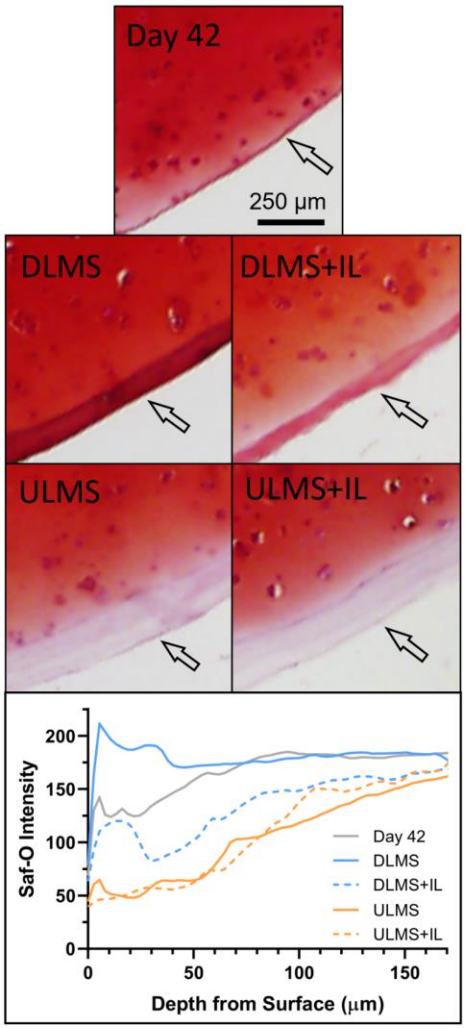

Figure 3.5 Representative safranin-o (saf-o) histology of cartilage construct cross-section at the surface (arrow) and corresponding relative staining intensity.

3.3.3 Confirmation of DLMS Implant Release Profile (Study 2)

A burst release of 64 µg DSP was observed in the first 48 hours. Fitting the subsequent release data to a line (R^2=0.98) over the next 8 days, a daily release rate of 1.4 µg DSP per day (95% CI, 1.1 to 1.6 µg DSP per day).

3.3.4 Clinically Based Assessments of *In Vivo* OATS Repairs (Study 2)

Gait was significantly worse at 6 months compared to baseline in OATS-CTL (p=0.031) and INJ (p=0.008) groups **(Table 3.1)**. Meanwhile, gait score was similar to baseline in DLMS specimens (p=0.39). Lameness was elevated in CTL compared to both DLMS (1.8 vs. 1.3; between-group difference, 0.5; p=0.099) and INJ (1.8 vs. 1.4; between-group difference, 0.4; p=0.20).

We did not observe significant between-group differences in animal's change in weight at the 6-month time point.

Table 3.1 Clinical outcome scores of OATS repairs at 6 months; *p<0.05, **p<0.01, ***p<0.001, ****p<0.0001

	Mean (95% CI)	**Mean Difference from Baseline (95% CI)**		
Measurement	**Baseline**	**OATS-CTL (N=5)**	**OATS-DLMS (N=6)**	**OATS-INJ (N=5)**
Gait	10.0 (10.0 to 10.0)	-2.9 (-5.5 to -0.2)*	-1.3 (-3.7 to 1.1)	-3.6 (-6.2 to -0.9)**
CROM (°)	108 (107 to 109)	-12 (-20 to -4)**	-8 (-15 to -0.0)*	-9 (-17 to -1)*
Lameness	0.0 (0.0 to 0.0)	1.8 (1.2 to 2.4)****	1.3 (0.8 to 1.9)****	1.4 (0.8 to 2.0)****
Pain	0.0 (0.0 to 0.0)	1.3 (0.2 to 2.4)*	1.1 (0.2 to 2.1)*	1.0 (0.0 to 2.1)
Effusion	0.0 (0.0 to 0.0)	2.0 (0.9 to 3.0)***	1.8 (0.9 to 2.8)***	1.3 (0.3 to 2.4)*

OATS, osteochondral autograft transfer system; CTL, no dexamethasone supplementation group; DLMS, dexamethasone-loaded microsphere implant group; INJ, dexamethasone injection group

3.3.5 Histological Assessment of OATS Repairs (Study 2)

Cartilage was visually intact in each group, with some evidence of lesions in OATS-INJ specimens **(Figure 3.6A-C)**. The combined OARSI cartilage score of DLMS specimens were more than twice as likely to be improved compared to CTL (p=0.003), but there was not a significantly increased likelihood compared to the INJ group (p=0.47) **(Table 3.2)**. OC scores, which specifically evaluated the graft-host junction, showed little pathology across groups **(Table 3.3)**.

Examining sub-scores **(Table 3.2)**, DLMS were nearly three times more likely to have better chondrocyte scores and more than three times more likely to have better proteoglycan sub-scores than both CTL (p=0.001 and 0.005, respectively) and INJ (p=0.078 and 0.048, respectively). Meanwhile, INJ was not significantly likely to differ from CTL in chondrocyte or proteoglycan score (p=0.92 and 0.95, respectively). Superior proteoglycan deposition in DLMS samples was evident from toluidine blue staining as well **(Figure 3.6G-I).**

DLMS were more than twice as likely to have a better collagen sub-score than both CTL (p=0.001) and INJ (p=0.068), which was further evidenced in picrosirius red staining **(Figure 3.6J-L)**. Collagen pathology in INJ was not significantly likely to differ from CTL (p=0.82).

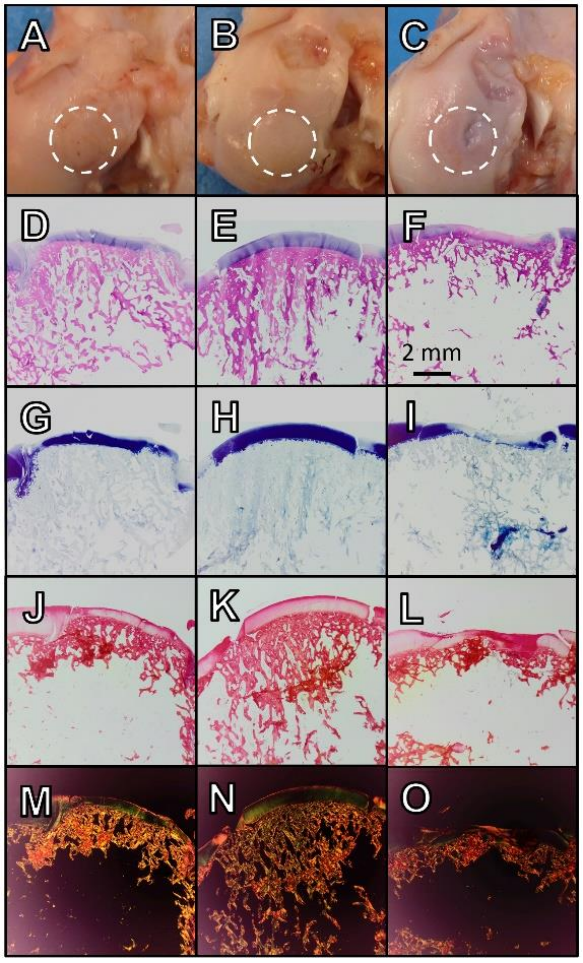

Figure 3.6 Gross imaging and histological staining for selected graft sites. **(A-C)** Gross morphology; **(D-F)** H&E; **(G-I)** Toluidine blue; **(J-L)** Picrosirius red; **(M-O)** Polarized light microscopy; OATS-CTL (A, D, G, J, M; 92-FCL), OATS-DLMS (B, E, H, K, N; 88-FCL), OATS-INJ (C, F, I, L, O; 112-FCL).

Table 3.2 OARSI cartilage scores and sub-scores; *p<0.05, **p<0.01, ***p<0.001

	Median (95% CI)			Odds Ratio (95% CI)		
Measurement	**OATS-CTL (N=5)**	**OATS-INJ (N=5)**	**OATS-DLMS (N=6)**	**INJ vs. CTL**	**DLMS vs. CTL**	**DLMS vs. INJ**
OARSI (Cartilage, combined)	12 (9 to 17)	12 (7 to 15)	8 (6 to 12)	1.3 (0.6 to 2.7)	2.2 (1.3 to 3.6)**	1.6 (0.7 to 3.7)
Structure	2 (2 to 3)	2 (1 to 3)	2 (1 to 3)	1.8 (0.9 to 3.5)	1.5 (0.9 to 2.8)	0.9 (0.4 to 2.0)
Chondrocytes	4 (2 to 4)	4 (2 to 4)	2 (1 to 3)	1.1 (0.4 to 3.2)	2.7 (1.5 to 5.1)**	2.6 (0.9 to 7.4)
Proteoglycans	3 (2 to 4)	3 (1 to 4)	2 (1 to 2)	1.0 (0.3 to 3.5)	3.3 (1.4 to 7.5)**	3.4 (1.0 to 11.4)*
Collagen	2 (1 to 3)	2 (1 to 3)	1 (1 to 2)	1.1 (0.4 to 2.9)	2.8 (1.5 to 5.1)**	2.5 (0.9 to 6.8)
Tidemark	1 (0 to 2)	0 (0 to 2)	0 (0 to 2)	1.8 (1.2 to 2.8)**	1.7 (1.1 to 2.8)*	1.0 (0.6 to 1.4)
Bone	1 (0 to 3)	0 (0 to 3)	3 (0 to 3)	1.1 (0.6 to 2.4)	0.7 (0.2 to 2.1)	0.6 (0.2 to 1.8)

OATS, osteochondral autograft transfer system; CTL, no dexamethasone supplementation group; DLMS, dexamethasone-loaded microsphere implant group; INJ, dexamethasone injection group

Table 3.3 OC scores.

	Median (95% CI)		
Measurement	**OATS-CTL (N=5)**	**OATS-DLMS (N=6)**	**OATS-INJ (N=5)**
OC (Total)	2 (1 to 4)	2 (1 to 3)	2 (1 to 3)
Fill	0 (0 to 0)	0 (0 to 0)	0 (0 to 0)
Edge Integration	1 (1 to 1)	1 (1 to 1)	1 (1 to 1)
Surface Congruity	0 (0 to 1)	1 (0 to 1)	0 (0 to 1)
Calcified Cartilage	0 (0 to 1)	0 (0 to 0)	0 (0 to 1)
Fibrosis	0 (0 to 1)	0 (0 to 1)	0 (0 to 1)
Inflammation	0 (0 to 0)	0 (0 to 0)	0 (0 to 0)

OATS, osteochondral autograft transfer system; CTL, no dexamethasone supplementation group; DLMS, dexamethasone-loaded microsphere implant group; INJ, dexamethasone injection group

3.3.6 Modulation of In Vivo Inflammatory Environment (Study 2)

Synovial fluid IL-6 levels peaked at 1 month in each group ($p<0.01$) **(Figure 3.7)**. The concentration of IL-6 at 1-month was significantly elevated in the OATS-DLMS group relative to CTL ($p=0.004$) and INJ ($p=0.011$). Significant differences were not detected in IL-8 levels.

MMP-2 was elevated at 1 month and remained significantly elevated at 3 months in all groups ($p<0.001$). MMP-3 levels peaked at 1 month in the DLMS group only ($p=0.012$). By 2 months, MMP-3 levels in DLMS had returned to baseline ($p=0.78$). The concentration of MMP-3 was significantly elevated in the DLMS group relative to CTL ($p=0.009$) and INJ ($p=0.008$) at the 1-month time point. No significant differences were observed in OARSI synovium scores, which were largely in the range of mild to moderate pathology **(Figure 3.8, Table 3.4)**.

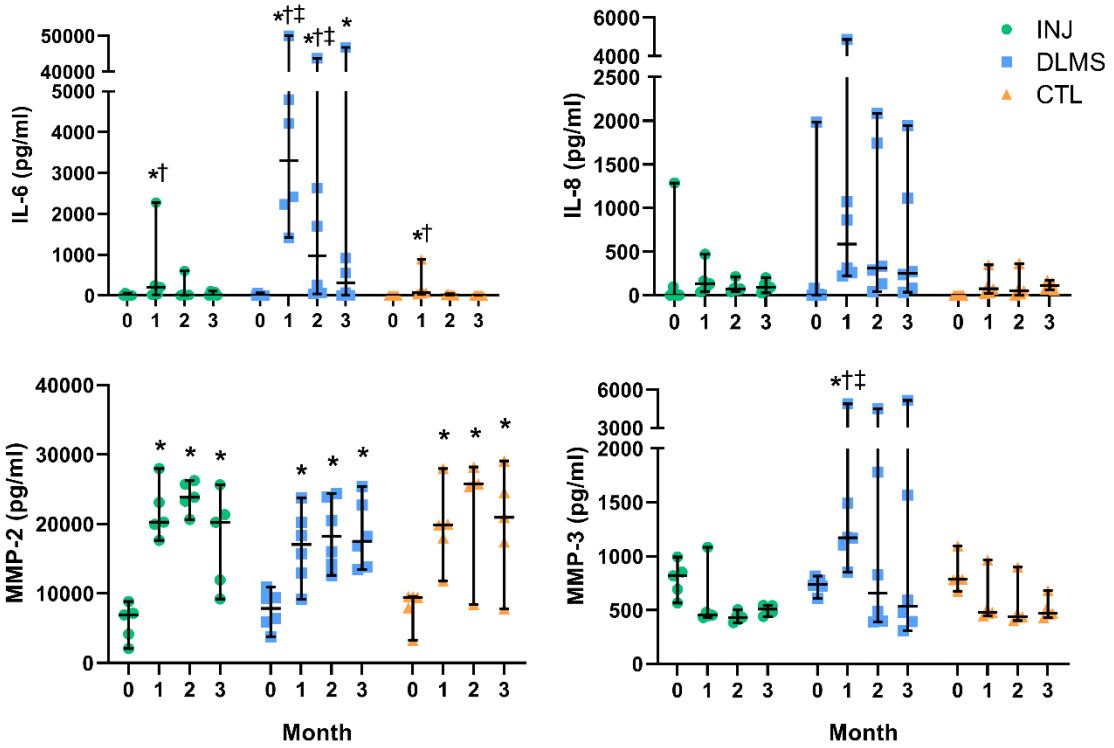

Figure 3.7 Synovial fluid composition of IL-6, IL-8, MMP-2, and MMP-3. *$p<0.05$ compared to Day 0 (same group), †$p<0.05$ compared to OATS-CTL (same time point), ‡$p<0.05$ compared to OATS-INJ (same time point). (bars show median and 95% CI)

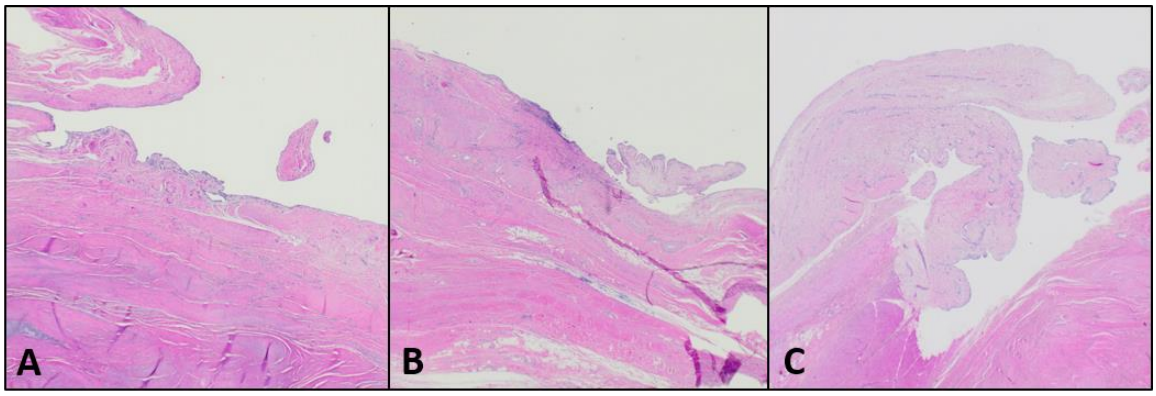

Figure 3.8 Representative synovium H&E. Mild to moderate synovitis was observed in **(A)** CTL (ID-92), **(B)** DLMS (ID-88), **(C)** INJ (ID-112) animals.

Table 3.4 Histological scoring of the synovium (OARSI).

	Median (95% CI)		
Measurement	**OATS-CTL (N=5)**	**OATS-DLMS (N=6)**	**OATS-INJ (N=5)**
OARSI (Synovium Total)	7 (5 to 9)	7 (6 to 11)	8 (6 to 10)
Lining Cells	2 (1 to 3)	2 (1 to 3)	3 (2 to 3)
Lining Characteristics	3 (3 to 5)	4 (2 to 5)	4 (3 to 4)
Cell Infiltration	1 (0 to 2)	2 (1 to 3)	1 (1 to 2)

OATS, osteochondral autograft transfer system; CTL, no dexamethasone supplementation group; DLMS, dexamethasone-loaded microsphere implant group; INJ, dexamethasone injection group

3.3.7 Evaluation of DLMS Implant in Donor Sites

Micro-CT reconstructions of the DLMS implant bone bases revealed significant bone fill-in and ingrowth **(Figure 3.9)**. Specifically, bone volume density (BV/TV) of the bone scaffold increased 17 ± 23% over the implantation period ($p=0.009$). There was also a significant decrease in plate-rod (PR) ratio ($p<0.001$).

Representative histology of the graft donor site, which also served as the DLMS implant site, showed a degree of fibrous tissue formation in CTL and INJ groups **(Figure 3.10)**.

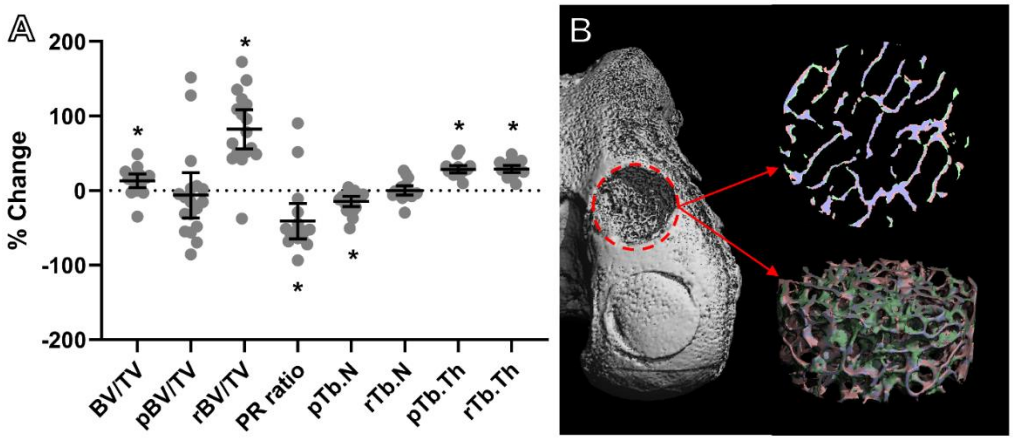

Figure 3.9 MicroCT reconstruction of autograft donor site. **(A)** Significant bone remodeling in the DLMS osteochondral implant; Bone volume density (BV/TV), plate density (pBV/TV), rod density (rBV/TV), plate-rod ratio (PR ratio), number of plate trabeculi (pTb.N), number of rod trabeculi (rTb.N), plate trabecular thickness (pTb.Th), and rod trabecular thickness (rTb.Th); **(B)** Reconstruction of DLMS bone base showing resorbed bone (pink), new bone (green), and unchanged bone (blue); *$p<0.05$ vs. baseline.

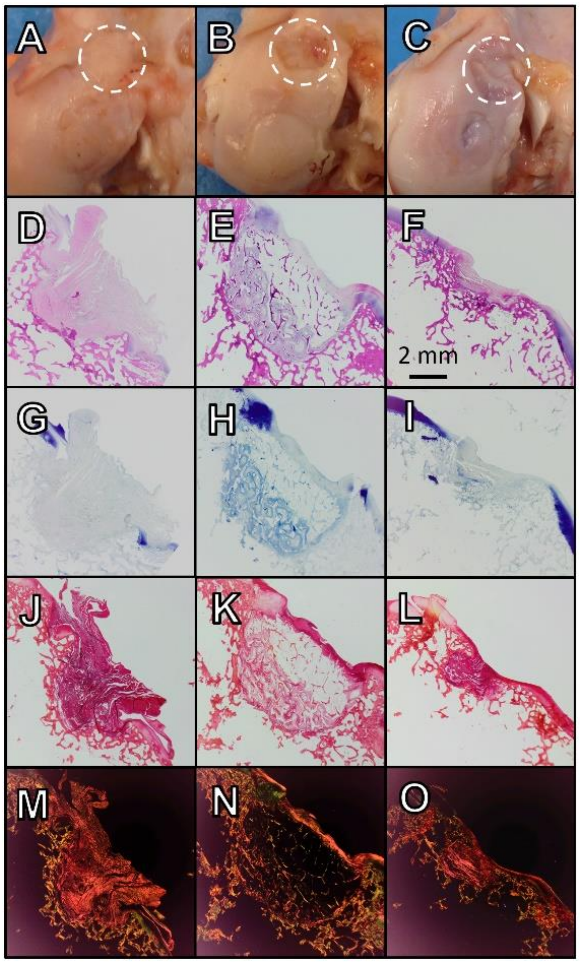

Figure 3.10 Gross imaging and histological staining for selected graft donor sites. **(A-C)** Gross morphology; **(D-F)** H&E; **(G-I)** Toluidine blue; **(J-L)** Picrosirius red; **(M-O)** Polarized light microscopy; OATS-CTL (A, D, G, J, M; 92-FCL), OATS-DLMS (B, E, H, K, N; 88-FCL), OATS-INJ (C, F, I, L, O; 112-FCL).

3.4 Discussion

The current study examined the influence of targeted, sustained low-dose DEX delivery, via PLGA microspheres embedded in an acellular agarose carrier, on suppressing synovial inflammation and promoting growth and repair of neighboring focal articular cartilage injuries (SA1e-f). While periodic intra-articular glucocorticoid injections have long been used to manage joint inflammation and pain (Cederlöf and Jonson, 1966), only recently have they been proposed as an early

intervention aimed at dampening the inflammatory cascade following joint injury and surgical repair (Grodzinsky et al., 2017; Heard et al., 2015; Huebner et al., 2014). To overcome issues with low residence time and negative local and systemic effects, MS glucocorticoid delivery platforms have entered development. One product, an already FDA-approved intra-articular microsphere injection of triamcinolone acetonide (TA), has demonstrated extended local drug release and improvements in pain, however no impact on tissue integrity (Bodick et al., 2015; Kraus et al., 2018; Spitzer et al., 2019). We anticipated that DEX, due to its elevated anti-inflammatory potency relative to TA (Buttgereit et al., 2002) and demonstrated strong pro-anabolic effects in cartilage cultures at low doses (Bian et al., 2010; Grodzinsky et al., 2017; Ng et al., 2010), would be a prime candidate to expedite and augment cartilage repair and restoration procedures that can be limited by graft durability and viability (Gomoll et al., 2012; Nover et al., 2015; Sgaglione and Kerker, 2008) as well as iatrogenic injury (Amin et al., 2017; Hooiveld et al., 2003; Sgaglione and Kerker, 2008). Overall, we accept our hypothesis that the DLMS implant provides chondroprotection and improved functional osteochondral integrity in both an *in vitro* cytokine-challenged environment (Study 1, SA1e) and a preclinical model of cartilage restoration surgery (Study 2, SA1f). However, results were inconclusive as to whether the DLMS implant directly affected synovial structure-function.

Study 1a confirmed DEX bioavailability not only to the bathing media (i.e. joint space), but also directly to the adjacent dense cartilage matrix. Glucocorticoid receptor binding, indicated by $p57^{Kip2}$ expression, demonstrated a radially-dependent concentration of DEX, with cartilage immediately adjacent to the DLMS-laden core expressing the most intense staining that declined toward the edge of the construct **(Figure 3.3)**. This local delivery rendered special targeting mechanisms, such as conjugating with avidin (Bajpayee et al., 2017), unnecessary.

In Study 1b, engineered cartilage derived from adult canine chondrocytes reached native levels for Young's modulus, dynamic modulus, and GAG content by day 42 in culture (Ng et al., 2010). And as anticipated, E_Y and GAG/ww were not significantly affected by IL insult in the DLMS group, indicating that the carrier was chondroprotective to these mature constructs *in vitro*. Meanwhile, specimens without DEX supplementation (ULMS), a positive control for IL-induced cartilage degradation (Roach et al., 2016b), decreased significantly in E_Y and GAG content when subjected to IL insult. ULMS+IL specimens had significantly lower E_Y than ULMS, which was likely due to the significant decrease in GAG/ww **(Figure 3.4A, C)** in the periphery of the constructs **(Figure 3.5)**. Cytokine treatment did not significantly decrease collagen content in IL-treated groups, regardless of DEX treatment, which is consistent with literature studies of two-week cytokine stimulation of engineered and explanted cartilage tissues (Lima et al., 2008c; Andrea R Tan et al., 2015).

Interestingly, constructs grown with DLMS in the absence of IL had a significant decrease in collagen content (%COL/ww). This was partially a byproduct of higher GAG content (i.e. wet weight) in the DLMS group, however absolute levels of collagen were still approximately 20% below pre-treatment values. In the absence of cytokines, adult cartilage explants are generally able to maintain mechanical and biochemical properties in culture regardless of DEX treatment (Bian et al., 2010). However in juvenile engineered tissues, there is evidence that collagen deposition later in culture can be higher without DEX (Lima et al., 2008c). It is possible that DEX levels accumulated too quickly *in vitro* and approached a deleterious level. DLMS groups ostensibly had variable DEX concentrations, which were dependent on release kinetics and media volume (estimated to be 1.6 μM DSP in the first 24 hours followed by 150 nM DSP per day) as well as drug clearance (half of media replaced 3x per week). However, even with accumulated DEX over

the course of the two week culture, concentrations likely remained at least an order of magnitude below the peak seen in a clinical setting (7.7 mM; based on 4 mg, 1 ml injection (Cardone, 2002)).

In Study 2, DLMS carriers were formulated to deliver an estimated burst release of 15-75 µM DSP in the first 24 hours followed by 1.4-7.0 µM DSP per carrier per day (based on estimated 0.5-2.5 ml synovial fluid volume). An *in vitro* release study of actual DLMS implants confirmed this estimate. While it is anticipated that *in vivo* release kinetics would be expedited compared to *in vitro* (Doty et al., 2017), studies have shown that extended *in vivo* release (at least 70 days) still occurs (Doty et al., 2017; Rudnik-Jansen et al., 2017). For PLGA-DEX microspheres, *in vitro* release is predictive of *in vivo* release kinetics (Zolnik and Burgess, 2008). Although expected to at times be higher than minimum values established to be chondroprotective (1 nM-10 µM) (Lu et al., 2011), we anticipated that concentrations would remain well below deleterious levels. The total dosage used in this study was estimated to be 0.63 mg DSP (3 implants per knee), whereas clinical injections contain 4 mg DSP.

At the terminal time point, the OATS-DLMS group showed superior knee function based on return to pre-surgery gait scores and improved lameness grades. Between-group differences in pain were not observed, likely due to the fact that OAT procedures are generally successful in restoring joint function (Ma et al., 2004). Further benefits of low dose DEX were observed in OARSI cartilage score, with DLMS specimens more than twice as likely to be improved compared to controls. Examining sub-scores, DLMS were nearly three times more likely to have better chondrocyte scores and more than three times more likely to have better proteoglycan sub-scores than both CTL and INJ. This supported the results of Study 1b, which showed enhanced GAG/ww in the DLMS group.

In our studies, DLMS and ULMS had mean diameters of approximately 25 µm and 46 µm, respectively, which were similar to TA-loaded PLGA MS products on the market administered via intra-articular injection (Kumar et al., 2012). In advanced OA patients, these TA-MS injections provided better pain relief and longer joint residence time than bolus TA injection (Kraus et al., 2018; Spitzer et al., 2019). However, TA-loaded MS did not affect cartilage pathology in this clinical trial (Spitzer et al., 2019) or an *in vivo* rat model of OA (Rudnik-Jansen et al., 2017). This may have been a result of TA toxicity; TA has been reported to be toxic to chondrocytes (Euppayo et al., 2016) and to significantly decrease the proliferative rate and inhibit chondrogenic differentiation at an equivalent DEX level established to be chondroprotective (1 µM TA ≈ 200 nM DEX) (Lu et al., 2011; Weiss et al., 1988). Alternatively, free floating MS in the joint space may have led to increased joint friction and cartilage wear (Estell, 2018). End point histological analyses of rats did not show visible TA-MS (Rudnik-Jansen et al., 2017), indicating that free-floating MS may not remain in place. To prevent this, our DLMS implant was composed of agarose-encapsulated MS. Furthermore, DLMS carriers were constructed on a bone scaffold base to aid integration **(Figure 3.2)**, ensuring that the carriers remained in place for the duration of the study **(Figure 3.10)**. It is also anticipated that by suspending MS in agarose, the effect of small variations in MS diameter and local pH changes would be mitigated.

DLMS were more than twice as likely to have a better collagen sub-score than both CTL and INJ, which was further evidenced by pronounced picrosirius red staining. While contrary to the results of Study 1b, DEX at 100 nM is known to promote the osteoblast phenotype and *in vivo* bone formation by transplanted human osteoblasts on collagen sponges (Yamanouchi et al., 2001). It should also be emphasized that *in vitro* studies were based only on activities of chondrocytes

seeded into the construct, whereas *in vivo* experiments incorporated the contributions of a complex milieu of other joint tissues, including synovial- and bone marrow-derived stem and immune cells.

Meanwhile, chondrocyte and proteoglycan scores were not significantly likely to differ from CTL in the high dose DEX group (OATS-INJ). In a rabbit PTOA model, frequent injections of high dose DEX were chondroprotective over three weeks but had severe systemic side effects, including weight loss and organ necrosis (Huebner et al., 2014). We did not observe significant weight gain or loss for any dog in the study and necropsy results showed no evidence for systemic pathology. Furthermore, neither impairment of healing nor infections were observed in our studies, each of which can be undesired side effects of glucocorticoids (Sherman et al., 2015).

Micro-CT reconstructions of the DLMS implants showed significant bone fill and ingrowth of donor sites with increasing trabecular bone density over the implantation period. Histologic assessment of donor sites also revealed improved donor site tissue fill and architecture compared to injection and control groups. These findings have important clinical significance in terms of their potential for reducing donor site morbidity, which is still a significant concern associated with OAT (Andrade et al., 2016; Shimozono et al., 2019). As such, this apparent dual benefit of the DLMS implants in terms of supporting cartilage restoration while also addressing potential donor site morbidity further enhances the attraction for clinical use. Other DEX delivery methods, such as an intra-articular DLMS patch, are also feasible if concerns regarding donor site morbidity persist or if other cartilage restoration techniques, such as OCA, ACI, or MACI, are selected.

Cytokine levels in the synovial fluid were inconclusive regarding a potential anti-inflammatory effect. Counterintuitively, both IL-6 and MMP-3 concentrations were increased at the 1-month time point in the OATS-DLMS group relative to CTL and INJ **(Figure 3.7)**. While elevated levels of these markers are typically associated with inflammation and arthritis

(Gaissmaier et al., 2008; Rose and Kooyman, 2016), in our study they were paired with the relative absence of synovitis and improved cartilage tissue quality in DLMS groups. IL-6 has been implicated as an anti-inflammatory mediator in OA, showing chondroprotective and anabolic effects (Gaissmaier et al., 2008; Westacott and Sharif, 1996). Meanwhile, MMP-2 and MMP-3 can be an indicator of wound healing early in repair (Rose and Kooyman, 2016). Further, MMP-3 is mainly expressed by fibroblasts and endothelial cells (Okada et al., 1992), indicating that changes to the synovium are likely contributing to observations in Study 2. Previous *in vitro* work has suggested that DEX modulates synovium behavior to IL-1 insult (Stefani et al., 2018), however the role of MMPs on synovium function is unclear. Ultimately, additional studies will be required to elucidate the mechanism of DEX-induced matrix remodeling *in vivo*.

It is unlikely that increased cytokine concentration was a pro-inflammatory reaction to the PLGA or agarose, as these are widely reported to be biocompatible at the levels used (Danhier et al., 2012; Selmi et al., 2008). We speculate that the bone substrate used with the DLMS carrier may have contributed to elevated levels, however devitalized bone has been successfully used by others (Tognana et al., 2005). We previously reported negative *in vitro* effects of bone with juvenile chondrocytes, but did not see any with adult chondrocytes (Lima et al., 2008a). Overall, conclusions based on measures of inflammation (synovitis and cytokines) were potentially limited by having multiple repairs per knee. If only one DLMS implant failed, one might expect to observe a global spike in synovial fluid cytokines while simultaneously seeing improved local tissue quality at other repair sites. To capitalize on the positive effects of DEX, future studies may utilize other porous base scaffolds such as titanium (Bal et al., 2010).

This preliminary *in vivo* experiment was potentially limited by sample size, which was improved by creating multiple defects per knee. Based on previous canine studies in our

laboratory, we determined a priori that a sample size of approximately 17 repairs per group would be required to achieve a power of at least 0.8. In addition, the 6-month end point provides only an initial assessment of healing, integration, and cartilage restoration for functional outcomes with longer term studies needed prior to clinical application. Nevertheless, trends and significant between-group differences were observed for the outcome measures, providing evidence for expedited early repair and providing rationale for long-term studies of sustained, targeted low-dose DEX delivery to the joint.

3.5 Conclusion

Using *in vitro* models (Study 1, SA1e) and confirmatory *in vivo* models (Study 2, SA1f) of cartilage restoration provide guidance for optimizing localized DEX delivery strategies to maximize cartilage graft survival and function. Utilizing a targeted DLMS carrier implant, we observed *in vitro* chondroprotection in the presence of IL-1-induced degradation and improved *in vivo* functional outcomes. These improved outcomes were correlated with superior histological cartilage scores and minimal-to-no comorbidity, but not necessarily a dampened inflammatory response. However, synovitis was low across groups, and synovium-associated MMPs were upregulated in response to DLMS, potentially indicative of increased healing rather than degradation. Together, the data confirms the anabolic and chondroprotective effects of DEX on cartilage, however a dampened inflammatory response was not observed in synovial measures. Therefore, the presented work is only partially supportive of the Part I global hypothesis.

Part II

Electric Fields as Catabolic, Anabolic, and Migratory Mediators in Synovium and Cartilage

Chapter 4

Pulsed Electromagnetic Fields Modulate the Response of Synovium Explants in Culture

4.1 Introduction

In vitro studies have established PEMFs as a modulator of inflammatory signaling in isolated FLS from both bovine and human arthritic sources (De Mattei et al., 2009; Ongaro et al., 2012), however it remains unclear how this translates to explants. Complicating the matter, the distribution and quantity of FLS, MLS, and non-resident immune cells in the synovium changes dramatically based on stage of OA and donor (O'Brien et al., 2017; Utomo et al., 2016). Studies have characterized behavior of macrophage cell lines to various strengths and duty cycles of PEMFs, showing variable effects on inflammatory mediators (Akan et al., 2010; Kawczyk-Krupka et al., 2002). Using this as motivation, as well as the observed modulation of cell phenotype by IL-1 and DEX **(Chapter 2)**, clinical stimulation parameters that have also been reported to have *in vitro, in vivo* and clinical benefits for cartilage and joint health (Collarile et al., 2018; Gobbi et al., 2014; Zorzi et al., 2007) were used to investigate the effect of PEMF on response to IL-1 and DEX in juvenile bovine and OA human synovium explants (SA2a). Specifically, *we hypothesized that PEMFs would decrease markers of inflammation in healthy bovine tissues and have an inconsistent effect on human OA tissues. Further, we hypothesized that the effect of PEMF would be altered by concurrent chemical treatment.*

4.2 Materials and Methods

4.2.1 PEMF System

The PEMF generators were custom made and calibrated to recapitulate clinical parameters by IGEA Clinical Biophysics (Carpi, Italy). The system consisted of electromagnetic coils made of copper wire and placed in a signal generator. This created a 1.5 ± 0.2 mT magnitude pulse with a duration of 1.3 ms and frequency of 75 Hz, yielding a duty cycle of 0.10. The magnetic peak field intensity was measured by the Hall probe (HTD61-0608-05-T, F.W. Bell, Sypris Solutions, Louisville, KY) of a gaussmeter (Walker Scientific, Auburn Hills, MI, USA) with a reading sensitivity equal to 0.2%. The induced electric field was measured by a standard coil probe (50 turns, 0.5 cm internal diameter of the coil probe, 0.2 copper diameter). A digital oscilloscope was used to evaluate the temporal pattern of the signal (Le Croy, Chestnut Ridge, NY). The shape and impulse length of the produced signal were maintained constant.

Studies were performed in a plexiglass chamber consisting of two parallel coils, also known as a Helmholtz pair **(Figure 4.1)**. The paired coils created a large region with uniform field, ideal for use with tissue culture plates.

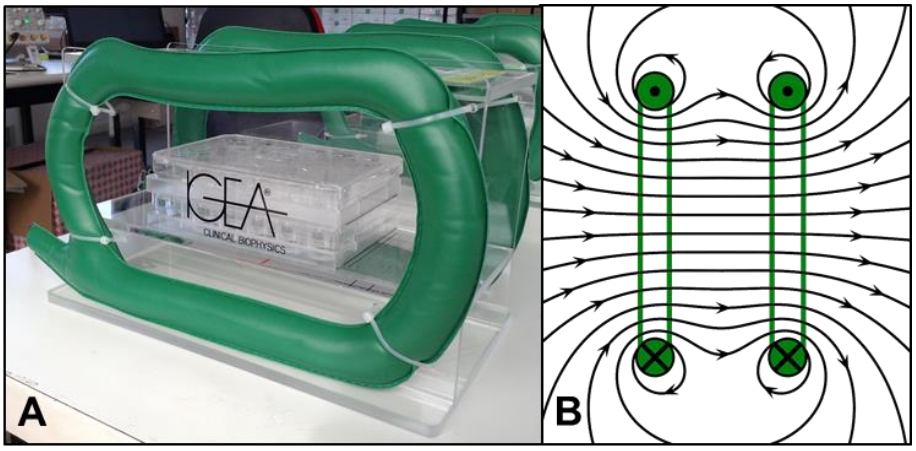

Figure 4.1 *In vitro* PEMF chamber consisting of **(A)** two electromagnetic coils (green) created a **(B)** uniform magnetic field in the culture area.

4.2.2 Synovium Explant Harvest

Fresh bovine synovial tissue was harvested, pooled, and cultured as described previously **(2.2.2.1)**. Human OA synovium explants were collected (IRB #AAAQ2703) from the region adjacent to the medial and lateral femoral condyle of 11 subjects during total knee arthroplasty **(Figure 4.2, Table 4.1)**. Explants were trimmed of excess adipose and outer capsule tissue before dicing. Human tissue was kept separated by donor for experiments.

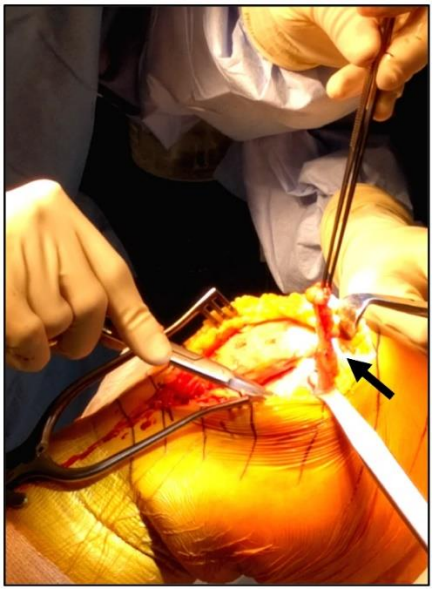

Figure 4.2 Human synovium explant harvest. Tissue (arrow) harvested from human OA patients during total knee arthroplasty.

Table 4.1 Human Donor Information.

Donor ID	Gender	OA Grade	Age
A	M	4	78
B	M	2	65
C	F	4	68
D	F	4	63
E	F	3	60
F	M	4	80
G	F	4	69
H	F	4	71
I	F	4	72
J	F	4	66
K	F	4	72
Human (mean ± stdev)		**3.7 ± 0.6**	**69 ± 6**

4.2.3 *In Vitro* Chemical Stimulation with or without PEMF

As previously described **(2.2.2.3)**, bovine explants were cultured for two weeks in: BM (CTL), BM supplemented with 10 ng/ml IL-1α, or BM supplemented with 100 nM DEX. Human explants were cultured in identical conditions, but interleukin-1α was substituted with interleukin-1β, as it is a more potent isoform in adult tissues (Kuroki et al., 2005). Specimens were cultured in PEMF chambers **(Figure 4.1)** which were active for either 8 hr per day or 0 hr per day (sham)[1].

[1] No detectable electromagnetic field in sham chambers (Tesla Meter, F.W. Bell).

4.2.4 Biochemistry

As previously described **(2.2.2.6)**, bovine explants (3 pooled donors; n=9-11) and human OA explants (11 individual donors; n=4-7 replicates per donor) were frozen, digested, and assayed for DNA, GAG, and total collagen content. Initial content shown in **Table A.1.1**.

4.2.5 Media Analyses

Media samples were assayed using the HA Quantikine ELISA Kit (Cat. No. DHYAL0; R&D Systems), PGE2 Parameter Assay Kit (Cat. No. KGE004B; R&D Systems), and Griess Reagent Kit for NO determination (Cat. No. G7921; ThermoFisher).

4.2.6 Histological and Immunohistochemical Characterization

Specimens were fixed and processed for H&E, alcian blue, and picrosirius red histology, as well as CD-14 immunostaining as described previously **(2.2.2.8)**.

4.2.7 Statistics

Statistical analyses were conducted as previously described **(2.2.2.9)**. Human data was analyzed using two- or three-way ANOVA (repeated measures) and Tukey HSD post-hoc test. Simple linear regression was performed on PGE2 data using Graphpad Prism software.

4.3 Results

4.3.1 Juvenile Bovine Synovium Explants

In the absence of PEMF, CTL and DEX specimens retained a native membrane-like morphology while IL specimens contracted and hardened **(Figure 4.3)**. With PEMF stimulation, morphology

only differed in the CTL media condition; specimens partially contracted and hardened, similar to IL groups. Total collagen content increased in culture only in the CTL media group without PEMF (p=0.018) **(Figure 4.4)**. Histological staining showed generally porous ECM in CTL and DEX groups, whereas IL specimens had a greater degree of matrix compaction **(Figure 4.5)**. Comparing H&E of IL±PEMF specimens **(Figure 4.5B, E)**, IL+PEMF had a lower degree of intimal hyperplasia more similar to CTL and DEX specimens.

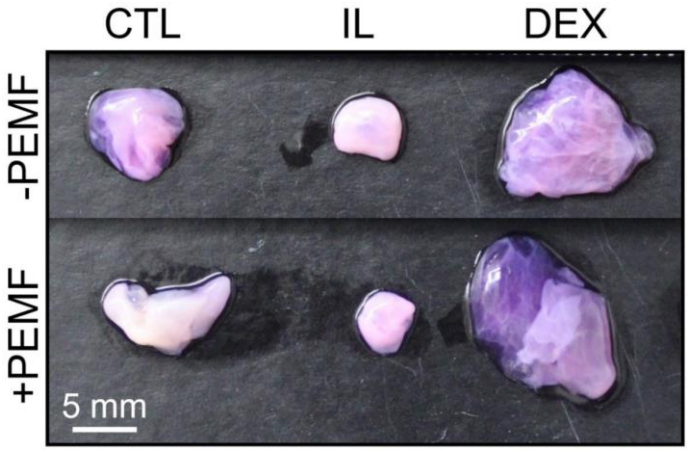

Figure 4.3 Gross morphology of bovine synovium explants exposed to CTL, IL, or DEX media in combination with PEMF stimulation for either: 0 hr (-PEMF) or 8 hr (+PEMF) per day for two weeks.

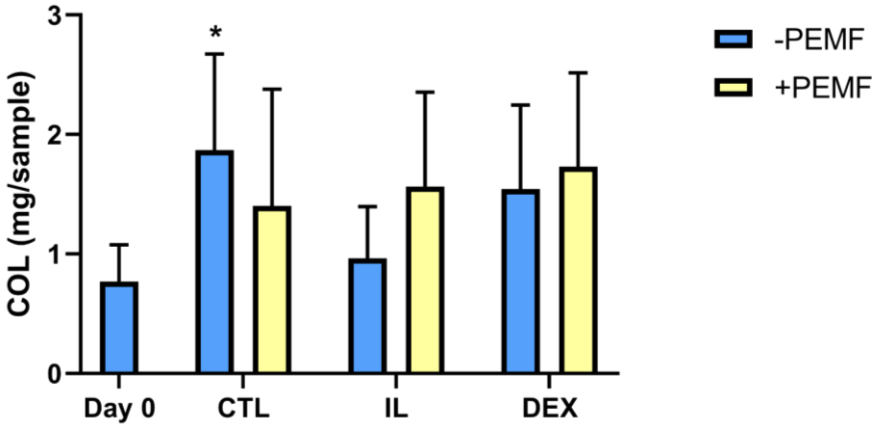

Figure 4.4 Total collagen content in PEMF-treated bovine synovium explants. *p<0.05 vs. Day 0

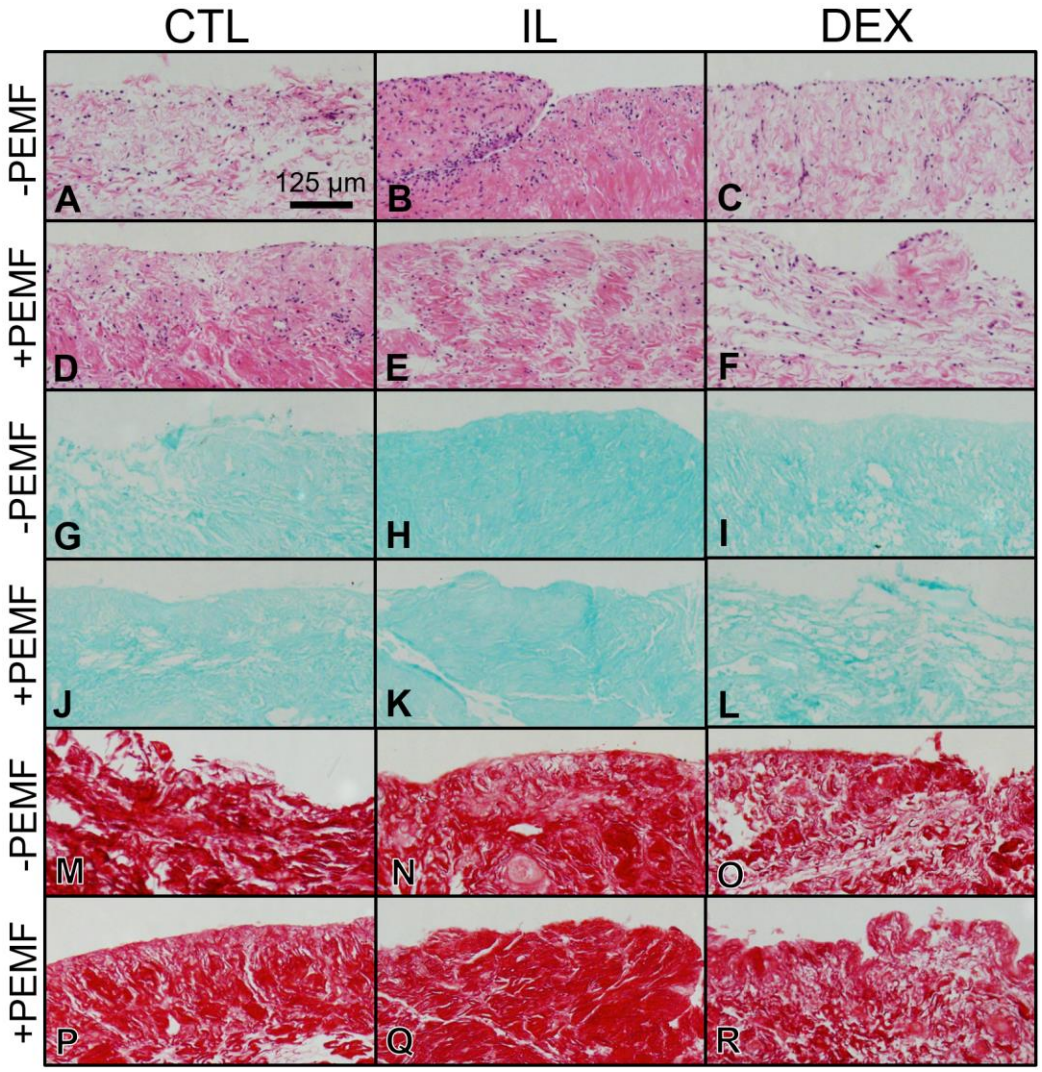

Figure 4.5 Histology of PEMF-treated bovine synovium explants. **(A-F)** H&E, **(G-L)** Alcian Blue, and **(M-R)** Picrosirius Red for **(A, G, M)** CTL-PEMF, **(D, J, P)** CTL+PEMF, **(B, H, N)** IL-PEMF, **(E, K, Q)** IL+PEMF, **(C, I, O)** DEX-PEMF, **(F, L, R)** DEX+PEMF.

Total NO secretion was significantly decreased by PEMF treatment in CTL culture conditions ($p<0.0001$) **(Figure 4.6)**. Meanwhile, PEMF treatment non-significantly lowered NO secretion in IL-treated specimens.

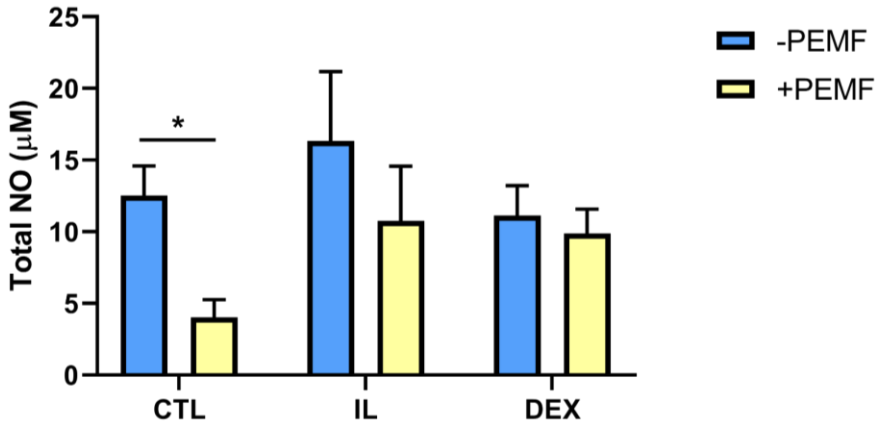

Figure 4.6 Total nitric oxide (NO) secretion in PEMF-treated bovine synovium explants. *p<0.0001

4.3.2 Human OA Synovium Explants

Gross morphology varied widely between donors and treatment groups, with synovial contractures and residual adipose tissue observed in many specimens **(Figure 4.7)**. DNA content was significantly affected by both media (p=0.027) and PEMF (p=0.011) **(Figure 4.8)**. In the CTL media group, PEMF treatment significantly decreased DNA content compared to no PEMF treatment (p=0.009). Overall, specimen dry weight was not significantly affected by PEMF (p=0.12), however there was a modest ~11% overall decrease with PEMF treatment across all groups. Significant PEMF effects were not observed in GAG or collagen content. Histological staining was similarly variable; however, matrix compaction was least apparent in the DEX+PEMF group **(Figure 4.9E, Q)**. Low intensity alcian blue staining was observed across all groups. In the absence of PEMF, CD14-positive cells were observed in all groups, however positive cells were absent in CTL+PEMF and DEX+PEMF **(Figure 4.9S-X)**.

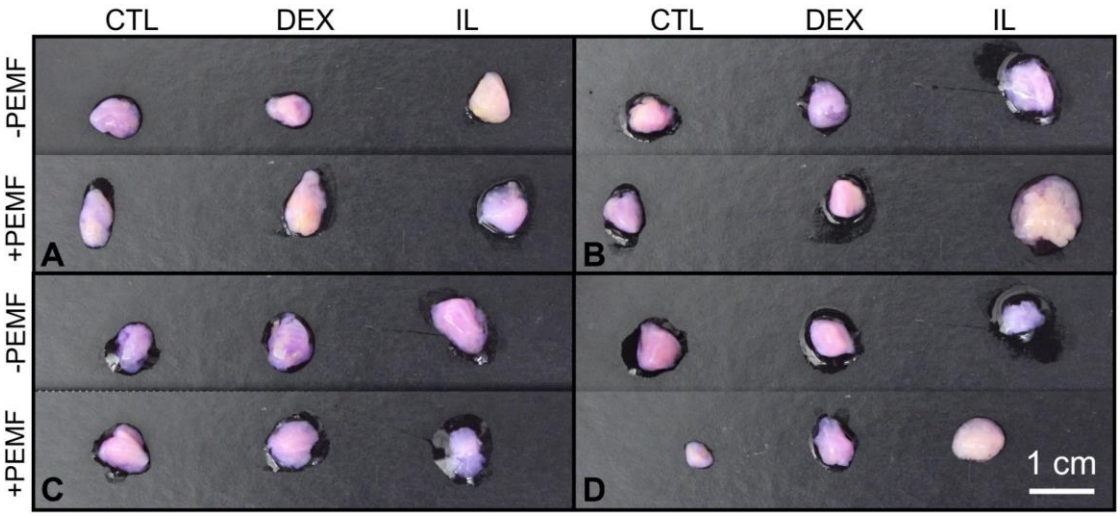

Figure 4.7 Gross morphology of selected OA human synovium explants exposed to CTL, DEX, or IL media in combination with PEMF stimulation for either: 0 hr (-PEMF) or 8 hr (+PEMF) per day for two weeks; **(A)** Donor H, **(B)** Donor I, **(C)** Donor J, and **(D)** Donor K.

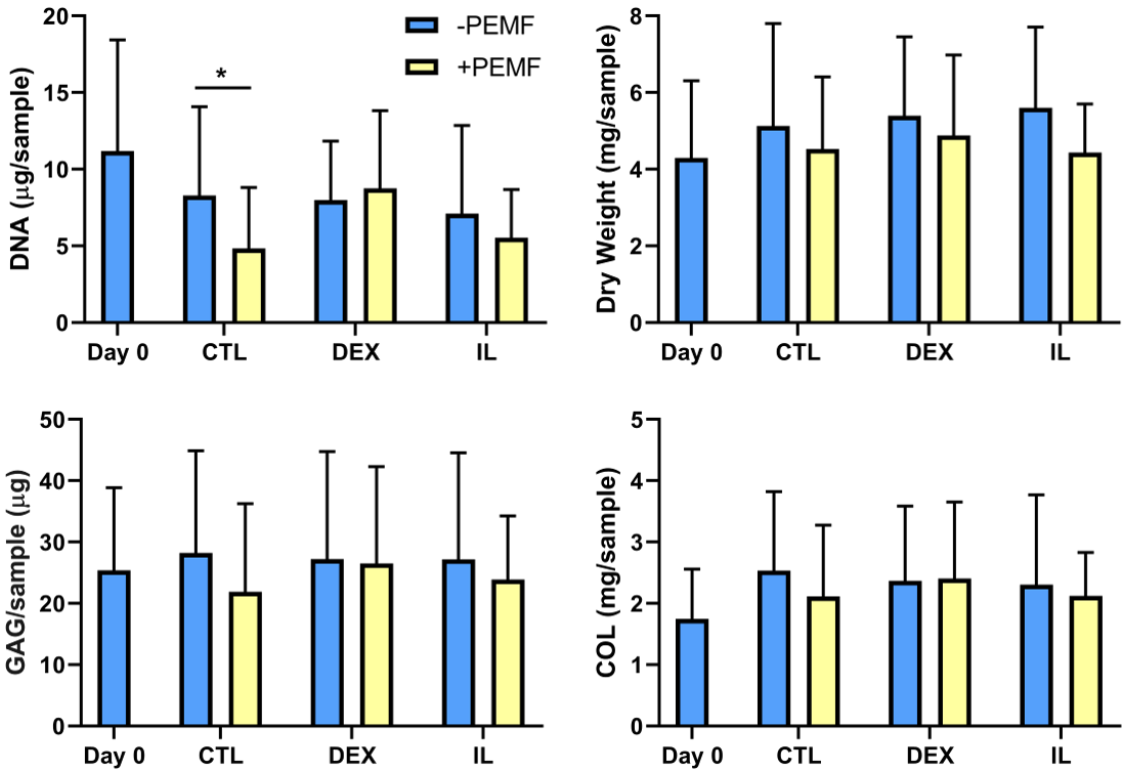

Figure 4.8 DNA, Dry weight, GAG, and collagen content in PEMF-treated human OA synovium explants. *p<0.05

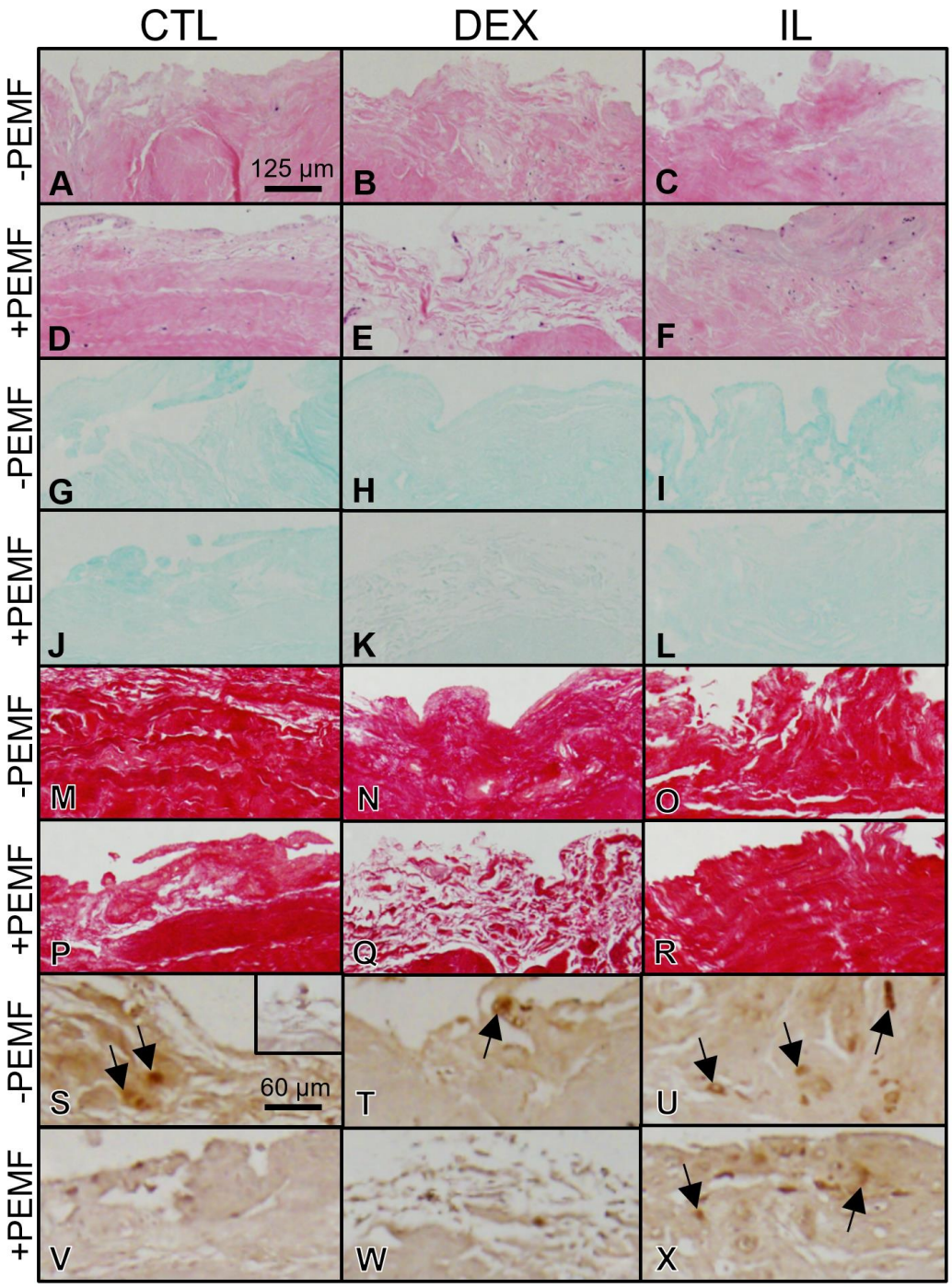

Figure 4.9 Histology of PEMF-treated OA human synovium explants. **(A-F)** H&E, **(G-L)** Alcian Blue, **(M-R)** Picrosirius Red, and **(S-X)** CD14 immunohistochemistry (red-brown DAB stain with purple hematoxylin counterstain, arrows point to $CD14^{+}$ positive cells, negative control inset in panel S) for Donor A; **(A, G, M, S)** CTL-PEMF, **(D, J, P, V)** CTL+PEMF, **(B, H, N, T)** IL-PEMF, **(E, K, Q, W)** IL+PEMF, **(C, I, O, U)** DEX-PEMF, **(F, L, R, X)** DEX+PEMF.

In the absence of PEMF, both HA and NO secretion were significantly decreased by DEX and increased by IL during the second week ($p<0.05$) **(Figure 4.10)**. Similarly, PGE2 secretion was decreased by DEX and increased by IL at both week 1 and week 2 ($p<0.0001$). There was not a significant effect of PEMF treatment on HA, NO, or PGE2 secretion. Post hoc linear regression analysis of donor age and PGE2 secretion yielded a significant positive correlation in IL+PEMF group only (Week 2, Slope=4.8, $r^2=0.53$, $p=0.012$) **(Figure 4.11)**.

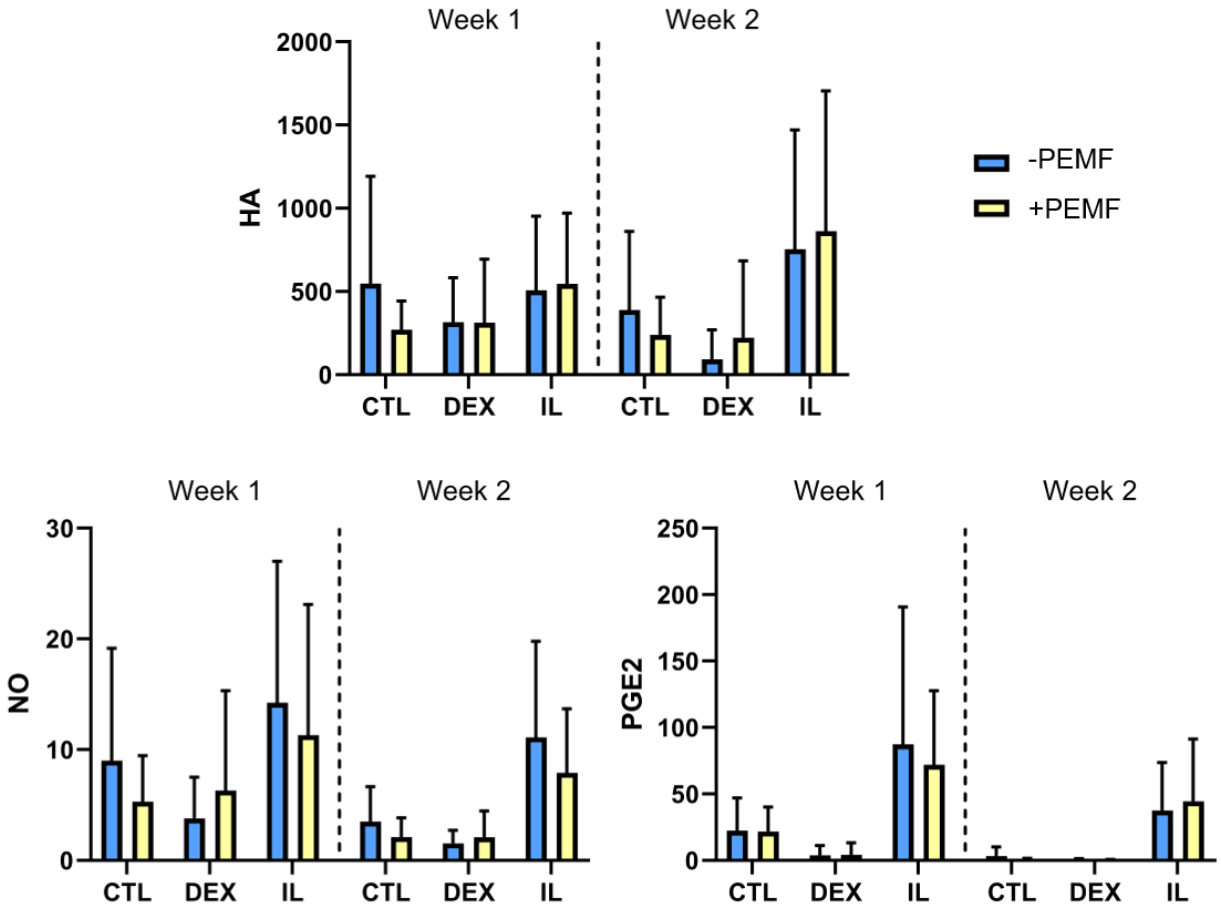

Figure 4.10 Hyaluronic acid, nitric oxide, and PGE2 secretion from PEMF-treated human OA synovium explants. All values are normalized to mean starting dry weight (g) for the respective donor. Non-normalized units: HA (µg), NO (mmol), PGE2 (µg)

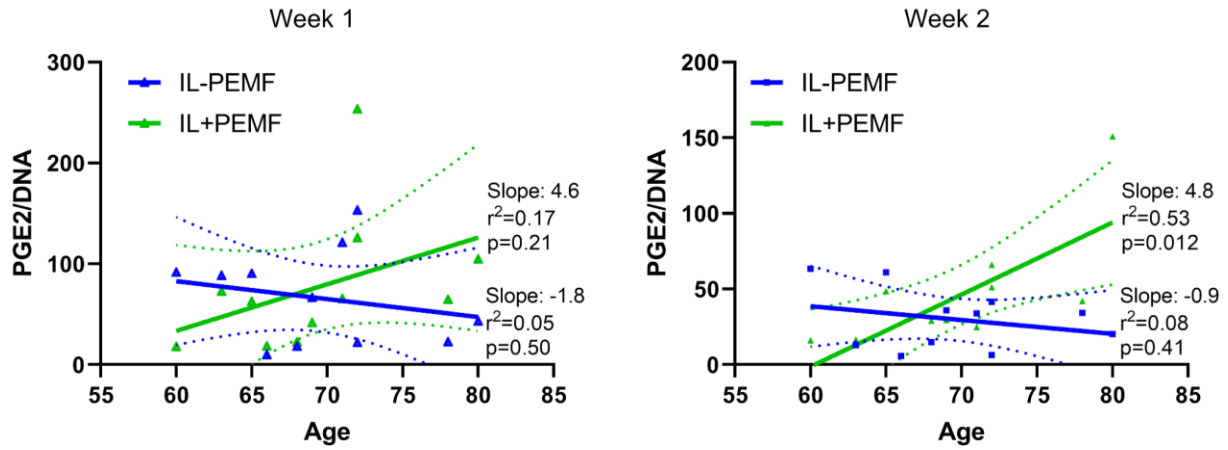

Figure 4.11 Linear regression of PGE2 secretion vs. donor age in IL-treated groups. Age had a significant positive correlation with PGE2 secretion in week 2.

4.4 Discussion

The presented studies characterized the response of healthy and OA synovial explants to PEMFs in control and chemical-stimulated culture conditions (SA2a). As hypothesized, a differential response to PEMF was observed in juvenile bovine and OA human synovium explants, and response was dependent on media treatment. PEMF treatment modulated collagen content, NO secretion, and gross morphology of bovine explants in CTL media conditions. Meanwhile, PEMF treatment had an effect on DNA and possibly CD14 content in human OA specimens, however other measures remained unchanged. Interestingly, secretion of NO from human OA explants followed a familiar pattern of decreased levels with DEX and increased with IL-1 that was previously observed in juvenile bovine explants **(2.2)**. However, HA secretion deviated from this behavior in that DEX treatment lowered levels compared to CTL **(Figure 4.10)** rather than increased **(Figure 2.6)**.

In the absence of PEMF, bovine CTL and DEX specimens retained a native-like membrane morphology while IL specimens contracted and hardened **(Figure 4.3)**. This is potentially

indicative of a fibrotic phenotype (Remst et al., 2015), and was also apparent in histological staining, where IL specimens had a greater degree of matrix compaction compared to CTL and DEX **(Figure 4.5A-C)**. A potent anti-inflammatory effect (i.e. decreased NO secretion) was observed in PEMF-stimulated CTL specimens, a nonsignificant effect in IL specimens, and no effect in DEX specimens **(Figure 4.6)**. It is possible that this was due to changing cell phenotype in IL and DEX-treated bovine explant cultures, as observed in **Chapter 2**.

Meanwhile, regardless of media condition, there was not a significant effect of PEMF treatment on HA or NO secretion in human OA tissues. This is in contrast with literature reports of reduced inflammatory signaling in bovine isolated bovine and human arthritic FLS (De Mattei et al., 2009; Ongaro et al., 2012). However, although an overall effect of PEMF on PGE2 secretion was not observed, there was a significant correlation with donor age in IL+PEMF specimens only **(Figure 4.11)**. In this group, specimens from older donors were more likely to have higher PGE2 secretion. This result warrants further study, as it is possible that the anti-inflammatory effect previously ascribed to PEMF is only present in a subset of specimens (possibly lower age). If such an effect were present, this would have obvious clinical implications and could also explain conflicting results for PEMF treatment in the literature.

In our study, human tissues showed qualitative evidence of an anti-inflammatory effect; in the absence of PEMF, $CD14^+$ cells were observed in all groups, however $CD14^+$ cells were absent in CTL+PEMF and DEX+PEMF specimens **(Figure 4.9S-X)**. Future studies should include flow cytometry analysis to robustly quantify potential changes in CD14 due to PEMF. Flow cytometry data for passaged synovial cells from selected donors is shown in **Table A.1.2**, however no differences were present.

Nevertheless, it is likely that variable quantities of FLS were present in the OA specimens, with a higher proportion of starting cells being MLS or lymphocytes **(1.3.1.2)**. The effect of PEMF on synovial immune cells has not been well characterized, however one study reported downregulation of TNFα and nuclear factor kappa B (NFκB) in a murine macrophage cell line (Ross and Harrison, 2013). NFκB serves critical immune system functions, including transcription of cytokines and regulation of cell differentiation, proliferation, and viability (Hayden et al., 2006). PEMF has also been shown to increase NO production in THP-1 cells, a human monocyte cell line (Akan et al., 2010). Therefore, it is quite possible that PEMF had counteracting effects in FLS and MLS, contributing to the inconclusive results in human OA explants.

In human specimens, PEMF treatment did have an effect on DNA content, leading to significantly decreased DNA content compared to no PEMF treatment. Similarly, there was a modest ~11% overall decrease in specimen dry weight with PEMF treatment across all groups. Together, these may be indicative of a reduction in synovial hyperplasia and/or fibrosis, however the clinical significance of this small effect, without concomitant reduction in inflammatory mediators, is unclear. Overall, these results support the Part II global hypothesis, however this comes with the caveats that PEMF did not have a consistent anti-catabolic effect in human OA tissues nor did it have an additive effect with DEX. These results are likely to have significant implications for selecting optimal patient populations for PEMF therapy.

4.5 Conclusion

Overall, the current studies (SA2a) support the Part II global hypothesis by demonstrating that PEMF modulates inflammatory signaling in bovine explant tissues, in agreement with previous reports of isolated FLS. However, the response of human tissues was far more variable and a robust

anti-catabolic effect of PEMF was not observed. This was likely due to the advanced disease state of these tissues and the variable cell content, with a significantly lower proportion of FLS cells compared to healthy tissue. A key limitation of this study was that we could not quantify exactly which cells in the tissue were responding to PEMF. It is likely that increased MLS and T lymphocytes within human OA specimens interact with PEMF in very different ways from FLS, likely also compounded by cellular communication/gap junctions. This motivates further evaluation of PEMF in synovial tissue obtained from healthy or early disease patients, where PEMF may be more effective.

Chapter 5

Pulsed Electromagnetic Fields Enhance Osteochondral Repair using Engineered Constructs

5.1 Introduction

Clinical studies of PEMFs have shown improvements in function following microfracture, OCA, MACI®, and bone marrow-derived stem cell transplantation (Cadossi et al., 2014; Collarile et al., 2018; Iwasa and Reddi, 2018). However, while these initial studies were promising, PEMFs have remained controversial for cartilage repair due to inconclusive clinical evidence of robust efficacy and few mechanistic studies on the matter (Bjordal et al., 2007; Gobbi et al., 2014). We suspect that the sometimes-conflicting data may stem from differences in methods and strengths/duty cycle of applied electric fields, anatomic geometry, repair type, and contributions from surrounding tissues.

Motivated by promising initial *in vitro* and clinical studies **(1.3.4.1)** and our own *in vitro* data supporting an anti-catabolic response in non-pathologic synovium explants **(Chapter 4)**, these studies aim to optimize parameters of PEMF stimulation in order to provide insights into successful clinical translation for engineered cartilage repair (SA2b-c). As engineered cartilage is especially susceptible to impacts from sub-optimal implantation properties and pro-inflammatory cytokines (Djouad et al., 2009; Hunter and Levenston, 2004; Obradovic et al., 2001b; Spalazzi et al., 2008), *we hypothesized that a standardized and optimized PEMF strategy would serve a dual*

role of stimulating cartilage anabolism and suppressing synovial-mediated catabolism following joint repair, leading to better post-operative outcomes using engineered cartilage.

To this end, we first assessed the effect of timing (Study 1) and orientation (Study 2) of PEMF stimulation on engineered cartilage growth and integration, two often cited factors contributing to clinical graft failure (Hunter and Levenston, 2004; Obradovic et al., 2001a). Study 1 and 2 were conducted *in vitro*, to serve as a best-case scenario permitting the evaluation of the intrinsic response of engineered cartilage to PEMF stimulation. Next, tissue quality and functional outcomes were assessed following an *in vivo* engineered osteochondral graft repair (Study 3). The adult canine preclinical model was selected for its similarities to humans in patellofemoral joint pathology and presentation of pain and discomfort via changes to gait (Bendele, 2001). To the author's knowledge, PEMFs have not previously been investigated in a preclinical engineered cartilage model or as a method for improving engineered cartilage growth and integration.

5.2 Materials and Methods

5.2.1 PEMF System

The PEMF system was configured as previously described **(4.2.1)**. *In vitro* studies (Study 1-2) were performed in a plexiglass chamber consisting of two parallel coils **(Figure 4.1, Figure 5.1A)**. Modeling of the PEMF-induced electrical field within engineered cartilage constructs was performed by means of COMSOL Multiphysics 5.4 software. The *in vivo* portion (Study 3) was performed using a single electromagnetic coil, which was strapped to the cranial (anterior) portion of the canine stifle (knee) joint, allowing for unrestricted range of motion **(Figure 5.2C)**.

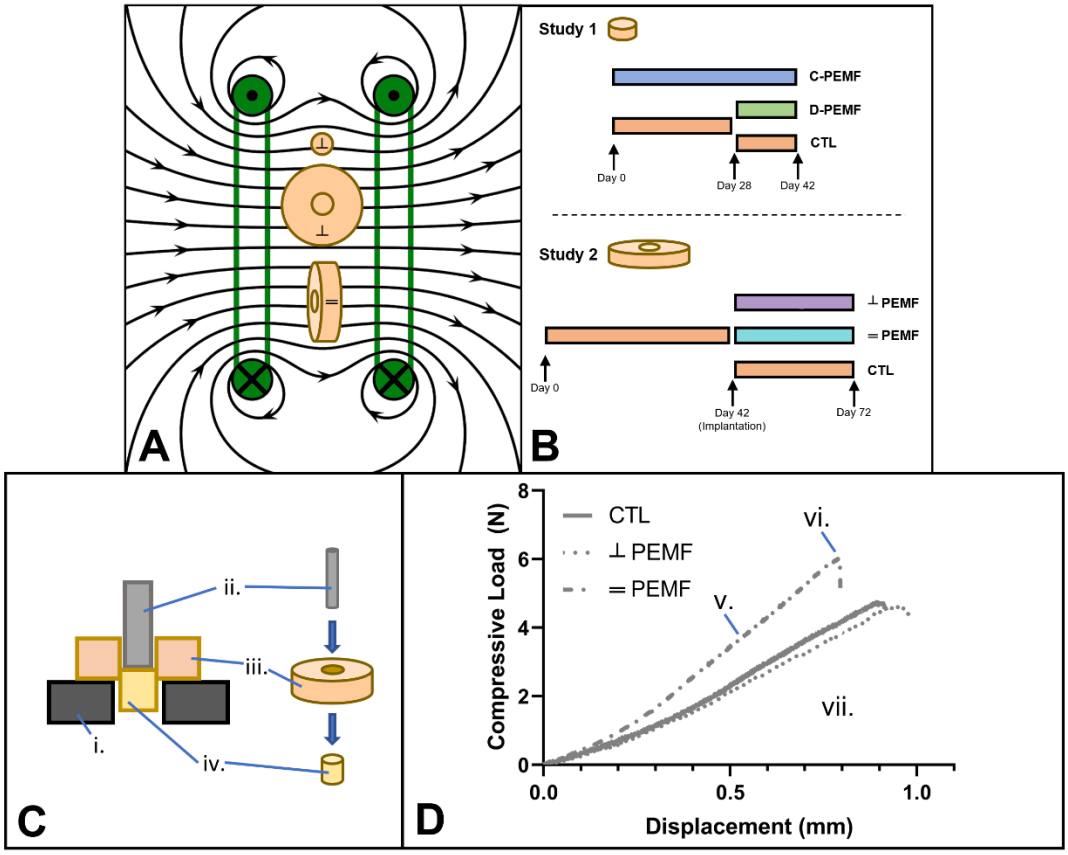

Figure 5.1 Schematic of *in vitro* PEMF application and push-out mechanical testing. **(A)** Magnetic field lines (modified from commons.wikimedia.org, labeled for reuse) with engineered constructs in perpendicular (⊥) or parallel (═) orientations; **(B)** Study 1 specimens were stimulated with PEMF starting at day 0 (continuous PEMF, C-PEMF), starting at day 28 (delayed PEMF, D-PEMF), or no PEMF (CTL) and cultured for a total of 42 days (all study 1 PEMF samples in perpendicular orientation). Study 2 specimens were pre-cultured for 42 days and then sub-cored, re-implanted, and stimulated with either perpendicular (⊥) or parallel (═) orientation or no PEMF (CTL) for an additional 1 month; **(C)** Schematic of push-out testing of engineered core/annulus units (Study 2) showing side view and deconstructed oblique view with construct holder (i.), indenter (ii.), construct annulus (iii.), and construct core (iv.); **(D)** Representative load-displacement curves from push-out tests for perpendicular, parallel, and no PEMF (Study 2).

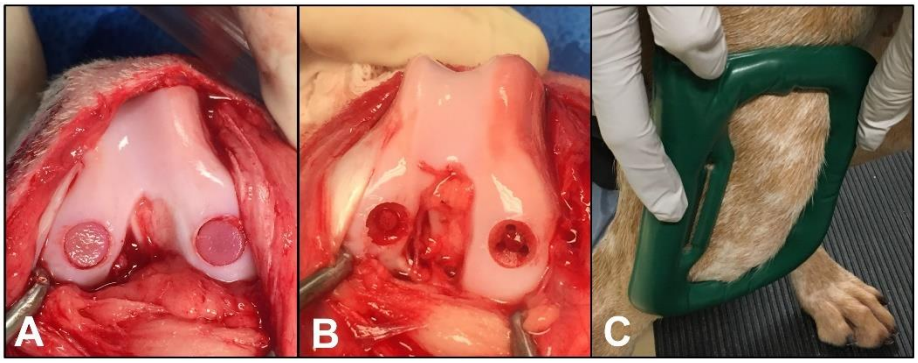

Figure 5.2 Schematic of *in vivo* osteochondral repairs and PEMF stimulation. **(A)** Two engineered osteochondral grafts (out of a total of 3 per joint, trochlear repair not shown) were implanted in the femoral condyles (Study 3); **(B)** Two microfracture procedures (total of 3 per joint, trochlear defect not shown) in the femoral condyles (Study 3); **(C)** Single electromagnetic coil (green) used for *in vivo* pilot allowed full range of motion (Study 3).

5.2.2 Preparation and Culture of Engineered Constructs

TE cartilage was prepared from adult canine cartilage and cultured as previously described **(3.2.2)**.

5.2.3 Effect of PEMF Timing on Engineered Cartilage Growth (Study 1)

Engineered constructs (Ø 3 mm x 2.4 mm thick) were placed in the PEMF device starting from 1 of 3 different times: 1) continuous PEMF starting from day 0 (C-PEMF), 2) delayed PEMF starting from day 28 (D-PEMF), and 3) no-PEMF (CTL) **(Figure 5.1A-C)**. PEMF was applied for 8 hr/day, 7 days/week, and a total culture time of 6 weeks. CTL specimens were cultured in adjacent sham chambers[2]. Biochemical properties were assessed at bi-weekly intervals over the 42-day culture period (n=6-8).

[2] No detectable electromagnetic field in sham chambers (Tesla Meter, F.W. Bell).

5.2.4 Effect of PEMF Orientation on Engineered Cartilage Integration (Study 2)

Cartilage constructs were prepared (Ø 8 mm x 2.4 mm thick) and cultured to maturity (42 days). At maturity, constructs were sub-punched using a 3 mm biopsy punch (Integra Miltex). The 3 mm cores were then randomly re-inserted into each annulus to create an implant-defect model. The core-annulus units were placed in 1 of 3 conditions: PEMF stimulation with electromagnetic coils oriented either perpendicular (⊥ PEMF) or parallel (═ PEMF) to the construct surface and no-PEMF controls (CTL) (**Figure 5.1A-C**). As in Study 1, PEMF was applied for 8 hr/day, 7 days/week.

Specimen biochemical properties were evaluated at 42 days (start of implantation) and 72 days (1-month post-implantation) (n=8-12). Integration of the core-annulus unit was evaluated using an indentation "push-out" test at the terminal time point **(Figure 5.1D-E)**. Briefly, an indenter was visually centered over the core before loading at a rate of 10 μm/sec (Lima et al., 2008a; van de Breevaart Bravenboer et al., 2004). The stiffness (slope of linear portion of force-displacement curve; **Figure 5.1E, v.**), failure load (maximum observed force; **Figure 5.1E, vi.**), and energy to failure (area under the load-displacement curve to the peak load and normalized to interface area; **Figure 5.1E, vii.**) were computed for each specimen. After the cores were separated from the annuli via this destructive mechanical testing, individual core/annulus specimens were solubilized using proteinase K and assayed for DNA, GAG, and COL, as before.

5.2.5 Preclinical Model of Engineered Osteochondral Repair with PEMF (Study 3)

Osteochondral grafts (Ø 6 mm x 6 mm thick) were prepared and cultured as previously described (Lima et al., 2008a). Briefly, bovine trabecular bone cores (Ø 6 mm x 5 mm thick) were devitalized and then infused with 2% (w/v) Type VII Agarose containing P2 canine chondrocytes (30 x 10^6

cells/ml) to produce layered osteochondral constructs with a 1 mm gel-only region, 1 mm gel bone interface, and 4 mm bone-only. Constructs were pre-cultured until the cartilage layer reached maturity (42 days).

Purpose-bred adult mongrel dogs (0.9 ± 0.07 yr, 24.0 ± 1.78 kg, all female) were anesthetized and prepared for aseptic surgery of the right stifle (University of Missouri-Columbia IACUC #9167). Mature osteochondral constructs (n=8 animals, n=3 grafts per animal) were press-fit into defects created using a 6 mm OATS® reamer with power pick (**Figure 5.2A,** trochlear repair not shown). Specifically, one defect each was created in the trochlear groove (TG), femoral condyle-medial (FCM), and femoral condyle-lateral (FCL) of the stifle joint. A parallel set of repairs were performed in defects (Ø 6 mm x 1 mm thick) using the microfracture (power pick) technique (n=8 animals, n=3 repairs per joint) (**Figure 5.2B,** trochlear repair not shown).

Starting on the first post-operative day, all animals were fitted with PEMF devices which were then worn for 6 hr/day, 7 days/week for 3 months. The stimulation time was shortened from the 8 hr/day used for *in vitro* experiments to 6 hr/day for the *in vivo* study due to practical reasons. Half of the devices were active (+ or PEMF, n=4) and the other half were sham control devices (- or CTL, n=4).

5.2.6 Clinically Based Assessments (Study 3)

Animals were examined, assessed, and had synovial fluid assayed as described in **Chapter 3.2.5**, with the addition of total pressure-index (TPI).

5.2.7 Histological Scoring (Study 3)

At the terminal 3-month time point, animals were sacrificed and tissue harvested for histopathology assessment, as previously described **(3.2.6)**. Additional immunohistochemical staining of osteochondral repair units was performed using collagen type II primary antibody (ab34712; Abcam) and DAB staining kit (ab64264; Abcam).

5.2.8 Statistics

Statistical analyses of *in vitro* data and power analysis were performed as previously described **(3.2.7)**. *In vivo* functional measures were compared using three-way ANOVA (repair type, PEMF, time) with time as a repeated measures factor and Tukey post-hoc test (α=0.05). These normally distributed data were presented as mean (95% Confidence Interval (95% CI)).

Modified OARSI scores and corresponding sub-scores were analyzed using a Generalized Linear Model. Specifically, data were fit to an ordinal multinomial probability distribution and cumulative logit link function with generalized estimating equations correction for repeated measures (location, scorer). The dependent (response) variable was the score (or sub-score) and the independent variables (predictors) were the categorical factors: repair type, PEMF, and/or repair location. Total OARSI scores were grouped into ordered categories for regression analysis in order to increase the number of observations per level of the dependent variable. Odds ratios (OR) and corresponding 95% CI were computed from the model's parameter estimates. OCA scores were evaluated using the Mann-Whitney test. Averages of non-normal datasets were presented as median (95% CI). Ordinal regression analyses were performed using IBM SPSS Statistics 25.

5.3 Results

5.3.1 Finite Element Modeling of Electric Field Distribution

In the perpendicular PEMF coil orientation, the induced electric field was predicted to peak at opposite ends of the construct resulting in an irregular charge distribution on the outer surface **(Figure 5.3)**. The parallel PEMF coil orientation generated an electrical field and consequent charge distribution peaking along the outer circumference of the cartilage construct. In this case, the field was symmetric with regards to the axis of the cylinder, generating a homogenous distribution.

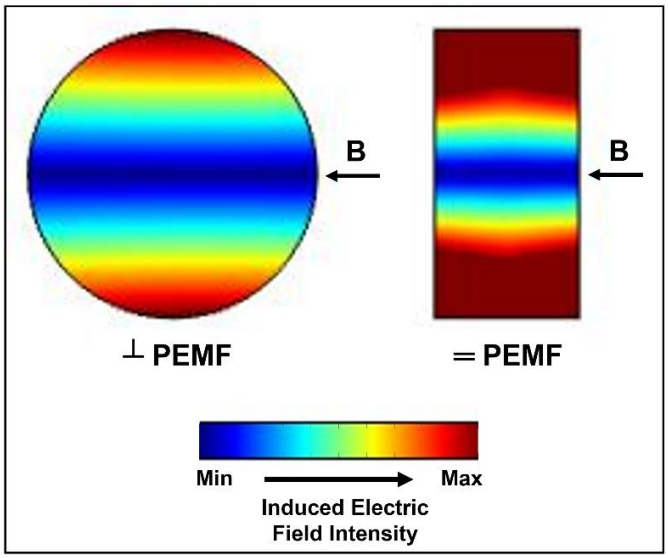

Figure 5.3 Finite element analysis of PEMF-stimulated engineered cartilage. Charge distribution changed dramatically dependent on PEMF orientation.

5.3.2 Effect of PEMF on Maturation of Engineered Cartilage (Study 1)

At day 42, delayed PEMF (D-PEMF) had significantly greater cell content (DNA/ww; 0.05 vs. 0.03 %ww; between-group difference, 0.01 %ww; p=0.022) and GAG content (GAG/ww; 2.8 vs. 2.3%; between-group difference, 0.5 %ww; p=0.031) compared to no-PEMF (CTL) **(Figure 5.4)**. In contrast, collagen content (COL/ww) was significantly elevated with continuous PEMF (C-

PEMF) compared to no PEMF (2.6 vs. 2.0 %ww; between-group difference, 0.7 %ww; p=0.046) **(Figure 5.4C)**. Meanwhile, there were no significant between-group differences in either GAG/DNA or COL/DNA at any time point.

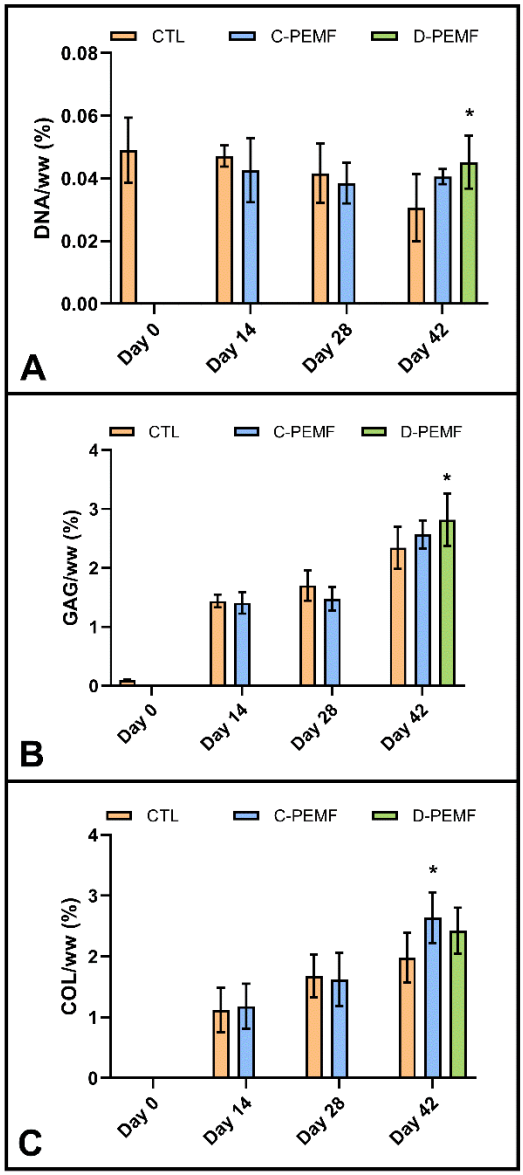

Figure 5.4 Biochemical properties of PEMF-stimulated engineered cartilage maturation. **(A)** DNA/ww, **(B)** GAG/ww, and **(C)** COL/ww in engineered constructs subjected to no PEMF (CTL), continuous PEMF (C-PEMF), or delayed PEMF (D-PEMF) (Study 1); *p<0.05 compared to CTL at same time point.

5.3.3 Effect of PEMF on Repair of Mature Engineered Cartilage Model (Study 2)

Repair stiffness was significantly greater in the parallel PEMF orientation compared to CTL (3.1 vs. 2.4 N/mm; between-group difference, 0.73 N/mm; p=0.012) and compared to perpendicular PEMF (3.1 vs. 2.4 N/mm; between-group difference, 0.71 N/mm; p=0.026) (**Figure 5.5A**). Additionally, there was a significant increase in failure load for the parallel PEMF orientation relative to CTL (**Figure 5.5B**; 6.4 vs. 4.6 N; between-group difference, 1.7 N; p=0.017) and a nonsignificant increase in energy to failure (**Figure 5.5C**; 310 vs. 197 J/m^2; between-group difference, 113 J/m^2; p=0.074) of the core-annulus unit.

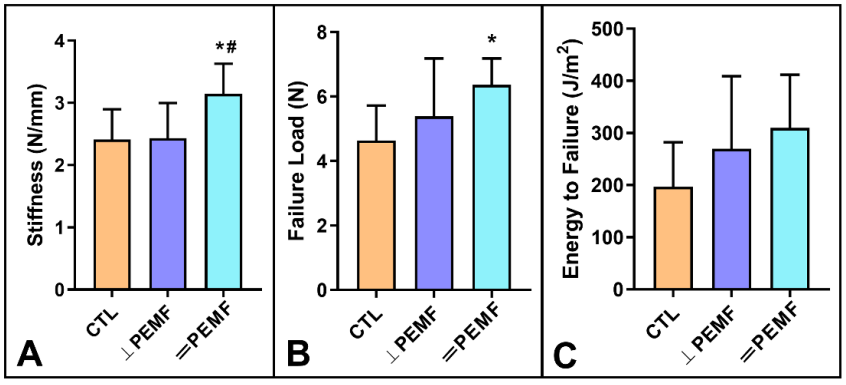

Figure 5.5 Mechanical properties of core-annulus repairs subjected to PEMF. **(A)** Stiffness (N/mm) was determined from the slope of the load-displacement curve, **(B)** failure load (N) from the peak load, and **(C)** energy to failure (J/m^2) from the area under the curve normalized to interface area. Each parameter was enhanced in the parallel (═PEMF) orientation relative to no PEMF (CTL); *p<0.05 compared to CTL, #p<0.05 compared to ⊥PEMF.

DNA content was not significantly affected by PEMF treatment in either the construct cores or annuli **(Figure 5.6A)**. Annuli in the perpendicular PEMF group had significantly greater GAG content compared to CTL (5.6 vs. 4.0 %ww; between-group difference, 1.6 %ww; p=0.010) **(Figure 5.6B)**. GAG content was similarly increased in parallel PEMF compared to CTL (5.6 vs. 4.0 %ww; between-group difference, 1.6 %ww; p=0.028). While there were no significant

differences in collagen content, perpendicular PEMF had a non-significant increase over parallel PEMF in the construct annuli (2.6 vs. 2.3 %ww; between-group difference, 0.3 %ww; p=0.12) **(Figure 5.6C)**.

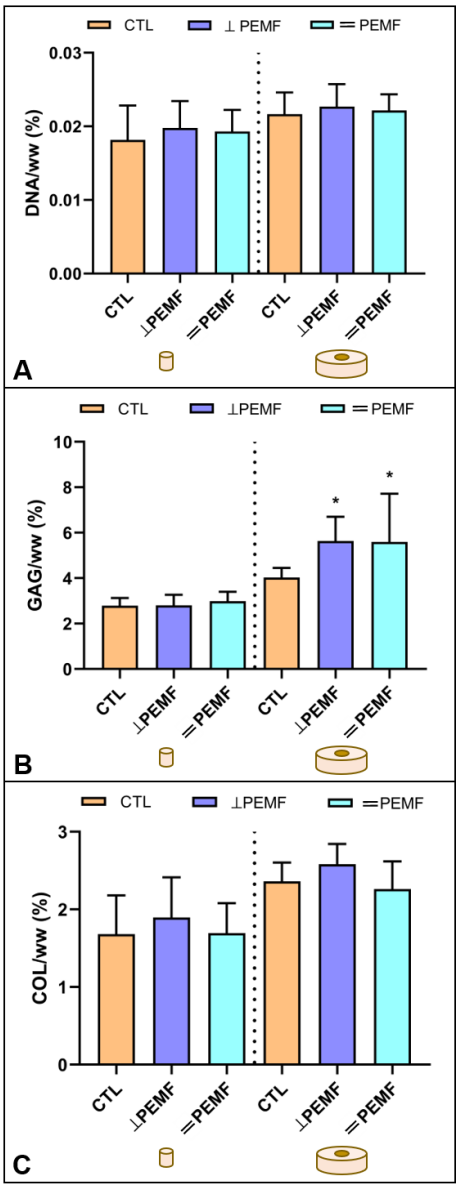

Figure 5.6 Biochemical properties of core-annulus repairs subjected to PEMF. **(A)** DNA/ww, **(B)** GAG/ww, and **(C)** COL/ww for the engineered construct cores (left) and annuli (right) in perpendicular (⊥) and parallel (═) PEMF groups compared to no PEMF (CTL) (Study 2); *p<0.05 compared to CTL.

5.3.4 Clinically Based Assessments of In Vivo PEMF-Stimulated Repairs (Study 3)

In animals with tissue-engineered repairs, five out of six parameters (gait, CROM, TPI, pain, effusion) were not significantly changed from baseline **(Table 5.1)**. At the same time, animals with microfracture repairs had significantly worse gait, CROM, and TPI scores. Tissue-engineered repairs led to less lameness than microfracture repairs in both no PEMF (1.3 vs. 2.0; between-group difference, 0.8; 95% CI, 0.01 to 1.5) and PEMF (1.3 vs. 2.0; between-group difference, 0.8; 95% CI, 0.01 to 1.5) conditions.

Table 5.1 Clinical outcome scores of OC repairs at 3 months; *p<0.05, **p<0.01, ***p<0.001, ****p<0.0001

	Mean (95% CI)			Mean (95% CI)			Mean (95% CI)	
	TE (Change from Baseline)		Difference in Change (TE- vs. TE+)	MF (Change from Baseline)		Difference in Change (MF- vs. MF+)	Difference in Change (TE- vs. MF-)	Difference in Change (TE+ vs. MF+)
Measurement	**TE-**	**TE+**		**MF-**	**MF+**			
Gait	-1.5 (-3.6 to 0.6)	-1.7 (-3.8 to 0.4)	-0.2 (-2.7 to 2.4)	-2.9 (-5.0 to -0.8) **	-3.9 (-5.9 to -1.8) ***	-0.9 (-3.4 to 1.6)	-1.4 (-3.9 to 1.1)	-2.2 (-4.7 to 0.3)
CROM	-7.5 (-20.2 to 5.2)	-10.8 (-23.4 to 1.9)	-3.3 (-18.4 to 11.9)	-17.5 (-30.2 to -4.8) **	-23.8 (-36.4 to -11.1) ***	-6.3 (-21.4 to 8.9)	-10.0 (-25.2 to 5.2)	-13.0 (-28.2 to 2.2)
TPI	-2.8 (-6.7 to 1.2)	-2.1 (-6.1 to 1.8)	0.7 (-4.1 to 5.4)	-4.4 (-8.4 to 0.5) *	-6.0 (-9.9 to -2.1) **	-1.6 (-6.3 to 3.1)	-1.7 (-6.4 to 3.1)	-3.9 (-8.6 to 0.8)
Lameness	1.3 (0.6 to 1.9) ***	1.3 (0.6 to 1.9) ***	0.0 (-0.7 to 0.7)	2.0 (1.4 to 2.6) ****	2.0 (1.4 to 2.6) ****	0.0 (-0.7 to 0.7)	0.8 (0.01 to 1.5) *	0.8 (0.01 to 1.5) *
Pain	1.3 (-0.6 to 3.2)	1.1 (-0.8 to 3.0)	-0.2 (-2.5 to 2.1)	1.5 (-0.5 to 3.4)	2.6 (0.7 to 4.5) **	1.2 (-1.1 to 3.5)	0.2 (-2.1 to 2.4)	1.6 (-0.7 to 3.8)
Effusion	1.3 (-1.7 to 4.3)	1.7 (-1.3 to 4.7)	0.5 (-3.1 to 4.0)	3.8 (0.8 to 6.8) **	2.6 (-0.4 to 5.5)	-1.2 (-4.8 to 2.3)	2.5 (-1.1 to 6.1)	0.8 (-2.7 to 4.4)

TE-, tissue-engineered osteochondral repairs without PEMF; TE+, tissue-engineered osteochondral repairs with PEMF; MF-, microfracture repairs without PEMF; MF+, microfracture repairs with PEMF; comfortable range of motion (CROM), total pressure index (TPI)

5.3.5 Histological Assessment of PEMF-Stimulated Repairs (Study 3)

PEMF-treated tissue-engineered osteochondral repairs (TE+) were approximately 70% less likely than those without PEMF (TE-) to have a worse (ie. higher) combined OARSI cartilage score (p=0.028) **(Table 5.2)**. Specifically, TE+ samples were about 80% less likely to have greater proteoglycan pathology (p=0.013) and 60% less likely (p=0.051) to have greater chondrocyte pathology than TE-. This was reflected by toluidine blue staining, which was homogenously distributed in TE+ specimens and almost nonexistent in the superficial zone of TE- specimens **(Figure 5.7I-J)**.

Table 5.2 OARSI cartilage scores and sub-scores. *p<0.05, ****p<0.0001

	Median (95% CI)			Median (95% CI)		
Measurement	TE-	TE+	Odds Ratio (95% CI)	MF-	MF+	Odds Ratio (95% CI)
OARSI (Cartilage, combined)	19 (14 to 20)	18.5 (12 to 19)	0.3 (0.1 to 0.9) *	16 (13 to 19)	16.5 (15 to 20)	1.8 (0.6 to 5.7)
Structure	4 (2 to 4)	4 (1 to 4)	0.7 (0.2 to 2.0)	3.5 (2 to 4)	3 (2 to 4)	0.9 (0.2 to 3.6)
Chondrocytes	4 (2 to 4)	3.5 (1 to 4)	0.4 (0.1 to 1.0)	3 (2 to 4)	3 (2 to 4)	0.9 (0.2 to 4.5)
Proteoglycans	3 (2 to 4)	3 (1 to 3)	0.2 (0.1 to 0.7) *	3 (3 to 3)	3 (3 to 4)	0.8 (0.1 to 5.0)
Collagen	3 (3 to 3)	3 (3 to 3)	N/A	3 (3 to 3)	3 (3 to 3)	N/A
Tidemark	2 (2 to 2)	2 (2 to 2)	N/A	2 (2 to 2)	2 (2 to 2)	N/A
Bone	3 (3 to 3)	3 (3 to 3)	N/A	2 (1 to 3)	3 (3 to 3)	55.3 (9.4 to 326) ****

TE-, tissue-engineered osteochondral repairs without PEMF; TE+, tissue-engineered osteochondral repairs with PEMF; MF-, microfracture repairs without PEMF; MF+, microfracture repairs with PEMF

There were no significant differences in repair quality at the graft-host junction (OC score; p=0.31) **(Table 5.3)**. However, H&E staining showed evidence of increased matrix fill-in for TE+ specimens compared to TE- **(Figure 5.7E-F)**.

Histologically, tissue-engineered repairs had superior deposition of both GAG **(Figure 5.7I-L)** and type II collagen **(Figure 5.7Q-T)** compared to microfracture. There was not a

significant effect of PEMF in determining overall cartilage pathology in microfracture (p=0.31). However, picrosirius red staining intensity was more intense in non-PEMF groups for both tissue-engineered and microfracture repairs **(Figure 5.7M-P)**.

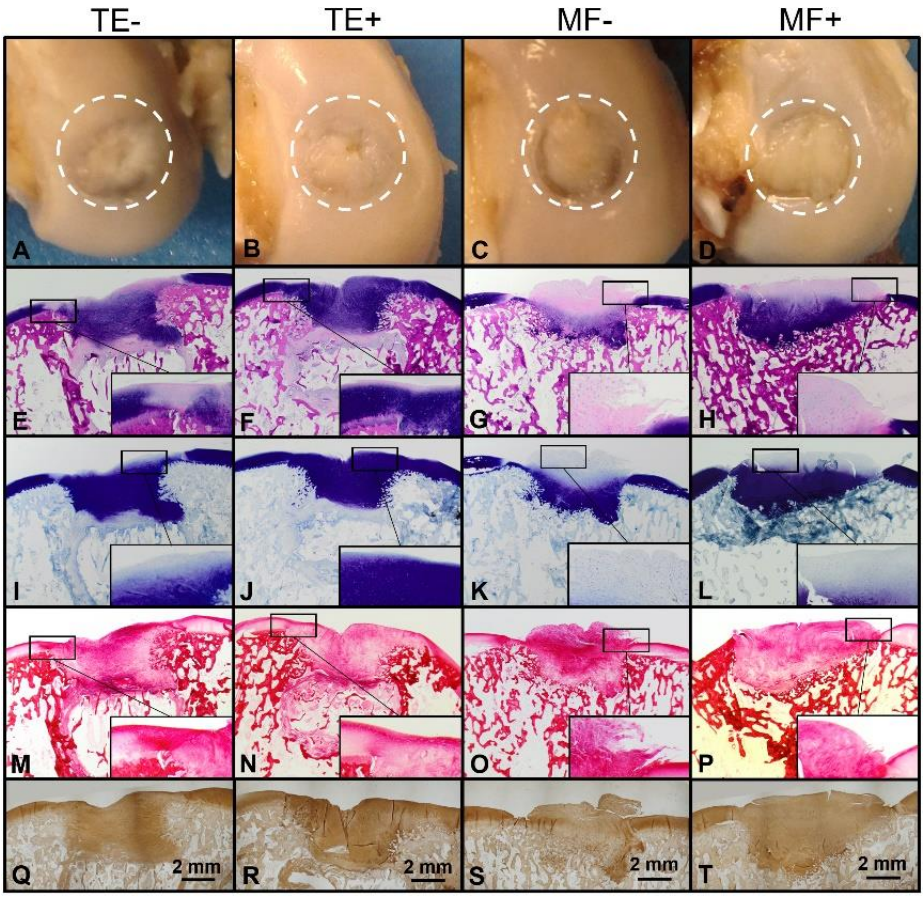

Figure 5.7 Gross imaging and histological staining for selected grafts sites. **(A-D)** Representative gross morphology, **(E-H)** H&E, **(I-L)** toluidine blue, **(M-P)** picrosirius red, and **(Q-T)** type II collagen immunohistochemistry of TE- (ID 90-FCM; A, E, I, M, Q), TE+ (ID 101-FCM; B, F, J, N, R), MF- (ID 105-FCM; C, G, K, O, S), and MF+ (ID 110-FCM; D, H, L, P, T) at 3-month time point (Study 3); Tissue-engineered osteochondral repairs without PEMF (TE-) and with PEMF (TE+); microfracture repairs without PEMF (MF-) and with PEMF (MF+).

Table 5.3 OC TE graft-host junction scores.

Measurement	Median (95% CI)	
	TE-	TE+
OC (Total)	7 (6 to 8)	6 (5 to 8)
Fill	2 (2 to 2)	2 (2 to 2)
Edge Integration	1 (1 to 1)	1 (0 to 2)
Surface Congruity	2 (1 to 2)	1 (0 to 2)
Fibrosis	1 (1 to 2)	1 (1 to 1)
Inflammation	1 (1 to 1)	1 (1 to 1)

TE-, tissue-engineered osteochondral repairs without PEMF; TE+, tissue-engineered osteochondral repairs with PEMF

5.3.6 Modulation of *In Vivo* Inflammatory Environment (Study 3)

TE- repairs had significantly elevated IL-6 ($p=0.0031$) and IL-8 ($p=0.012$) at the 1-month time point **(Figure 5.8)**. With PEMF treatment, TE+ repairs did not have significantly elevated levels of IL-6 ($p=0.32$) or IL-8 ($p=0.62$) at the same time point. Meanwhile, KC was elevated after 1 month for TE+ ($p=0.010$) but not for TE- ($p=0.35$). There were no between-group differences in MCP-1, MMP-1, MMP-2, or MMP-3.

For microfracture repairs, there were no significant increases above baseline for IL-6, IL-8, KC, or MMP-3. Microfracture with PEMF had significantly elevated MCP-1 at both 1-month ($p<0.001$) and 2-months ($p=0.0072$) but repairs without PEMF did not ($p=0.36$ and $p=0.82$, respectively) **(Figure 5.8)**.

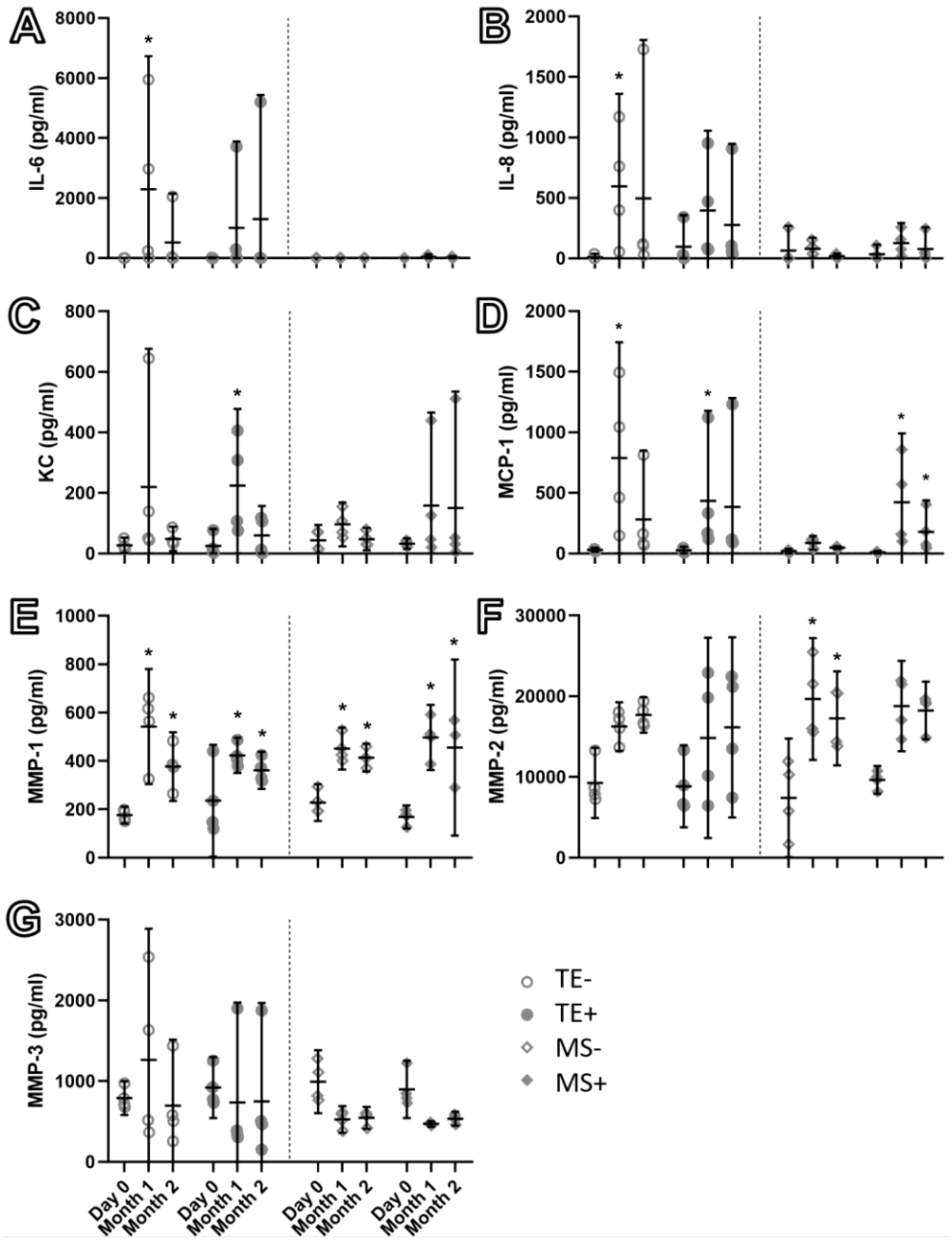

Figure 5.8 Synovial fluid panel of OA-related cytokines. **(A)** IL-6, **(B)** IL-8, **(C)** KC, **(D)** MCP-1, **(E)** MMP-1, **(F)** MMP-2, and **(G)** MMP-3; *p<0.05 compared to Day 0.

TE+ repairs were approximately 1.6x more likely than TE- to have greater overall synovium pathology (p=0.043) **(Table 5.4)**. Specifically, TE+ repairs were about 4x more likely than TE- to have increased pathologic lining characteristics (p=0.014). This disparity was apparent

in synovium histology, which showed synovial villous hyperplasia **(Figure 5.9, arrows)**. No significant differences were observed in number of lining cells or degree of cell infiltration. While synovium in microfracture repairs was not significantly affected by PEMF, TE groups were approximately 3x more likely to present cell infiltration than microfracture groups (p=0.021).

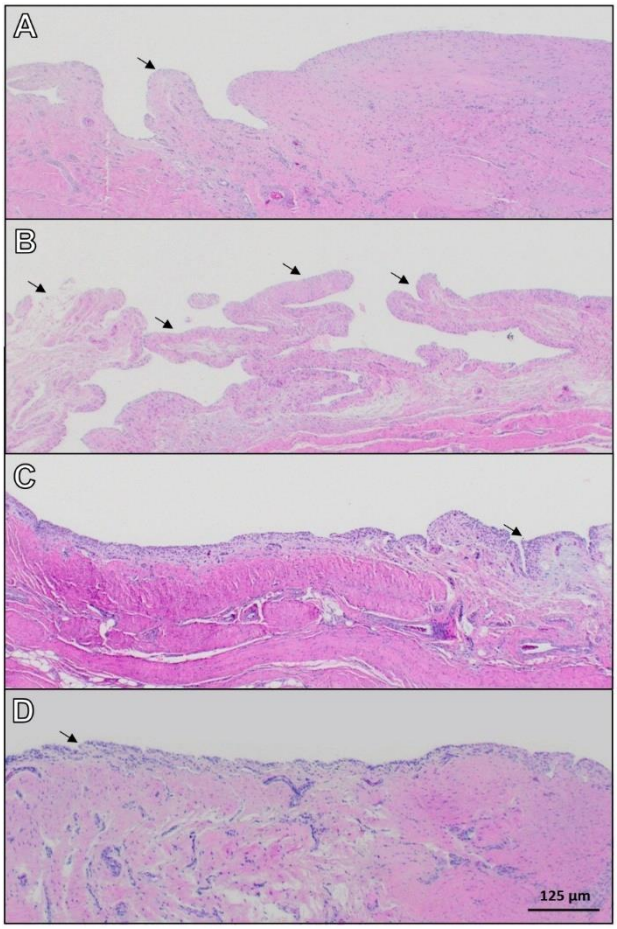

Figure 5.9 Representative H&E of synovium in PEMF-stimulated repairs showing increased villous hyperplasia in TE+PEMF (arrows); **(A)** TE-, **(B)** TE+, **(C)** MS-, and **(D)** MS+.

Table 5.4 Histological scoring of the synovium (OARSI). *p<0.05

	Median (95% CI)			Median (95% CI)		
Measurement	**TE-**	**TE+**	**Odds Ratio (95% CI)**	**MF-**	**MF+**	**Odds Ratio (95% CI)**
OARSI (Synovium Total)	5 (3 to 7)	6.5 (4 to 8)	2.6 (1.0 to 6.4) *	4 (3 to 7)	4.5 (4 to 6)	1.1 (0.4 to 3.2)
Lining Cells	2 (1 to 2)	2 (1 to 3)	1.7 (0.8 to 3.7)	2 (1 to 3)	2 (1 to 3)	1.1 (0.5 to 2.3)
Lining Characteristics	2 (1 to 3)	3 (2 to 4)	4.0 (1.3 to 11.9) *	2 (1 to 3)	2 (1 to 3)	0.9 (0.3 to 2.8)
Cell Infiltration	1 (0 to 1)	1 (0 to 2)	1.3 (0.6 to 3.0)	0 (0 to 1)	0 (0 to 1)	0.8 (0.2 to 3.1)

TE-, tissue-engineered osteochondral repairs without PEMF; TE+, tissue-engineered osteochondral repairs with PEMF; MF-, microfracture repairs without PEMF; MF+, microfracture repairs with PEMF

5.4 Discussion

Although not currently the standard of care, engineered cartilage repair techniques (e.g. MACI) are increasingly gaining clinical acceptance. By improving strategies for preparation and implantation of tissue engineered cartilage, their full potential can be more fully realized. The current studies examined the influence of PEMF on engineered cartilage fabricated from an agarose hydrogel with passaged adult canine chondrocytes (SA2b-c). Overall, PEMF enhanced engineered cartilage repair by modulation of growth (Study 1, SA2b) and integration (Study 2, SA2b) *in vitro*. Specifically, delayed PEMF application improved DNA and GAG content while the parallel PEMF orientation was superior for integrative repair. Furthermore, PEMF significantly improved functional outcomes and cartilage tissue quality *in vivo* (Study 3, SA2c), despite also increasing synovial hyperplasia and only modestly decreasing inflammatory cytokines. As a result of the inconclusive synovial measures, we can only partially accept the hypothesis.

In Study 1, delayed PEMF stimulation led to significantly greater cell content and GAG deposition in immature engineered constructs **(Figure 5.4)**. While GAG/DNA was not also increased, an increase in overall GAG deposition may lead to increased tissue strength. PEMFs

have been implicated in stimulating FGF-2 production (Tepper et al., 2004), which may have contributed to chondrocyte growth and survival in culture.

The time-dependent effect of PEMF suggested a role of cell-matrix adhesions, which had not yet formed at the onset of stimulation in the continuous PEMF group. Previous studies have established that isolated chondrocytes were only responsive to PEMFs in the presence of serum, which is necessary for forming such adhesions (Pezzetti et al., 2014). Furthermore, PEMFs have been shown to stimulate chondrocyte proliferation and GAG synthesis in mature cartilage explants (De Mattei et al., 2007; Ongaro et al., 2011).

PEMF had a similar robust effect on GAG deposition when applied to mature engineered constructs, however the difference was only observed in the construct annuli (Study 2; **Figure 5.6)**. No differences were observed in constructs cores, perhaps due to shielding by the annuli. This theory was supported by finite element modeling, which showed that charge density was concentrated in the annuli for both PEMF orientations **(Figure 5.3)**.

While the increase in GAG deposition was not orientation dependent, parallel PEMF outperformed perpendicular PEMF and CTL in terms of repair stiffness and ultimate failure load **(Figure 5.5)**. This was potentially a result of the more uniform charge density created by the parallel PEMF orientation, particularly at the core-annulus junction **(Figure 5.3)**. Increased collagen content in the perpendicular group may have played a role as well, as it would counteract GAG-induced tissue swelling in the annulus thereby lowering the perceived integration strength.

EF-induced cell migration at the core-annulus interface was another potential contributor to improved graft integration in parallel PEMF specimens. Endogenous EFs are known to guide cell migration and proliferation in developing embryos (Robinson, 1985). Analogous to their role in development, DC EF gradients of 1-10 V/cm guide cell migration during tissue regeneration in

adult animals (Baker et al., 1974; Lippiello et al., 1990; Nessler and Mass, 1987) and cause *in vitro* directed movement of musculoskeletal cells (Chao et al., 2007; O'Connell et al., 2015; Sun et al., 2004). The PEMF system used in this study created a relatively low intensity induced EF of approximately 0.071 V/cm (Benazzo et al., 2008), however it was applied over an extended time period. The EF, which is perpendicular to the magnetic field lines **(Figure 5.1)**, would be offset by 90° in the two orientations, likely causing different patterns of migration. Although migration behavior was not analyzed in this study, future experiments could examine this potential mechanism by tracking cell migration using labeling techniques.

In vivo (Study 3), PEMF-stimulated tissue-engineered repairs were significantly less likely than no PEMF controls to have cartilage pathology (OARSI cartilage score, **Table 5.2**). Specifically, PEMF-treated specimens were less likely to have proteoglycan- and chondrocyte-related pathology than control, which was also apparent from comparatively diffuse toluidine blue staining in the superficial zone of control specimens **(Figure 5.7)**. A similar result was observed in a guinea pig model of OA (Veronesi et al., n.d.); this may have been due to increased TGFβ expression (Aaron and Ciombor, 2004) and chondrogenesis (Ciombor et al., 2002; De Mattei et al., 2007; Ongaro et al., 2011).

In apparent agreement with the results of Study 2, tissue-engineered repair integration was improved by PEMF (**Table 5.3**), although not significantly. H&E staining of the graft-host junction was more intense in PEMF-treated repairs **(Figure 5.7)**. It is possible that only a weak effect was observed in OC sub-scores due to inconsistent PEMF orientation, which was likely dependent on degree of knee flexion and repair location (TG vs. FCL or FCM). Due to coil placement and animals being allowed to walk freely, we speculated that repairs would primarily be exposed to parallel PEMF orientation. However, controlling knee flexion in animals was

inherently difficult, limiting orientation-related conclusions that could be drawn from Study 3. Furthermore, while the animals were all the same size and gender, clinical PEMF dosing is complicated by the varied conductance of different tissue types and different patient sizes (Petrofsky, 2008).

In contrast to cartilage scores, PEMF slightly increased synovial pathology. TE+ repairs were significantly more likely than TE- to have villous hyperplasia **(Figure 5.9, Table 5.4)**. PEMF has been shown to increase collagen I expression and VEGF (de Girolamo et al., 2013), which may have led to the observed synovial pathology. While no differences in lining thickness or inflammatory cell recruitment were observed, PEMF is known to increase FGF-2 production (Tepper et al., 2004), which may have had the unintended effect of stimulating synovial fibroblast proliferation.

Interestingly, the increased synovial pathology did not coincide with increased synovial fluid inflammatory markers (nor worse clinical outcomes). For example, TE- repairs had significantly elevated IL-6 and IL-8 at the 1-month time point (**Figure 5.8**), whereas levels in TE+ repairs were not significantly elevated over baseline. PEMF has been shown to increase adenosine receptor activity in synovial cells and chondrocytes, resulting in the inhibition of pro-inflammatory cytokines (De Mattei et al., 2009; Vincenzi et al., 2013).

Overall, disparate effects of PEMF were observed in microfracture and tissue-engineered osteochondral repairs. Microfracture repairs had a significantly increased likelihood of having subchondral bone pathology in PEMF compared to no PEMF control. The bone pathology presented as increased subchondral bone density, which was apparent in picrosirius red staining **(Figure 5.7)**. This was likely driven in part by increased TGF-β1, BMP-2, and BMP-4 expression

in osteoblasts (Bodamyali et al., 1998; Zhuang et al., 1997), as well as increased osteoblast proliferation and reduced osteoclast formation (Chang et al., 2005; Otter et al., 1998).

Increased bone growth has also been observed at the transplant-host junction of the subchondral bone in an *in vivo* autograft model (Benazzo et al., 2008). While it was considered beneficial for early graft stabilization and preventing bone resorption, it is possible that PEMF dosage would need to be modified (i.e. lowered) in microfracture repairs to prevent this pathologic bone thickening. It is further speculated that due to tissue density and maturity, OCA repair, the current standard of care, would perhaps require an elevated PEMF dose in order to observe similar integrative benefits to cartilage that were seen in tissue-engineered constructs.

Microfracture repair tissue is often described as sub-optimal in quality (Mithoefer et al., 2009), and this was reflected in the improved functional outcome of engineered vs. microfracture repairs in Study 3. Microfracture had significantly worse scores at 3 months, compared to baseline, for gait, CROM, and TPI **(Table 5.1)**. Meanwhile, these parameters were not significantly different from baseline in tissue-engineered groups, indicating a near absence of functional limitations. Engineered repairs outperformed microfracture in lameness score as well. This was likely due to superior cartilage tissue quality, as demonstrated by increased deposition of both GAG and type II collagen **(Figure 5.7)**.

Despite the positive clinical outcome measures, elevated baseline cytokine levels (**Figure 5.8**) were observed in engineered construct groups. This may have been indicative of increased overall metabolic activity and tissue healing, as proposed in the discussion of **Chapter 3**. Alternatively, we speculate that the observed differences between microfracture and engineered cartilage repairs may have been a result of the allogenic cells in the engineered constructs. *In vitro* studies described herein were based only on activities of chondrocytes seeded into the construct,

whereas *in vivo* experiments incorporated the contributions of a complex milieu of other joint tissues, including synovial- and bone marrow-derived stem and immune cells. The cell content and matrix structure of synovium is altered dramatically in different stages of disease (Stefani et al., 2018), and likely changing the overall effects of PEMF as well.

Although the devitalized bone bases did not elicit an immunogenic response in biocompatibility tests (data not shown), future studies may choose to utilize a more robust porous titanium scaffold (Bal et al., 2010). Overall, we anticipate that engineered cartilage is analogous to allogeneic cartilage allografts, which have been used clinically for decades and not thought to pose a significant immunogenic risk (Bugbee et al., 2016).

To the authors knowledge, this is the first report of PEMF for improved engineered cartilage growth and integration, both *in vitro* and *in vivo*. This preliminary *in vivo* experiment was potentially limited by sample size, which was improved by creating multiple defects per knee. Based on previous canine studies in our laboratory, we determined a priori that a sample size of approximately 17 repairs per group would be required to achieve a power of at least 0.8. Nevertheless, trends and significant between-group differences were observed for many of the outcome measures. While some success in alleviating pain has been reported in previous clinical PEMF studies, our preclinical model provides a valuable platform for optimizing focal defect repair protocols based on individual mechanisms of action. It will be important to determine if benefits to growth translate to improved long-term clinical repairs.

5.5 Conclusion

The current studies, which utilized clinically relevant parameters associated with the IGEA device, demonstrated that applied PEMFs can enhance engineered cartilage repair through modulation of

cartilage growth and healing. And while it is possible that increased synovial hyperplasia observed here, in the absence of increased inflammatory cytokines, was indicative of non-catabolic changes to synovium structure-function, additional studies will be required to confirm this. Therefore, the presented data is partially supportive of the global hypothesis outlined for Part II. In order to capitalize on potential anti-inflammatory behavior in synovium, further evaluation of structure-function in response to PEMF will be needed, perhaps utilizing the engineered model described in **Chapter 2**.

Using *in vitro* models (Study 1 and 2, SA2b) and confirmatory *in vivo* models (Study 3, SA2c) of cartilage restoration provide guidance for optimizing PEMF strategies to maximize clinical cartilage graft survival and function. Engineered osteochondral grafts were pre-cultured for 42 days prior to implantation and initiation of PEMF stimulation (Study 3), mimicking the delayed PEMF protocol evaluated in Study 1. Furthermore, the PEMF coil was oriented on the frontal plane to maximize time spent in a "parallel" orientation during normal movement. Moving forward, we hypothesize that PEMF dosage can be further optimized to target improved pre-implantation cartilage properties and decreased catabolic activities post-implantation, leading to better long-term clinical outcomes. Although not currently the standard of care, engineered cartilage repair techniques are increasingly gaining clinical acceptance. By improving strategies for preparation and implantation of tissue engineered cartilage, the full potential of tissue engineered constructs can be more fully realized.

Chapter 6

Direct Current Electric Fields Increase Mobilization of Synovial Cells

6.1 Introduction

In addition to being key effector cells within the synovium in both IL and DEX-treated **(Chapter 2)** and PEMF-stimulated **(Chapter 4)** conditions, synovial cells have also been directly implicated in cartilage repair (Bilgen et al., 2007; Rui et al., 2010; Sampat et al., 2011a). FLS are recruited to the site of partial thickness defects *in vivo*, however the efficiency of their migration into the wound site is generally insufficient for effective healing (Hunziker and Rosenberg, 1996). Meanwhile, proliferation of resident MLS and infiltration of peripheral blood mononuclear cells (PBMCs) contribute to the pro-inflammatory environment and further joint degeneration (O'Brien et al., 2017; Utomo et al., 2016). Development of a method to direct migration of one or more cell types of interest may facilitate the natural healing process or serve as a method for repopulating devitalized allogenic and xenogeneic tissues.

DC EFs, which have been shown to induce galvanotaxis *in vitro* **(1.3.4.2)**, may allow the selective homing of repair cells (Chao et al., 2000; Finkelstein et al., 2007; Tan et al., 2011) and exclusion of immune cells (Douglas et al., 2019; Orida and Feldman, 1982). Furthermore, migration behavior likely differs based on biological substrate or culture within three-dimensional matrices. Galvanotaxis of FLS and MLS (or adherent PBMCs) has not been explored in a 3D repair model, either as a method to increase homing of FLS repair cells or to exclude inflammatory cells.

Such an *in vitro* model will be crucial in translating findings to a preclinical system that will ostensibly require implanted electrodes.

Below, we explore strategies to enhance and direct cell migration in the joint to be used to amplify the intrinsic repair process of cartilage as well as to support cell-based therapies of cartilage repair. First, we evaluated potential galvanotactic behavior of adherent PBMCs in the existing 2D experimental chamber used by our laboratory (SA2d). Next, we modified this chamber in order to view migration of FLS within a collagen repair matrix (SA2e). Finally, we designed and validated a new culture chamber capable of applying DC EFs to 3D tissues in a sterile and biomimetic culture configuration (SA2f). Overall, *we hypothesized that adherent PBMCs and FLS exposed to DC EFs, in 2D and 3D, respectively, would exhibit directed migration. Furthermore, development of new bioreactor approaches would facilitate application of DC EFs to three-dimensional synovium and cartilage specimens in biomimetic configurations.*

6.2 DC EFs Increase Migration Speed of Adherent Inflammatory Cells

6.2.1 Introduction

Under DC EF stimulation, macrophages have been shown to migrate towards the anode (Orida and Feldman, 1982), whereas FLS may migrate in the opposite direction (i.e. cathode) at certain passage numbers (Tan et al., 2011). Although the exact mechanism of galvanotaxis is not known, it is thought to be dependent on cell adherence and therefore not an electrophoretic phenomena (Finkelstein et al., 2007). Monocytes and macrophages are major constituents of PBMCs (Ulmer et al., 1984) that invade the joint, and they can easily be separated and isolated via their ability to adhere to substrates (Bennett and Breit, 1994). This study aimed to investigate DC EF-induced migration of adherent PBMCs (i.e. monocytes and macrophages) in culture (SA2d). Given the

important role of MLS in driving structural changes in synovium **(2.3)**, the ability to direct migratory behavior of inflammatory cells may impact the progression of OA symptoms and synovial hyperplasia.

6.2.2 Materials and Methods

6.2.2.1 2D Galvanotaxis Chamber

The galvanotaxis chamber **(Figure 6.1)** was based on a modified flow chamber assembly (A. R. Tan et al., 2015b). Briefly, silver–silver chloride electrodes were fabricated from silver wire soaked for one hour in a hypochlorite solution (Clorox Bleach) and interfaced with ports on each side of the galvanotaxis channel via a pair of 30-cm long, 2% agarose–PBS bridges. These bridges prevented contamination of the cells from electrolysis products generated during current application using a power supply (Keithley Instruments). The conductive media was DMEM supplemented with 5% FBS, which had adequate protein concentration for cellular adherence and ion concentrations for current flow. The chamber also consists of a glass window, facilitating real-time microscopic analysis.

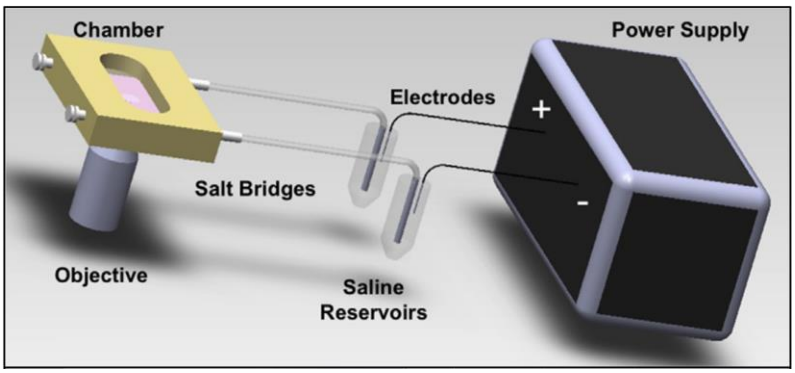

Figure 6.1 Schematic of classic 2D galvanotaxis system. Cells are plated on a glass slide and exposed to EF gradient for three hours with continuous microscopic monitoring (A. R. Tan et al., 2015b).

6.2.2.2 Preparation, Culture, and DC EF Stimulation of Adherent PBMCs

A leukopak, obtained from a healthy blood donor (n=1, Type O+), was purchased from New York Blood Center (New York, NY). PBMCs were isolated via density centrifugation with Ficoll-Paque (GE Healthcare, Cat. No. 17144002) (Ulmer et al., 1984).

Prior to assembling the galvanotaxis chamber, PBMCs were precultured for 2 hours at 37°C in DMEM supplemented with 5% FBS on un-coated glass slides with removable silicone wells (10^5 cells/cm^2). Silicone wells were then removed and non-adherent cells were thoroughly rinsed from the slides before placing in the galvanotaxis chamber. Subsequently, a current of 3.33 mA was applied, resulting in an EF = 6 V/cm, for 3 hours at room temperature. Control slides were cultured in parallel chambers with no EF stimulation.

6.2.2.3 Image Analysis

Photomicrographs (10x magnification with phase contrast filter on an Olympus IX-70 inverted microscope) were collected at 10-min intervals during the 3-hour stimulation period. Resulting images were manually analyzed using custom MATLAB code in order to extract overall speed, incremental speed, migration direction, and directed velocity (A. R. Tan et al., 2015b). Briefly, coordinates of each cell's centroid were tracked, using the initial starting position as the origin. Overall speed was derived from the overall net displacement (i.e. magnitude of the vector starting at the origin and ending at the final cell position) divided by the 3-hr experimental period. Incremental speed was computed at each individual 10 min interval. Migration direction was defined based on the position of the migration vector, whereby the cathode (-) and anode (+) were positioned at 90° and 270°, respectively. Directed velocity was defined as the component of the

speed directed toward the cathode (90°). Mean angle was computed as the average of unit vectors for each cell. A total of 19-20 cells were evaluated for each run (n=3-4).

6.2.2.4 Statistics

Statistical comparisons were made with the Mann Whitney test ($\alpha = 0.05$). Values were presented as median ± interquartile range (IQR). Computations were all made with Graphpad Prism 8 (La Jolla, CA).

6.2.3 Results

6.2.3.1 Adherent PBMC Migration

Mean incremental speed computed over the three-hour stimulation period was significantly decreased by DC EF application (19 vs. 15 μm/h; between-group difference, -4 μm/h; p=0.0017) **(Figure 6.2)**. There was no statistical difference in overall migration speed (p=0.20) or directed velocity (p=0.12). Mean migration angle was 272° for EF and 177° for CTL.

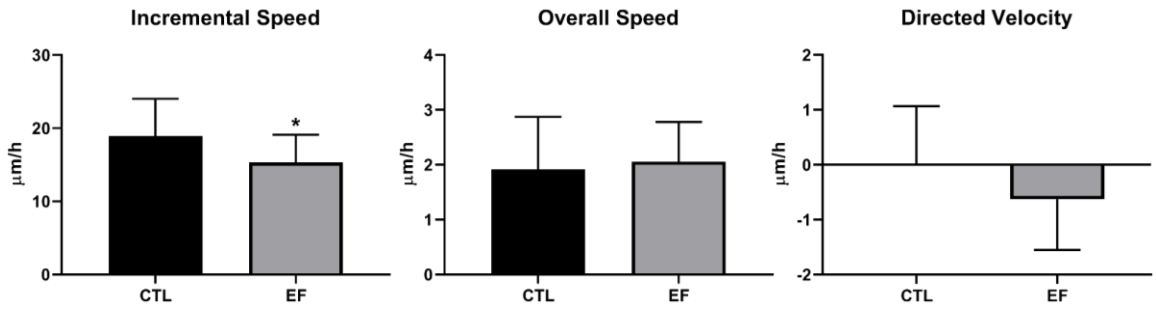

Figure 6.2 Effect of DC EFs on incremental speed, overall speed, and directed velocity of adherent PBMCs in 2D. *p<0.01 compared to CTL (no EF); Total cells analyzed for CTL (n=59) and EF (n=80) over three and four separate runs, respectively; Median and IQR shown in plots.

6.2.4 Discussion

Infiltration of PBMCs from the vasculature is a hallmark of OA synovium (O'Brien et al., 2017; Utomo et al., 2016). A majority of these infiltrating mononuclear cells have been identified as $CD14^+$ monocytes and macrophages (Moradi et al., 2015; Pessler et al., 2008), which are unique among PBMCs in that they adhere to substrates in culture (Bennett and Breit, 1994). In the preceding experiments, DC EF-induced migration of the adherent subpopulation of PBMCs was explored (SA2d). We observed increased kinetic activity in response to a DC EF, however no preferential migration direction **(Figure 6.2)**. Therefore, the presented data does not support our hypothesis.

Both incremental and overall speed were evaluated in this study. Incremental speed was derived from the cell displacement observed in each individual 10-min interval. Overall speed, however, considers only the start and end point of each cell over the 3-hr stimulation. The increase in incremental speed without a corresponding increase in overall speed was characteristic of increased random cell motility. This was also evident from the lack of difference in directed velocity between groups. This result was unanticipated, based on previous research showing preferential migration of macrophages in culture (Douglas et al., 2019; Orida and Feldman, 1982). However, it should be noted that the mean angle of migration in EF-stimulated samples was 272°, almost exactly towards the anode. While this may have been by chance, it possibly indicates an extremely low level of direction preference.

Although likely not useful for excluding these cells from the joint (i.e. the original hypothesis), increased overall kinetic behavior may have other implications. Additional work will be required to assess any concurrent changes in PBMC function and viability. PBMCs are thought to be major contributors to synovial pannus formation, so disrupting this function could have

clinical benefit. Induced EFs have also been shown to affect the immunogenic response of macrophages to bacterial infection (Akan et al., 2010). Modulation of PBMC behavior may also be used to complement other modes of joint repair; PBMCs have been shown to enhance migration of chondrocytes both *in vitro* and *in vivo* (Hopper et al., 2015b, 2015a).

6.3 DC EFs Induce Migration of FLS within a Collagen Repair Matrix

6.3.1 Introduction

Galvanotaxis of FLS has been demonstrated on 2D substrates, however the preferential migration direction was dependent on passage number (Tan et al., 2011). It is anticipated that migration behavior may differ on biological substrates or within three-dimensional matrices, and understanding this phenomenon will be critical for eventual clinical translation. Directed migration may also be useful in populating or re-populating scaffolds for tissue engineering applications (Rajabi et al., 2015). 3D collagen- or Matrigel- based migration assays have been described using Transwells or culture dishes (Timpson et al., 2011), however to our knowledge these systems have not been used to evaluate galvanotaxis of FLS. In this study, we modified the classic galvanotaxis chamber **(Figure 6.1)** in order to view migration of FLS within a collagen hydrogel (SA2e), similar to (Sun et al., 2004).

6.3.2 Materials and Methods

6.3.2.1 Cell Isolation and Culture

Juvenile bovine FLS were isolated and passaged (P2) as previously described **(2.2.2)**.

6.3.2.2 Galvanotaxis Chamber Assembly and Application of DC EF

The galvanotaxis chamber and parameters described in the previous section **(6.2.2.1)** were used. However, instead of culturing cells directly on glass slides, FLS (10^5 cells/ml) were encapsulated directly in a type I collagen hydrogel (2 mg/ml; ThermoFisher, Cat. No. A1064401). This resulted in a thin collagen gel with the exact geometry of the channel. Briefly, concentrated collagen was diluted, osmotically balanced with 10x PBS, and neutralized with 1 N NaOH prior to thoroughly mixing in cells, on ice. This FLS-seeded collagen gel (100 µl per chamber) was allowed to solidify directly in the chamber for 2 hours at 37°C prior to DC EF stimulation (6 V/cm) at room temperature for 4 hours. Control samples without applied DC EF were performed in parallel.

6.3.2.3 Image Analysis

Photomicrographs were collected and analyzed as previously described **(6.2.2.3)**. A total of 20-24 cells were evaluated for each run (n=1).

6.3.2.4 Statistics

Statistical analyses were performed as previously described **(6.2.2.4)**.

6.3.3 Results

DC EF-application led to significantly increased incremental speed (6.9 vs. 1.9 µm/h; between-group difference, 5.0 µm/h; $p<0.0001$), overall migration speed (2.5 vs. 1.4 µm/h; between-group difference, 1.0 µm/h; $p<0.0001$), and directed velocity towards the anode (1.9 vs. 0.5 µm/h; between-group difference, 1.4 µm/h; $p<0.001$), **(Figure 6.3)**. Mean migration angle was 46° for

EF and 156° for CTL, which was clearly reflected in plots showing the path of each individual cell **(Figure 6.4)**.

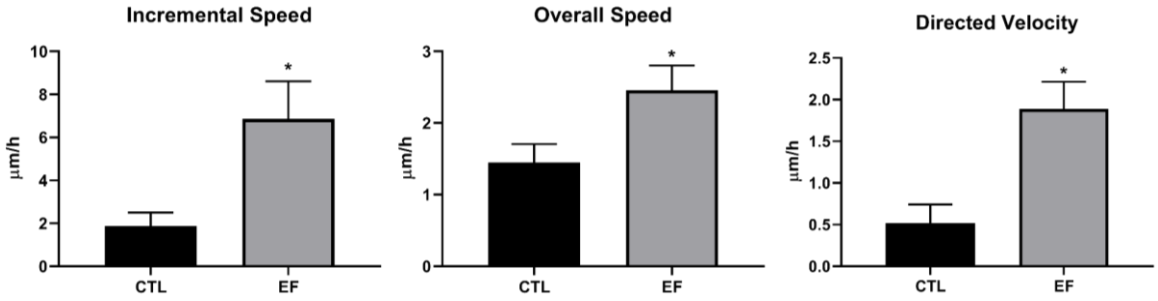

Figure 6.3 Effect of DC EFs on overall speed, incremental speed, and directed velocity of bovine FLS in 3D. *p<0.001 compared to CTL (no EF); Total cells analyzed for CTL (n=20) and EF (n=24); Median and IQR shown in plots.

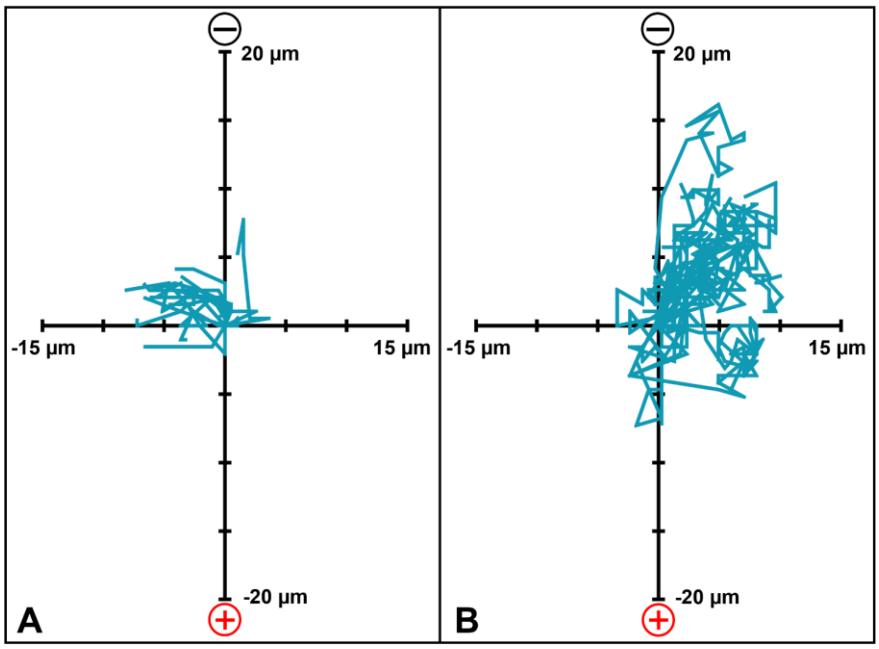

Figure 6.4 Individual migration paths for FLS in 3D collagen gel. **(A)** E- (n=20), **(B)** E+ (n=24) Tracking of each cell began at the origin, with positive y-displacement indicating cathodal migration.

6.3.4 Discussion

Galvanotaxis of bovine FLS within a 3D collagen hydrogel was explored (SA2e) through the modification an established system for evaluating 2D migration (Chao et al., 2007, 2000; O'Connell et al., 2015; Tan et al., 2011). In the collagen substrate, FLS exhibited cathodal-directed migration as well as an increase in overall and incremental speed. Therefore, we accept the hypothesis that FLS exhibit directed migration in 3D culture conditions.

In our hands, P2 FLS had a cathodal-directed velocity of 1.9 μm/hr when exposed to a 6 V/cm EF **(Figure 6.3)**. This was similar to previous work from our laboratory, which showed that P4 FLS demonstrated cathodal-directed velocity of up to 5 μm/hr in 2D (Tan et al., 2011). In one study of human fibroblasts embedded in 0.58 mg/ml collagen and exposed to 0.1 V/cm, cells migrated at a velocity of 13.8 μm/h, however the same cells did not migrate in 2D or in 1.08 mg/ml collagen (Sun et al., 2004). The clinical relevance of such a low collagen concentration is dubious, due to the extremely low mechanical properties. In a follow-up study by the same group, human fibroblasts in 2 mg/ml collagen and exposed to 10 V/cm did not migrate, but did realign perpendicularly to the EF (Sun et al., 2006).

The mode of cell tracking, via the centroid, may have underestimated migration distance in our experiment. Mesenchymal cells typically migrate via dendritic outgrowths (Friedl and Wolf, 2010), which may not have been observed using an inverted microscope with brightfield illumination. It is also likely that cells formed additional focal matrix adhesions in the collagen gel, which can complicate migration (Qu et al., 2019; Sun et al., 2006). This, along with the porosity of collagen hydrogel, may have contributed to slower directed migration observed here. In anticipation of this, the collagen concentration used in the current work (2 mg/ml) was chosen for being the lowest concentration that formed a stiff gel. However, other work has shown that 2

mg/ml collagen hydrogels have an average pore size of 2 μm^2 (Miron-Mendoza et al., 2010). Cells and their nuclei can constrict to fit through pores as small as 3 μm^2, but cell translocation becomes limited at pore sizes below 25 μm^2 (Qu et al., 2019).

6.4 Development of a 3D Bioreactor Capable of Modeling FLS Migration within a Cartilage Defect

6.4.1 Introduction

In this study, migration of synovial repair cells was demonstrated *in situ* on cartilage explants using a custom, versatile galvanotaxis chamber (SA2f). The chamber was designed with the goal of applying DC EFs to 3D specimens to simulate the migration of endogenous and/or exogenous repair cells into a substrate or defect. To demonstrate the capabilities of the system, EFs were directionally applied through a piece of synovium overlaid in apposition with cartilage explants (Ng et al., 2010). This tissue configuration was chosen to mimic the proximity of the synovium and cartilage in the diarthrodial joint and provide a route for FLS to contribute to the limited repair of cartilage observed after injury (Bhattaram and Chandrasekharan, 2016; Hunziker and Rosenberg, 1996). FLS migration into the mock defect was quantified and long-term viability of EF-exposed cells was confirmed. Finally, to characterize the electrokinetic conditions associated with the applied EF in our custom chamber, we employed finite element modeling to describe the current density distribution for the different experiments performed.

6.4.2 Materials and Methods

6.4.2.1 Chamber Design

Using an established flow-chamber based galvanotaxis system **(Figure 6.1)** as a basis, a novel 3D galvanotaxis chamber **(Figure 6.5B)** was designed using CAD software (Solidworks, Waltham, MA). The upper and lower chamber is separated by an O-ring and held together with screws, thereby accommodating cylindrical specimens while preventing current leakage. As such, a sealed cylindrical channel with a 5-mm diameter and a 1-mm height was formed to accommodate the specimen. The well-defined chamber geometry permitted the electric field strength (E) and current density (J) to be calculated using Ohm's Law. The resistance of the chamber was 35.8 kΩ, which was consistent with theoretical calculations.

The anode (+) and cathode (-) were positioned above and below the sample chamber, respectively. The power supply, electrodes, and salt bridges were prepared as before **(6.2.2.1)**. The total chamber volume was approximately 2.5 ml, allowing sufficient media supplementation for large constructs and ion concentration to conduct current.

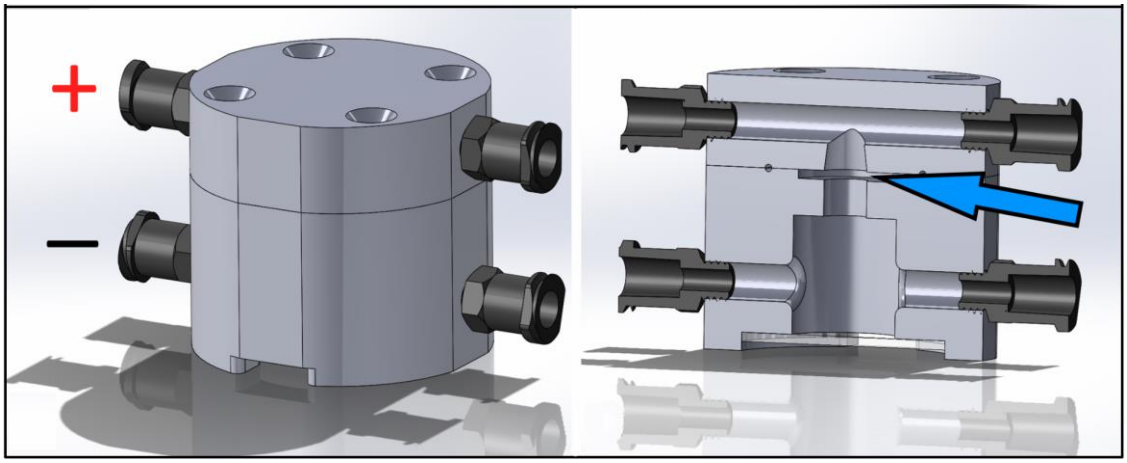

Figure 6.5 Schematic of novel 3D galvanotaxis system. The chamber allows application of EF gradients (electrode positions denoted (+ and -) to 3D tissues and constructs (blue arrow indicates specimen location).

6.4.2.2 3D Printing of Chamber

The chamber was 3D printed using an Ultimaker S5 (Cura v4.2.1; Utrecht, Netherlands) with Taulman Nylon 680 filament. Nylon filament was selected due to FDA approval and compatibility with autoclaving and ethanol sterilization ("Nylon 680 Spec," 2016). The main parameters necessary for good results are 100% infill with modified: printing speed, temperature, ironing setting, layer height, build plate temperature, retraction speed/distance, fan speed, build plate adhesion, and support material **(Table A.2.1)**.

After printing, the support material was removed by soaking in warm water. Then the chamber assembly was tapped and drilled. Once all of the holes are threaded and drilled, the final the clear acrylic cap for the bottom chamber of the bioreactor was prepared. The acrylic cap was laser cut from an acrylic sheet between 1.2 mm to 1.6 mm in thickness and adhered to the assembly with Loctite® 4902 cyanoacrylate adhesive.

6.4.2.3 Finite Element Analysis of Chamber

FEBio (v. 2.6.0) was used to model the current flow within a the cartilage explant system (Maas et al., 2012). The cartilage and bath were modeled as multiphasic materials with neo-Hookean solids. Na^+ and Cl^- solutes were permitted to transport throughout the system as this framework maintains electroneutrality throughout all of the material phases (Ateshian et al., 2013). The material properties and solute transport properties is supplied in the supplemental materials **(Table A.2.2)**.

Geometries were based on: a PBS bath with a ∅5 mm × 2 mm cartilage ring with a central (a) ∅1 mm × 2 mm defect, (b) ∅1.5 mm × 2 mm defect, (c) ∅2.0mm × 2 mm defect, or (d) ∅5.0mm × 2 mm defect (empty). After establishing equilibrium conditions **(Equation 6.1)**,

current density was imposed (in a manner similar to the experimental procedure) using an effective prescribed solute flux to represent the flow of Cl^- based on the Ag-AgCl kinetics. Models were kept electrically-grounded through a linear constraint to maintain $c^{Na^+} = c^{Cl^-}$ within the middle of the collagen gel, in the middle of the analysis. Axisymmetric boundaries were imposed to reduce model size while maintaining the experimental cylindrical geometry.

Equation 6.1 Equilibrium conditions for finite element modeling.

$$c^{Na^+} = c^{Cl^-} = 150\ mM; p = 0\ MPa;\ cartilage\ fixed - charge\ density = -200\ mM$$

6.4.2.4 Tissue Harvest and Culture

Fresh bovine cartilage and synovial tissue was harvested and maintained as before **(2.2.2.1)**. Ø5mm full thickness osteochondral cores were harvested from the femoral condyles and trimmed to remove subchondral bone.

6.4.2.5 FLS Migration into a Cartilage Defect

To create a cartilage defect, Ø1mm cores were removed from each cartilage explant with a biopsy punch. An intact section of juvenile bovine synovium (~5 mm × 5 mm × 1 mm thickness) was then labeled with a lipophilic membrane dye (Vybrant DiI, Life Technologies) and placed in direct apposition to the cartilage explant prior to EF stimulation **(Figure 6.6)**. Explants were pre-cultured overnight in DMEM supplemented with 5% FBS. Explants were placed in the chamber and current was applied for three hours, generating an applied field strength E= 6 V/cm (E+). Control samples (E-) were handled similarly, but without the application of the EF.

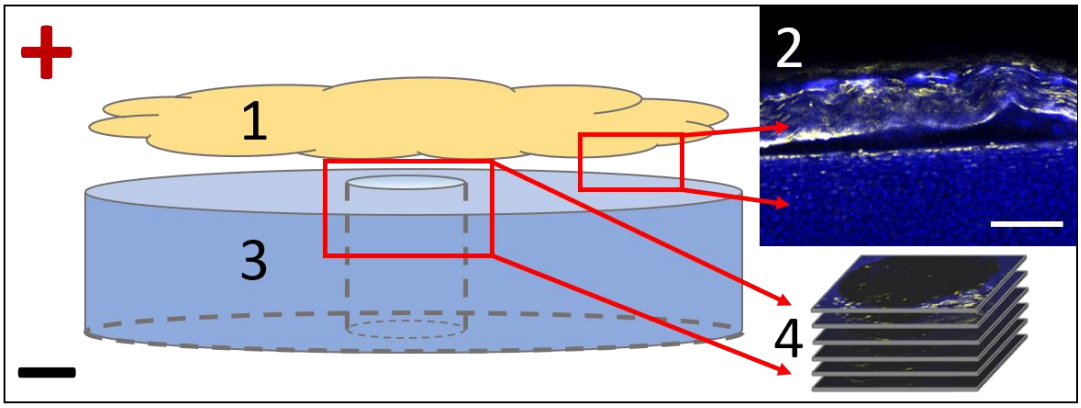

Figure 6.6 Schematic of cartilage-synovium defect-repair model. The chamber's anode (+) and cathode (-) were positioned above and below the specimen, respectively. DiI-labeled synovium (1, yellow) was placed in direct contact (2) with DAPI-labeled cartilage (3, blue). Synovium removed for confocal z-stack imaging (4), leaving migrated cells on cartilage specimen. Scale bar = 100 µm

6.4.2.6 Confocal Imaging

A subset of samples was set aside and immediately analyzed for viability in each condition (Live/Dead kit, Thermofisher). The remainder of samples were fixed in 4% paraformaldehyde overnight. The synovium was then removed from the explant, leaving migrated cells behind. Specimens were subsequently stained with DAPI (Sigma Aldrich) for co-localization of endogenous cartilage cells with the migrated synovial cells (stained with DiI) on the cartilage explant. A confocal microscope (Zeiss) was used to visualize cell accumulation at the cartilage surface and cartilage defect site. Additionally, z-stacks with a 40 µm step-size were used to characterize the migration distances within the constructs **(Figure 6.6)**. This step size was chosen to ensure that no FLS were missed or double counted in the subsequent image analysis. Only FLS that had adhered to the cartilage explant were evaluated. These were identified by co-localization of DAPI and DiI stains on the cartilage surface. Cells were classified as either "transferred" or "migrated," meaning that they were either in contact with the upper rim of the defect (visible in

first z-stack image) or visible at ≥40 μm depth, respectively. The number of migrated cells was normalized to the total number of transferred plus migrated cells. Directed velocity was computed assuming constant cell migration over the 3-hour experiment, and non-migrating cells (i.e. transferred to cartilage surface only) were considered to have a velocity of 0.

6.4.2.7 Statistics

The proportion of migrated vs. transferred cells was analyzed via Fisher's Exact Test ($p<0.05$). Transferred and migrated cells were counted and pooled from N=3 constructs in each EF condition, yielding 237 total FLS in the E+ condition and 132 total FLS in the E- condition. Directed velocity of transferred cells was analyzed using the Mann Whitney Test ($p<0.05$) and values were expressed as mean ± standard deviation.

6.4.3 Results

6.4.3.1 Chamber Validation and FEBio Modeling

Finite Element Analysis Showed Distinct Current Gradients Dependent on Specimen Geometry and Material. At equilibrium, current density **(Figure 6.7)** was concentrated at the defect site, as expected from electrical computations. The highest concentration of current was seen at the inner cut surface of cartilage defect, throughout its entire depth. The empty chamber had a homogeneous current density profile. Electrical computations and FEBio outputs were validated by taking measurements of the chamber with varying sized cartilage (conductive) and rubber (insulative) constructs with varying defect sizes **(Table 6.1)**.

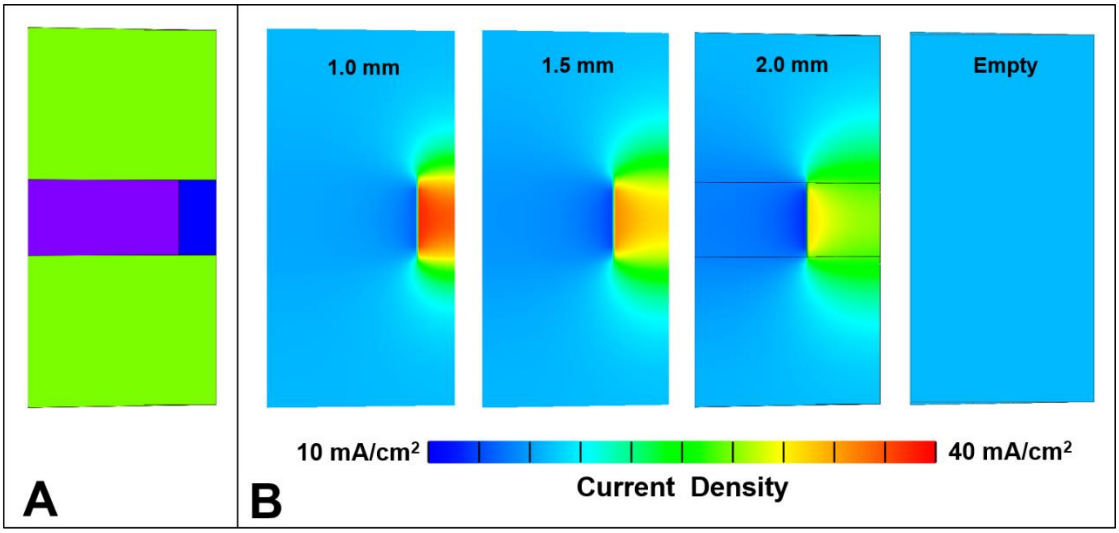

Figure 6.7 Estimated current density as estimated with FEBio. (**A**) The system was modeled in FEBio as two bathing solutions (green) above and below the cartilage explant (purple), with a biopsy punch defect in the center (blue). To simplify computations, the symmetric sample and chamber was modeled as a wedge. (**B**) Current density at equilibrium was concentrated in the defect. Gradients were sensitive to small changes in defect size (3.33 mA applied).

Table 6.1 Theoretical and actual specimen voltage drop in galvanotaxis chamber.

Defect Diameter (mm)	**$E_{Theoretical,\ Ohm's\ Law}$ (V/cm)**	**E_{actual} (V/cm)**	**$J_{Theoretical,\ FEBio}$ (mA/cm^2)**
1.0	4.8	6	~34-40
1.5	4.1	4	~31-34
2.0	3.4	3	~28-31
5.0 (Empty)	1.1	-	~16-19

Voltage drop (E, V/cm); Current density (J, mA/cm^2); Theoretical Ohm's Law values were predicted using Ohm's Law and an applied current of 3.33 mA, media resistivity of 0.6579 Ωm, cartilage resistivity of 3.268 Ωm (Binette et al., 2004), and 2.2 mm sample thickness. FEBio-predicted values were approximated from resulting heat maps.

6.4.3.2 FLS Migration in Wound Repair Model

EF-Stimulation Increased Both Cell Recruitment and Average Migration Velocity in an Explant Model. EF specimens (E+) showed enhanced migration into the defect site and a larger number of adherent FLS overall **(Figure 6.8)**. Approximately 89% of adherent cells had migrated at least 40 µm into the defect in the EF group, compared to 45% in controls (E-). Additionally, EF increased directed velocity of FLS into the defect relative to control **(Figure 6.9).**

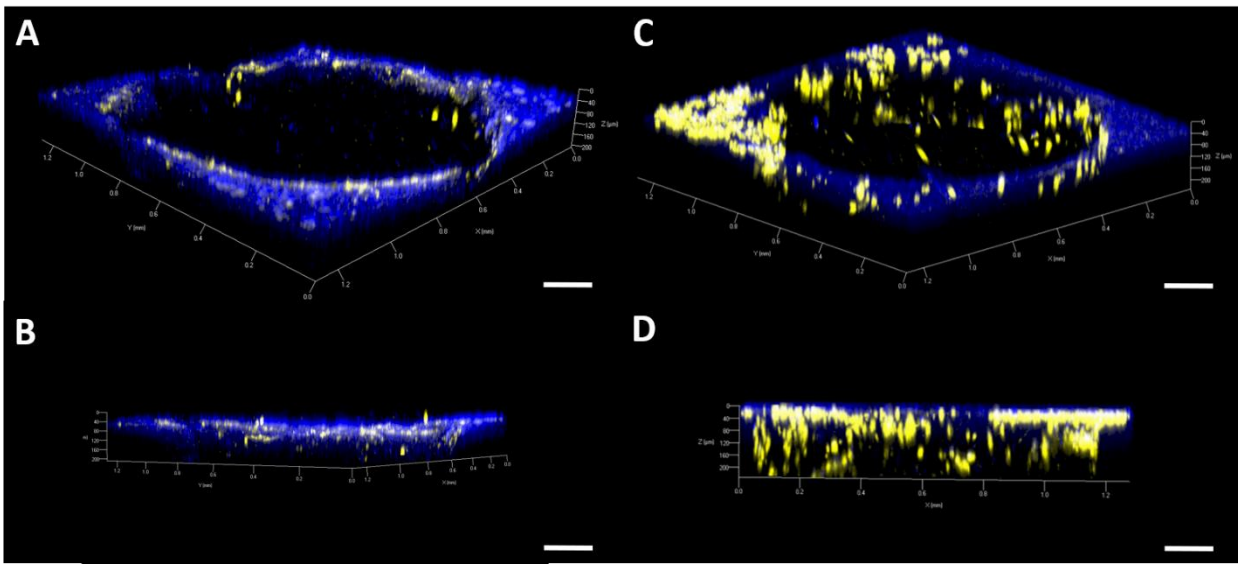

Figure 6.8 Representative confocal reconstructions of FLS migrating into cartilage defect. (**A**) top and (**B**) side view of control (E-) showing minimal FLS migration. (**C**) Top and (**D**) side view of explant exposed to DC EF for 3 hours (E+) showing migration to a depth of up to 200 µm. Synovium was removed for imaging, leaving migrated cells behind. Scale bars = 200 µm

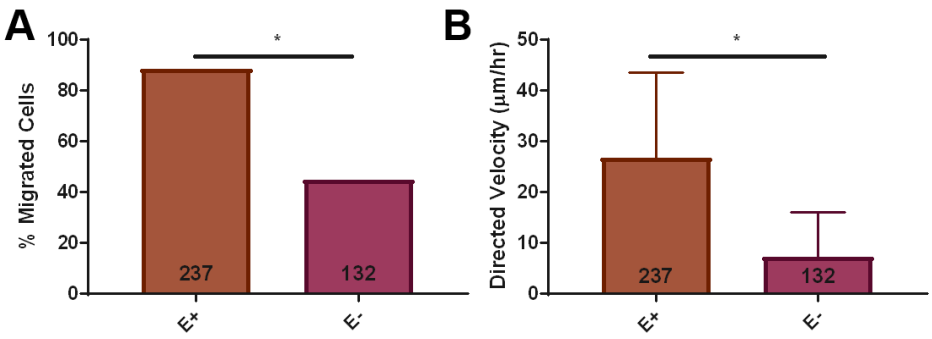

Figure 6.9 Cell migration affinity and directed velocity. **(A)** Effect of EF on FLS migration into the cartilage defect. Significantly more FLS migrated in the E+ (6 V/cm) group, compared to E- ($p<0.05$). **(B)** Effect of EF on FLS directed velocity into a cartilage defect. FLS had significantly greater velocity towards the cathode in E+ groups compared to E- ($p<0.05$). N reported on each bar, pooled across triplicate samples.

6.4.4 Discussion

A custom galvanotaxis chamber was designed, tested, and characterized to evaluate cell migration on a biological substrate due to applied EF strengths of magnitude similar to those reported to promote galvanotaxis in 2D (SA2f). The system was modeled and validated using finite element analysis, basic circuit computations, and multimeter measurements. In a pilot study using the system, cathodal migration of synovial repair cells was observed in a cartilage explant defect repair model. Passaged SDSCs have been shown to migrate preferentially towards the anode (+) or cathode (-) at early or late passages, respectively (A. R. Tan et al., 2015b; Tan et al., 2011). While our current experiments did not allow for examination of bi-directional migration, the system can be easily modified to do so by culturing labeled cells on multiple surfaces of the construct. Overall, we accept the hypothesis that development of novel bioreactors can facilitate application of DC EFs to tissue specimens and subsequent cellular analysis.

FLS have been shown to have a speed of up to 10 µm/hr (E=6 V/cm) and 25 µm/hr (E=10 V/cm) in 2D galvanotaxis systems (Chao et al., 2000; A. R. Tan et al., 2015b). We demonstrated

an average directed velocity of 26.7 ± 15 μm/hr with an estimated E=6 V/cm and J=73 mA/cm^2 **(Figure 6.9)**. These high field strengths are on par for what chondrocytes may see *in vivo*, with magnitudes of up to 15 V/cm and current densities of up to 100 mA/cm^2 (Mow and Huiskes, 2005). Higher EFs and current densities than those seen *in vivo* may be necessary to stimulate more significant and robust migration, but must be balanced with any detrimental effects on cell health, such as Joule heating. Our pilot studies confirmed that cells remained viable under the conditions tested. In future studies, it will be important to parse out mechanisms that mediate differences in cell attachment and interaction between the substrates examined (i.e. 2D glass slide vs. 2D cartilage vs. 3D). The effect of EFs can also be studied where a collagen gel (or other cell carrier) is superimposed with the cylindrical cartilage explant to study integrative properties of cartilage repair (Hunter and Levenston, 2004; Obradovic et al., 2001a). Results of **Section 6.3** provide a foundation for these experiments. Some studies have reported perpendicular migration of MSCs and fibroblasts in 3D matrices, however these reports utilized either very small continuous DC EFs (Sun et al., 2004) or low duty cycle pulsed EFs (Yuan et al., 2014).

While the present system is unable to perform real-time cell tracking, it does permit for maintenance of aseptic conditions, multiple treatments over time, and subsequent cell, tissue and media analyses. The applied current necessary to achieve a desired electric field strength can be calculated from Ohm's Law and knowledge of the impedance of the current path. Our FE model is able to faithfully determine the average current density as calculated from measurements of chamber impedance and electrokinetic properties of the electrolyte. Moreover, it is able to describe the spatially-varying current density distribution in the experiments not able to be determined experimentally. The latter may support efforts to better understand the mechanisms that mediate galvanotaxis, particularly when coupled with multiphasic models of the cell (Ateshian et al., 2013).

This model can serve as the basis of future efforts to describe electrokinetic conditions where more complex geometries and tissue properties (such as may be found with OA tissue) are considered. As a singular example, we envision modeling cellular migration into varying degrees of damaged and porous arthritic tissue. In this study, the chamber was used successfully to direct FLS migration out of 3D synovium tissue onto cut 2D cartilage surfaces.

6.5 Conclusion

Together with successful applications of applied DC EFs for bone fractures and spinal fusion (Veronesi et al., 2015), our findings (SA2e-f) suggest that galvanotaxis may be a promising tool for encouraging and promoting the migration of both endogenous and exogenously-delivered FLS repair cells to sites of articular cartilage injury (Ng et al., 2010). However, directed migration of adherent PBMCs was not observed (SA2d), and additional studies will be required to elucidate any potential benefits of the observed kinetic response. Therefore, the results are supportive of the Part II global hypothesis with regard to FLS but not necessarily other cell types present in the synovium. It is envisioned that future iterations of applied EFs could include modifying the time course of stimulation. After directing migration of cells via galvanotaxis imposed by DC EFs, time-varying EFs, such as PEMFs **(Chapter 4 and Chapter 5)**, may be applied using field parameters reported to stimulate biosynthesis of chondrocytes and repair cells (Ongaro et al., 2011; Varani et al., 2008).

Part III

Conclusions and Future Directions

Chapter 7

Conclusions and Future Directions

The overall aim of this dissertation is two-fold: 1) characterize synovium structure-function in response to pro-inflammatory cytokine insult and glucocorticoid treatment **(Part I)**; 2) investigate electrotherapeutic strategies for modulating synovium behavior and cartilage repair **(Part II)**. Towards this goal, this dissertation uncovered new findings related to synovium structure-function and shed light on potential glucocorticoid and electrotherapeutic strategies that may support cartilage repair via modulation of the synovium. The studies described here utilized both tissue engineering and explant culture techniques to elucidate specific mechanisms of altered synovial structure-function as well as preclinical animal models and new bioreactor culture systems to explore translation of findings and new strategies targeting synovial-mediated repair. Together, these models allowed us to capture the complexity of synovium behavior in health and disease and the potential for synovial-based therapies in joint repair. In conclusion, we first present a summary of experimental findings in the context of the global hypotheses. Finally, future studies motivated by this work are suggested.

7.1 Conclusions

7.1.1 Dexamethasone is a Metabolic Mediator in Synovium and Cartilage

In **Part I**, we began by describing a functional tissue engineered synovium model that was validated against explant behavior **(Chapter 2)**. We were able to recapitulate many of the unique

structural and functional characteristics of synovium, including protein expression, intimal lining formation, solute transport, and friction coefficient. Additionally, engineered synovium behavior mirrored that of explants when treated with IL-1 or DEX. Notably, IL-1 and DEX treatment both induced a hyperplastic response that was correlated with reduced solute permeability, despite both treatments otherwise eliciting the expected secretory response. The engineered synovium model was then expanded to include resident MLS, demonstrating the key role that these cells play in structural reorganization of synovium. An exaggerated IL-1-induced hyperplastic response and co-localization of FLS and MLS was observed, highlighting the importance of MLS in synovium structure-function. Finally, the model was translated to a human system with co-cultured T lymphocytes. We observed reduced intimal hyperplasia in engineered synovium co-cultured with T lymphocytes that correlated with increased specimen dry weight, suggesting an alternative T cell-mediated mechanism of hyperplasia and/or pannus formation. Overall, these studies highlight the complexity of the response to IL-1 and DEX as well as the interaction of cell types present at different stages and presentations of OA, with specific impact on synovium structure-function.

Finally, in part motivated by insights into solute transport in the synovium as well as its strong anti-inflammatory response to DEX, we developed a sustained low-dose DEX delivery platform for mitigating synovial inflammation while simultaneously stimulating cartilage growth **(Chapter 3)**. We observed *in vitro* chondroprotection in the presence of IL-1-induced degradation and improved *in vivo* functional outcomes following a preclinical model of OAT repair. These improved outcomes were correlated with superior histological cartilage scores and minimal-to-no comorbidity, but not necessarily a dampened inflammatory response. However, synovitis was low across groups, and synovium-associated MMPs were upregulated in response to DLMS, potentially indicative of increased healing rather than degradation. Together, the data confirms the

anabolic and chondroprotective effects of DEX on cartilage, however a dampened inflammatory response was not observed in synovial measures. Therefore, the global hypothesis for Part I was accepted, in part. Together, these results support a strong role for IL-1 and DEX in altered synovium structure-function *in vitro*, however *in vivo* preclinical data did not strongly support a connection between the improved outcomes and altered synovial function.

7.1.2 Electric Fields as Metabolic & Migratory Mediators in Synovium & Cartilage

In **Part II**, we evaluated synovium behavior and cartilage repair in response to two different modes of electrical stimulation. For the first time, we characterized the biological response of both healthy bovine and OA human synovium explants to PEMFs, showing distinct anti-inflammatory behavior in bovine tissues, in agreement with literature reports of isolated bovine FLS **(Chapter 4)**. However, the response of human OA tissues was far more variable and a robust anti-catabolic effect of PEMF was not observed. This was likely due to the advanced disease state of these tissues and the variable cell content, with a significantly lower proportion of FLS cells compared to healthy tissue. A correlation was observed between age and PGE2 secretion in response to PEMF, suggesting a potential avenue of future research with immediate clinical implications. A key limitation of this study was that we could not quantify exactly which cells in the tissue were responding to PEMF. It is likely that increased MLS and T lymphocytes within human OA specimens interact with PEMF in very different ways from FLS, likely also compounded by cellular communication/gap junctions.

Motivated by the potent anti-inflammatory effect seen in normal tissue and previous work demonstrating a pro-anabolic and anti-catabolic effect on cartilage, the PEMF system was then adapted for use with a preclinical adult canine model of engineered cartilage repair **(Chapter 5)**.

Using clinically relevant stimulation parameters, we demonstrated that PEMFs can enhance engineered cartilage repair through modulation of cartilage growth and healing. Counterintuitively, increased synovial hyperplasia was also observed, however this was in the absence of increased inflammatory cytokines. Additional studies, perhaps utilizing the engineered synovium described in Chapter 2, will be required to elucidate the mechanism of this seemingly contradictory synovial behavior. Finally, we investigated the potential for direct synovial cell-mediated cartilage repair via induced migration with DC EFs **(Chapter 6)**. Results suggested that galvanotaxis may be a promising tool for promoting the migration and transfer of FLS repair cells within ECM or to sites of articular cartilage injury. The novel tissue-scale bioreactor was capable of applying well-defined DC EFs in sterile culture conditions to three-dimensional constructs, providing a crucial tool in translating culture findings to a preclinical system. Overall, the global hypothesis for Part II was accepted, in part. Together, these results support the role of electrotherapeutic strategies in promoting metabolic and migratory behavior of FLS *in vitro*, and metabolic behavior of engineered cartilage both *in vitro* and *in vivo*. However, despite positive overall outcomes, a complex role of synovium-mediated *in vivo* repair was evident.

7.2 Future Directions

7.2.1 Computational Modeling of Synovium Transport

To complement structure-function data from solute transport studies **(2.2.3.3)**, we are working to develop constitutive models of the Transwell system **(Figure 7.1)** and synovium **(Figure 7.2)**. The computational analyses, based on the mixture theory constitutive framework (Ateshian et al., 2013, 2010; Gu et al., 1998), will serve as a tool to provide more accurate interpretation of our data.

In the current solute transport analysis **(2.2.2.4)**, extraction of solute permeability coefficient relies on assumptions that the top reservoir remains at a constant concentration and the bottom reservoir concentration is negligible. However, these assumptions do not hold true for our Transwell-based system, as the three compartments (top reservoir, tissue, and bottom reservoir) all have comparable volumes. Therefore, we plan to use finite element analyses (FEBio, febio.org) to determine the time-evolution of solute concentration in the bottom well, and fit the model to experimental data **(Figure 2.9)**. A representative finite element mesh for an axisymmetric analysis of the tissue inside a Transwell of known dimensions is shown in **(Figure 7.1a)**. At the initial time t=0, the solute concentration is uniform in the top well; as the solute diffuses through the specimen to the bottom well, the concentrations in the top and bottom well evolve, demonstrating that the assumption of constant concentrations in the top and bottom reservoirs is erroneous **(Figure 7.1b)**.

We plan to generate parametric curves for the bottom well concentrations at specific time points, taking into account that the bottom well is refreshed at each sampling time point (i.e. the bottom concentration will be reset to zero at those intervals). These curves will be generated for a range of permeability values and sample thicknesses, and used to fit the experimental data to find the optimal permeability coefficient for each tissue sample. Additionally, fluorescence recovery after photobleaching (FRAP) may be used to assess spatial variations (Albro et al., 2008) that may occur between the highly cellular intimal lining and more acellular subintimal lining.

Compartmental modeling of the synovial joint has been used by others to describe how the synovium modulates synovial fluid composition in disease and therapeutic conditions (Blewis et al., 2010a; Hui et al., 2012). Our findings can provide information that may help to further refine the model, such as by defining parameters that are influenced by tissue loading and deformation. One proposed mechanism is based on the presented work **(Figure 2.9)**; we suspect that solute

transport is affected by both tissue geometry (i.e. thickness) and cellular compaction, which both increase the effective diffusion distance for solutes **(Figure 7.2)**.

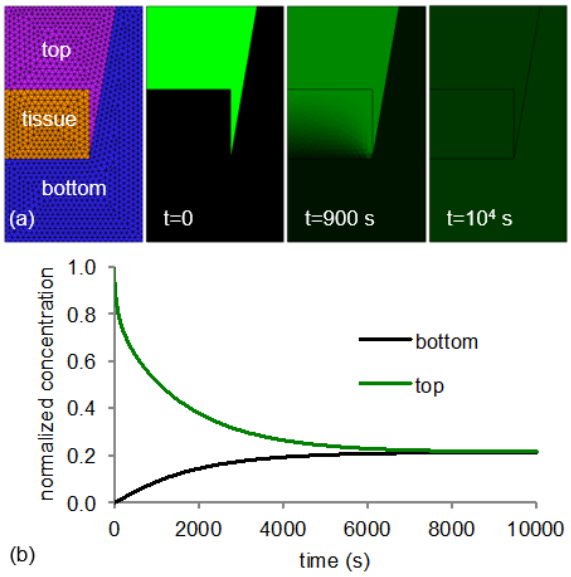

Figure 7.1 FEBio modeling of solute transport assay in Transwell. **(a)** Finite element mesh for axisymmetric model of tissue sample (Ø4.26 mm × 1.75 mm) in Transwell. Subsequent panels show the time evolution of dextran concentration as it diffuses across the tissue sample down to the bottom reservoir; **(b)** The temporal evolution of dextran concentration in the bottom reservoir may be fitted to experimental data to extract the dextran permeability.

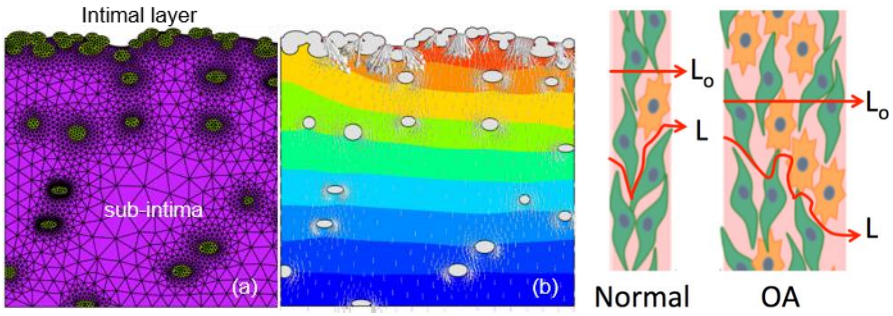

Figure 7.2 FEBio modeling of solute transport within the synovium. **(a)** Finite element mesh of synovium intima and subintima, including cells; **(b)** Solute concentration (color contours) and solute molar flux (arrows) showing transport from the synovial cavity into the sub-intima; **(right)** Drawing of potential route (L) of solute transport across synovium in normal versus OA tissue with thickness L_0 that has undergone hyperplasia and tissue thickening.

7.2.2 Advanced Cell Tracking and Isolation

In **Chapter 2**, lipophilic membrane dyes were used to track the individual contributions and phenotype of individual cell populations. Lipophilic membrane dyes are convenient and do not alter cell behavior, but have the potential for dye transfer and do not persist after 1-2 population doublings (Lassailly et al., 2010). Another option for robust, long-term cell tracking is through constitutive labeling with lentiviral trackers. In preliminary work, human OA FLS were successfully transfected with ILV-EF-1α-tdTomato (Vectalys, Toulouse, France) to constitutively express tdTomato fluorescent protein **(Figure 7.3)**. After one additional passage (P3-P4), transfection efficiency was assessed to be nearly 100% at a multiplicity of infection (MOI) of 20 and 100% at MOI of 40. This lentivirus was reported by the manufacturer to label primary fibroblasts at 100% efficiency and MSCs at least 90% efficiency. These results demonstrate our ability to culture and robustly track isolated human OA FLS from multiple donors. These cells remained viable in 2D. Additional work needs to be completed to assess functional aspects of these cells and to optimize labeling for other synovial cell types.

Further, in our studies, Dynabead sorting was utilized to isolate and count cell populations of interest. A more efficient and accurate method is through multicolor flow cytometry sorting. This will allow precise donor matching of immune cell populations, through isolation directly from synovial explant tissues. This will be especially useful for further translating the engineered synovium model to the human system, where normal tissues may consist of tiny fragments with few cells. Initial optimization has begun to take place in our laboratory through collaborations with Columbia Stem Cell Initiative flow cytometry core facility. Alternatively, matching donor tissues and cell types may be obtained from tissue procurement facilities such as the National Disease Research Interchange (NDRI, Philadelphia, PA), for which we have recently submitted a protocol.

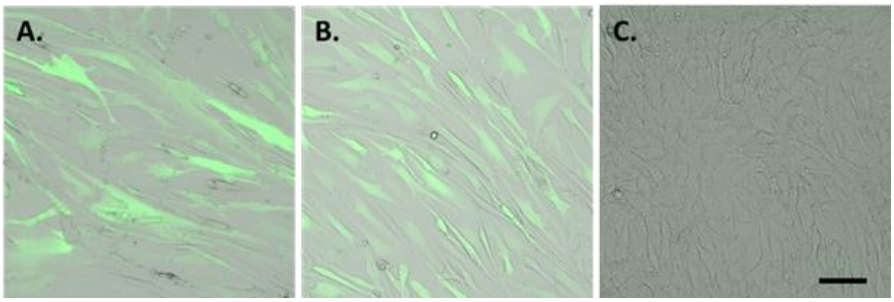

Figure 7.3 Confocal images, transmitted light with overlaid fluorescence signal. Human OA FLS were isolated by CD14 Dynabead negative isolation and subsequently transfected to constitutively express tdTomato. **(A)** MOI 20; **(B)** MOI 40; **(C)** Control cells. Transfection was stable over at least one passage and multiple weeks of culture. Scale bar = 10 μm

7.2.3 Cartilage-Synovium Cross-Talk

As the ultimate goal of studying the synovium is to more accurately predict and influence whole-joint outcomes, our engineered synovium model will ostensibly require addition of additional tissue types. This was apparent in **Chapter 3** and **Chapter 5**, where it was difficult to decouple the effects of DEX and PEMF on the synovium vs. cartilage or bone. Others have conducted simplistic co-culture studies with synovium and cartilage **(1.3.2)**, however functional analyses were limited. In a more complex system, the Tuan lab group proposed a lab-on-a-chip inspired model composed of bone, cartilage, synovium, and fat cells (Li et al., 2019). However, this system also lacks analyses of synovium structure-function, relying instead on modeling secretory behavior of isolated FLS only. Our laboratory has begun to perform cartilage-synovium co-culture studies **(Figure 7.4)**, and preliminary data has appeared in a previous thesis (Silverstein, 2016).

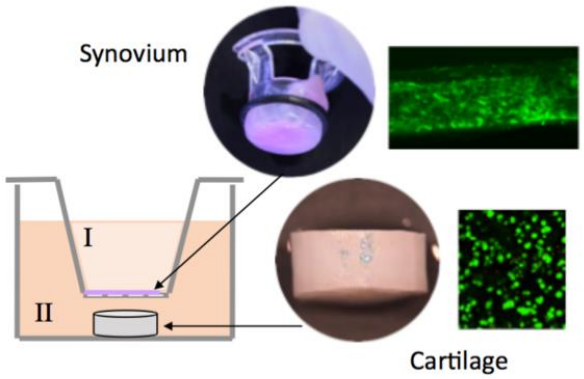

Figure 7.4 Transwell-based synovium-cartilage co-culture system.

7.2.4 Modeling Synovium-related Pain

The normal synovial sub-lining is highly vascularized and innervated (Smith, 2011), and nerve and vascular density have been observed to increase with OA (Ghilardi et al., 2012). Inflammation caused by cartilage and synovium injury influence dorsal root ganglion (DRG) neurons and sensitize pain perception (i.e. nociception) (Felson, 2005). Alterations in the functional properties of sensory neurons are a key determinant of the severity of OA pain (Li et al., 2011). Interestingly, the density of calcitonin gene-related peptide (CGRP)-positive sensory nerve fibers was higher in OA than in RA, and density of substance P-positive nerve fibers tended to be higher in RA (Dirmeier et al., 2008). While both are considered to be pro-inflammatory (Wang et al., 2015), this data suggests alternate mechanisms of pain transmission.

Substance P is produced by FLS from patients with RA and OA (Inoue et al., 2001). In initial work, we have observed substance P in human OA synovium and engineered synovium, respectively **(Figure 7.5)**. These findings suggest that IL-1 and TNF-α regulate nerve growth factor (NGF) expression and production in MLS and FLS in OA joints (Stoppiello et al., 2014; Takano et al., 2017). Importantly, the influence of FLS on DRG neurons is dependent on their state of activity, soluble factors, as well as direct cellular contacts (von Banchet et al., 2007). FLS may

contribute to the pain response through expression of neuropeptide markers in response to FGF-2 (Liu et al., 2011). In preliminary work, we have shown that FGF-2-treated FLS express neurofilament-M+H **(Figure 7.6A-B)**. Additionally, IL-treated FLS in three-dimensional culture have the capacity to express β3-tubulin **(Figure 7.6C-D)**, which is considered a robust marker of neuronal cells (Takeshita et al., 2012).

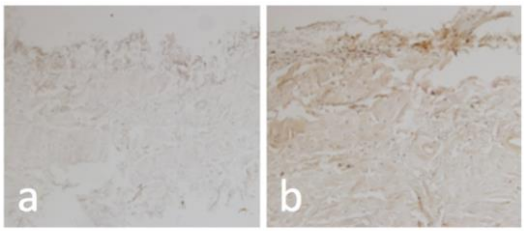

Figure 7.5 Immunohistochemistry of pain marker in synovium. Substance P staining of human OA synovium (a: no-antibody control, b: positive DAB staining).

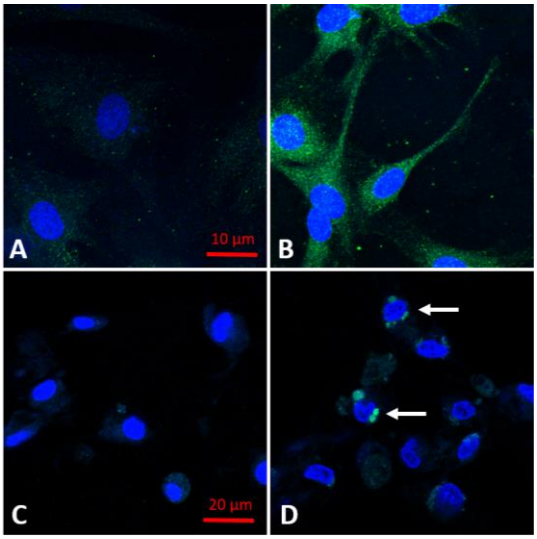

Figure 7.6 Neurofilament-M+H and β3-tubulin immunohistochemistry of FLS. P3 juvenile bovine FLS were cultured on a collagen-coated dish at a density of 3000 cells/cm^2 in **(A)** CTL or **(B)** FGF-2-treated (25 ng/ml) conditions for 10 days. Robust positive expression of neurofilament-M+H (FITC, green) was observed in FGF-2-treated FLS. Separately, P3 juvenile bovine FLS were encapsulated in 2 mg/ml type I collagen hydrogel at 2.5 million cells/ml and cultured in **(C)** CTL

or **(D)** IL-treated (10 ng/ml) conditions for 10 days. Positive expression of β3-tubulin (FITC, green) was observed in a subset of IL-treated FLS (arrows).

Anti-NGF treatments have shown some promise in animal models (Lascelles et al., 2015), however clinical investigations have revealed significant downsides such as increased OA progression, higher incidence of joint replacement, and neurological side effects (Seidel et al., 2013). A sophisticated *in vitro* model **(Chapter 2)** may be useful in supplementing clinical pain studies, where outcomes are difficult to interpret and compare as they often lack standard protocols (Chu et al., 2019) and can be confounded by placebo effect (Saltzman et al., 2017). We propose a modification to the engineered synovium model whereby DRG neurons are encapsulated within a Matrigel matrix and layered above or below the synovial intima **(Figure 7.7)**. A preliminary version of the co-culture system demonstrated axon formation by DRG cells that were placed in apposition with engineered synovium.

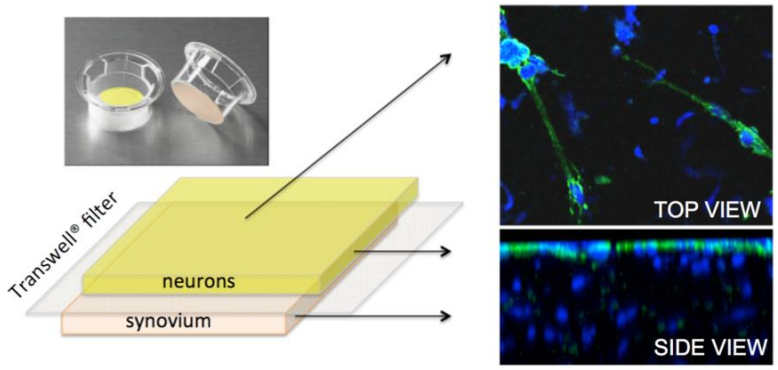

Figure 7.7 Schematic of layered co-culture of DRG neurons and synovium in Transwell. Immunohistochemistry of β3-tubulin (green) and DAPI counterstain showing axon formation by DRG cells in top view **(top-right)** and FLS co-cultured in lower layer with DAPI only **(bottom-right)**.

7.2.5 Developing Drug Delivery Strategies Targeting Synovium

In **Chapter 3**, we described intra-articular delivery of DEX via an acellular osteochondral implant in OAT repairs. While promising, this delivery method is incompatible with repairs that do not leave behind an empty graft donor site, such as OCA, ACI, or microfracture procedures. Further, depending on the drug and mode of action, osteochondral delivery may not be ideal. For example, SB-431542 (SB), a selective small molecule inhibitor of TGF-β/activin type I receptor kinase activity developed by GlaxoSmithKline, has been shown to reduce rotator cuff fibrosis after injury in a mouse model (Davies et al., 2016). Osteochondral delivery of a TGF-β inhibitor would likely impede cartilage healing.

Elevated levels of TGF-β1 during various stages of the wound response leads to differentiation of resident synovial fibroblasts to activated myofibroblasts (Bauer et al., 2006). Studies suggest that myofibroblastic differentiation represents a potential mechanism by which TGF-β1 enhances the arthrofibrotic process (Unterhauser et al., 2004). Our preliminary data shows that SB can inhibit synovium contraction and myofibroblast differentiation of synovial fibroblasts (Cai et al., 2018; Lee et al., 2020).

By instead incorporating drug-loaded microspheres into a biocompatible vitrified collagen (Takezawa et al., 2004) patch, which can be sutured directly to the synovial intima **(Figure 7.8)**, precisely targeted intra-articular drug delivery can be accomplished. However, robust *in vitro* models will still be necessary to assess potential unforeseen changes in synovium structure-function induced by SB **(Chapter 2)**.

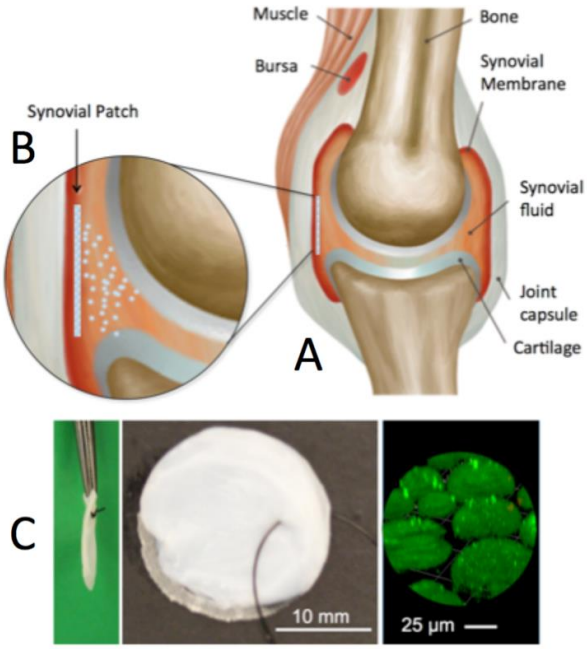

Figure 7.8 Schematic of proposed synovial patch for targeted drug delivery. **(A)** Model of idealized knee joint showing possible location of synovial patch. **(B)** Microspheres embedded within the patch release drug into the joint space. **(C)** A synovial patch composed of high-density collagen vitrigel is capable of being sutured. Fluorescently labeled microspheres can be seen on the patch surface (right).

Part IV

References and Appendices

References

Aaron, R.K., Ciombor, D.M., 2004. Pain in osteoarthritis. Med Health R I 87, 205–209.

Agarwal, S.K., Brenner, M.B., 2006. Role of adhesion molecules in synovial inflammation. Curr Opin Rheumatol 18, 268–276. https://doi.org/10.1097/01.bor.0000218948.42730.39

Akan, Z., Aksu, B., Tulunay, A., Bilsel, S., Inhan-Garip, A., 2010. Extremely low-frequency electromagnetic fields affect the immune response of monocyte-derived macrophages to pathogens. Bioelectromagnetics 31, 603–612. https://doi.org/10.1002/bem.20607

Albro, M.B., Chahine, N.O., Li, R., Yeager, K., Hung, C.T., Ateshian, G.A., 2008. Dynamic loading of deformable porous media can induce active solute transport. J Biomech 41, 3152–3157. https://doi.org/10.1016/j.jbiomech.2008.08.023

Alegre-Aguarón, E., Sampat, S.R., Xiong, J.C., Colligan, R.M., Bulinski, J.C., Cook, J.L., Ateshian, G.A., Brown, L.M., Hung, C.T., 2014. Growth Factor Priming Differentially Modulates Components of the Extracellular Matrix Proteome in Chondrocytes and Synovium-Derived Stem Cells. PLOS ONE 9, e88053. https://doi.org/10.1371/journal.pone.0088053

Allen, D.B., 1996. GROWTH SUPPRESSION BY GLUCOCORTICOID THERAPY. Endocrinology and Metabolism Clinics of North America 25, 699–717. https://doi.org/10.1016/S0889-8529(05)70348-0

American Academy of Orthopaedic Surgeons Board of Directors, 2013. Treatment of osteoarthritis of the knee: evidence-based guideline, 2nd ed. American Academy of Orthopaedic Surgeons, Rosemont, IL.

Amin, A.K., Simpson, A.H.R.W., Hall, A.C., 2017. Iatrogenic articular cartilage injury: the elephant in the operating theatre. The Bone & Joint Journal 99-B, 1555–1556. https://doi.org/10.1302/0301-620X.99B12.BJJ-2017-1337

Andrade, R., Vasta, S., Pereira, R., Pereira, H., Papalia, R., Karahan, M., Oliveira, J.M., Reis, R.L., Espregueira-Mendes, J., 2016. Knee donor-site morbidity after mosaicplasty - a systematic review. J Exp Orthop 3, 31. https://doi.org/10.1186/s40634-016-0066-0

Armstrong, R.D., English, J., Gibson, T., Chakraborty, J., Marks, V., 1981. Serum methylprednisolone levels following intra-articular injection of methylprednisolone acetate. Annals of the Rheumatic Diseases 40, 571–574. https://doi.org/10.1136/ard.40.6.571

Ateshian, G.A., Maas, S., Weiss, J.A., 2013. Multiphasic Finite Element Framework for Modeling Hydrated Mixtures With Multiple Neutral and Charged Solutes. J Biomech Eng 135, 1110011–11100111. https://doi.org/10.1115/1.4024823

Ateshian, G.A., Morrison, B., Hung, C.T., 2010. Modeling of active transmembrane transport in a mixture theory framework. Ann Biomed Eng 38, 1801–1814. https://doi.org/10.1007/s10439-010-9980-y

Ateshian, G.A., Warden, W.H., Kim, J.J., Grelsamer, R.P., Mow, V.C., 1997. Finite deformation biphasic material properties of bovine articular cartilage from confined compression experiments. Journal of Biomechanics 30, 1157–1164. https://doi.org/10.1016/S0021-9290(97)85606-0

Attur, M., Samuels, J., Krasnokutsky, S., Abramson, S.B., 2010. Targeting the synovial tissue for treating osteoarthritis (OA): where is the evidence? Best Practice & Research Clinical Rheumatology, Osteoarthritis 24, 71–79. https://doi.org/10.1016/j.berh.2009.08.011

Backes, J.R., Bentley, J.C., Politi, J.R., Chambers, B.T., 2013. Dexamethasone Reduces Length of Hospitalization and Improves Postoperative Pain and Nausea After Total Joint Arthroplasty: A Prospective, Randomized Controlled Trial. The Journal of Arthroplasty 28, 11–17. https://doi.org/10.1016/j.arth.2013.05.041

Bajpayee, A., Scheu, M., Varady, N., Yannatos, I., Brown, L., Krishnan, Y., Fitzsimons, T., Bhattacharya, P., Frank, E., Grodzinsky, A., Porter, R., 2017. Sustained intra-cartilage delivery of low dose dexamethasone using a cationic carrier for treatment of post traumatic osteoarthritis. eCM 34, 341–364. https://doi.org/10.22203/eCM.v034a21

Baker, B., Becker, R.O., Spadaro, J., 1974. A study of electrochemical enhancement of articular cartilage repair. Clin. Orthop. Relat. Res. 251–267.

Bal, B.S., Rahaman, M.N., Jayabalan, P., Kuroki, K., Cockrell, M.K., Yao, J.Q., Cook, J.L., 2010. In vivo outcomes of tissue-engineered osteochondral grafts. Journal of Biomedical Materials Research Part B: Applied Biomaterials 93B, 164–174. https://doi.org/10.1002/jbm.b.31571

Barland, P., Novikoff, A.B., Hamerman, D., 1962. ELECTRON MICROSCOPY OF THE HUMAN SYNOVIAL MEMBRANE. J Cell Biol 14, 207–220.

Bartok, B., Firestein, G.S., 2010. Fibroblast-like synoviocytes: key effector cells in rheumatoid arthritis. Immunol. Rev. 233, 233–255. https://doi.org/10.1111/j.0105-2896.2009.00859.x

Bauer, C., Niculescu-Morzsa, E., Jeyakumar, V., Kern, D., Späth, S.S., Nehrer, S., 2016. Chondroprotective effect of high-molecular-weight hyaluronic acid on osteoarthritic chondrocytes in a co-cultivation inflammation model with M1 macrophages. Journal of Inflammation 13, 31. https://doi.org/10.1186/s12950-016-0139-y

Bauer, S., Jendro, M.C., Wadle, A., Kleber, S., Stenner, F., Dinser, R., Reich, A., Faccin, E., Gödde, S., Dinges, H., Müller-Ladner, U., Renner, C., 2006. Fibroblast activation protein is expressed by rheumatoid myofibroblast-like synoviocytes. Arthritis Research & Therapy 8, R171. https://doi.org/10.1186/ar2080

Becker, R.O., Spadaro, J.A., Marino, A.A., 1977. Clinical experiences with low intensity direct current stimulation of bone growth. Clin Orthop Relat Res 75–83.

Beekhuizen, M., Bastiaansen-Jenniskens, Y.M., Koevoet, W., Saris, D.B.F., Dhert, W.J.A., Creemers, L.B., van Osch, G.J.V.M., 2011. Osteoarthritic synovial tissue inhibition of proteoglycan production in human osteoarthritic knee cartilage: Establishment and characterization of a long-term cartilage-synovium coculture. Arthritis & Rheumatism 63, 1918–1927. https://doi.org/10.1002/art.30364

Benazzo, F., Cadossi, M., Cavani, F., Fini, M., Giavaresi, G., Setti, S., Cadossi, R., Giardino, R., 2008. Cartilage repair with osteochondral autografts in sheep: Effect of biophysical stimulation with pulsed electromagnetic fields. J. Orthop. Res. 26, 631–642. https://doi.org/10.1002/jor.20530

Bendele, A.M., 2001. Animal models of osteoarthritis. J Musculoskel Neuron Interact 1, 363–376.

Bennett, S., Breit, S.N., 1994. Variables in the isolation and culture of human monocytes that are of particular relevance to studies of HIV. J. Leukoc. Biol 236–240.

Berthelot, J.-M., Le Goff, B., Maugars, Y., 2013. Side effects of corticosteroid injections: What's new? Joint Bone Spine 80, 363–367. https://doi.org/10.1016/j.jbspin.2012.12.001

Betti, E., Marchetti, S., Cadossi, R., Faldini, C., Faldini, A., 1999. Effect of Stimulation by Low-Frequency Pulsed Electromagnetic Fields in Subjects with Fracture of the Femoral Neck,

in: Electricity and Magnetism in Biology and Medicine. Springer, Boston, MA, pp. 853–855. https://doi.org/10.1007/978-1-4615-4867-6_204

Bhattaram, P., Chandrasekharan, U., 2016. The joint synovium: A critical determinant of articular cartilage fate in inflammatory joint diseases. Seminars in Cell & Developmental Biology. https://doi.org/10.1016/j.semcdb.2016.05.009

Bian, L., Stoker, A.M., Marberry, K.M., Ateshian, G.A., Cook, J.L., Hung, C.T., 2010. Effects of Dexamethasone on the Functional Properties of Cartilage Explants During Long-Term Culture. Am J Sports Med 38, 78–85. https://doi.org/10.1177/0363546509354197

Bilgen, B., Orsini, E., Aaron, R.K., Ciombor, D.McK., 2007. FBS suppresses TGF-β1-induced chondrogenesis in synoviocyte pellet cultures while dexamethasone and dynamic stimuli are beneficial. J Tissue Eng Regen Med 1, 436–442. https://doi.org/10.1002/term.56

Binette, J.S., Garon, M., Savard, P., McKee, M.D., Buschmann, M.D., 2004. Tetrapolar Measurement of Electrical Conductivity and Thickness of Articular Cartilage. J Biomech Eng 126, 475–484. https://doi.org/10.1115/1.1785805

Bjordal, J.M., Johnson, M.I., Lopes-Martins, R.A.B., Bogen, B., Chow, R., Ljunggren, A.E., 2007. Short-term efficacy of physical interventions in osteoarthritic knee pain. A systematic review and meta-analysis of randomised placebo-controlled trials. BMC Musculoskelet Disord 8, 51. https://doi.org/10.1186/1471-2474-8-51

Blasioli, D.J., Matthews, G.L., Kaplan, D.L., 2014. The degradation of chondrogenic pellets using cocultures of synovial fibroblasts and U937 cells. Biomaterials 35, 1185–1191. https://doi.org/10.1016/j.biomaterials.2013.10.050

Blewis, M.E., Lao, B.J., Jadin, K.D., McCarty, W.J., Bugbee, W.D., Firestein, G.S., Sah, R.L., 2010a. Semi-permeable membrane retention of synovial fluid lubricants hyaluronan and proteoglycan 4 for a biomimetic bioreactor. Biotechnology and Bioengineering n/a-n/a. https://doi.org/10.1002/bit.22645

Blewis, M.E., Lao, B.J., Schumacher, B.L., Bugbee, W.D., Sah, R.L., Firestein, G.S., 2010b. Interactive cytokine regulation of synoviocyte lubricant secretion. Tissue Eng Part A 16, 1329–1337. https://doi.org/10.1089/ten.TEA.2009.0210

Blewis, M.E., Nugent-Derfus, G.E., Schmidt, T.A., Schumacher, B.L., Sah, R.L., 2007. A model of synovial fluid lubricant composition in normal and injured joints. Eur Cell Mater 13, 26–39.

Bodamyali, T., Bhatt, B., Hughes, F.J., Winrow, V.R., Kanczler, J.M., Simon, B., Abbott, J., Blake, D.R., Stevens, C.R., 1998. Pulsed electromagnetic fields simultaneously induce osteogenesis and upregulate transcription of bone morphogenetic proteins 2 and 4 in rat osteoblasts in vitro. Biochem. Biophys. Res. Commun. 250, 458–461. https://doi.org/10.1006/bbrc.1998.9243

Bodick, N., Lufkin, J., Willwerth, C., Kumar, A., Bolognese, J., Schoonmaker, C., Ballal, R., Hunter, D., Clayman, M., 2015. An Intra-Articular, Extended-Release Formulation of Triamcinolone Acetonide Prolongs and Amplifies Analgesic Effect in Patients with Osteoarthritis of the Knee: A Randomized Clinical Trial. The Journal of Bone and Joint Surgery-American Volume 97, 877–888. https://doi.org/10.2106/JBJS.N.00918

Bondeson, J., 2015. The Role of Synovial Macrophages in Rheumatoid Arthritis and Osteoarthritis: Its Implications for Radiosynovectomy, in: Kampen, W.U., Fischer, M. (Eds.), Local Treatment of Inflammatory Joint Diseases: Benefits and Risks. Springer International Publishing, Cham, pp. 31–48. https://doi.org/10.1007/978-3-319-16949-1_2

Bondeson, J., Blom, A.B., Wainwright, S., Hughes, C., Caterson, B., Berg, W.B. van den, 2010. The role of synovial macrophages and macrophage-produced mediators in driving inflammatory and destructive responses in osteoarthritis. Arthritis & Rheumatism 62, 647–657. https://doi.org/10.1002/art.27290

Bozynski, C.C., Kuroki, K., Stannard, J.P., Smith, P.A., Stoker, A.M., Cook, C.R., Cook, J.L., 2015. Evaluation of Partial Transection versus Synovial Debridement of the ACL as Novel Canine Models for Management of ACL Injuries. J Knee Surg 28, 404–410. https://doi.org/10.1055/s-0035-1544975

Braddock, M., Campbell, C.J., Zuder, D., 1999. Current therapies for wound healing: electrical stimulation, biological therapeutics, and the potential for gene therapy. Int. J. Dermatol. 38, 808–817.

Branchet, M.C., Boisnic, S., Blétry, O., Robert, L., Charron, D., Francès, C., 1992. Expression of HLA class II antigens on skin fibroblasts in scleroderma. Br. J. Dermatol. 126, 431–435.

Brocklehurst, R., Bayliss, M., Maroudas, A., Coysh, H., Freeman, M., Revell, P., Ali, S., 1984. The composition of normal and osteoarthritic articular cartilage from human knee joints. With special reference to unicompartmental replacement and osteotomy of the knee. The Journal of Bone & Joint Surgery 66, 95–106.

Bugbee, W.D., Pallante-Kichura, A.L., Görtz, S., Amiel, D., Sah, R., 2016. Osteochondral allograft transplantation in cartilage repair: Graft storage paradigm, translational models,

and clinical applications. Journal of Orthopaedic Research 34, 31–38. https://doi.org/10.1002/jor.22998

Buttgereit, F., Silva, J.A.P.D., Boers, M., Burmester, G.-R., Cutolo, M., Jacobs, J., Kirwan, J., Köhler, L., Riel, P. van, Vischer, T., Bijlsma, J.W.J., 2002. Standardised nomenclature for glucocorticoid dosages and glucocorticoid treatment regimens: current questions and tentative answers in rheumatology. Annals of the Rheumatic Diseases 61, 718–722. https://doi.org/10.1136/ard.61.8.718

Byrne, R., Dalwigk, K. von, Hladik, A., Steiner, G., Smolen, J.S., Kiener, H., Scheinecker, C., 2014a. A8.30 Analysis of monocyte-fibroblast interaction in 3D synovial micromass tissue cultures. Annals of the Rheumatic Diseases 73, A88–A88. https://doi.org/10.1136/annrheumdis-2013-205124.204

Byrne, R., Dalwigk, K. von, Steiner, G., Holinka, J., Windhager, R., Smolen, J.S., Kiener, H., Scheinecker, C., 2014b. SAT0552 Fibroblast-Like Synovial Cells and Monocytes TEAM up in the Organization and the Dynamic Modeling of the Synovial Tissue. Annals of the Rheumatic Diseases 73, 790–791. https://doi.org/10.1136/annrheumdis-2014-eular.3514

Cadossi, M., Buda, R.E., Ramponi, L., Sambri, A., Natali, S., Giannini, S., 2014. Bone Marrow–derived Cells and Biophysical Stimulation for Talar Osteochondral Lesions: A Randomized Controlled Study. Foot & Ankle International 35, 981–987. https://doi.org/10.1177/1071100714539660

Cai, C.C., Stefani, R.M., Mahoney, C.M., Ateshian, G.A., Marra, K.G., Shah, R., Hung, C.T., 2018. Efficacy of SB-431542 in Disrupting TGF-b□1-induced Synovial Fibroblast-Seeded Collagen Gel Contraction. Presented at the Orthopaedic Research Society, p. 1.

Calvo, I.O., Byrne, R.A., Karonitsch, T., Niederreiter, B., Kartnig, F., Alasti, F., Holinka, J., Ertl, P., Kiener, H.P., 2017. 04.19 3D synovial organoid culture reveals cellular mechanisms of tissue formation and inflammatory remodelling. Annals of the Rheumatic Diseases 76, A49–A50. https://doi.org/10.1136/annrheumdis-2016-211051.19

Carballo, C.B., Nakagawa, Y., Sekiya, I., Rodeo, S.A., 2017. Basic Science of Articular Cartilage. Clinics in Sports Medicine 36, 413–425. https://doi.org/10.1016/j.csm.2017.02.001

Cardone, D.A., 2002. Joint and Soft Tissue Injection 66, 6.

Cederlöf, S., Jonson, G., 1966. Intraarticular prednisolone injection for osteoarthritis of the knee. A double blind test with placebo. Acta Chir Scand 132, 532–537.

Chang, E.Y., Pallante-Kichura, A.L., Bae, W.C., Du, J., Statum, S., Wolfson, T., Gamst, A.C., Cory, E., Amiel, D., Bugbee, W.D., Sah, R.L., Chung, C.B., 2014. Development of a Comprehensive Osteochondral Allograft MRI Scoring System (OCAMRISS) With Histopathologic, Micro–Computed Tomography, and Biomechanical Validation. CARTILAGE 5, 16–27. https://doi.org/10.1177/1947603513514436

Chang, K., Chang, W.H.-S., Huang, Sherry, Huang, Smile, Shih, C., 2005. Pulsed electromagnetic fields stimulation affects osteoclast formation by modulation of osteoprotegerin, RANK ligand and macrophage colony-stimulating facto. Journal of Orthopaedic Research 23, 1308–1314. https://doi.org/10.1016/j.orthres.2005.03.012.1100230611

Chao, P.G., Lu, H.H., Hung, C.T., Nicoll, S.B., Bulinski, J.C., 2007. Effects of Applied DC Electric Field on Ligament Fibroblast Migration and Wound Healing. Connective Tissue Research 48, 188–197. https://doi.org/10.1080/03008200701424451

Chao, P.-H.G., Roy, R., Mauck, R.L., Liu, W., Valhmu, W.B., Hung, C.T., 2000. Chondrocyte Translocation Response to Direct Current Electric Fields. J Biomech Eng 122, 261–267. https://doi.org/10.1115/1.429661

Chrysis, D., Ritzen, E.M., Sävendahl, L., 2003. Growth retardation induced by dexamethasone is associated with increased apoptosis of the growth plate chondrocytes. Journal of Endocrinology 176, 331–337.

Chu, C.R., Rodeo, S., Bhutani, N., Goodrich, L.R., Huard, J., Irrgang, J., LaPrade, R.F., Lattermann, C., Lu, Y., Mandelbaum, B., Mao, J., McIntyre, L., Mishra, A., Muschler, G.F., Piuzzi, N.S., Potter, H., Spindler, K., Tokish, J.M., Tuan, R., Zaslav, K., Maloney, W., 2019. Optimizing Clinical Use of Biologics in Orthopaedic Surgery: Consensus Recommendations From the 2018 AAOS/NIH U-13 Conference. J Am Acad Orthop Surg 27, e50–e63. https://doi.org/10.5435/JAAOS-D-18-00305

Ciombor, D.M., Lester, G., Aaron, R.K., Neame, P., Caterson, B., 2002. Low frequency EMF regulates chondrocyte differentiation and expression of matrix proteins. J. Orthop. Res. 20, 40–50. https://doi.org/10.1016/S0736-0266(01)00071-7

Coleman P. J., Scott D., Mason R. M., Levick J. R., 2004a. Role of hyaluronan chain length in buffering interstitial flow across synovium in rabbits. The Journal of Physiology 526, 425–434. https://doi.org/10.1111/j.1469-7793.2000.00425.x

Coleman P. J., Scott D., Ray J., Mason R. M., Levick J. R., 2004b. Hyaluronan Secretion into the Synovial Cavity of Rabbit Knees and Comparison with Albumin Turnover. The Journal of Physiology 503, 645–656. https://doi.org/10.1111/j.1469-7793.1997.645bg.x

Collarile, M., Sambri, A., Lullini, G., Cadossi, M., Zorzi, C., 2018. Biophysical stimulation improves clinical results of matrix-assisted autologous chondrocyte implantation in the treatment of chondral lesions of the knee. Knee Surg Sports Traumatol Arthrosc 26, 1223–1229. https://doi.org/10.1007/s00167-017-4605-8

Cook, J.L., Kuroki, K., Stoker, A., Fox, H.S. and D.B., 2007. Review of In Vitro Models and Development and Initial Validation of a Novel Co-Culture Model for the Study of Osteoarthritis [WWW Document]. Current Rheumatology Reviews. URL http://www.eurekaselect.com/78627/article (accessed 1.12.18).

Cook, J.L., Kuroki, K., Visco, D., Pelletier, J.-P., Schulz, L., Lafeber, F.P.J.G., 2010. The OARSI histopathology initiative – recommendations for histological assessments of osteoarthritis in the dog. Osteoarthritis and Cartilage 18, S66–S79. https://doi.org/10.1016/j.joca.2010.04.017

Cooper, C.A., Brown, K.K., Meletis, C.D., Zabriskie, N., 2008. Inflammation and Hyaluronic Acid. Alternative and Complementary Therapies 14, 78–84. https://doi.org/10.1089/act.2008.14201

Danhier, F., Ansorena, E., Silva, J.M., Coco, R., Le Breton, A., Préat, V., 2012. PLGA-based nanoparticles: An overview of biomedical applications. Journal of Controlled Release 161, 505–522. https://doi.org/10.1016/j.jconrel.2012.01.043

Davies, M.R., Liu, X., Lee, L., Laron, D., Ning, A.Y., Kim, H.T., Feeley, B.T., 2016. TGF-β Small Molecule Inhibitor SB431542 Reduces Rotator Cuff Muscle Fibrosis and Fatty Infiltration By Promoting Fibro/Adipogenic Progenitor Apoptosis. PLOS ONE 11, e0155486. https://doi.org/10.1371/journal.pone.0155486

de Girolamo, L., Stanco, D., Galliera, E., Viganò, M., Colombini, A., Setti, S., Vianello, E., Corsi Romanelli, M.M., Sansone, V., 2013. Low frequency pulsed electromagnetic field affects proliferation, tissue-specific gene expression, and cytokines release of human tendon cells. Cell Biochem. Biophys. 66, 697–708. https://doi.org/10.1007/s12013-013-9514-y

De Mattei, M., Fini, M., Setti, S., Ongaro, A., Gemmati, D., Stabellini, G., Pellati, A., Caruso, A., 2007. Proteoglycan synthesis in bovine articular cartilage explants exposed to different low-frequency low-energy pulsed electromagnetic fields. Osteoarthritis and Cartilage 15, 163–168. https://doi.org/10.1016/j.joca.2006.06.019

De Mattei, M., Varani, K., Masieri, F.F., Pellati, A., Ongaro, A., Fini, M., Cadossi, R., Vincenzi, F., Borea, P.A., Caruso, A., 2009. Adenosine analogs and electromagnetic fields inhibit

prostaglandin E2 release in bovine synovial fibroblasts. Osteoarthritis and Cartilage 17, 252–262. https://doi.org/10.1016/j.joca.2008.06.002

Dirmeier, M., Capellino, S., Schubert, T., Angele, P., Anders, S., Straub, R.H., 2008. Lower density of synovial nerve fibres positive for calcitonin gene-related peptide relative to substance P in rheumatoid arthritis but not in osteoarthritis. Rheumatology 47, 36–40. https://doi.org/10.1093/rheumatology/kem301

Djouad, F., Rackwitz, L., Song, Y., Janjanin, S., Tuan, R.S., 2009. ERK1/2 Activation Induced by Inflammatory Cytokines Compromises Effective Host Tissue Integration of Engineered Cartilage. Tissue Engineering Part A 15, 2825–2835. https://doi.org/10.1089/ten.tea.2008.0663

Donlin, L.T., Jayatilleke, A., Giannopoulou, E.G., Kalliolias, G.D., Ivashkiv, L.B., 2014. Modulation of TNF-induced macrophage polarization by synovial fibroblasts. J. Immunol. 193, 2373–2383. https://doi.org/10.4049/jimmunol.1400486

Doty, A.C., Weinstein, D.G., Hirota, K., Olsen, K.F., Ackermann, R., Wang, Y., Choi, S., Schwendeman, S.P., 2017. Mechanisms of in vivo release of triamcinolone acetonide from PLGA microspheres. Journal of Controlled Release 256, 19–25. https://doi.org/10.1016/j.jconrel.2017.03.031

Douglas, T.A., Alinezhadbalalami, N., Balani, N., Schmelz, E.M., Davalos, R.V., 2019. Separation of Macrophages and Fibroblasts Using Contactless Dielectrophoresis and a Novel ImageJ Macro. Bioelectricity 1, 49–55. https://doi.org/10.1089/bioe.2018.0004

Dragoo, J.L., Danial, C.M., Braun, H.J., Pouliot, M.A., Kim, H.J., 2012. The chondrotoxicity of single-dose corticosteroids. Knee Surg Sports Traumatol Arthrosc 20, 1809–1814. https://doi.org/10.1007/s00167-011-1820-6

Duerr, S., Stremme, S., Soeder, S., Bau, B., Aigner, T., n.d. MMP-2/gelatinase A is a gene product of human adult articular chondrocytes and is increased in osteoarthritic cartilage 6.

Edwards, J.C.W., 1982. The Origin of Type A Synovial Lining Cells. Immunobiology 161, 227–231. https://doi.org/10.1016/S0171-2985(82)80078-8

Elsaid, K.A., Fleming, B.C., Oksendahl, H.L., Machan, J.T., Fadale, P.D., Hulstyn, M.J., Shalvoy, R., Jay, G.D., 2008. Decreased lubricin concentrations and markers of joint inflammation in the synovial fluid of patients with anterior cruciate ligament injury. Arthritis & Rheumatism 58, 1707–1715. https://doi.org/10.1002/art.23495

Ene, R., Sinescu, R.D., Ene, P., Cîrstoiu, M.M., Cîrstoiu, F.C., 2015. Synovial inflammation in patients with different stages of knee osteoarthritis. Rom J Morphol Embryol 56, 169–173.

Esposito, M., Lucariello, A., Costanzo, C., Fiumarella, A., Giannini, A., Riccardi, G., Riccio, I., 2013. Differentiation of Human Umbilical Cord-derived Mesenchymal Stem Cells, WJ-MSCs, into Chondrogenic Cells in the Presence of Pulsed Electromagnetic Fields. In Vivo 27, 495–500.

Estell, E.G., 2018. Modulation of Synovium Mechanobiology and Tribology in the Osteoarthritic Environment. Columbia University, New York, NY.

Estell, E.G., Murphy, L.A., Silverstein, A.M., Tan, A.R., Shah, R.P., Ateshian, G.A., Hung, C.T., 2017. Fibroblast-like synoviocyte mechanosensitivity to fluid shear is modulated by interleukin-1α. J Biomech 60, 91–99. https://doi.org/10.1016/j.jbiomech.2017.06.011

Euppayo, T., Siengdee, P., Buddhachat, K., Pradit, W., Chomdej, S., Ongchai, S., Nganvongpanit, K., 2016. In vitro effects of triamcinolone acetonide and in combination with hyaluronan on canine normal and spontaneous osteoarthritis articular cartilage. In Vitro Cell.Dev.Biol.-Animal 52, 723–735. https://doi.org/10.1007/s11626-016-0022-4

Fam, H., Kontopoulou, M., Bryant, J.T., 2009. Effect of concentration and molecular weight on the rheology of hyaluronic acid/bovine calf serum solutions. Biorheology 46, 31–43. https://doi.org/10.3233/BIR-2009-0521

Faul, F., Erdfelder, E., Lang, A.-G., Buchner, A., 2007. G*Power 3: A flexible statistical power analysis program for the social, behavioral, and biomedical sciences. Behavior Research Methods 39, 175–191. https://doi.org/10.3758/BF03193146

Fell, H.B., 1978. Synoviocytes. J Clin Pathol Suppl (R Coll Pathol) 12, 14–24.

Felson, D.T., 2005. The sources of pain in knee osteoarthritis. Current Opinion in Rheumatology 17, 624. https://doi.org/10.1097/01.bor.0000172800.49120.97

Fichadiya, A., Bertram, K.L., Ren, G., Yates, R.M., Krawetz, R.J., 2016. Characterizing heterogeneity in the response of synovial mesenchymal progenitor cells to synovial macrophages in normal individuals and patients with osteoarthritis. J Inflamm (Lond) 13. https://doi.org/10.1186/s12950-016-0120-9

Finkelstein, E.I., Chao, P.G., Hung, C.T., Bulinski, J.C., 2007. Electric field-induced polarization of charged cell surface proteins does not determine the direction of galvanotaxis. Cell Motil. Cytoskeleton 64, 833–846. https://doi.org/10.1002/cm.20227

Florine, E.M., Miller, R.E., Porter, R.M., Evans, C.H., Kurz, B., Grodzinsky, A.J., 2013. Effects of Dexamethasone on Mesenchymal Stromal Cell Chondrogenesis and Aggrecanase Activity: Comparison of Agarose and Self-Assembling Peptide Scaffolds. CARTILAGE 4, 63–74. https://doi.org/10.1177/1947603512455196

Fraser, J.R.E., Kimpton, W.G., Pierscionek, B.K., Cahill, R.N.P., 1993. The kinetics of hyaluronan in normal and acutely inflamed synovial joints: Observations with experimental arthritis in sheep. Seminars in Arthritis and Rheumatism 22, 9–17. https://doi.org/10.1016/S0049-0172(10)80015-0

Friedl, P., Wolf, K., 2010. Plasticity of cell migration: a multiscale tuning model. The Journal of Cell Biology 188, 11–19. https://doi.org/10.1083/jcb.200909003

Furuzawa-Carballeda, J., Macip-Rodríguez, P.M., Cabral, A.R., 2008. Osteoarthritis and rheumatoid arthritis pannus have similar qualitative metabolic characteristics and pro-inflammatory cytokine response. Clin. Exp. Rheumatol. 26, 554–560.

Gaissmaier, C., Koh, J.L., Weise, K., 2008. Growth and differentiation factors for cartilage healing and repair. Injury, Cartilage Repair 39, 88–96. https://doi.org/10.1016/j.injury.2008.01.035

Garcia, A.N., Vogel, S.M., Komarova, Y.A., Malik, A.B., 2011. Permeability of Endothelial Barrier: Cell Culture and <Emphasis Type="Italic">In Vivo</Emphasis> Models, in: Permeability Barrier, Methods in Molecular Biology. Humana Press, pp. 333–354. https://doi.org/10.1007/978-1-61779-191-8_23

Gerwin, N., Hops, C., Lucke, A., 2006. Intraarticular drug delivery in osteoarthritis. Advanced Drug Delivery Reviews, Drug Delivery in Degenerative Joint Disease 58, 226–242. https://doi.org/10.1016/j.addr.2006.01.018

Ghilardi, J.R., Freeman, K.T., Jimenez-Andrade, J.M., Coughlin, K.A., Kaczmarska, M.J., Castaneda-Corral, G., Bloom, A.P., Kuskowski, M.A., Mantyh, P.W., 2012. Neuroplasticity of sensory and sympathetic nerve fibers in a mouse model of a painful arthritic joint. Arthritis & Rheumatism 64, 2223–2232. https://doi.org/10.1002/art.34385

Gitter, B.D., Labus, J.M., Lees, S.L., Scheetz, M.E., 1989. Characteristics of human synovial fibroblast activation by IL-1 beta and TNF alpha. Immunology 66, 196–200.

Gobbi, A., Lad, D., Petrera, M., Karnatzikos, G., 2014. Symptomatic Early Osteoarthritis of the Knee Treated With Pulsed Electromagnetic Fields: Two-Year Follow-up. CARTILAGE 5, 78–85. https://doi.org/10.1177/1947603513515904

Goesling, J., Moser, S.E., Zaidi, B., Hassett, A.L., Hilliard, P., Hallstrom, B., Clauw, D.J., Brummett, C.M., 2016. Trends and Predictors of Opioid Use Following Total Knee and Total Hip Arthroplasty. Pain 157, 1259–1265. https://doi.org/10.1097/j.pain.0000000000000516

Gomoll, A.H., Filardo, G., Almqvist, F.K., Bugbee, W.D., Jelic, M., Monllau, J.C., Puddu, G., Rodkey, W.G., Verdonk, P., Verdonk, R., Zaffagnini, S., Marcacci, M., 2012. Surgical treatment for early osteoarthritis. Part II: allografts and concurrent procedures. Knee Surg Sports Traumatol Arthrosc 20, 468–486. https://doi.org/10.1007/s00167-011-1714-7

Gonçalves, R., Mosser, D.M., 2001. The Isolation and Characterization of Murine Macrophages, in: Current Protocols in Immunology. John Wiley & Sons, Inc. https://doi.org/10.1002/0471142735.im1401s111

Graabaek, P.M., 1984. Characteristics of the two types of synoviocytes in rat synovial membrane. An ultrastructural study. Lab Invest 50, 690–702.

Grodzinsky, A.J., Wang, Y., Kakar, S., Vrahas, M.S., Evans, C.H., 2017. Intra-articular dexamethasone to inhibit the development of post-traumatic osteoarthritis. Journal of Orthopaedic Research 35, 406–411. https://doi.org/10.1002/jor.23295

Gu, W.Y., Lai, W.M., Mow, V.C., 1998. A mixture theory for charged-hydrated soft tissues containing multi-electrolytes: passive transport and swelling behaviors. J Biomech Eng 120, 169–180.

Gunja, N.J., Dujari, D., Chen, A., Luengo, A., Fong, J.V., Hung, C.T., 2011. Migration responses of outer and inner meniscus cells to applied direct current electric fields. J. Orthop. Res. 30, 103–111. https://doi.org/10.1002/jor.21489

Habib, G.S., 2009. Systemic effects of intra-articular corticosteroids. Clin Rheumatol 28, 749–756. https://doi.org/10.1007/s10067-009-1135-x

Hamilton, J.A., Butler, D.M., Stanton, H., 1994. Cytokine interactions promoting DNA synthesis in human synovial fibroblasts. J. Rheumatol. 21, 797–803.

Hardy, M.M., Seibert, K., Manning, P.T., Currie, M.G., Woerner, B.M., Edwards, D., Koki, A., Tripp, C.S., 2002. Cyclooxygenase 2-dependent prostaglandin E2 modulates cartilage proteoglycan degradation in human osteoarthritis explants. Arthritis Rheum. 46, 1789–1803. https://doi.org/10.1002/art.10356

Hayden, M.S., West, A.P., Ghosh, S., 2006. NF- κ B and the immune response. Oncogene 25, 6758–6780. https://doi.org/10.1038/sj.onc.1209943

Haynes, B.F., Grover, B.J., Whichard, L.P., Hale, L.P., Nunley, J.A., McCollum, D.E., Singer, K.H., 1988. Synovial microenvironment-T cell interactions. Human T cells bind to fibroblast-like synovial cells in vitro. Arthritis Rheum. 31, 947–955. https://doi.org/10.1002/art.1780310802

Haywood, L., Walsh, D.A., 2001. Vasculature of the normal and arthritic synovial joint. Histol. Histopathol. 16, 277–284.

Heard, B.J., Barton, K.I., Chung, M., Achari, Y., Shrive, N.G., Frank, C.B., Hart, D.A., 2015. Single intra-articular dexamethasone injection immediately post-surgery in a rabbit model mitigates early inflammatory responses and post-traumatic osteoarthritis-like alterations. Journal of Orthopaedic Research 33, 1826–1834. https://doi.org/10.1002/jor.22972

Hehenberger, K., Kratz, G., Hansson, A., Brismar, K., 1998. Fibroblasts derived from human chronic diabetic wounds have a decreased proliferation rate, which is recovered by the addition of heparin. Journal of Dermatological Science 16, 144–151. https://doi.org/10.1016/S0923-1811(97)00042-X

Hitchon, C.A., El-Gabalawy, H.S., 2011. The Synovium in Rheumatoid Arthritis. Open Rheumatol J 5, 107–114. https://doi.org/10.2174/1874312901105010107

Hollander, A.P., Heathfield, T.F., Webber, C., Iwata, Y., Bourne, R., Rorabeck, C., Poole, A.R., 1994. Increased damage to type II collagen in osteoarthritic articular cartilage detected by a new immunoassay. J Clin Invest 93, 1722–1732. https://doi.org/10.1172/JCI117156

Hooiveld, M., Roosendaal, G., Wenting, M., van den Berg, M., Bijlsma, J., Lafeber, F., 2003. Short-Term Exposure of Cartilage to Blood Results in Chondrocyte Apoptosis. Am J Pathol 162, 943–951.

Hopper, N., Henson, F., Brooks, R., Ali, E., Rushton, N., Wardale, J., 2015a. Peripheral blood derived mononuclear cells enhance osteoarthritic human chondrocyte migration. Arthritis Research & Therapy 17, 199. https://doi.org/10.1186/s13075-015-0709-z

Hopper, N., Wardale, J., Brooks, R., Power, J., Rushton, N., Henson, F., 2015b. Peripheral Blood Mononuclear Cells Enhance Cartilage Repair in in vivo Osteochondral Defect Model. PLOS ONE 10, e0133937. https://doi.org/10.1371/journal.pone.0133937

Huch, K., Stöve, J., Günther, K.P., Puhl, W., 2001. Interactions between human osteoarthritic chondrocytes and synovial fibroblasts in co-culture. Clin. Exp. Rheumatol. 19, 27–33.

Huebner, K.D., Shrive, N.G., Frank, C.B., 2014. Dexamethasone inhibits inflammation and cartilage damage in a new model of post-traumatic osteoarthritis. Journal of Orthopaedic Research 32, 566–572. https://doi.org/10.1002/jor.22568

Hügle, T., Geurts, J., 2017. What drives osteoarthritis?-synovial versus subchondral bone pathology. Rheumatology (Oxford) 56, 1461–1471. https://doi.org/10.1093/rheumatology/kew389

Hui, A.Y., McCarty, W.J., Masuda, K., Firestein, G.S., Sah, R.L., 2012. A systems biology approach to synovial joint lubrication in health, injury, and disease. Wiley Interdisciplinary Reviews: Systems Biology and Medicine 4, 15–37. https://doi.org/10.1002/wsbm.157

Hung, C.T., Lima, E.G., Mauck, R.L., Taki, E., LeRoux, M.A., Lu, H.H., Stark, R.G., Guo, X.E., Ateshian, G.A., 2003. Anatomically shaped osteochondral constructs for articular cartilage repair. Journal of Biomechanics 36, 1853–1864. https://doi.org/10.1016/S0021-9290(03)00213-6

Hunter, C.J., Levenston, M.E., 2004. Maturation and integration of tissue-engineered cartilages within an in vitro defect repair model. Tissue Eng. 10, 736–746. https://doi.org/10.1089/1076327041348310

Hunter, D.J., Bierma-Zeinstra, S., 2019. Osteoarthritis. The Lancet 393, 1745–1759. https://doi.org/10.1016/S0140-6736(19)30417-9

Hunziker, E.B., Rosenberg, L.C., 1996. Repair of partial-thickness defects in articular cartilage: cell recruitment from the synovial membrane. J Bone Joint Surg Am 78, 721–733.

Ikeuchi, M., Kamimoto, Y., Izumi, M., Fukunaga, K., Aso, K., Sugimura, N., Yokoyama, M., Tani, T., 2014. Effects of dexamethasone on local infiltration analgesia in total knee arthroplasty: a randomized controlled trial. Knee Surg Sports Traumatol Arthrosc 22, 1638–1643. https://doi.org/10.1007/s00167-013-2367-5

Inoue, H., Shimoyama, Y., Hirabayashi, K., Kajigaya, H., Yamamoto, S., Oda, H., Koshihara, Y., 2001. Production of neuropeptide substance P by synovial fibroblasts from patients with rheumatoid arthritis and osteoarthritis. Neuroscience Letters 303, 149–152. https://doi.org/10.1016/S0304-3940(01)01713-X

Iwasa, J., Engebretsen, L., Shima, Y., Ochi, M., 2009. Clinical application of scaffolds for cartilage tissue engineering. Knee Surg Sports Traumatol Arthrosc 17, 561–577. https://doi.org/10.1007/s00167-008-0663-2

Iwasa, K., Reddi, A.H., 2018. Pulsed Electromagnetic Fields and Tissue Engineering of the Joints. Tissue Engineering Part B: Reviews 24, 144–154. https://doi.org/10.1089/ten.teb.2017.0294

Jamieson, C.A.M., Yamamoto, K.R., 2000. Crosstalk pathway for inhibition of glucocorticoid-induced apoptosis by T cell receptor signaling. PNAS 97, 7319–7324. https://doi.org/10.1073/pnas.97.13.7319

Jay, G.D., 1992. Characterization of a bovine synovial fluid lubricating factor. I. Chemical, surface activity and lubricating properties. Connect. Tissue Res. 28, 71–88.

Jay, G.D., Britt, D.E., Cha, C.J., 2000a. Lubricin is a product of megakaryocyte stimulating factor gene expression by human synovial fibroblasts. J. Rheumatol. 27, 594–600.

Jay, G.D., Britt, D.E., Cha, C.J., 2000b. Lubricin is a product of megakaryocyte stimulating factor gene expression by human synovial fibroblasts. J. Rheumatol. 27, 594–600.

Jay, G.D., Torres, J.R., Rhee, D.K., Helminen, H.J., Hytinnen, M.M., Cha, C.-J., Elsaid, K., Kim, K.-S., Cui, Y., Warman, M.L., 2007. Association between friction and wear in diarthrodial joints lacking lubricin. Arthritis Rheum 56, 3662–3669. https://doi.org/10.1002/art.22974

Jiang, D., Liang, J., Noble, P.W., 2011. Hyaluronan as an Immune Regulator in Human Diseases. Physiological Reviews 91, 221–264. https://doi.org/10.1152/physrev.00052.2009

Katagiri, K., Matsukura, Y., Muneta, T., Ozeki, N., Mizuno, M., Katano, H., Sekiya, I., 2017. Fibrous Synovium Releases Higher Numbers of Mesenchymal Stem Cells Than Adipose Synovium in a Suspended Synovium Culture Model. Arthroscopy 33, 800–810. https://doi.org/10.1016/j.arthro.2016.09.033

Kawczyk-Krupka, A., Sieron, A., Shani*, J., Czuba, Z.P., Krol, W., 2002. Biological Effects of Extremely Low-Frequency Magnetic Fields on Stimulated Macrophages J774.2 in Cell

Culture. Electromagnetic Biology and Medicine 21, 141–153. https://doi.org/10.1081/JBC-120006786

Kiener, H.P., Brenner, M.B., 2005. Building the synovium: cadherin-11 mediates fibroblast-like synoviocyte cell-to-cell adhesion. Arthritis Res Ther 7, 49. https://doi.org/10.1186/ar1495

Kiener, H.P., Lee, D.M., Agarwal, S.K., Brenner, M.B., 2006. Cadherin-11 Induces Rheumatoid Arthritis Fibroblast-Like Synoviocytes to Form Lining Layers in Vitro. The American Journal of Pathology 168, 1486–1499. https://doi.org/10.2353/ajpath.2006.050999

Kiener, H.P., Watts, G.F.M., Cui, Y., Wright, J., Thornhill, T.S., Sköld, M., Behar, S.M., Niederreiter, B., Lu, J., Cernadas, M., Coyle, A.J., Sims, G.P., Smolen, J., Warman, M.L., Brenner, M.B., Lee, D.M., 2010. Synovial fibroblasts self-direct multicellular lining architecture and synthetic function in three-dimensional organ culture. Arthritis & Rheumatism 62, 742–752. https://doi.org/10.1002/art.27285

Kloth, L.C., 2005. Electrical Stimulation for Wound Healing: A Review of Evidence From In Vitro Studies, Animal Experiments, and Clinical Trials. International Journal of Lower Extremity Wounds 4, 23–44. https://doi.org/10.1177/1534734605275733

Kraus, V.B., Conaghan, P.G., Aazami, H.A., Mehra, P., Kivitz, A.J., Lufkin, J., Hauben, J., Johnson, J.R., Bodick, N., 2018. Synovial and systemic pharmacokinetics (PK) of triamcinolone acetonide (TA) following intra-articular (IA) injection of an extended-release microsphere-based formulation (FX006) or standard crystalline suspension in patients with knee osteoarthritis (OA). Osteoarthritis and Cartilage 26, 34–42. https://doi.org/10.1016/j.joca.2017.10.003

Krishnan, R., Caligaris, M., Mauck, R.L., Hung, C.T., Costa, K.D., Ateshian, G.A., 2004. Removal of the superficial zone of bovine articular cartilage does not increase its frictional coefficient. Osteoarthritis and Cartilage 12, 947–955. https://doi.org/10.1016/j.joca.2004.08.009

Kumar, A., Bendele, A.M., Blanks, R.C., Bodick, N., 2012. Sustained efficacy of intra-articular FX006 in a rat model of osteoarthritis.

Kuroki, K., Stoker, A.M., Cook, J.L., 2005. Effects of proinflammatory cytokines on canine articular chondrocytes in a three-dimensional culture. Am. J. Vet. Res. 66, 1187–1196.

Labens, R., Lascelles, B.D.X., Charlton, A.N., Ferrero, N.R., Wettere, A.J.V., Xia, X.-R., Blikslager, A.T., 2013. Ex vivo effect of gold nanoparticles on porcine synovial membrane. Tissue Barriers 1, e24314. https://doi.org/10.4161/tisb.24314

Labus, J., Häckel, S., Lucka, L., Danker, K., 2014. Interleukin-1β induces an inflammatory response and the breakdown of the endothelial cell layer in an improved human THBMEC-based in vitro blood–brain barrier model. Journal of Neuroscience Methods 228, 35–45. https://doi.org/10.1016/j.jneumeth.2014.03.002

Lai, W.M., Hou, J.S., Mow, V.C., 1991. A triphasic theory for the swelling and deformation behaviors of articular cartilage. J Biomech Eng 113, 245–258.

Lascelles, B.D., Knazovicky, D., Case, B., Freire, M., Innes, J.F., Drew, A.C., Gearing, D.P., 2015. A canine-specific anti-nerve growth factor antibody alleviates pain and improves mobility and function in dogs with degenerative joint disease-associated pain. BMC Veterinary Research 11, 101. https://doi.org/10.1186/s12917-015-0413-x

Lassailly, F., Griessinger, E., Bonnet, D., 2010. "Microenvironmental contaminations" induced by fluorescent lipophilic dyes used for noninvasive in vitro and in vivo cell tracking. Blood 115, 5347–5354. https://doi.org/10.1182/blood-2009-05-224030

Lee, A.J., Murphy, L.A., Ateshian, G.A., Thomopoulos, S.A., Shah, R.P., Hung, C.T., 2020. SB-431542 Modulates the Wound Healing Response of Ligament Fibroblasts: Implications Following ACL Reconstruction. Presented at the Orthopaedic Research Society, p. 1.

Lee, C.M., Kisiday, J.D., McIlwraith, C.W., Grodzinsky, A.J., Frisbie, D.D., 2013. Synoviocytes protect cartilage from the effects of injury in vitro. BMC Musculoskeletal Disorders 14, 54. https://doi.org/10.1186/1471-2474-14-54

Lee, D.M., Kiener, H.P., Agarwal, S.K., Noss, E.H., Watts, G.F.M., Chisaka, O., Takeichi, M., Brenner, M.B., 2007. Cadherin-11 in Synovial Lining Formation and Pathology in Arthritis. Science 315, 1006–1010. https://doi.org/10.1126/science.1137306

Lee, H.G., Cowman, M.K., 1994. An Agarose Gel Electrophoretic Method for Analysis of Hyaluronan Molecular Weight Distribution. Analytical Biochemistry 219, 278–287. https://doi.org/10.1006/abio.1994.1267

Lee, J.H., Fitzgerald, J.B., DiMicco, M.A., Cheng, D.M., Flannery, C.R., Sandy, J.D., Plaas, A.H., Grodzinsky, A.J., 2009. Co-culture of Mechanically Injured Cartilage with Joint Capsule Tissue Alters Chondrocyte Expression Patterns and Increases ADAMTS5 Production. Arch Biochem Biophys 489, 118–126. https://doi.org/10.1016/j.abb.2009.07.006

Levick, J. R., et al., 1999. Physiology of synovial fluid and trans-synovial flow, in: Biology of the Synovial Joint. pp. 235–252.

Levick, J.R., McDonald, J.N., 1995. Fluid movement across synovium in healthy joints: role of synovial fluid macromolecules. Ann Rheum Dis 54, 417–423.

Levick, J.R., McDonald, J.N., 1989. Ultrastructure of transport pathways in stressed synovium of the knee in anaesthetized rabbits. J Physiol 419, 493–508.

Li, X., Kim, J.-S., van Wijnen, A.J., Im, H.-J., 2011. Osteoarthritic tissues modulate functional properties of sensory neurons associated with symptomatic OA pain. Mol Biol Rep 38, 5335–5339. https://doi.org/10.1007/s11033-011-0684-7

Li, Z., Lin, Z., Lopez, M.R., O'Donnell, B., Li, X., Moran, I.J., Alexander, P.G., Goodman, S.B., Lin, H., Tuan, R.S., 2019. Organ-on-a-chip System for the Modeling of Synovial Joint Pathologies. Presented at the Orthopaedic Research Society, p. 1.

Lima, E.G., Bian, L., Ng, K.W., Mauck, R.L., Byers, B.A., Tuan, R.S., Ateshian, G.A., Hung, C.T., 2007. The Beneficial Effect of Delayed Compressive Loading on Tissue-Engineered Cartilage Constructs Cultured with TGF-β3. Osteoarthritis Cartilage 15, 1025–1033. https://doi.org/10.1016/j.joca.2007.03.008

Lima, E.G., Grace Chao, P., Ateshian, G.A., Bal, B.S., Cook, J.L., Vunjak-Novakovic, G., Hung, C.T., 2008a. The effect of devitalized trabecular bone on the formation of osteochondral tissue-engineered constructs. Biomaterials 29, 4292–4299. https://doi.org/10.1016/j.biomaterials.2008.07.018

Lima, E.G., Tan, A.R., Tai, T., Bian, L., Stoker, A.M., Ateshian, G.A., Cook, J.L., Hung, C.T., 2008b. Differences in Interleukin-1 Response Between Engineered and Native Cartilage. Tissue Engineering Part A 14, 1721–1730. https://doi.org/10.1089/ten.tea.2007.0347

Lima, E.G., Tan, A.R., Tai, T., Bian, L., Stoker, A.M., Ateshian, G.A., Cook, J.L., Hung, C.T., 2008c. Differences in Interleukin-1 Response Between Engineered and Native Cartilage. Tissue Engineering Part A 14, 1721–1730. https://doi.org/10.1089/ten.tea.2007.0347

Lippiello, L., Chakkalakal, D., Connolly, J.F., 1990. Pulsing direct current-induced repair of articular cartilage in rabbit osteochondral defects. J. Orthop. Res. 8, 266–275. https://doi.org/10.1002/jor.1100080216

Liu, X.S., Sajda, P., Saha, P.K., Wehrli, F.W., Bevill, G., Keaveny, T.M., Guo, X.E., 2007. Complete Volumetric Decomposition of Individual Trabecular Plates and Rods and Its Morphological Correlations With Anisotropic Elastic Moduli in Human Trabecular Bone. Journal of Bone and Mineral Research 23, 223–235. https://doi.org/10.1359/jbmr.071009

Liu, Z., Long, X., Li, J., Wei, L., Gong, Z., Fang, W., 2011. Differentiation of temporomandibular joint synovial mesenchymal stem cells into neuronal cells in vitro: an in vitro study. Cell Biology International 35, 87–91. https://doi.org/10.1042/CBI20100144

Loeser, R.F., Goldring, S.R., Scanzello, C.R., Goldring, M.B., 2012. Osteoarthritis: a disease of the joint as an organ. Arthritis Rheum. 64, 1697–1707. https://doi.org/10.1002/art.34453

Lotz, M., Terkeltaub, R., Villiger, P.M., 1992. Cartilage and joint inflammation. Regulation of IL-8 expression by human articular chondrocytes. The Journal of Immunology 148, 466–473.

Lu, Y.C., Evans, C.H., Grodzinsky, A.J., 2011. Effects of short-term glucocorticoid treatment on changes in cartilage matrix degradation and chondrocyte gene expression induced by mechanical injury and inflammatory cytokines. Arthritis Research & Therapy 13, R142. https://doi.org/10.1186/ar3456

Ma, H.-L., Hung, S.-C., Wang, S.-T., Chang, M.-C., Chen, T.-H., 2004. Osteochondral autografts transfer for post-traumatic osteochondral defect of the knee—2 to 5 years follow-up. Injury 35, 1286–1292. https://doi.org/10.1016/j.injury.2004.02.013

Maas, S.A., Ellis, B.J., Ateshian, G.A., Weiss, J.A., 2012. FEBio: Finite Elements for Biomechanics. J Biomech Eng 134, 11005-NaN. https://doi.org/10.1115/1.4005694

Manferdini, C., Paolella, F., Gabusi, E., Gambari, L., Piacentini, A., Filardo, G., Fleury-Cappellesso, S., Barbero, A., Murphy, M., Lisignoli, G., 2017. Adipose stromal cells mediated switching of the pro-inflammatory profile of M1-like macrophages is facilitated by PGE2: in vitro evaluation. Osteoarthritis and Cartilage 25, 1161–1171. https://doi.org/10.1016/j.joca.2017.01.011

Marks, P.H., Donaldson, M.L.C., 2005. Inflammatory Cytokine Profiles Associated With Chondral Damage in the Anterior Cruciate Ligament–Deficient Knee. Arthroscopy: The Journal of Arthroscopic & Related Surgery 21, 1342–1347. https://doi.org/10.1016/j.arthro.2005.08.034

Mathiessen, A., Conaghan, P.G., 2017. Synovitis in osteoarthritis: current understanding with therapeutic implications. Arthritis Res Ther 19. https://doi.org/10.1186/s13075-017-1229-9

Mattei, M.D., Caruso, A., Pezzetti, F., Pellati, A., Stabellini, G., Sollazzo, V., Traina, G.C., 2001. Effects of Pulsed Electromagnetic Fields on Human Articular Chondrocyte Proliferation. Connective Tissue Research 42, 269–279. https://doi.org/10.3109/03008200109016841

Mauck, R.L., Soltz, M.A., Wang, C.C.B., Wong, D.D., Chao, P.-H.G., Valhmu, W.B., Hung, C.T., Ateshian, G.A., 2000. Functional Tissue Engineering of Articular Cartilage Through Dynamic Loading of Chondrocyte-Seeded Agarose Gels. J Biomech Eng 122, 252–260. https://doi.org/10.1115/1.429656

McAlindon, T.E., LaValley, M.P., Harvey, W.F., Price, L.L., Driban, J.B., Zhang, M., Ward, R.J., 2017. Effect of Intra-articular Triamcinolone vs Saline on Knee Cartilage Volume and Pain in Patients With Knee Osteoarthritis: A Randomized Clinical Trial. JAMA 317, 1967–1975. https://doi.org/10.1001/jama.2017.5283

McKee, C.M., Penno, M.B., Cowman, M., Burdick, M.D., Strieter, R.M., Bao, C., Noble, P.W., 1996. Hyaluronan (HA) fragments induce chemokine gene expression in alveolar macrophages. The role of HA size and CD44. J Clin Invest 98, 2403–2413. https://doi.org/10.1172/JCI119054

McNamara, L.E., McMurray, R.J., Biggs, M.J.P., Kantawong, F., Oreffo, R.O.C., Dalby, M.J., 2010. Nanotopographical control of stem cell differentiation. J Tissue Eng 2010, 120623. https://doi.org/10.4061/2010/120623

Miron-Mendoza, M., Seemann, J., Grinnell, F., 2010. The differential regulation of cell motile activity through matrix stiffness and porosity in three dimensional collagen matrices. Biomaterials 31, 6425–6435. https://doi.org/10.1016/j.biomaterials.2010.04.064

Mitani, G., Sato, M., Yamato, M., Kokubo, M., Takagaki, T., Ebihara, G., Okano, T., Mochida, J., 2014. Potential utility of cell sheets derived from the anterior cruciate ligament and synovium fabricated in temperature-responsive culture dishes. J. Biomed. Mater. Res. 102, 2927–2933. https://doi.org/10.1002/jbm.a.34962

Mithoefer, K., McAdams, T., Williams, R.J., Kreuz, P.C., Mandelbaum, B.R., 2009. Clinical Efficacy of the Microfracture Technique for Articular Cartilage Repair in the Knee: An Evidence-Based Systematic Analysis. Am J Sports Med 37, 2053–2063. https://doi.org/10.1177/0363546508328414

Moradi, B., Rosshirt, N., Tripel, E., Kirsch, J., Barié, A., Zeifang, F., Gotterbarm, T., Hagmann, S., 2015. Unicompartmental and bicompartmental knee osteoarthritis show different patterns of mononuclear cell infiltration and cytokine release in the affected joints. Clinical & Experimental Immunology 180, 143–154. https://doi.org/10.1111/cei.12486

Mow, V.C., Huiskes, R., 2005. Basic Orthopaedic Biomechanics & Mechano-biology. Lippincott Williams & Wilkins.

Mwangi, T.K., Berke, I.M., Nieves, E.H., Bell, R.D., Adams, S.B., Setton, L.A., 2018. Intra-articular clearance of labeled dextrans from naive and arthritic rat knee joints. Journal of Controlled Release 283, 76–83. https://doi.org/10.1016/j.jconrel.2018.05.029

Myers, S.L., Brandt, K.D., Eilam, O., 1995. Even low-grade synovitis significantly accelerates the clearance of protein from the canine knee: implications for measurement of synovial fluid "markers" of osteoarthritis. Arthritis & Rheumatism 38, 1085–1091. https://doi.org/10.1002/art.1780380810

Nade, S., Newbold, P.J., 1983. Factors determining the level and changes in intra-articular pressure in the knee joint of the dog. The Journal of Physiology 338, 21–36. https://doi.org/10.1113/jphysiol.1983.sp014657

Nakamura, H., Yoshino, S., Kato, T., Tsuruha, J., Nishioka, K., 1999. T-cell mediated inflammatory pathway in osteoarthritis. Osteoarthritis and Cartilage 7, 401–402. https://doi.org/10.1053/joca.1998.0224

Nessler, J.P., Mass, D.P., 1987. Direct-current electrical stimulation of tendon healing in vitro. Clin. Orthop. Relat. Res. 303–312.

Neustadt, D.H., 2006. Intra-articular injections for osteoarthritis of the knee. Cleveland Clinic journal of medicine 73, 897–8, 901–4, 906–11.

Ng, K.W., Lima, E.G., Bian, L., O'Conor, C.J., Jayabalan, P.S., Stoker, A.M., Kuroki, K., Cook, C.R., Ateshian, G.A., Cook, J.L., Hung, C.T., 2010. Passaged Adult Chondrocytes Can Form Engineered Cartilage with Functional Mechanical Properties: A Canine Model. Tissue Eng Part A 16, 1041–1051. https://doi.org/10.1089/ten.tea.2009.0581

Nover, A.B., Stefani, R.M., Lee, S.L., Ateshian, G.A., Stoker, A.M., Cook, J.L., Hung, C.T., 2015. Long-term storage and preservation of tissue engineered articular cartilage. J. Orthop. Res. 34, 141–148. https://doi.org/10.1002/jor.23034

Nylon 680 Spec [WWW Document], 2016. . taulman3D. URL http://taulman3d.com/nylon-680-spec.html (accessed 10.2.19).

Obradovic, B., Martin, I., Freed, L.E., Vunjak-Novakovic, G., 2001a. Bioreactor studies of natural and tissue engineered cartilage. Ortop Traumatol Rehabil 3, 181–189.

Obradovic, B., Martin, I., Padera, R.F., Treppo, S., Freed, L.E., Vunjak-Navakovic, G., 2001b. Integration of engineered cartilage. J. Orthop. Res. 19, 1089–1097. https://doi.org/10.1016/S0736-0266(01)00030-4

O'Brien, K., Tailor, P., Leonard, C., DiFrancesco, L.M., Hart, D.A., Matyas, J.R., Frank, C.B., Krawetz, R.J., 2017. Enumeration and Localization of Mesenchymal Progenitor Cells and Macrophages in Synovium from Normal Individuals and Patients with Pre-Osteoarthritis or Clinically Diagnosed Osteoarthritis. International Journal of Molecular Sciences 18, 774. https://doi.org/10.3390/ijms18040774

O'Connell, G.D., Tan, A.R., Cui, V., Bulinski, J.C., Cook, J.L., Attur, M., Abramson, S.B., Ateshian, G.A., Hung, C.T., 2015. Human chondrocyte migration behaviour to guide the development of engineered cartilage. J Tissue Eng Regen Med n/a-n/a. https://doi.org/10.1002/term.1988

Ohyama, H., Nishimura, F., Meguro, M., Takashiba, S., Murayama, Y., Matsushita, S., 2002. Counter-antigen presentation: fibroblasts produce cytokines by signalling through HLA class II molecules without inducing T-cell proliferation. Cytokine 17, 175–181. https://doi.org/10.1006/cyto.2001.0976

Okada, Y., Shinmei, M., Tanaka, O., Naka, K., Kimura, A., Nakanishi, I., Bayliss, M.T., Iwata, K., Nagase, H., 1992. Localization of matrix metalloproteinase 3 (stromelysin) in osteoarthritic cartilage and synovium. Lab Invest 66, 680–690.

Olson, S.A., Horne, P., Furman, B., Huebner, J., Al-Rashid, M., Kraus, V.B., Guilak, F., 2014. The Role of Cytokines in Posttraumatic Arthritis: Journal of the American Academy of Orthopaedic Surgeons 22, 29–37. https://doi.org/10.5435/JAAOS-22-01-29

Ongaro, A., Pellati, A., Masieri, F.F., Caruso, A., Setti, S., Cadossi, R., Biscione, R., Massari, L., Fini, M., De Mattei, M., 2011. Chondroprotective effects of pulsed electromagnetic fields on human cartilage explants. Bioelectromagnetics 32, 543–551. https://doi.org/10.1002/bem.20663

Ongaro, A., Varani, K., Masieri, F. f., Pellati, A., Massari, L., Cadossi, R., Vincenzi, F., Borea, P. a., Fini, M., Caruso, A., De Mattei, M., 2012. Electromagnetic fields (EMFs) and adenosine receptors modulate prostaglandin E2 and cytokine release in human osteoarthritic synovial fibroblasts. J. Cell. Physiol. 227, 2461–2469. https://doi.org/10.1002/jcp.22981

Orida, N., Feldman, J.D., 1982. Directional protrusive pseudopodial activity and motility in macrophages induced by extracellular electric fields. Cell Motility 2, 243–255. https://doi.org/10.1002/cm.970020305

Ospelt, C., 2017. Synovial fibroblasts in 2017. RMD Open 3, e000471. https://doi.org/10.1136/rmdopen-2017-000471

Otter, M.W., McLeod, K.J., Rubin, C.T., 1998. Effects of Electromagnetic Fields in Experimental Fracture Repair: Clinical Orthopaedics and Related Research 355S, S90–S104. https://doi.org/10.1097/00003086-199810001-00011

Palmer, D.G., 1967. Synovial villi: An examination of these structures within the anterior compartment of the knee and metacarpo-phalangeal joints. Arthritis & Rheumatism 10, 451–458. https://doi.org/10.1002/art.1780100507

Patwari, P., Lin, S.N., Kurz, B., Cole, A.A., Kumar, S., Grodzinsky, A.J., 2009. Potent inhibition of cartilage biosynthesis by coincubation with joint capsule through an IL-1-independent pathway. Scand J Med Sci Sports 19, 528–535. https://doi.org/10.1111/j.1600-0838.2009.00911.x

Peck, Y., Leom, L.T., Low, P.F.P., Wang, D.-A., 2018. Establishment of an in vitro three-dimensional model for cartilage damage in rheumatoid arthritis. Journal of Tissue Engineering and Regenerative Medicine 12, e237–e249. https://doi.org/10.1002/term.2399

Pelletier, J.P., Martel-Pelletier, J., Abramson, S.B., 2001. Osteoarthritis, an inflammatory disease: potential implication for the selection of new therapeutic targets. Arthritis Rheum. 44, 1237–1247. https://doi.org/10.1002/1529-0131(200106)44:6<1237::AID-ART214>3.0.CO;2-F

Penatti, A., Facciotti, F., De Matteis, R., Larghi, P., Paroni, M., Murgo, A., De Lucia, O., Pagani, M., Pierannunzii, L., Truzzi, M., Ioan-Facsinay, A., Abrignani, S., Geginat, J., Meroni, P.L., 2017. Differences in serum and synovial CD4+ T cells and cytokine profiles to stratify patients with inflammatory osteoarthritis and rheumatoid arthritis. Arthritis Research & Therapy 19, 103. https://doi.org/10.1186/s13075-017-1305-1

Pessler, F., Chen, L.X., Dai, L., Gomez-Vaquero, C., Diaz-Torne, C., Paessler, M.E., Scanzello, C., Çakir, N., Einhorn, E., Schumacher, H.R., 2008. A histomorphometric analysis of synovial biopsies from individuals with Gulf War Veterans' Illness and joint pain compared to normal and osteoarthritis synovium. Clin Rheumatol 27, 1127–1134. https://doi.org/10.1007/s10067-008-0878-0

Petrofsky, J., 2008. The effect of the subcutaneous fat on the transfer of current through skin and into muscle. Medical Engineering & Physics 30, 1168–1176. https://doi.org/10.1016/j.medengphy.2008.02.009

Pezzetti, F., Mattei, M.D., Caruso, A., Cadossi, R., Zucchini, P., Carinci, F., Traina, G.C., Sollazzo, V., 2014. Effects of Pulsed Electromagnetic Fields on Human Chondrocytes: An In Vitro Study. Calcif Tissue Int 65, 396–401. https://doi.org/10.1007/s002239900720

Pietschmann, M.F., Horng, A., Niethammer, T., Pagenstert, I., Sievers, B., Jansson, V., Glaser, C., Müller, P.E., 2009. Cell quality affects clinical outcome after MACI procedure for cartilage injury of the knee. Knee Surg Sports Traumatol Arthrosc 17, 1305–1311. https://doi.org/10.1007/s00167-009-0828-7

Pober, J.S., Collins, T., Gimbrone, M.A., Cotran, R.S., Gitlin, J.D., Fiers, W., Clayberger, C., Krensky, A.M., Burakoff, S.J., Reiss, C.S., 1983. Lymphocytes recognize human vascular endothelial and dermal fibroblast Ia antigens induced by recombinant immune interferon. Nature 305, 726–729. https://doi.org/10.1038/305726a0

Pretzel, D., Pohlers, D., Weinert, S., Kinne, R.W., 2009. In vitro model for the analysis of synovial fibroblast-mediated degradation of intact cartilage. Arthritis Res Ther 11, R25. https://doi.org/10.1186/ar2618

Price, F.M., Levick, J.R., Mason, R.M., 1996. Glycosaminoglycan concentration in synovium and other tissues of rabbit knee in relation to synovial hydraulic resistance. J Physiol 495, 803–820.

Pulkki, K., 1986. The effects of synovial fluid macrophages and interleukin-1 on hyaluronic acid synthesis by normal synovial fibroblasts. Rheumatol Int 6, 121–125. https://doi.org/10.1007/BF00270348

Qu, F., Guilak, F., Mauck, R.L., 2019. Cell migration: implications for repair and regeneration in joint disease. Nature Reviews Rheumatology 15, 167. https://doi.org/10.1038/s41584-018-0151-0

Rajabi, A.H., Jaffe, M., Arinzeh, T.L., 2015. Piezoelectric materials for tissue regeneration: A review. Acta Biomaterialia 24, 12–23. https://doi.org/10.1016/j.actbio.2015.07.010

Remst, D.F.G., Davidson, B., N, E., Kraan, V.D., M, P., 2015. Unravelling osteoarthritis-related synovial fibrosis: a step closer to solving joint stiffness. Rheumatology (Oxford) 54, 1954–1963. https://doi.org/10.1093/rheumatology/kev228

Reyes, L.I., León, F., González, P., Rozas, M.F., Labarca, C., Segovia, A., Neira, O., Naves, R., 2008. Dexamethasone inhibits BAFF expression in fibroblast-like synoviocytes from

patients with rheumatoid arthritis. Cytokine 42, 170–178. https://doi.org/10.1016/j.cyto.2007.12.005

Riesle, J., Hollander, A.P., Langer, R., Freed, L.E., Vunjak-Novakovic, G., 1998. Collagen in tissue-engineered cartilage: types, structure, and crosslinks. J. Cell. Biochem. 71, 313–327.

Roach, B.L., 2017. Modulation of the in vitro mechanical and chemical environment for the optimization of tissue-engineered articular cartilage. Columbia University, New York, NY.

Roach, B.L., Kelmendi-Doko, A., Balutis, E.C., Marra, K.G., Ateshian, G.A., Hung, C.T., 2016a. Dexamethasone Release from Within Engineered Cartilage as a Chondroprotective Strategy Against Interleukin-1α. Tissue Eng Part A. https://doi.org/10.1089/ten.TEA.2016.0018

Roach, B.L., Kelmendi-Doko, A., Balutis, E.C., Marra, K.G., Ateshian, G.A., Hung, C.T., 2016b. Dexamethasone Release from Within Engineered Cartilage as a Chondroprotective Strategy Against Interleukin-1α. Tissue Eng Part A. https://doi.org/10.1089/ten.TEA.2016.0018

Robinson, K.R., 1985. The responses of cells to electrical fields: a review. J. Cell Biol. 101, 2023–2027.

Rocha, B., Haston, W.S., Freitas, A.A., 1984. Lymphocyte Migration into Collagen Gels: Role of Lymph. Scandinavian Journal of Immunology 19, 297–305. https://doi.org/10.1111/j.1365-3083.1984.tb00934.x

Rose, B.J., Kooyman, D.L., 2016. A Tale of Two Joints: The Role of Matrix Metalloproteases in Cartilage Biology. Dis Markers 2016. https://doi.org/10.1155/2016/4895050

Ross, C.L., Harrison, B.S., 2013. Effect of pulsed electromagnetic field on inflammatory pathway markers in RAW 264.7 murine macrophages. J Inflamm Res 6, 45–51. https://doi.org/10.2147/JIR.S40269

Rubin, J.P., DeFail, A., Rajendran, N., Marra, K.G., 2009. Encapsulation of adipogenic factors to promote differentiation of adipose-derived stem cells. Journal of Drug Targeting 17, 207–215. https://doi.org/10.1080/10611860802669231

Rudnik-Jansen, I., Colen, S., Berard, J., Plomp, S., Que, I., van Rijen, M., Woike, N., Egas, A., van Osch, G., van Maarseveen, E., Messier, K., Chan, A., Thies, J., Creemers, L., 2017. Prolonged inhibition of inflammation in osteoarthritis by triamcinolone acetonide released

from a polyester amide microsphere platform. Journal of Controlled Release 253, 64–72. https://doi.org/10.1016/j.jconrel.2017.03.014

Rui, Y.-F., Du, L., Wang, You, Wang, Yang, Lui, P.P.-Y., Tang, T.-T., Chan, K.-M., Dai, K.-R., 2010. Bone morphogenetic protein 2 promotes transforming growth factor β3-induced chondrogenesis of human osteoarthritic synovium-derived stem cells. Chin. Med. J. 123, 3040–3048.

Ryang We, S., Koog, Y.H., Jeong, K.-I., Wi, H., 2013. Effects of pulsed electromagnetic field on knee osteoarthritis: a systematic review. Rheumatology 52, 815–824. https://doi.org/10.1093/rheumatology/kes063

Sabaratnam S., Arunan V., Coleman P. J., Mason R. M., Levick J. R., 2005. Size selectivity of hyaluronan molecular sieving by extracellular matrix in rabbit synovial joints. The Journal of Physiology 567, 569–581. https://doi.org/10.1113/jphysiol.2005.088906

Saito, S., Katoh, M., Masumoto, M., Matsumoto, S., Masuho, Y., 1999. Dexamethasone Inhibits Collagen Degradation Induced by the Combination of Interleukin-1 and Plasminogen in Cartilage Explant Culture. Biological and Pharmaceutical Bulletin 22, 727–730. https://doi.org/10.1248/bpb.22.727

Saltzman, B.M., Leroux, T., Meyer, M.A., Basques, B.A., Chahal, J., Bach, B.R., Yanke, A.B., Cole, B.J., 2017. The Therapeutic Effect of Intra-articular Normal Saline Injections for Knee Osteoarthritis: A Meta-analysis of Evidence Level 1 Studies. Am J Sports Med 45, 2647–2653. https://doi.org/10.1177/0363546516680607

Sampat, S.R., O'Connell, G.D., Fong, J.V., Alegre-Aguarón, E., Ateshian, G.A., Hung, C.T., 2011a. Growth Factor Priming of Synovium-Derived Stem Cells for Cartilage Tissue Engineering. Tissue Engineering Part A 17, 2259–2265. https://doi.org/10.1089/ten.tea.2011.0155

Sampat, S.R., O'Connell, G.D., Fong, J.V., Alegre-Aguarón, E., Ateshian, G.A., Hung, C.T., 2011b. Growth Factor Priming of Synovium-Derived Stem Cells for Cartilage Tissue Engineering. Tissue Engineering Part A 17, 2259–2265. https://doi.org/10.1089/ten.tea.2011.0155

Samuelsson, M.K.R., Pazirandeh, A., Davani, B., Okret, S., 1999. p57Kip2, a Glucocorticoid-Induced Inhibitor of Cell Cycle Progression in HeLa Cells. Mol Endocrinol 13, 1811–1822. https://doi.org/10.1210/mend.13.11.0379

Sarin, A., Wu, M.-L., Henkart, P.A., 1996. Different Interleukin-1β Converting Enzyme (ICE) Family Protease Requirements for the Apoptotic Death of T Lymphocytes Triggered by Diverse Stimuli. Journal of Experimental Medicine 184, 2445–2450. https://doi.org/10.1084/jem.184.6.2445

Scanzello, C.R., Goldring, S.R., 2012a. The role of synovitis in osteoarthritis pathogenesis. Bone, Osteoarthritis 51, 249–257. https://doi.org/10.1016/j.bone.2012.02.012

Scanzello, C.R., Goldring, S.R., 2012b. The role of synovitis in osteoarthritis pathogenesis. Bone, Osteoarthritis 51, 249–257. https://doi.org/10.1016/j.bone.2012.02.012

Schmidt, T.A., Sah, R.L., 2007. Effect of synovial fluid on boundary lubrication of articular cartilage. Osteoarthritis and Cartilage 15, 35–47. https://doi.org/10.1016/j.joca.2006.06.005

Schor, S.L., 1983. Lymphocyte migration into three-dimensional collagen matrices: a quantitative study. J Cell Biol 96, 1089–1096.

Seidel, M.F., Wise, B.L., Lane, N.E., 2013. Nerve growth factor: an update on the science and therapy. Osteoarthritis and Cartilage, Pain in Osteoarthritis 21, 1223–1228. https://doi.org/10.1016/j.joca.2013.06.004

Sellam, Jérémie, Berenbaum, F., 2010. The role of synovitis in pathophysiology and clinical symptoms of osteoarthritis. Nature Reviews Rheumatology 6, 625–635. https://doi.org/10.1038/nrrheum.2010.159

Sellam, Jeremie, Berenbaum, F., 2010. The role of synovitis in pathophysiology and clinical symptoms of osteoarthritis. Nature Reviews Rheumatology 6, 625+.

Selmi, T.A.S., Neyret, P., Verdonk, P.C.M., Barnouin, L., 2007. Autologous Chondrocyte Transplantation in Combination With an Alginate-Agarose Based Hydrogel (Cartipatch). Techniques in Knee Surgery 6, 253–258. https://doi.org/10.1097/BTK.0b013e318148b797aB

Selmi, T.A.S., Verdonk, P., Chambat, P., Dubrana, F., Potel, J.-F., Barnouin, L., Neyret, P., 2008. Autologous chondrocyte implantation in a novel alginate-agarose hydrogel: OUTCOME AT TWO YEARS. The Journal of Bone and Joint Surgery. British volume 90-B, 597–604. https://doi.org/10.1302/0301-620X.90B5.20360

Sgaglione, N., Kerker, J., 2008. Autologous Osteochondral Transplantation. OKOJ 6, 22.

Sherman, S.L., James, C., Stoker, A.M., Cook, C.R., Khazai, R.S., Flood, D.L., Cook, J.L., 2015. In Vivo Toxicity of Local Anesthetics and Corticosteroids on Chondrocyte and Synoviocyte Viability and Metabolism. CARTILAGE 6, 106–112. https://doi.org/10.1177/1947603515571001

Shibakawa, A., Aoki, H., Masuko-Hongo, K., Kato, T., Tanaka, M., Nishioka, K., Nakamura, H., 2003. Presence of pannus-like tissue on osteoarthritic cartilage and its histological character. Osteoarthr. Cartil. 11, 133–140.

Shimozono, Y., Seow, D., Yasui, Y., Fields, K., Kennedy, J.G., 2019. Knee-to-Talus Donor-Site Morbidity Following Autologous Osteochondral Transplantation: A Meta-Analysis with Best-case and Worst-case Analysis. Clin. Orthop. Relat. Res. 477, 1915–1931. https://doi.org/10.1097/CORR.0000000000000719

Shiozawa, S., Shiozawa, K., Fujita, T., 1983. Presence of HLA-DR antigen on synovial type A and B cells: an immunoelectron microscopic study in rheumatoid arthritis, osteoarthritis and normal traumatic joints. Immunology 50, 587–594.

Silverstein, A.M., 2016. Development of Biofidelic Culture Models of Osteoarthritis. Columbia University.

Silverstein, A.M., Stefani, R.M., Sobczak, E., Tong, E.L., Attur, M.G., Shah, R.P., Bulinski, J.C., Ateshian, G.A., Hung, C.T., 2017. Toward understanding the role of cartilage particulates in synovial inflammation. Osteoarthr. Cartil. 25, 1353–1361. https://doi.org/10.1016/j.joca.2017.03.015

Smith, M.D., 2011. The Normal Synovium. Open Rheumatol J 5, 100–106. https://doi.org/10.2174/1874312901105010100

Soong, H.K., Parkinson, W.C., Bafna, S., Sulik, G.L., Huang, S.C., 1990. Movements of cultured corneal epithelial cells and stromal fibroblasts in electric fields. Invest. Ophthalmol. Vis. Sci. 31, 2278–2282.

Spalazzi, J.P., Dagher, E., Doty, S.B., Guo, X.E., Rodeo, S.A., Lu, H.H., 2008. In vivo evaluation of a multiphased scaffold designed for orthopaedic interface tissue engineering and soft tissue-to-bone integration. Journal of Biomedical Materials Research Part A 86A, 1–12. https://doi.org/10.1002/jbm.a.32073

Spitzer, A.I., Richmond, J.C., Kraus, V.B., Gomoll, A., Jones, D.G., Huffman, K.M., Peterfy, C., Cinar, A., Lufkin, J., Kelley, S.D., 2019. Safety and Efficacy of Repeat Administration of Triamcinolone Acetonide Extended-release in Osteoarthritis of the Knee: A Phase 3b,

Open-label Study. Rheumatol Ther 6, 109–124. https://doi.org/10.1007/s40744-019-0140-z

Stannus, O., Jones, G., Cicuttini, F., Parameswaran, V., Quinn, S., Burgess, J., Ding, C., 2010. Circulating levels of IL-6 and TNF-α are associated with knee radiographic osteoarthritis and knee cartilage loss in older adults. Osteoarthritis and Cartilage 18, 1441–1447. https://doi.org/10.1016/j.joca.2010.08.016

Stefani, R.M., Halder, S.S., Estell, E.G., Lee, A.J., Silverstein, A.M., Sobczak, E., Chahine, N.O., Ateshian, G.A., Shah, R.P., Hung, C.T., 2018. A Functional Tissue-Engineered Synovium Model to Study Osteoarthritis Progression and Treatment. Tissue Engineering Part A. https://doi.org/10.1089/ten.tea.2018.0142

Stern, R., 2004. Hyaluronan catabolism: a new metabolic pathway. European Journal of Cell Biology; Stuttgart 83, 317–25.

Stoppiello, L.A., Mapp, P.I., Wilson, D., Hill, R., Scammell, B.E., Walsh, D.A., 2014. Structural Associations of Symptomatic Knee Osteoarthritis. Arthritis & Rheumatology 66, 3018–3027. https://doi.org/10.1002/art.38778

Sugawara, S., Sugiyama, A., Nemoto, E., Rikiishi, H., Takada, H., 1998. Heterogeneous Expression and Release of CD14 by Human Gingival Fibroblasts: Characterization and CD14-Mediated Interleukin-8 Secretion in Response to Lipopolysaccharide. Infect. Immun. 66, 3043–3049.

Sun, H.B., Nalim, R., Yokota, H., 2003. Expression and Activities of Matrix Metalloproteinases under Oscillatory Shear in IL-1-Stimulated Synovial Cells. Connective Tissue Research 44, 42–49. https://doi.org/10.1080/03008200390151954

Sun, S., Titushkin, I., Cho, M., 2006. Regulation of mesenchymal stem cell adhesion and orientation in 3D collagen scaffold by electrical stimulus. Bioelectrochemistry 69, 133–141. https://doi.org/10.1016/j.bioelechem.2005.11.007

Sun, S., Wise, J., Cho, M., 2004. Human Fibroblast Migration in Three-Dimensional Collagen Gel in Response to Noninvasive Electrical Stimulus. I. Characterization of Induced Three-Dimensional Cell Movement. Tissue Engineering 10, 1548–1557. https://doi.org/10.1089/ten.2004.10.1548

Sutton, S., Clutterbuck, A., Harris, P., Gent, T., Freeman, S., Foster, N., Barrett-Jolley, R., Mobasheri, A., 2009. The contribution of the synovium, synovial derived inflammatory

cytokines and neuropeptides to the pathogenesis of osteoarthritis. Vet. J. 179, 10–24. https://doi.org/10.1016/j.tvjl.2007.08.013

Swärd, P., Wang, Y., Hansson, M., Lohmander, L.S., Grodzinsky, A.J., Struglics, A., 2017. Coculture of bovine cartilage with synovium and fibrous joint capsule increases aggrecanase and matrix metalloproteinase activity. Arthritis Res. Ther. 19, 157. https://doi.org/10.1186/s13075-017-1318-9

Takano, S., Uchida, K., Inoue, G., Miyagi, M., Aikawa, J., Iwase, D., Iwabuchi, K., Matsumoto, T., Satoh, M., Mukai, M., Minatani, A., Takaso, M., 2017. Nerve growth factor regulation and production by macrophages in osteoarthritic synovium. Clinical & Experimental Immunology 190, 235–243. https://doi.org/10.1111/cei.13007

Takeshita, M., Nakamura, J., Ohtori, S., Inoue, G., Orita, S., Miyagi, M., Ishikawa, T., Takahashi, K., 2012. Sensory innervation and inflammatory cytokines in hypertrophic synovia associated with pain transmission in osteoarthritis of the hip: a case–control study. Rheumatology 51, 1790–1795. https://doi.org/10.1093/rheumatology/kes173

Takezawa, T., Ozaki, K., Nitani, A., Takabayashi, C., Shimo-Oka, T., 2004. Collagen Vitrigel: A Novel Scaffold That Can Facilitate a Three-Dimensional Culture for Reconstructing Organoids. Cell Transplantation 13, 463–473. https://doi.org/10.3727/000000004783983882

Tan, A.R., Alegre-Aguarón, E., Dujari, D.N., Sampat, S.R., Bulinski, J.C., Ateshian, G.A., Hung, C.T., 2011. Effects of Passaging on the Migration Response of Synovium-Derived Stem Cells to an Applied DC Electric Field 401–402. https://doi.org/10.1115/SBC2011-53674

Tan, A. R., Alegre-Aguarón, E., O'Connell, G.D., VandenBerg, C.D., Aaron, R.K., Vunjak-Novakovic, G., Chloe Bulinski, J., Ateshian, G.A., Hung, C.T., 2015a. Passage-dependent relationship between mesenchymal stem cell mobilization and chondrogenic potential. Osteoarthritis and Cartilage 23, 319–327. https://doi.org/10.1016/j.joca.2014.10.001

Tan, A. R., Alegre-Aguarón, E., O'Connell, G.D., VandenBerg, C.D., Aaron, R.K., Vunjak-Novakovic, G., Chloe Bulinski, J., Ateshian, G.A., Hung, C.T., 2015b. Passage-dependent relationship between mesenchymal stem cell mobilization and chondrogenic potential. Osteoarthritis and Cartilage 23, 319–327. https://doi.org/10.1016/j.joca.2014.10.001

Tan, Andrea R, VandenBerg, C.D., Attur, M., Abramson, S.B., Knight, M.M., Bulinski, J.C., Ateshian, G.A., Cook, J.L., Hung, C.T., 2015. Cytokine preconditioning of engineered cartilage provides protection against interleukin-1 insult. Arthritis Res. Ther. 17, 361. https://doi.org/10.1186/s13075-015-0876-y

Tepper, O.M., Callaghan, M.J., Chang, E.I., Galiano, R.D., Bhatt, K.A., Baharestani, S., Gan, J., Simon, B., Hopper, R.A., Levine, J.P., Gurtner, G.C., 2004. Electromagnetic fields increase in vitro and in vivo angiogenesis through endothelial release of FGF-2. FASEB J. 18, 1231–1233. https://doi.org/10.1096/fj.03-0847fje

Timpson, P., Mcghee, E.J., Erami, Z., Nobis, M., Quinn, J.A., Edward, M., Anderson, K.I., 2011. Organotypic Collagen I Assay: A Malleable Platform to Assess Cell Behaviour in a 3-Dimensional Context. J Vis Exp. https://doi.org/10.3791/3089

Tognana, E., Padera, R.F., Chen, F., Vunjak-Novakovic, G., Freed, L.E., 2005. Development and remodeling of engineered cartilage-explant composites in vitro and in vivo. Osteoarthritis and Cartilage 13, 896–905. https://doi.org/10.1016/j.joca.2005.05.003

Trock, D.H., Bollet, A.J., Dyer, R.H., Fielding, L.P., Miner, W.K., Markoll, R., 1993. A double-blind trial of the clinical effects of pulsed electromagnetic fields in osteoarthritis. J. Rheumatol. 20, 456–460.

Ulmer, A.J., Scholz, W., Ernst, M., Brandt, E., Flad, H.-D., 1984. Isolation and Subfractionation of Human Peripheral Blood Mononuclear Cells (PBMC) by Density Gradient Centrifugation on Percoll. Immunobiology 166, 238–250. https://doi.org/10.1016/S0171-2985(84)80042-X

Unterhauser, F.N., Bosch, U., Zeichen, J., Weiler, A., 2004. α-Smooth muscle actin containing contractile fibroblastic cells in human knee arthrofibrosis tissue. Arch Orthop Trauma Surg 124, 585–591. https://doi.org/10.1007/s00402-004-0742-x

Utomo, L., van Osch, G.J.V.M., Bayon, Y., Verhaar, J.A.N., Bastiaansen-Jenniskens, Y.M., 2016. Guiding synovial inflammation by macrophage phenotype modulation: an in vitro study towards a therapy for osteoarthritis. Osteoarthritis and Cartilage 24, 1629–1638. https://doi.org/10.1016/j.joca.2016.04.013

Valencia, X., Higgins, J.M.G., Kiener, H.P., Lee, D.M., Podrebarac, T.A., Dascher, C.C., Watts, G.F.M., Mizoguchi, E., Simmons, B., Patel, D.D., Bhan, A.K., Brenner, M.B., 2004. Cadherin-11 Provides Specific Cellular Adhesion between Fibroblast-like Synoviocytes. J Exp Med 200, 1673–1679. https://doi.org/10.1084/jem.20041545

van Buul, G.M., Villafuertes, E., Bos, P.K., Waarsing, J.H., Kops, N., Narcisi, R., Weinans, H., Verhaar, J.A.N., Bernsen, M.R., van Osch, G.J.V.M., 2012. Mesenchymal stem cells secrete factors that inhibit inflammatory processes in short-term osteoarthritic synovium

and cartilage explant culture. Osteoarthr. Cartil. 20, 1186–1196. https://doi.org/10.1016/j.joca.2012.06.003

van de Breevaart Bravenboer, J., In der Maur, C.D., Bos, P.K., Feenstra, L., Verhaar, J.A., Weinans, H., van Osch, G.J., 2004. Improved cartilage integration and interfacial strength after enzymatic treatment in a cartilage transplantation model. Arthritis Res Ther 6, R469. https://doi.org/10.1186/ar1216

Varani, K., De Mattei, M., Vincenzi, F., Gessi, S., Merighi, S., Pellati, A., Ongaro, A., Caruso, A., Cadossi, R., Borea, P.A., 2008. Characterization of adenosine receptors in bovine chondrocytes and fibroblast-like synoviocytes exposed to low frequency low energy pulsed electromagnetic fields. Osteoarthritis and Cartilage 16, 292–304. https://doi.org/10.1016/j.joca.2007.07.004

Veronesi, F., Cadossi, M., Giavaresi, G., Martini, L., Setti, S., Buda, R., Giannini, S., Fini, M., 2015. Pulsed electromagnetic fields combined with a collagenous scaffold and bone marrow concentrate enhance osteochondral regeneration: an in vivo study. BMC Musculoskeletal Disorders 16, 233. https://doi.org/10.1186/s12891-015-0683-2

Veronesi, F., Torricelli, P., Giavaresi, G., Sartori, M., Cavani, F., Setti, S., Cadossi, M., Ongaro, A., Fini, M., n.d. In vivo effect of two different pulsed electromagnetic field frequencies on osteoarthritis. Journal of Orthopaedic Research 32, 677–685. https://doi.org/10.1002/jor.22584

Vincenzi, F., Targa, M., Corciulo, C., Gessi, S., Merighi, S., Setti, S., Cadossi, R., Goldring, M.B., Borea, P.A., Varani, K., 2013. Pulsed Electromagnetic Fields Increased the Anti-Inflammatory Effect of A2A and A3 Adenosine Receptors in Human T/C-28a2 Chondrocytes and hFOB 1.19 Osteoblasts. PLoS One 8. https://doi.org/10.1371/journal.pone.0065561

von Banchet, G.S., Richter, J., Hückel, M., Rose, C., Bräuer, R., Schaible, H.-G., 2007. Fibroblast-like synovial cells from normal and inflamed knee joints differently affect the expression of pain-related receptors in sensory neurones: a co-culture study. Arthritis Research & Therapy 9, R6. https://doi.org/10.1186/ar2112

Wang, H., Zhang, X., He, J.-Y., Zheng, X.-F., Li, D., Li, Z., Zhu, J.-F., Shen, C., Cai, G.-Q., Chen, X.-D., 2015. Increasing expression of substance P and calcitonin gene-related peptide in synovial tissue and fluid contribute to the progress of arthritis in developmental dysplasia of the hip. Arthritis Research & Therapy 17, 4. https://doi.org/10.1186/s13075-014-0513-1

Warnock, J.J., Baker, L., Ballard, G.A., Ott, J., 2013. In vitro synthesis of tensioned synoviocyte bioscaffolds for meniscal fibrocartilage tissue engineering. BMC Veterinary Research 9, 242. https://doi.org/10.1186/1746-6148-9-242

Warnock, J.J., Bobe, G., Duesterdieck-Zellmer, K.F., Spina, J., Ott, J., Baltzer, W.I., Bay, B.K., 2014. Growth factor treated tensioned synoviocyte neotissues: Towards meniscal bioscaffold tissue engineering. The Veterinary Journal 200, 22–30. https://doi.org/10.1016/j.tvjl.2014.01.010

Weiss, A., Livne, E., Silbermann, M., 1988. Glucocorticoid hormone adversely affects the growth and regeneration of cartilage in vitro. Growth Dev Aging 52, 67–75.

Wenham, C.Y.J., Conaghan, P.G., 2010. The Role of Synovitis in Osteoarthritis. Ther Adv Musculoskelet Dis 2, 349–359. https://doi.org/10.1177/1759720X10378373

Westacott, C.I., Sharif, M., 1996. Cytokines in osteoarthritis: Mediators or markers of joint destruction? Seminars in Arthritis and Rheumatism 25, 254–272. https://doi.org/10.1016/S0049-0172(96)80036-9

Widuchowski, W., Widuchowski, J., Trzaska, T., 2007. Articular cartilage defects: Study of 25,124 knee arthroscopies. The Knee 14, 177–182. https://doi.org/10.1016/j.knee.2007.02.001

Wilusz, R.E., Weinberg, J.B., Guilak, F., McNulty, A.L., 2008. Inhibition of integrative repair of the meniscus following acute exposure to interleukin-1 in vitro. Journal of Orthopaedic Research 26, 504–512. https://doi.org/10.1002/jor.20538

Wu, P.-H., Giri, A., Sun, S.X., Wirtz, D., 2014. Three-dimensional cell migration does not follow a random walk. PNAS 111, 3949–3954. https://doi.org/10.1073/pnas.1318967111

Yamanouchi, K., Satomura, K., Gotoh, Y., Kitaoka, E., Tobiume, S., Kume, K., Nagayama, M., 2001. Bone Formation by Transplanted Human Osteoblasts Cultured Within Collagen Sponge with Dexamethasone In Vitro. Journal of Bone and Mineral Research 16, 857–867. https://doi.org/10.1359/jbmr.2001.16.5.857

Yang, K.G.A., Saris, D. b. f., Verbout, A. j., Creemers, L. b., Dhert, W. j. a., 2006. The Effect of Synovial Fluid from Injured Knee Joints on in Vitro Chondrogenesis. Tissue Engineering 12, 2957–2964. https://doi.org/10.1089/ten.2006.12.2957

Younes, M., Neffati, F., Touzi, M., Hassen-Zrour, S., Fendri, Y., Béjia, I., Ben Amor, A., Bergaoui, N., Najjar, M.F., 2007. Systemic effects of epidural and intra-articular glucocorticoid injections in diabetic and non-diabetic patients. Joint Bone Spine 74, 472–476. https://doi.org/10.1016/j.jbspin.2006.10.009

Yuan, G.-H., Tanaka V.M.D., M., Masuko-Hongo, K., Shibakawa, A., Kato, T., Nishioka, K., Nakamura, H., 2004. Characterization of cells from pannus-like tissue over articular cartilage of advanced osteoarthritis. Osteoarthritis and cartilage / OARS, Osteoarthritis Research Society 12, 38–45. https://doi.org/10.1016/j.joca.2003.08.004

Yuan, S.Y., Rigor, R.R., 2010. Methods for Measuring Permeability. Morgan & Claypool Life Sciences.

Yuan, X., Arkonac, D.E., Chao, P.G., Vunjak-Novakovic, G., 2014. Electrical stimulation enhances cell migration and integrative repair in the meniscus. Scientific Reports 4, srep03674. https://doi.org/10.1038/srep03674

Zhao, M., Agius-Fernandez, A., Forrester, J.V., McCaig, C.D., 1996. Directed migration of corneal epithelial sheets in physiological electric fields. Invest. Ophthalmol. Vis. Sci. 37, 2548–2558.

Zhuang, H., Wang, W., Seldes, R.M., Tahernia, A.D., Fan, H., Brighton, C.T., 1997. Electrical stimulation induces the level of TGF-beta1 mRNA in osteoblastic cells by a mechanism involving calcium/calmodulin pathway. Biochem. Biophys. Res. Commun. 237, 225–229. https://doi.org/10.1006/bbrc.1997.7118

Zimmermann, T., Kunisch, E., Pfeiffer, R., Hirth, A., Stahl, H.-D., Sack, U., Laube, A., Liesaus, E., Roth, A., Palombo-Kinne, E., Emmrich, F., Kinne, R.W., 2001. Isolation and characterization of rheumatoid arthritis synovial fibroblasts from primary culture — primary culture cells markedly differ from fourth-passage cells. Arthritis Res 3, 72–76.

Zolnik, B.S., Burgess, D.J., 2008. Evaluation of in vivo–in vitro release of dexamethasone from PLGA microspheres. Journal of Controlled Release 127, 137–145. https://doi.org/10.1016/j.jconrel.2008.01.004

Zorzi, C., Dall'Oca, C., Cadossi, R., Setti, S., 2007. Effects of pulsed electromagnetic fields on patients' recovery after arthroscopic surgery: prospective, randomized and double-blind study. Knee Surg Sports Traumatol Arthr 15, 830–834. https://doi.org/10.1007/s00167-007-0298-8

Appendix A

Supplementary Results

This appendix provides additional results to supplement studies described in this dissertation. A related second-author publication is also provided to show tangential work being performed in our laboratory using synovium-based models.

A.1 Supplementary Human Donor Data

Table A.1.1 Initial biochemical content for human and bovine synovium explants.

Donor Info				Initial Biochemical Content*				
Donor	**Gender**	**OA Grade**	**Age**	**DNA/DW (%)**	**GAG/DW (%)**	**GAG/DNA (µg/µg)**	**COL/DW (%)**	**COL/DNA (µg/µg)**
A	M	4	78	0.17 ± 0.18	0.71 ± 0.38	6.38 ± 3.8	43.73 ± 12.6	458.6 ± 262.6
B	M	2	65	0.30 ± 0.11	1.02 ± 0.18	3.72 ± 1.0	54.11 ± 7.88	210.1 ± 94.3
C	F	4	68	0.14 ± 0.06	0.82 ± 0.36	5.68 ± 1.0	38.69 ± 14.9	282.1 ± 39.4
D	F	4	63	0.27 ± 0.13	0.93 ± 0.30	3.75 ± 1.1	64.24 ± 9.57	317.7 ± 133.9
E	F	3	60	0.47 ± 0.26	1.10 ± 0.61	2.35 ± 0.7	35.25 ± 15.5	89.8 ± 44.1
F	M	4	80	0.43 ± 0.20	1.19 ± 0.56	2.69 ± 0.6	51.32 ± 13.7	135.9 ± 46.7
G	F	4	69	0.13 ± 0.06	0.60 ± 0.23	5.11 ± 2.6	42.35 ± 14.6	366.6 ± 179.8
H	F	4	71	0.20 ± 0.13	0.19 ± 0.17	0.86 ± 0.5	28.15 ± 16.4	354.1 ± 677.9
I	F	4	72	0.45 ± 0.50	0.46 ± 0.55	1.03 ± 0.5	42.23 ± 46.7	109.4 ± 59.8
J	F	4	66	0.26 ± 0.07	0.58 ± 0.22	2.52 ± 1.7	74.42 ± 23.0	333.7 ± 218.2
K	F	4	72	0.26 ± 0.25	0.34 ± 0.22	1.56 ± 1.1	33.90 ± 19.1	208.2 ± 91.8
Human Average (11 donors)		**3.7 ± 0.6**	**69 ± 6**	**0.28 ± 0.1**	**0.72 ± 0.3**	**4.24 ± 1.5**	**48.02 ± 13.1**	**260.6 ± 119**
Bovine Average (4 donors)		**0**	**Juvenile**	**0.53 ± 0.1**	**1.27 ± 0.2**	**2.52 ± 0.7**	**51.71 ± 11.1**	**105.5 ± 46.4**

***Values presented as mean ± standard deviation**

Table A.1.2 Percent positive surface marker expression of OA human FLS (P1).

	Synovial Fibroblasts		Inflamed synovium		Endothelial	Leukocytes		Macrophages	HSC
Donor	**CD73**	**CD90**	**CD105**	**CD106**	**CD31**	**CD11B**	**CD45**	**CD14**	**CD34**
A	90.3	52.6	10.7	50.7	16.6	1.01	1.1	1.39	2.25
B	99.5	89.7	48.2	51.6	17.5	0.653	0.653	0.917	1.58
C	82.2	56.6	12.2	82.2	15.2	1.02	1.02	2.12	2.03
D	65	35.8	34.2	59.5	9.77	0.22	0	1.01	3.01
E	94.2	75	52.2	57	8.95	1	0.32	1.2	3.27
F	96	62.5	61	77	17.1	0.5	0	2	5.14
G	87.7	52.9	42.2	63.7	10.5	0.5	0.41	1.12	3.58

A.2 Galvanotaxis Chamber Parameters

Table A.2.1 Optimal 3D printing settings.

Setting	Optimal Value*
Precision	20 µm
Extrusion Speed	Slow, ~35 mm/sec
Extrusion Temperature	255°C +/- 5°C
Fan Speed	40%
Optional Cura Settings	Ironing
Layer Height	0.2 mm
Nozzle Size	0.4 mm
Build Plate Temperature	45°C
Retraction Distance	3.5 mm
Retraction Speed	25 mm/sec
Build Plate Adhesion Method	Brim (support material extruder)

*Ultimaker S5 model printer, Cura version 4.2.1

Table A.2.2 Material properties of the finite element analysis.

Property		Cartilage	Collagen	Bath
Neo-Hookean	$E\ (MPa)$	0.4	0.01	0.1
	$\upsilon\ (-)$	0	0	0
	$\varphi^s\ (-)$	0.002	0.21	10^{-6}
	$FCD\ (mM)$	0	-200	0
	$k\ (mm^4 \times N \times s^{-1})$	0.28	0.0035	1
Na^+	$D^w\ (mm^2 s^{-1})$	1.15×10^{-3}	1.15×10^{-3}	1.15×10^{-3}
	$D^{sw}\ (mm^2 s^{-1})$	4.6×10^{-4}	7.5×10^{-4}	1.15×10^{-3}
	$\kappa\ (-)$	1	1	1
Cl^-	$D^w\ (mm^2 s^{-1})$	1.18×10^{-3}	1.18×10^{-3}	1.18×10^{-3}
	$D^{sw}\ (mm^2 s^{-1})$	7.2×10^{-4}	9×10^{-4}	1.18×10^{-3}
	$\kappa(-)$	1	1	1
Temperature	(K)	310	310	310

E = Young's modulus, υ = Poisson's ratio, φ^s = solid volume fraction, FCD=fixed-charge density, k = permeability, D^w = solute diffusion through PBS solution, D^{sw} = solute diffusion through mixture matrix, κ = partition coefficient

A.3 Toward Understanding the Role of Cartilage Particulates in Synovial Inflammation

Amy M. Silverstein, Robert M. Stefani, Evie Sobczak, Eric L. Tong, Mukundan G. Attur, Roshan P. Shah, J. Chloe Bulinski, Gerard A. Ateshian, Clark T. Hung

Osteoarthritis and Cartilage 25 (2017) 1353–1361

Osteoarthritis and Cartilage

Toward understanding the role of cartilage particulates in synovial inflammation

A.M. Silverstein †, R.M. Stefani †, E. Sobczak †, E.L. Tong †, M.G. Attur §, R.P. Shah ||, J.C. Bulinski ¶, G.A. Ateshian † ‡, C.T. Hung † *

† *Department of Biomedical Engineering, Columbia University, New York, NY, USA*
‡ *Department of Mechanical Engineering, Columbia University, New York, NY, USA*
§ *Division of Rheumatology, Department of Medicine, New York University School of Medicine and NYU Langone Medical Center, New York, NY, USA*
|| *Department of Orthopedic Surgery, Columbia University, New York, NY, USA*
¶ *Department of Biological Sciences, Columbia University, New York, NY, USA*

ARTICLE INFO

Article history:
Received 21 October 2016
Accepted 23 March 2017

Keywords:
Synovium
Cartilage
Wear particles
Inflammation

SUMMARY

Objective: Arthroscopy with lavage and synovectomy can remove tissue debris from the joint space and the synovial lining to provide pain relief to patients with osteoarthritis (OA). Here, we developed an *in vitro* model to study the interaction of cartilage wear particles with fibroblast-like synoviocytes (FLS) to better understand the interplay of cartilage particulates with cytokines on cells of the synovium.
Method: In this study sub-10 μm cartilage particles or 1 μm latex particles were co-cultured with FLS ±10 ng/mL interleukin-1α (IL-1α) or tumor necrosis factor-α (TNF-α). Samples were analyzed for DNA, glycosaminoglycan (GAG), and collagen, and media samples were analyzed for media GAG, nitric oxide (NO) and prostaglandin-E2 (PGE2). The nature of the physical interaction between the particles and FLS was determined by microscopy.
Results: Both latex and cartilage particles could be phagocytosed by FLS. Cartilage particles were internalized and attached to the surface of both dense monolayers and individual cells. Co-culture of FLS with cartilage particulates resulted in a significant increase in cell sheet DNA and collagen content as well as NO and PGE2 synthesis compared to control and latex treated groups.
Conclusion: The proliferative response of FLS to cartilage wear particles resulted in an overall increase in extracellular matrix (ECM) content, analogous to the thickening of the synovial lining observed in OA patients. Understanding how cartilage particles interface with the synovium may provide insight into how this interaction contributes to OA progression and may guide the role of lavage and synovectomy for degenerative disease.

Introduction

Tissue wear occurs as the result of articulation between load bearing surfaces[1]. Increased cartilage wear, leading to formation of loose particles in the joint space, has been linked to aging, overuse and obesity[2], often leading to osteoarthritis (OA). Several studies have investigated the use of synovial fluid aspirates to diagnose OA by characterizing cartilage wear particles in the synovial joint[3–5]. Clinically, it has been observed that cartilage and bone debris are bound to the surface or embedded deep within the synovial membrane of patients suffering from capsular synovial hyperplasia and metaplasia[6]. It has been hypothesized that the fibrotic shortening of the synovial capsule and synovitis result in OA-associated pain and contribute to further degradation of cartilage[6,7]. To provide pain relief to patients with OA, surgeons often use arthroscopy with lavage and synovectomy to remove tissue debris from the joint space and the synovium, however its success as a preventative measure has been widely debated[8,9]. Characterizing the interaction between cartilage particulates and the synovium is important for understanding why lavage is successful in some but not all patients;

*Address correspondence and reprint requests to: C.T. Hung, Columbia University, Department of Biomedical Engineering, 1210 Amsterdam Avenue, 351 Engineering Terrace, New York 10027, NY, USA. Fax: 1-212-854-8725.
E-mail addresses: ams2396@columbia.edu (A.M. Silverstein), rms2216@columbia.edu (R.M. Stefani), es3351@columbia.edu (E. Sobczak), elt2128@columbia.edu (E.L. Tong), mukundan.attur@nyumc.org (M.G. Attur), rs3464@cumc.columbia.edu (R.P. Shah), jcb4@biology.columbia.edu (J.C. Bulinski), ateshian@columbia.edu (G.A. Ateshian), cth6@columbia.edu (C.T. Hung).

http://dx.doi.org/10.1016/j.joca.2017.03.015
1063-4584/

it may also explain how increased concentrations of cartilage debris may contribute to the progression of osteoarthritic changes via the synovium. Despite mounting *in vitro* and *in vivo* evidence of the deleterious effects of cartilage particulates on joint health, the mechanisms that mediate their negative interactions with synovial cells remain poorly understood.

In vivo studies have investigated the biological effects of cartilage wear particles on synovial joint health and disease progression in animal models[10–12]. For the latter, animals developed synovitis shortly after joint injection with particulates, which persisted and was accompanied by the infiltration of mononuclear cells and capsular, fibrotic thickening of the synovium[10]. Notably, the injected particles were still present and embedded within the synovium months later[10,11].

Monolayer cell and particulate co-cultures have previously been used to study the effects of biologic and synthetic particles on cells. While the most common method of determining particle-induced effects is to apply a specific number of particles per cell[13–15], measuring particulate mass per number of cells is also commonly used[16,17]. Adding wear particles of any material to cells can change cellular viability, metabolic activity, function and expression of OA specific markers. Specifically, treatment of human fibroblast-like synoviocytes (FLS) or chondrocytes with cartilage particles results in increased proteinase activity[16] and tumor necrosis factor-α (TNF-α) gene expression[17]. Lacking the availability of techniques to measure precisely the number or size of particles being used for treatment, previous studies examined biologic wear particles by mass, with an undefined size distribution. As such, it has been difficult to determine if the mechanism involved in driving the response of FLS to cartilage particulates is mediated by phagocytosis, cell surface contact or a combination of both.

Studies typically use synthetic particles that are 0.2–7 μm in size[13–15,18,19], as particles <15 μm in diameter, are readily phagocytosed by chondrocytes, macrophages, FLS and mesenchymal stem cells (MSCs)[20,21]. Compared to these non-biologic (metal or plastic) wear particles, biologic (cartilage) wear particles are more complex to study because they are composed of extracellular matrix (ECM) proteins that can be phagocytosed or degraded by, or bound to cells. This study aims to better understand the interplay of cartilage particulates with cytokines on cells of the synovium to foster the development of effective strategies to mitigate the inflammatory effect of cartilage particulates in OA.

Methods

Experimental design

Three studies are discussed in this paper (outlined in Fig. 1). Study 1 optimized the treatment dosage of sub-10 μm cartilage or 1 μm latex particles. Particle concentrations up to 1000 particles per cell were cultured for 5 days with confluent FLS monolayers to determine a dose that would elicit a cellular response without compromising cell viability ($n = 3–4$/group). The lowest particle dose that resulted in significantly altered metabolic activity, as determined by the MTT (3-(4,5-Dimethylthiazol-2-yl)-2,5-Diphenyltetrazolium Bromide) assay, while preserving cell viability, was selected for subsequent experiments. A dosage of 250 particles per cell was selected for future experimentation for both latex and cartilage particles.

In study 2, cells were co-cultured for 5 days with ±250 cartilage particles (CART) per cell in the presence or absence of 10 ng/mL of interleukin-1α (IL-1α, Life Technologies, Carlsbad, CA) or TNF-α (Life Technologies) ($n = 6–8$/group). These concentrations are previously established for studies of cytokine effects on joint tissues[22–24]. FLS were also cultured ±250 latex particles per cell to establish a baseline non-biologic particle response. In study 3, designated donor cultures were maintained in media in the presence (FLS + CART) or absence (FLS only) of 250 cartilage particles per cell for 5 days. In parallel, cell-free cultures with (CART only) or without particles (media only) were maintained for 5 days under the same conditions. Conditioned media was removed from the four donor culture groups (media only, CART only, FLS only, FLS + CART), and particles were removed via filtration with a 0.22 μm filter in the particle groups. This conditioned media was split with fresh growth media and added to the recipient FLS monolayers for 5 days ($n = 5–8$/group).

Isolation and culture of FLS and cartilage explants

Synovial tissue was harvested from three freshly slaughtered juvenile bovine knee joints (2–4 weeks old) and digested in collagenase type II (Worthington Biochemical Corporation, Lakewood, NJ) for 2 h with stirring at 37°C. Digested cells (FLS) were filtered through a 70 μm porous nylon mesh. Viable cells were counted and plated at a density of 1.76×10^3 cells/cm^2. To obtain a pure cell population, FLS were expanded for two passages in α-Minimal Essential Medium (α-MEM, Life Technologies) containing 10% fetal bovine serum (FBS), 1% antibiotic-antimycotic and bFGF-2 (Life Technologies)[25,26]. Articular cartilage explants were cored using a disposable biopsy punch (10 mm diameter, Acuderm® Inc., Fort Lauderdale, FL) and cultured in cartilage explant media[27] supplemented with 1% antibiotic-antimycotic, 1% non-essential amino acids (Sigma–Aldrich, St. Louis, MO), 1 mg/mL bovine serum albumin (BSA), 50 μg/mL ascorbic acid (Sigma–Aldrich), 0.01 μg/mL hydrocortisone (Sigma–Aldrich) and 0.002 μg/mL insulin (BD Biosciences, San Jose, CA) until use.

Creation and characterization of in vitro synovium model

Confluent FLS were trypsinized, counted, re-suspended and plated at a density of 50×10^4 cells/cm^2 in α-MEM (10% FBS, 1% antibiotic–antimycotic) supplemented with 50 μg/mL ascorbic acid to allow the formation of a dense cell monolayer. After 5 days, confluent monolayers were fixed in 4% paraformaldehyde (PFA, Sigma–Aldrich) overnight at 4°C before being washed in phosphate buffered saline (PBS, Life Technologies). Cell monolayers were stained to determine the presence of Type I collagen (rabbit polyclonal anti-collagen I, Abcam, Cambridge, MA), lubricin (rabbit polyclonal anti-lubricin, Abcam) and DNA (4′,6-Diamidino-2-Phenylindole, Dihydrochloride, DAPI, Life Technologies).

Particulate preparation and characterization of particles

Cartilage particles were generated aseptically from the superficial and middle zones by manually abrading cartilage submerged in phosphate buffered saline (PBS) with waterproof 120 grit sandpaper (McMaster-Carr, Elmhurst, IL). Potential residual sandpaper particulates were removed gravimetrically and via sub-sequent filtration, as was confirmed through microscopic inspection of the particulate solution. The resulting cartilage particle solution was sequentially filtered with 70 μm, 40 μm, and 10 μm porous nylon mesh filters to achieve a sub-10 μm particulate size. An aliquot of either cartilage particles or 1 μm latex particulates (Sigma–Aldrich) was further diluted in PBS, counted and sized using a Multisizer 4 Coulter Counter (Beckman Coulter, Brea, CA) to determine the concentration of both the cartilage particulate and latex particle solutions[28]. An average of four aliquots was used to determine the particle concentration of the stock solutions and the average

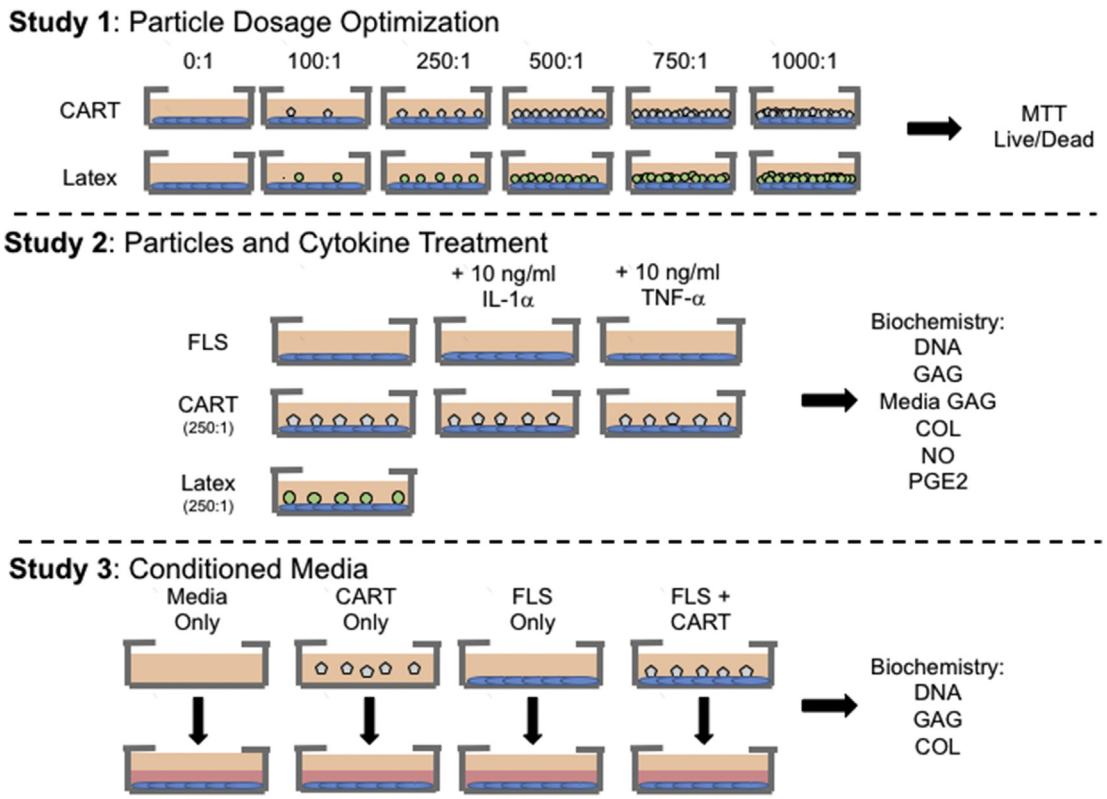

Fig. 1. Schematic of the experimental study design. In study 1, FLS were cultured for 5 days with increasing concentrations of latex or cartilage particulates (up to 1000:1 particles:cells). In study 2, FLS were cultured for 5 days in the presence or absence of 250 latex or cartilage particles per cell and 10 ng/mL IL-1α or TNF-α. In study 3, FLS were cultured in the presence (FLS + CART) or absence (FLS) of 250 cartilage wear particles (CART) per cell for 5 days. Concurrently, media alone (media only) and particles alone (CART only) were also cultured. Conditioned media from each donor group was combined with fresh media and added to recipient cultures for 5 days.

particulate size. Toxicity of sandpaper exposure to the cartilage surface was evaluated by co-culturing suspended pieces of 120 grit sandpaper with passage 2 FLS plated at a density of 50×10^4 cells/cm^2 in α-MEM (10% FBS, 1% antibiotic-antimycotic) supplemented with 50 μg/mL ascorbic acid. Viability and metabolic activity were assessed after 30 min, 60 min and 24 h using the LIVE/DEAD Viability/Cytotoxicity kit (Life Technologies) and MTT assay (Sigma–Aldrich)[29]. Cell monolayers were incubated for 4 h with 0.5 mg/mL MTT in growth media. The media was replaced and the dye was solubilized in a 1:1 solution of isopropanol and dimethyl sulfoxide.

Microscope analysis of cell-particle interactions

To better characterize the interactions between latex and cartilage particles, cartilage particulates were labeled with 20 μM dichlorotriazinylaminofluorescein (DTAF, Sigma–Aldrich)[28]. FLS were plated at either a low or high density overnight before treatment with 250 fluorescently labeled cartilage particles, green-yellow or unlabeled latex beads (Sigma–Aldrich) per cell for 2 days on glass coverslips. Prior to imaging, synovial cells were stained with CellTrace™ Calcein Red-Orange AM (Life Technologies) to identify if particles were internalized or in contact with the cell surface. Alternatively, cells were cultured and fixed in 4% PFA overnight, permeabilized with 0.1% Triton X (Sigma–Aldrich) and washed with PBS. After blocking with 1% BSA in PBS, cells were stained with TRITC-conjugated Phalloidin (EMD Millipore, Billerica, MA) and counterstained with DAPI. Z-stack images were taken and reconstructed using a Zeiss LSM700 Confocal microscope (Zeiss, Oberkochen, Germany). For actin-DAPI stained images with latex particles, non-fluorescent latex beads were used to eliminate the effects of channel bleed-through. For quantification of cell-particle interactions and spatial characterization, three blinded reviewers each counted 170 cells and 108 cells cultured with cartilage and latex particles, respectively.

Biochemistry

Confluent cell sheets and media samples were frozen at −20°C until use. Frozen monolayers and cartilage particulates were lyophilized prior to digestion for 16 h at 56°C in 0.5 mg/mL of proteinase K (MP Biomedicals, Santa Ana, CA) in 50 mM Tris buffered saline containing 1 mM EDTA, 1 mM iodoacetamide and 10 μg/mL pepstatin A (Sigma–Aldrich)[30]. Samples were analyzed using the Picogreen (Life Technologies), 1,9 dimethylmethylene blue (DMMB, Sigma–Aldrich) dye-binding[31], and orthohydroxproline (OHP) assays to determine DNA, glycosaminoglycan (GAG) and collagen content using, respectively. For the OHP assay, the proteinase K digested sample was hydrolyzed with 12 N HCl at 110°C for 16 h and dried before re-suspension in assay buffer. OHP content was determined after reacting chloramine T with dimethylaminobenzaldehyde (Sigma–Aldrich) and quantified using a 1:7.64 OHP-to-collagen mass ratio[32]. GAG content in the media was analyzed using the DMMB assay and normalized by DNA. Nitric oxide (NO) and prostaglandin-E2 (PGE2) released into the media was determined using the Greiss Reagent Kit for nitrite quantification (Life Technologies) and the PGE2 Parameter Assay Kit (R&D Systems Inc., Minneapolis, MN), respectively. Biochemical content or media product concentrations of particles alone were subtracted from the measured values of the resulting

synovial sheet with particles to determine the contribution of treated FLS alone.

Statistical analysis

Data sets were tested for normality and homogeneity using the Kolmogorov–Smirnov Test and Levene's test, respectively. Non-normal and non-homogeneous data were adjusted using a log transformation prior to analysis. For MTT dosage studies and conditioned media studies, a one-way analysis of variance (ANOVA) with Tukey's post-hoc test was performed. For cartilage biochemical analyses, a two-way ANOVA with Tukey's post-hoc tests with main factors set to cytokine and particle treatment was utilized. For latex biochemical analyses, student's unpaired *t*-test with unequal variances was used. Statistical analyses were performed in Statistica (Statsoft, Tulsa, OK) and R version 3.3.2 with $\alpha = 0.05$. Each data point represents the mean and 95% confidence interval.

Results

Characterization of FLS synovium culture

After 5 days, FLS organized into a multi-layer cell sheet that stained positive for collagen type I and lubricin (Fig. 2). Collagen I staining indicated the synthesis of a dense fibrous network whereas lubricin staining was primarily co-localized intracellularly.

Optimization of particle treatment dose

Latex and cartilage particles had average diameters of 1.05 ± 0.0002 μm and 0.85 ± 0.002 μm, respectively. Exposure to sandpaper up to 60 min had no toxic effects on the FLS as determined by viability or metabolic activity (not shown). To identify an effective treatment dose of cartilage particles, dense monolayers were co-cultured with up to 1000 particles per cell (Fig. 3). Increasing the dose of cartilage particles had no effect on cellular viability, as confirmed by increasing metabolic activity observed in the MTT assay. Metabolic activity significantly increased compared to controls for all doses ≥250 particles per cell ($P = 0.002$; 250:1 vs 0:1 particles per cell, Fig. 3(A)). Thus, a dosage of 250 particles per cell was chosen for future experimentation, as it was the lowest dose that increased metabolic activity without compromising viability.

Only a dose of 1000 latex particles per cell resulted in significantly decreased metabolic activity and viability ($P = 0.003$) compared to no-particle controls [Fig. 3(B)]. 250 latex particles per cell resulted in a significant increase in metabolic activity ($P = 0.04$; vs 0:1 particles:cells, Fig. 3(B)), while maintaining cell viability. Thus, 250:1 particles:cell was chosen for subsequent experiments. For both latex and cartilage particles, 250 particles per cell comprised a dose that was <0.002%v/v.

Characterization of the interaction between particles and synovium

Both latex and cartilage particles were phagocytosed by FLS [Figs. 4, 6(A) and 6(B)]. Latex particles were readily phagocytosed by FLS (73 ± 7%), with 5–20 particles internalized per cell [Fig. 6(A)]. Meanwhile, cartilage particles were selectively phagocytosed by FLS, with positive cells only internalizing 1–5 particles [Fig. 4(A) and (B)]. Z-stack reconstructions revealed two potential mechanisms of action: cartilage particle internalization or attachment to the surface of both dense monolayers and individual cells (Fig. 4). 79 ± 7% of FLS were associated with a particle (either phagocytosis or surface contact). Of these, 72 ± 11% of cells had cartilage particles within their cell boundaries (i.e., as a result of phagocytosis) while 32 ± 5% of the cells had cartilage particles in contact with the surface. 24 ± 5% of the cells had particles both within the cell boundary and in contact with the cell. Actin cytoskeleton staining revealed nuclear (internal) and cortical (external) remodeling of the actin cytoskeleton around cartilage particles [Fig. 4(C) and (D)], compared to only nuclear (internal) remodeling of latex particulates [Fig. 6(B)].

Effect of cytokines and cartilage or latex particles

Exposure to IL-1α or TNF-α had no effect on FLS proliferation ($P = 0.56$, Fig. 5(A)), however, cytokines modulated the total ECM composition of the FLS sheets as well as the release of ECM components and inflammatory markers to the media. Cytokine treatment had a significant effect on GAG ($P < 0.00001$) and collagen synthesis ($P < 0.00001$). TNF-α treatment resulted in a decrease in GAG content ($P = 0.003$, Fig. 5(B)), while both IL-1α ($P < 0.00001$) and TNF-α ($P < 0.00001$) resulted in a significant decrease in collagen content compared to non-cytokine controls [Fig. 5(C)]. Overall, cytokine treatment resulted in a significant increase in media GAG ($P < 0.00001$), NO ($P < 0.00001$), and PGE2 ($P < 0.00001$) when normalized by DNA content [Fig. 5(D–F)]. IL-1α had the greatest impact on PGE2 synthesis ($P = 0.0001$; vs no cytokine control), while TNF-α had the greatest effect on NO synthesis ($P = 0.0001$; vs no cytokine control). Total GAG synthesis (sum of FLS GAG + media GAG) was increased in IL-1α ($P = 0.0003$; vs no cytokine control) and TNF-α stimulated cultures ($P = 0.0003$; vs no cytokine control).

Co-culture of FLS with cartilage particulates resulted in a significant increase in DNA content of the cell sheet ($P < 0.00001$, Fig. 5(A)). The DNA content of the cartilage particles themselves constituted <1% that of the DNA of the cell monolayer (not shown). Treatment with cytokines did not have an interactive effect on the

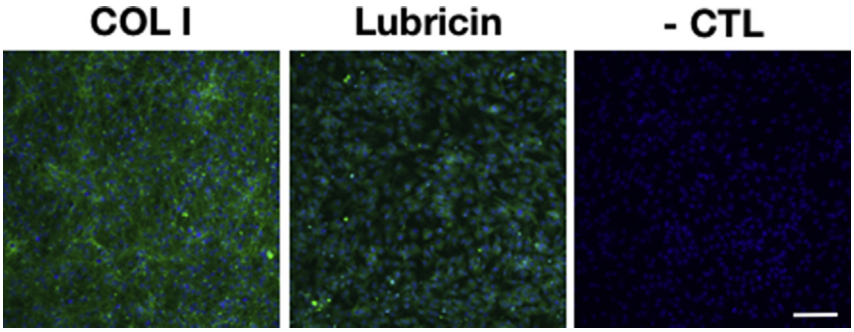

Fig. 2. Collagen I (green, A) and lubricin (green, B) vs negative (C) staining of a FLS cells sheet model of synovium. DAPI staining appears blue. Scale bar = 100 μm.

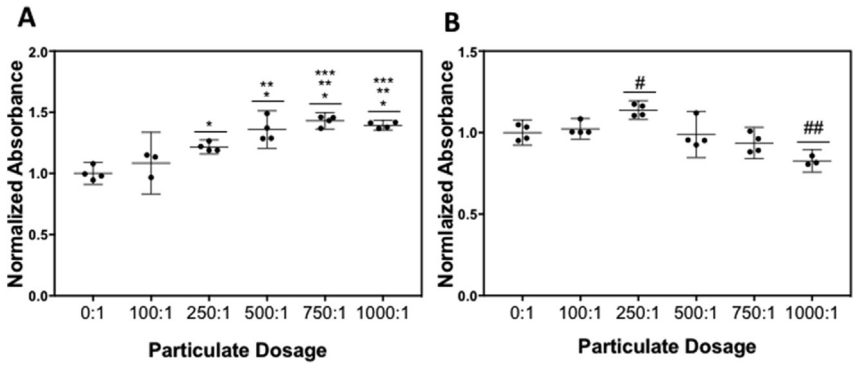

Fig. 3. MTT assay for assessing the effect of increasing concentrations of cartilage (A) and latex (B) particles on cellular metabolic activity. Data presented as mean and 95% confidence interval. $^{*}P < 0.05$ vs control (0:1 particles:cell), $^{**}P < 0.05$ vs 100:1 cartilage particles:cell, $^{***}P < 0.05$ vs 250:1 cartilage particles:cell. #$P < 0.05$ vs control 0:1, 500:1, 750:1 and 1000:1 latex particles:cells, ##$P < 0.05$ vs 0:1, 100:1, 250:1, and 500:1 latex particles:cells.

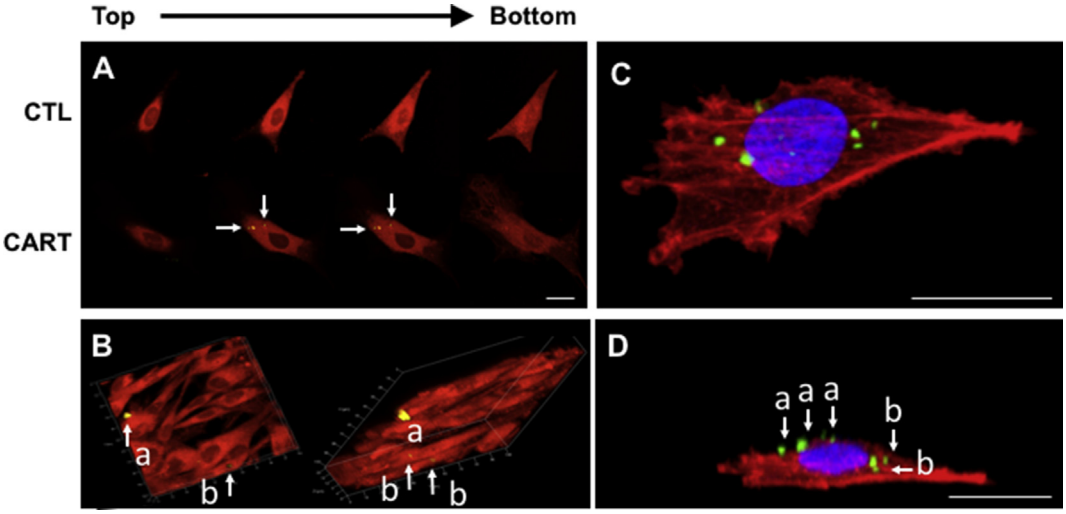

Fig. 4. (A) Z-stacks of a synovial cell (red) cultured without (CTL) and with (CART) cartilage wear particles (yellow/green). (B) 3D reconstruction. Top (C) and side (D) views of the 3D reconstructions of actin staining from the cartilage particles are found on the cell surface (a) and internalized by the cells (b). Particles indicated by white arrows. Scale bar = 20 μm.

proliferative behavior of FLS treated with cartilage particles ($P = 0.46$, Fig. 5(A)). In the absence of cytokine insult, co-culture with cartilage particles had no effect on GAG content ($P = 0.09$, Fig. 5(B)) and resulted in a significant change collagen content ($P < 0.00001$, Fig. 5(C)) of the cell sheet. Cartilage particles and cytokines together significantly reduced the GAG ($P = 0.01$) and collagen content ($P = 0.02$).

Overall, GAG content in the media was modulated by cytokines and particles together ($P < 0.00001$, Fig. 5(D)). NO levels were elevated as a result of cartilage particle ($P = 0.00003$) and cytokine ($P < 0.00001$) treatments, as well as the combined cartilage particle and cytokine treatment ($P = 0.003$). Cell sheets treated with TNF-α had NO levels equivalent to their cartilage particle treated counterparts ($P = 0.83$, Fig. 5(E)). Lastly, cartilage particle treatment had an effect on the release of PGE2 compared to control cells ($P < 0.00001$). Cytokine and cartilage particles together also resulted in a significant increase in PGE2 media concentrations compared to non-treated controls ($P < 0.00001$, Fig. 5(F)).

Treatment with latex particles alone had no effect on FLS proliferation ($P = 0.37$, Fig. 6(C)). Co-culture with latex particles resulted in a decrease in the overall collagen synthesis by FLS ($P < 0.00001$, Fig. 6(D)). NO synthesis was not altered by culture with latex particles ($P = 0.39$, Fig. 6(E)). PGE2 was detectable only in latex particle treated samples, after pooling. No PGE2 was detected in control samples compared to 27.6 ± 42.4 pg of PGE2/μg of DNA in latex treated samples ($P = 0.11$).

Conditioned media study

FLS treated with Media only and CART only conditioned media proliferated to a greater extent than FLS treated with FLS only conditioned media ($P = 0.0005$) and FLS + CART conditioned media ($P = 0.01$, Fig. 7(A)), respectively. No differences were observed between media only and CART + media groups ($P = 0.90$) and FLS + media only and CART + media + FLS ($P = 0.70$, Fig. 7(A)). No differences were detected in GAG synthesis ($P = 0.17$, Fig. 7(B)) and collagen synthesis across all groups ($P = 0.20$, Fig. 7(C)). As such, the response of FLS to cartilage particles appears to require particulate surface binding and/or phagocytosis.

Discussion

Previous research has identified the deleterious effects of cartilage wear particles on FLS and suggested that they play an important role in the pathogenesis of OA and degenerative joint changes[16]. Here, we adopted FLS monolayer cultures as a two-dimensional synovium model to further characterize the interaction of cartilage particles with FLS. The *in vitro* FLS system was

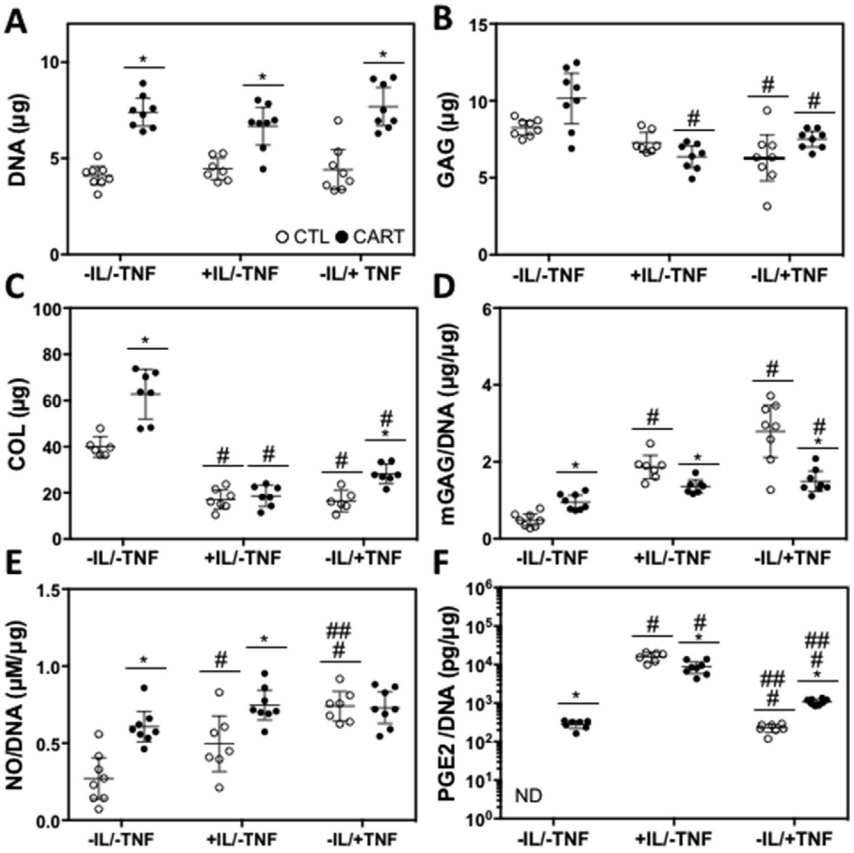

Fig. 5. Analysis of FLS cells sheets cultured ± IL-1α or TNF-α and ± cartilage wear particles (CART). The DNA, ECM synthesis and media NO and PGE2 of the particles alone was subtracted from the total to determine the final values. DNA (A), FLS cell sheet GAG (B), FLS cell sheet collagen (COL) (C), media GAG/DNA (D), media NO/DNA (E) and media PGE2/DNA (F). Data presented as mean and 95% confidence interval. ND = not detected. *$P < 0.05$ vs non-particle treated control (CTL) with same cytokine treatment. #$P < 0.05$ vs −IL/−TNF, ##$P < 0.05$ vs +IL/−TNF within CTL or CART treated samples respectively.

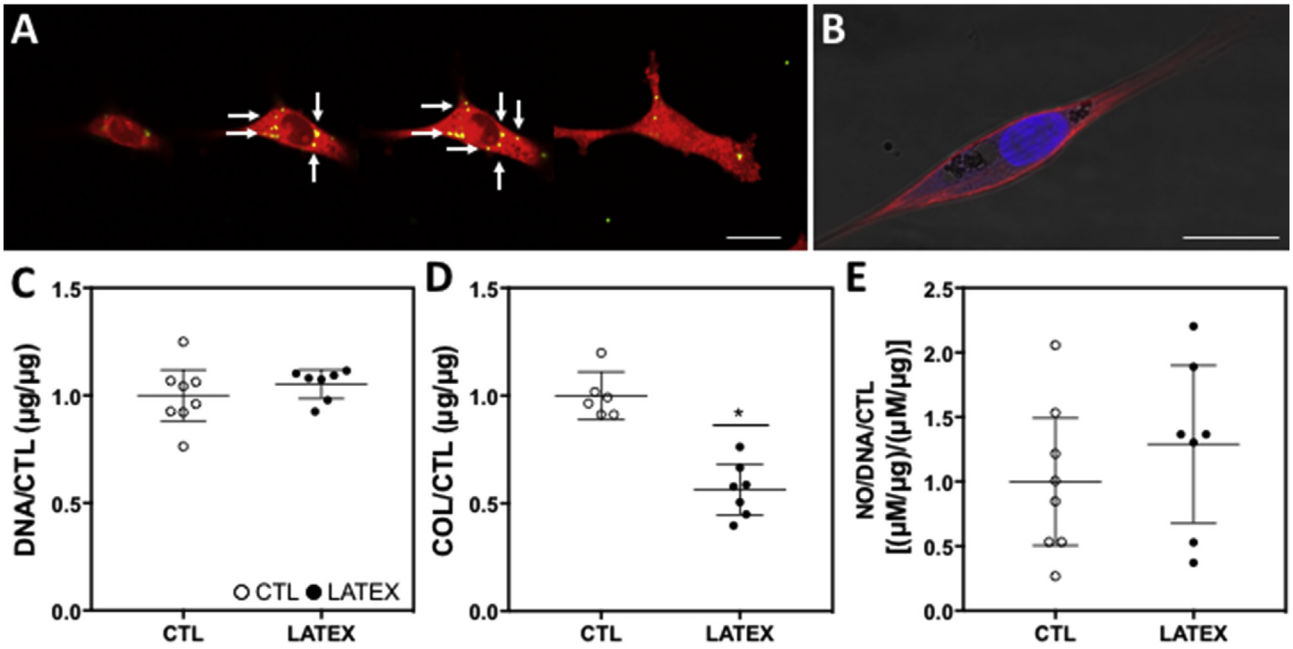

Fig. 6. (A) Z-stacks of a synovial cell (red) cultured with latex wear particles (yellow). (B) Actin (red)-DAPI (blue) staining showing remodeling of the cytoskeleton around the ingested latex beads. Scale bar = 20 μm. Analysis of FLS cell sheets cultured ± latex particles for DNA (C), FLS cell sheet COL (D) and media NO/DNA (E), all normalized by corresponding control (CTL) values. Data presented as mean and 95% confidence interval. *$P < 0.05$ vs non-particle treated control (CTL).

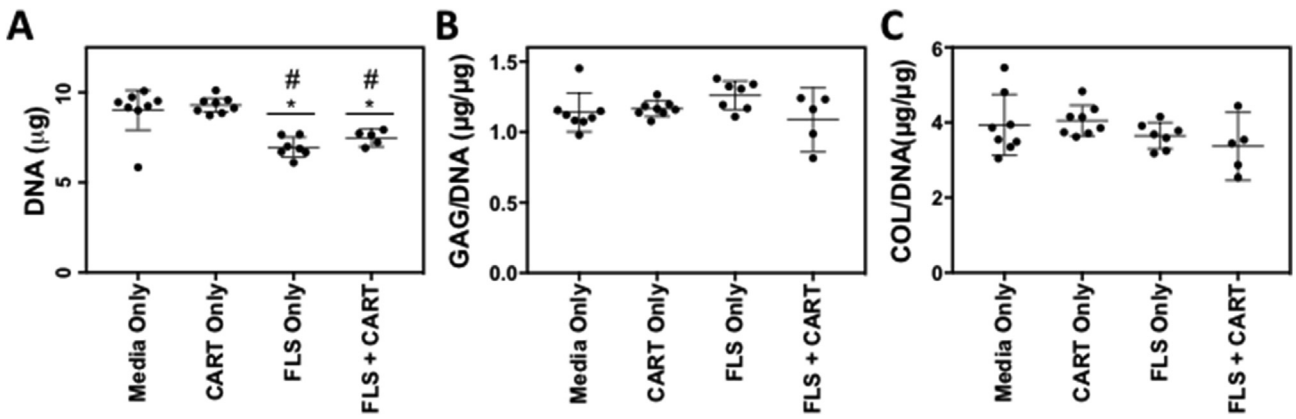

Fig. 7. DNA (A), FLS cell sheet GAG/DNA (B), and COL/DNA (C) for the conditioned media experiment. Data presented as mean and 95% confidence interval. *$P < 0.05$ vs Media only. #$P < 0.05$ vs CART only.

comprised of a dense cell sheet that was a few cells thick and positively expressed both collagen I and lubricin, similar to the native synovial lining[33–35]. The results of this study demonstrate the inflammatory response of FLS to sub-10 μm cartilage particles cartilage debris *in vitro* and evaluates two potential mechanisms of action: phagocytosis and surface contact.

The particulate doses (up to 1000:1 particles per cell) examined and used in this study may be compared to the range of values used for previous wear particles studies on various adult cell types involving cartilage[16], latex[19], polyethylene[15,18] and titanium[14,19,36] that quantified dose in terms of weight/cell[16,17], volume percentage[14,18,36] and particles per cell[13,19]. Similar to other non-biologic particles such as titanium, the viability of the synovial sheet cultures was decreased by increasing concentrations of latex particles[14].

Microscopy confirmed that sub-10 μm cartilage particles interact with FLS through both phagocytosis and surface contact. Both latex control and cartilage particles showed re-arrangement of the actin cytoskeleton around the wear particulate [Figs. 4(C,D) and 6(B)], as has been previously observed for osteoprogenitors and MSCs[14,19] treated with titanium particles. Here, we observed a remodeling of the actin cytoskeleton at the surface to form a U-shaped organization at the cell-cartilage particulate contact site [Fig. 4(D)].

Treatment of the synovium model with IL-1α and TNF-α, commonly utilized cytokines for *in vitro* modeling of OA[37], modulated ECM composition and increased secretion of inflammatory factors. Specifically, FLS treated with cytokines demonstrated a marked drop in cell sheet collagen content and increased media concentrations of NO and PGE2, indicative of an inflammatory response. Previous research on the effect of human FLS cells has shown that inflammatory cytokines increase cell proliferation, perhaps explaining the thickening of the synovial capsule observed in OA-associated synovitis[23,38,39]. The previously observed proliferative stimulus provided by these pro-inflammatory cytokines may have inhibited by the presence of growth factors in FBS used to supplement the culture media in the present study[40,41]. Cytokine stimulated FLS have been shown to produce a number of inflammatory factors involved in OA and RA, including IL-6, IL-8, NO, and PGE2[23,38,39,42] that can lead to matrix degradation, as observed here. PGE2 is known to activate MMP expression leading to cartilage degeneration[43], reinforcing the role of the synovium in continued cartilage matrix degradation.

Co-culture of FLS with cartilage particles resulted in proliferation of FLS that was not further modulated by the addition of inflammatory cytokines [Fig. 5(A)]. Moreover, exposure to cartilage particles alone resulted in increased production of key inflammatory factors (i.e., NO, PGE2) and thickening of the cell sheet through increased collagen content [Fig. 5(B) and (C)]. These *in vitro* findings confirm the results of previous animal model studies showing that cartilage particles alone can lead to synovitis and increased capsular thickening[10,11]. Supplementation of cartilage particle treated FLS cell sheets with inflammatory cytokines did differentially modulate the ECM composition, suggesting that the response of cartilage wear particles may have differing effects on synovial tissue health and cartilage degradation in late stage OA when cytokine levels are significantly upregulated.

Cells with media only and particle conditioned media proliferated greater than cells treated with FLS or FLS + Particle conditioned media, likely due to the depletion of nutrients in cell conditioned media. Conditioned media studies with media from cartilage particles alone and cartilage particle treated cells showed that the particles themselves are not leaching factors driving the rapid proliferative or inflammatory response of treated fibroblasts. Accordingly, contact is required for the mechanisms of action to have an impact on cellular response. Cartilage is composed primarily of type II collagen and proteoglycan[44], thus particulate binding to FLS surface receptors via integrins has the potential to activate a number of pathways and increase expression of matrix metalloproteinases[45]. Numerous studies have looked at cellular activation through ECM binding to FLS integrins[46] using ECM (collagen, fibronectin, etc.)-coated beads. These studies have shown that integrin engagement through collagen binding increases cellular proliferation and decreases collagenase synthesis. These results support the outcomes reported here for cartilage particle treatment (Fig. 5). Further, treatment of activated cells with TNF-α was able to increase collagenase synthesis[46], observed via treatment of FLS with cartilage particles and TNF-α (Fig. 5).

The change in ECM composition and release of products into the media of FLS co-cultured with latex particles was used as a non-biologic control to isolate the effects of phagocytosis alone on the observed responses. Latex particles did not affect the proliferation of particle treated FLS, as has been shown previously in FLS[47] and MSCs[19]. Latex particulates did induce decreased synthesis of collagen. Previous studies on the effects of sub-15 μm latex particulates in rabbits have shown increased synthesis of collagenase and neutral proteinases[20,47]. These studies have also shown that cells in the same culture as cells that have phagocytosed latex particulates also synthesize greater concentrations of collagenase, suggesting that phagocytosis results in the release of an active stimulatory factor.

Cartilage particles induced more proliferation and inflammation than latex particles alone, illustrating the importance of both cell

surface contact and presumably activation of integrins in the response of FLS to cartilage particles. Phagocytosis, cell surface binding and actin reorganization together may affect how FLS synthesize other molecules beyond the ECM proteins or inflammatory factors studied here in response to physical stimuli presented to FLS in the synovial joint environment (e.g., fluid shear or mechanical stretch)[48–50].

The work presented here provides a platform to study how the synovium responds to cartilage wear particulates *in vivo*. Targeting the interaction of cartilage particles by phagocytosis or surface binding may provide a means to slow the onset and progression of OA by mitigating the deleterious effects of cartilage particle-mediated synovitis. Future work will further investigate the exact mechanisms (e.g., integrin activation) responsible for rapid FLS proliferation and determine how cellular activation by cartilage wear particles influences cell–cell communication[47]. These insights may guide the optimization of arthroscopic lavage and debridement techniques to better address joint pain and inflammation[7–9].

Authors' contributions

All authors contributed significantly to the work reported in this manuscript. AMS and CTH designed the experiments. AMS, RMS, ES, and ETT carried out the experiments and collected the data. MGA, RPS, JCB and GAA and CTH supervised and advised the work. AMS, MGA, RPS, JCB, GAA, and CTH wrote the paper. All authors have read and approved the final submitted manuscript.

Conflict of interest statement

None of authors had a financial or personal relationship with organizations that could influence the work presented in this manuscript.

Role of the funding sources

The funding sources detailed in the acknowledgement had no role in the study design, data collection, data analysis or in the preparation and submission of the manuscript.

Acknowledgements

The authors would like to thank Raphael Gerraty for assistance with statistical analysis. Research reported in this publication was supported by NIAMS, NCRR, and NIBIB of the National Institutes of Health under Award Numbers AR060361, AR059038, AR043628, 1S10RR027943, and 5P41EB002520. The content is solely the responsibility of the authors and does not necessarily represent the official views of the National Institutes of Health.

References

1. Jay GD, Torres JR, Rhee DK, Helminen HJ, Hytinnen MM, Cha C-J, *et al*. Association between friction and wear in diarthrodial joints lacking lubricin. Arthritis Rheum 2007:3662–9.
2. Griffin TM, Guilak F. The role of mechanical loading in the onset and progression of osteoarthritis. Exerc Sport Sci Rev 2005;33:195–200.
3. Kuster MS, Podsiadlo P, Stachowiak GW. Shape of wear particles found in the human knee joint and their relationship to osteoarthritis. Rheumatology 1998:978–84.
4. Hakshur K, Benhar I, Bar-Ziv Y, Halperin N, Segal D, Eliaz N. The effect of hyaluronan injections into human knees on the number of bone and cartilage wear particles captured by bioferrography. Acta Biomater 2011:848–57.
5. Evans CH, Mears DC, Mcknight JL. A preliminary ferrographic survey of the wear particles in human synovial fluid. Arthritis Rheum 1981:912–8.
6. Lloyd-Roberts GC. The role of capsular changes in osteoarthritis of the hip joint. J Bone Joint Surg Br 1953;35-B:627–42.
7. Attur M, Samuels J, Krasnokutsky S, Abramson SB. Targeting the synovial tissue for treating osteoarthritis (OA): where is the evidence? Best Pract Res Clin Rheumatol 2010:71–9.
8. Felson DT. Arthroscopy as a treatment for knee osteoarthritis. Best Pract Res Clin Rheumatol 2010;24:47–50.
9. Pitta M, Davis 3rd W, Argintar EH. Arthroscopic management of osteoarthritis. J Am Acad Orthop Surg 2016;24:74–82.
10. Evans CH, Mazzocchi RA, Nelson DD, Rubash HE. Experimental arthritis induced by intraarticular injection of allogenic cartilaginous particles into rabbit knees. Arthritis Rheum 1984:200–7.
11. Chrisman OD, Fessel JM, Southwick WO. Experimental production of synovitis and marginal articular exostoses in the knee joints of dogs. Yale J Biol Med 1965;37:409–12.
12. Hurtig MB. Use of autogenous cartilage particles to create a model of naturally occurring degenerative joint disease in the horse. Equine Vet J Suppl 1988:19–22.
13. Chang C-H, Fang H-W, Ho Y-C, Huang H-T. Chondrocyte acting as phagocyte to internalize polyethylene wear particles and leads to the elevations of osteoarthritis associated NO and PGE2. Biochem Biophys Res Commun 2008:884–8.
14. Haleem-Smith H, Argintar E, Bush C, Hampton D, Postma WF, Chen FH, *et al*. Biological responses of human mesenchymal stem cells to titanium wear debris particles. J Orthop Res 2011:853–63.
15. Park DY, Min B-H, Kim D-W, Song BR, Kim M, Kim YJ. Polyethylene wear particles play a role in development of osteoarthritis via detrimental effects on cartilage, meniscus, and synovium. Osteoarthritis Cartilage 2013:2021–9.
16. Evans CH, Mears DC, Cosgrove JL. Release of neutral proteinases from mononuclear phagocytes and synovial cells in response to cartilaginous wear particles in vitro. Biochim Biophys Acta 1981:287–94.
17. Cameron-Donaldson M, Holland C, Hungerford DS, Frondoza CG. Cartilage debris increases the expression of chondrodestructive tumor necrosis factor-alpha by articular chondrocytes. Arthroscopy 2004:1040–3.
18. Chiu R, Ma T, Smith RL, Goodman SB. Ultrahigh molecular weight polyethylene wear debris inhibits osteoprogenitor proliferation and differentiation in vitro. J Biomed Mater Res 2008:242–7.
19. Okafor CC, Haleem-Smith H, Laqueriere P, Manner PA, Tuan RS. Particulate endocytosis mediates biological responses of human mesenchymal stem cells to titanium wear debris. J Orthop Res 2006:461–73.
20. Greis PE, Georgescu HI, Fu FH, Evans CH. Particle-induced synthesis of collagenase by synovial fibroblasts: an immunocytochemical study. J Orthop Res 1994;12:286–93.
21. Olson EJ, Kang JD, Fu FH, Georgescu HI, Mason GC, Evans CH. The biochemical and histological effects of artificial ligament wear particles: in vitro and in vivo studies. Am J Sports Med 1988;16:558–70.
22. Lima EG, Tan AR, Tai T, Bian L, Stoker AM, Ateshian GA, *et al*. Differences in interleukin-1 response between engineered and native cartilage. Tissue Eng Part A 2008:1721–30.
23. Gitter BD, Labus JM, Lees SL, Scheetz ME. Characteristics of human synovial fibroblast activation by IL-1 beta and TNF alpha. Immunology 1989;66:196–200.
24. Mohanraj B, Hou C, Meloni GR, Cosgrove BD, Dodge GR, mauck RL. A high throughput mechanical screening device for cartilage tissue engineering. J Biomech 2013:2130–6.

25. Sampat SR, O'Connell G, Fong JV, Alegre-Aguaron E, Ateshian GA, Hung CT. Growth factor priming of synovium derived stem cells for cartilage tissue engineering. Tissue Eng Part A 2011;17:2259–65.
26. Tan A, Alegre-Aguaron E, O'Connell G, VandenBerg C, Aaron R, Vunjak-Novakovic G, *et al*. Passage-dependent relationship between mesenchymal stem cell mobilization and chondrogenic potential. Osteoarthritis Cartilage 2014:319–27.
27. Albro MB, Durney KM, Shim JJ, Singh A, Cigan AD, Nims RJ, *et al*. Synovial fluid and physiologic levels of cortisol, insulin, and glucose in media maintain the homeostasis of immature bovine cartilage explants over long term culture. In: 2014 Annual Meeting of the Orthopaedic Research Society. New Orleans, LA 2014:1304.
28. Oungoulian SR, Chang S, Bortz O, Hehir KE, Zhu K, Willis CE, *et al*. Articular cartilage wear characterization with a particle sizing and counting analyzer. J Biomech Eng 2013;135. 024501-1-4.
29. Kupcsik L. Estimation of cell number based on metabolic activity: the MTT reduction assay. Methods Mol Biol 2011;740:13–9.
30. Riesle J, Hollander AP, Langer R, Freed LE, Vunjak-Novakovic G. Collagen in tissue-engineered cartilage: types, structure, and crosslinks. J Cell Biochem 1998;71:313–27.
31. Farndale RW, Buttle DJ, Barrett AJ. Improved quantitation and discrimination of sulphated glycosaminoglycans by use of dimethylmethylene blue. Biochim Biophys Acta 1986:173–7.
32. Hollander AP, Heathfield TF, Webber C, Iwata Y, Bourne R, Rorabeck C, *et al*. Increased damage to type II collagen in osteoarthritic articular cartilage detected by a new immunoassay. J Clin Invest 1994;93:1722–32.
33. Smith MD. The normal synovium. Open Rheumatol J 2011;5: 100–6.
34. Kiener HP, Watts GF, Cui Y, Wright J, Thornhill TS, Sköld M, *et al*. Synovial fibroblasts self-direct multicellular lining architecture and synthetic function in three-dimensional organ culture. Arthritis Rheum 2010:742–52.
35. Ashhurst DE, Bland YS, Levick JR. An immunohistochemical study of the collagens of rabbit synovial interstitium. J Rheumatol 1991;18:1669–72.
36. Seo SW, Lee D, Cho SK, Kim AD, Minematsu H, Celil Aydemir AB, *et al*. ERK signaling regulates macrophage colony-stimulating factor expression induced by titanium particles in MC3T3.E1 murine calvarial preosteoblastic cells. Ann N Y Acad Sci 2007;1117:151–8.
37. Goldring MB. The role of cytokines as inflammatory mediators in osteoarthritis: lessons from animal models. Connect Tissue Res 1999:1–11.
38. Pulkki K. The effects of synovial fluid macrophages and interleukin-1 on hyaluronic acid synthesis by normal synovial fibroblasts. Rheumatol Int 1986;6:121–5.
39. Nishimoto N, Ito A, Ono M, Tagoh H, Matsumoto T, Tomita T, *et al*. IL-6 inhibits the proliferation of fibroblastic synovial cells from rheumatoid arthritis patients in the presence of soluble IL-6 receptor. Int Immunol 2000;12:187–93.
40. Blewis ME, Lao BJ, Jadin KD, McCarty WJ, Bugbee WD, Firestein GS, *et al*. Semi-permeable membrane retention of synovial fluid lubricants hyaluronan and proteoglycan 4 for a biomimetic bioreactor. Biotechnol Bioeng 2010;106: 149–60.
41. Russell FD, Hamilton KD. Nutrient deprivation increases vulnerability of endothelial cells to proinflammatory insults. Free Radic Biol Med 2014;67:408–15.
42. Ribel-Madsen S, Bartels EM, Stockmarr A, Borgwardt A, Cornett C, Danneskiold-Samsoe B, *et al*. A synoviocyte model for osteoarthritis and rheumatoid arthritis: response to ibuprofen, betamethasone, and ginger extract-a cross-sectional in vitro study. Arthritis 2012;2012:505842.
43. Attur M, Al-Mussawir HE, Patel J, Kitay A, Dave M, Palmer G, *et al*. Prostaglandin E2 exerts catabolic effects in osteoarthritis cartilage: evidence for signaling via the EP4 receptor. J Immunol 2008;181:5082–8.
44. Buckwalter JA, Mankin HJ. Articular cartilage: tissue design and chondrocyte-matrix interactions. AAOS Instr Course Lect 1998;47:477–86.
45. Guan JL. Role of focal adhesion kinase in integrin signaling. Int J Biochem Cell Biol 1997;29:1085–96.
46. Sarkissian M, Lafyatis R. Integrin engagement regulates proliferation and collagenase expression of rheumatoid synovial fibroblasts. J Immunol 1999;162:1772–9.
47. Werb Z, Reynolds JJ. Stimulation by endocytosis of the secretion of collagenase and neutral proteinase from rabbit synovial fibroblasts. J Exp Med 1974;140:1482–97.
48. Yanagida-Suekawa T, Tanimoto K, Tanne Y, Mitsuyoshi T, Hirose N, Su S, *et al*. Synthesis of hyaluronan and superficial zone protein in synovial membrane cells modulated by fluid flow. Eur J Oral Sci 2013;121:566–72.
49. Sun HB, Nalim R, Yokota H. Expression and activities of matrix metalloproteinases under oscillatory shear in IL-1 stimulated synovial cells. Connect Tissue Res 2003;44:42–9.
50. Sun HB, Yokota H. Reduction of cytokine-induced expression and activity of MMP-1 and MMP-13 by mechanical strain in MH7A rheumatoid synovial cells. Matrix Biol 2002;21: 263–70.

Appendix B

Thesis Publications

B.1 Full Length Manuscripts

Nover AB, Stefani RM, Lee SL, Ateshian G, Stoker AM, Cook JL, Hung CT. "Long-term storage and preservation of tissue engineered articular cartilage." J Orthop Res. 2016 Jan;34(1):141-8. doi: 10.1002/jor.23034. Epub 2015 Sep 8.

Silverstein AM, Stefani RM, Sobczak E, Tong EL, Attur MG, Shah RP, Bulinski JC, Ateshian GA, Hung CT. "Toward Understanding the Role of Cartilage Particulates in Synovial Inflammation." Osteoarthritis Cartilage. 2017 Aug;25(8):1353-1361. doi: 10.1016/j.joca.2017.03.015. Epub 2017 Mar 30.

Stefani RM, Halder SS, Estell EG, Lee AJ, Silverstein AM, Sobczak E, Chahine NO, Ateshian GA, Shah RP, Hung CT. "A Functional Tissue Engineered Synovium Model to Study Osteoarthritis Progression and Treatment." Tissue Eng Part A. 2019 Apr;25(7-8):538-553. doi: 10.1089/ten.TEA.2018.0142. Epub 2018 Oct 31.

Estell EG, Silverstein AM, Stefani RM, Murphy LA, Shah RP, Ateshian GA, Hung CT. "Cartilage Wear Particles Induce Inflammatory and Degradative Response Similar to Pro-Inflammatory Cytokines in Human Fibroblast-like Synoviocytes." J Orthop Res. 2019 Sep;37(9):1979-1987. doi: 10.1002/jor.24340. Epub 2019 May 17.

Stefani RM, Lee AJ, Tan AR, Halder SS, Hu Y, Guo XE, Stoker AM, Ateshian GA, Marra KG, Cook JL, Hung CT. "Sustained Low-Dose Dexamethasone Delivery Via a PLGA Microsphere-embedded Agarose Implant for Enhanced Osteochondral Repair." Acta Biomater. 2019. doi: 10.1016/j.actbio.2019.11.052. Epub 2019 Dec 2.

Stefani RM, Barbosa S, Tan AR, Setti S, Stoker AM, Ateshian GA, Cadossi R, Vunjak-Novakovic G, Aaron RK, Cook JL, Bulinski JC, Hung CT. "Pulsed Electromagnetic Fields Promote Repair of Focal Articular Cartilage Defects with Engineered Osteochondral Constructs." *In Revision at Biotechnology and Bioengineering (19-803.R1)*

Stefani RM, Lyons CM, Halder SS, Setti S, Ateshian GA, Cadossi R, Shah RP, Bulinski JC, Hung CT. "Biological Response of Synovium Explants to Pulsed Electromagnetic Fields is Modulated by Interleukin and Dexamethasone." *In Preparation.*

Stefani RM, Roach BL, Silverstein AM, Medberry PM, Lee J, Tan AR, Ateshian GA, Bulinski JB, Hung CT. "Applied Direct Current Electric Field Bioreactor to Induce Cell Migration into a 3D Cartilage Defect Model." *In preparation.*

Estell EG, Murphy LA, Stefani RM, Lee AJ, Shah RP, Ateshian GA, Hung CT. "Interleukin-1β Increases Human Synoviocyte Mechanosensitivity to Fluid-Induced Shear Stress be Modulating the Primary Cilia." *In preparation.*

Lee AJ, Ichinose R, Yu WT, Stefani RM, Mahoney CM, Marra KG, Ateshian GA, Shah RP, Hung CT. "SB-431542-Encapsulated Poly(Lactide-co-Glycolide) Microspheres as a Strategy to Prevent Arthrofibrosis." *In preparation.*

Murphy LA, Stefani RM, Sakhrani N, Gangi LR, Lee AJ, Kenawy HM, Ateshian GA, Shah RP, Hung CT. "Synovial Wrap for Supporting Primary Intra-Articular Ligament Repair" *In preparation.*

B.2 Conference Abstracts

Nover AB, Lee SL, Yu WT, Stefani RM, Ateshian GA, Stoker AM, Cook JL, Hung CT: "Long-Term Storage and Preservation of Tissue Engineered Articular Cartilage." Orthopaedic Research Society Annual Meeting, Las Vegas, NV, March 28-31, 2015.

Stefani RM, Nover AB, Ateshian G, Hung CT: "Characterization of a Model System to Study Synovial Membrane Transport Properties." Orthopaedic Research Society Annual Meeting, Las Vegas, NV, March 28-31, 2015.

Silverstein AM, Tong ET, Stefani RM, Attur MG, Ateshian GA, Bulinski JC, Hung CT: "Toward Understanding the Mechanism by which Cartilage Microparticulates Induce Synovial Inflammation in Osteoarthritis." Orthopaedic Research Society Annual Meeting, Orlando, FL, March 5-8, 2016.

Silverstein AM*, Stefani RM*, Sobczak E, Halder SS, Medberry P, Shah RP, Ateshian GA, Hung CT: "Design and Characterization of a Tissue Engineered Synovium Model to Study Pro-Inflammatory and Chondroprotective Mediators in Osteoarthritis." Orthopaedic Research Society Annual Meeting, San Diego, CA, March 19-27, 2017. *Authors contributed equally to this work.

Silverstein AM, Stefani RM, Sobczak E, Attur MG, Shah RP, Bulinski JC, Ateshian GA, Hung CT: "Cell Contact-Mediated Response of Fibroblast-like Synoviocytes to Cartilaginous Debris." Orthopaedic Research Society Annual Meeting, San Diego, CA, March 19-27, 2017.

Stefani RM, Roach BL, Silverstein AM, Nims RJ, Lee JH, Ateshian GA, Bulinski JC, Hung CT: "Electric Field Modulation of Synovial Fibroblast Migration for Cartilage Repair." Orthopaedic Research Society Annual Meeting, San Diego, CA, March 19-27, 2017.

Lee JH, Yu WT, Cai CC, Stefani RM, Mahoney CM, Ateshian GA, Marra KG, Shah RP, Hung CT: "Efficacy of SB-431542 in disrupting TGF-B1-induced synovial fibroblast-seeded collagen gel contraction." Orthopaedic Research Society Annual Meeting, New Orleans, LA, March 10-13, 2018.

Cai CC, Stefani RM, Mahoney CM, Ateshian GA, Marra KG, Shah RP, Hung CT: "Efficacy of SB-431542 in Disrupting Synovial Fibroblast-Seeded Collagen Gel Contraction." Orthopaedic Research Society Annual Meeting, New Orleans, LA, March 10-13, 2018.

Stefani RM, Tan AR, Barbosa S, Yu WT, Halder SS, Bozynski C, Setti S, Ateshian GA, Cadossi R, Stoker A, Aaron RK, Cook JL, Bulinski JC, Hung CT: "Application of Pulsed Electromagnetic Fields for Promoting Cartilage Repair of Engineered Constructs." Orthopaedic Research Society Annual Meeting, New Orleans, LA, March 10-13, 2018.

Stefani RM, Silverstein AM, Halder SS, Lyons CM, Ateshian GA, Bulinski JC, Shah RP, Hung CT: "Modulation of Synovial Fibroblast to Macrophage Ratio by Proinflammatory Cytokine and Corticosteroid: Implications for OA and Therapeutics." Orthopaedic Research Society Annual Meeting, New Orleans, LA, March 10-13, 2018. *Podium Presentation.*

Lee JH, Yu WT, Stefani RM, Mahoney CM, Marra KG, Ateshian GA, Shah RP, Hung CT: "SB-431542 encapsulated microspheres as a strategy to prevent arthrofibrosis" Biomedical Engineering Society Annual Meeting, Atlanta, GA, October 17-20, 2018. *Podium Presentation.*

Murphy LA, Stefani RM, Estell EG, Gangi LR, Kenawy HM, Ateshian GA, Shah RP, Hung CT: "Wound Healing of PCL Fibroblasts is Inhibited by Synovial Fibroblasts Production of Hyaluronan." Orthopaedic Research Society Annual Meeting, Austin, TX, February 2-5, 2019.

Stefani RM, Lee AJ, Gangi LR, Kenawy HM, Barbosa S, Tan AR, Durney KM, Hu Y, Ateshian GA, Guo XE, Marra KG, Bozynski CC, Stoker AM, Cook JL, Hung CT: "Sustained Low-Dose Dexamethasone Delivery is Chondroprotective & Enhances Clinical Repair of Cartilage Lesions." Orthopaedic Research Society Annual Meeting, Austin, TX, February 2-5, 2019.

Sakhrani N, Murphy LA, Lee AJ, Stefani RM, Semler, EJ, Shah RP, Visco CJ, Yuan X, Hung CT: "Synoviocyte Mechanosensitivity is Modulated by Glucose Preconditioning in an In Vitro Model of Diabetic Osteoarthritis and Synovial Joint Insulin Resistance." Orthopaedic Research Society Annual Meeting, Phoenix, AZ, February 8-11, 2020. *Podium Presentation.*

Murphy LA, Stefani RM, Sakhrani N, Gangi LR, Lee AJ, Kenawy HM, Ateshian GA, Shah RP, Hung CT: "Synovial Wrap for Supporting Primary Intra-Articular Ligament Repair." Orthopaedic Research Society Annual Meeting, Phoenix, AZ, February 8-11, 2020.

Murphy LA, Gangi LR, Stefani RM, Kenawy HM, Lee AJ, Ateshian GA, Shah RP, Hung CT: "Interleukin-1a Decreases Coefficient of Friction of Synovium *ex vivo*." Orthopaedic Research Society Annual Meeting, Phoenix, AZ, February 8-11, 2020.

Lee AJ, Gangi LR, Zandkarimi F, Stefani RM, Stockwell BR, Hung CT: "Ferrostatin-1 as an Inhibitor of Blood-Induced Chondrocyte Cell Death." Orthopaedic Research Society Annual Meeting, Phoenix, AZ, February 8-11, 2020. *Podium Presentation.*

Gangi LR, Kenawy HM, Stefani RM, Sakhrani N, Stoker AM, Cook JL, Chahine NO, Ateshian GA, Hung CT: "Impact of Sex-Based Differences on Cartilage Tissue Engineering with Canine Chondrocytes." Orthopaedic Research Society Annual Meeting, Phoenix, AZ, February 8-11, 2020.